DOCTOR OF PHILOSOPHY

The role of central IL-6 signalling in the development of Type 2 Diabetes

Yiannakas, Adonis

Award date:
2016

THE ROLE OF CENTRAL IL-6 SIGNALLING IN THE DEVELOPMENT OF TYPE 2 DIABETES

By

Adonis Yiannakas

A thesis submitted to the University of Dundee for the degree of

Doctor of Philosophy

JANUARY 2016

Contents

Declaration

I hereby declare this thesis to be my own work and has not been previously accepted for a higher degree. The nature and extent of contribution of other authors has been acknowledged accordingly.

……

Adonis Yiannakas
Dundee
January 2016

Conditions regarding relevant Ordinance and Regulations have been fulfilled.

……

Prof Rory McCrimmon
Dundee
January 2016

Acknowledgments

I would like to thank Dr. Alison McNeilly, Jen Gallagher and Kathryn Wright for their help and guidance throughout my studies, as well as Prof. Rory McCrimmon for this opportunity. Special thanks to my family, as well as Joe and Jake Birchenall for their friendship and support during my 8 years in Scotland.

I wish to dedicate this thesis to Artemis, for the love, patience and belief in me.

Abstract

Diets induced obesity and Type 2 diabetes affect an alarming number of people in the world. Patients exhibit a number of associated co-morbidities that require treatment and reduce life expectancy. The development of Type 2 diabetes results from a chronic disruption of glucose homeostasis as a consequence of environmental and genetic factors. The regulation of hypothalamic metabolic signalling is understood to be critical to the dynamic and long-term maintenance of glucose homeostasis by virtue of its influence on peripheral effectors (pancreas, liver, muscle and fat). Prolonged periods of inflammation observed in the development of diet-induced obesity and diabetes and accumulating evidence suggests this may negatively affect the maintenance of these neuroendocrine networks.

Interleukin 6 (IL-6) is a pleiotropic cytokine involved in the acute, as well as the resolving and adaptive phase of inflammatory responses. The IL-6 receptor has recently been shown to exhibit extensive localization in key regions of the human and rodent hypothalamus involved in glucose and energy homeostasis regulation. Recent work at Prof. Rory McCrimmon's lab investigating the role of IL-6 in the development of hypoglycaemia unawareness in Type 1 Diabetes identified the development of a glucose-sensing defect in hypothalamic glucose-sensing mouse cultures (GT1-7) in response to antecedent IL-6. These studies provided preliminary evidence to suggest that inflammatory cytokines such as IL-6 could directly modulate hypothalamic glucose sensing neurons and therefore might influence whole body glucose and energy homeostasis.

The body of work contained in this thesis sets out to examine the hypothesis that down-regulation of central IL-6 signaling would disturb the ability of mammals to regulate energy homeostasis, and would exacerbate defects in glucose clearance, insulin sensitivity and body composition typically observed in during the development of Type 2 Diabetes through chronic energy excess. To test this hypothesis cre-lox technology was used to generate a CRE-mediated nervous-system specific NesCreIL-6Rα knock-down (KD) mouse. Chronic administration of high-fat diet (>40% fat) in mice is commonly used to model the effects of diet-induced obesity and the progression to type 2 diabetes in humans. To examine the effects of this intervention in the development of diet induced obesity and diabetes, age (8-10 weeks

old) and sex-matched KD and control animals on standard chow (SC -15% fat) and high fat diet (HFD - 60% fat) were characterized using an array of *in vivo* metabolic phenotyping tests over a period of 20 weeks.

To generate a brain-specific IL-6Rα KD, heterozygous *B6.Cg-Tg (Nes-cre) 1Kln/J* mice were crossed with B6 (SJL)-*Il6ra*$^{tm.1.1Drew}$*/J* animals (IL-6Rα$^{flox/flox}$). The Nestin promoter exhibits brain-specific expression, while the IL-6Rα gene is flanked by 2 *loxP* sites in IL-6Rα$^{flox/flox}$ mice that would theoretically allow for brain-specific disruption of the receptor gene in offspring of this cross. Incorporation of the CRE gene in NesCre+ mice, and the presence of loxP sites in the genome of IL-6Rα$^{flox/flox}$ colony were confirmed by standard PCR **(Figures 1.1, 1.2)**. Offspring of the cross bearing the CRE gene were classified as KD, while the rest were considered wild-type littermates. Disruption of the IL-6Rα gene was confirmed at the mRNA level using real-time PCR (**Figure 1.3.2)**, with KD mice exhibiting down-regulation of the gene at the hypothalamus (~50%) and hippocampus (~35%). The effects of the NesCre-mediated down-regulation of the IL-6Rα were also examined using *in vivo* and *ex vivo* approaches, in relation to the induction of the STAT3 phosphorylation typically observed in response to IL-6. Administration of IL-6 in the periphery failed to induce STAT3 phosphorylation in the hypothalamus and hippocampus of KD mice, even though similar responses to control animals were observed in peripheral organs **(Figures 1.4, 1.5)**. Furthermore, examination of IL-6Rα protein expression by immunohistochemistry, confirmed decreases in the number of IL-6Rα-positive neuronal cells in NesCreIL-6Rα KDs compared to control mice **(Figures 1.7.1-4)**.

Brain-specific IL-6Rα down-regulation in NesCreIL-6Rα KDs was associated with a dramatic suppression of *in vivo* GSIS **(Figure 2.5.4)**, but was of little consequence to the blood glucose response to insulin **(Figures 2.4.1-3).** Examination of insulin and glucagon immunohistochemistry and *ex vivo* hormone release, KD and control islets were found to produce and release similar levels of the hormones in isolation, implicating a central component in the effect observed *in vivo* **(Figures 2.8.1-3)**. Body weight was closely matched between KD and control animals on SC diet, while dramatic increases observed in control animals on HFD were mirrored in HF-fed KDs **(Figure 2.1)**. Paradoxically, KD SC mice were significantly leaner than control mice, despite being hyperphagic **(Figures 2.2.1-5, 2.3, 2.9.1)**, hypoactive and hypothermogenic **(Figure 2.6.2-4)**. Hyperphagia and suppression of energy

expenditure was also observed in the HF-fed KDs, but in this case the leaner phenotype was progressively reversed through the course of 20 weeks of diet **(Figures 2.2.1-5, 2.6.2-4)**. Examination of a separate cohort of SC mice indicated that increases in food intake and body fat in response to chronic diet, were not a consequence of differences in leptin sensitivity between KD and control animals **(Figures 2.9.1-2).**

Collectively, data presented in this thesis suggest central IL-6 to play a fundamental role in the ability of the body to release insulin and regulate glycaemia in response to a glucose challenge. KD mice exhibited increased food intake and decreased energy expenditure and activity, that were only associated with increased body fat following chronic HF-feeding. This would suggest that increases in peripheral IL-6 observed in obese patients are part of a protective response to chronic energy excess, acting centrally to promote energy expenditure at least in part through increases in circulating insulin and thermogenic fat oxidation.

List of Abbreviations

2-deoxy-D-Glucose - 2-DG

A Desintegrin and Metalloprotease - ADAM

Activator Protein 1 - AP-1

Adenosine Diphosphate - ADP

Adenosine Monophosphate activated Kinase - AMPK

Adenosine Triphosphate - ATP

Adrenocorticotropic Hormone - ACTH

Agouti-Related Peptide - AgRP

Alpha 1 Acid Glycoprotein - AG

Arcuate Hypothalamic Nucleus - ARC

Body Mass Index -BMI

Brown Adipose Tissue - BAT

C Reactive Protein - CRP

Chemokine C-X-C motif Ligand 1 - CXCL1

Chemokine C-X-C motif Ligand 3 – CXCL3

Chemokine C-X-C motif Ligand 5 - CXCL5

Chemokine C-X-C motif Ligand 6 - CXCL6

Chemokine C-X-C motif Ligand 8 - CXCL8

C-jun Kinase – JNK

Cocaine and Amphetamine-Regulated Transcript - CART

Cyclic Adenosine Monophosphate - cAMP

Cyclic Adenosine Monophosphate Response Element-Binding protein - CREB

Diet Induced Obesity - DIO

Deoxyribonucleic Acid - DNA

Dosromedial Hypothalamus - DMN

ER – Endoplasmic Reticulum

Extracellular Receptor Kinase ½ - ERK1/2

Forkhead Box O1 - FoXO1

Glucagon-like Peptide 1 – GLP1

Glucose Stimulated Insulin Secretion – GSIS

Glucose Transporter - GLUT

Glucose-6-Phosphatase - G6Pase

Glycated Haemoglobin - HbA1c

Glyceraldehyde 3-phosphate dehydrogenase - GAPDH

Glycoprotein 130 – gp130

G-Protein Coupled Receptors - GPCRs

Guanosine Triphosphate - GTP

Hepatitis B Virus - HBV

High Fat Diet - HFD

Hormone Sensitive Lipase - HSL

Inducible Nitric Oxide Synthase - iNOS

Inhibitor of Nuclear Factor Kappa Beta Kinase Substrate Beta - IKKβ

Insulin Receptor Substrate 1 - IRS-1

Insulin Tolerance Test - ITT

Interferon Gamma – IFN-γ

Interleukin 1 Beta – IL-1β

Interleukin 10 – IL-10

Interleukin 13 – IL-13

Interleukin 4 – IL-4

Interleukin 6 – IL-6

Interleukin 6 Receptor Alpha Subunit – IL-6Rα

Interleukin 4 Receptor Alpha Subunit – IL-4Rα

Intra-peritoneal - IP

Janus kinase - JAK

Lateral Hypothalamus - LH

Lipopolysaccharide - LPS

Mitogen Activated Protein Kinase - MAPK

Messenger Ribonucleic Acid - mRNA

Muscarinic Acetylcholine Receptor - mAChR

NesCre1 (B6.Cg-Tg (Nes-cre) 1Kln/J mice - CRE

NesCreIL-6Rα KD mice - KD

Non-significant – ns

Not Assessed – N/A

Neuropeptide Y - NPY

Nuclear Factor for Interleukin 6 - NF-IL-6

Nuclear Factor Kappa Beta- NF-κB

Oral Glucose Tolerance Test – oGTT

Parathyroid Hormone - PTH

Paraventricular Hypothalamus - PVN

Peroxisome Proliferator-Activated Receptor Gamma – PPARγ

PPARγ co-activator 1α - PGC-1α

Phosphatidylinositide 3-Kinase - PI3K

Pro-Opiomelanocortin - POMC

Protein Kinase B - PKB/Akt

Protein Kinase C - PKC

Reactive Oxygen Species - ROS

Serotonin - 5-HT

Signal Transducer and Activator of Transcription - STAT

Soluble Interleukin 6 Receptor – sIL-6Rα

Soluble-glycoprotein 130 analogue - sgp130Fc

Standard Chow - SC

Suppressor of Cytokine Signaling 3 – SOCS3

Toll-like Receptor- TLR

Tumor Necrosis Factor Alpha - TNF-α

Type 2 Diabetes – T2D

Uncoupling protein 1 - UCP1

Ventromedial Hypothalamus – VMH

Wild Type Littermate mice of the NesCre+ x IL-6Rα$^{flox/flox}$ cross - WT

White Adipose Tissue -WAT

World Health Organization – WHO

List of Figures

List of Tables

Chapter 1: Introduction

Diet Induced Obesity and Diabetes: A Modern Epidemic

Obesity is a medical condition characterized by excess body fat, leading to decreased life expectancy through the accumulation of a range of pathologies in patients (Haslam & James, 2005; WHO, 2000). It is among the leading causes of preventable death (Yoon, et al., 2014), as it is associated with type 2 diabetes, hypertension and hyperlipidaemia - major precursors to cardiovascular disease (Eckel, 1997; Poirier & Eckel, 2002). Obesity is most frequently the consequence of a combination of environmental factors (excess food intake, lack of physical activity) and genetic susceptibility (Lau, et al., 2007). In rare cases, obesity is caused by genetic mutations, endocrine disorders, medications or psychiatric illness (Barness, et al., 2007). Body mass index (BMI) is currently the primary focus in obesity treatment recommendations, in relation to obesity-related comorbidities such as hypertension and hyperlipidaemia (WHO, 2000). Patients are generally characterized as individuals with a BMI above 30kg/m^2, with the normal range being around 25kg/m^2.

Figure 1.1: The Body Mass Index Scale

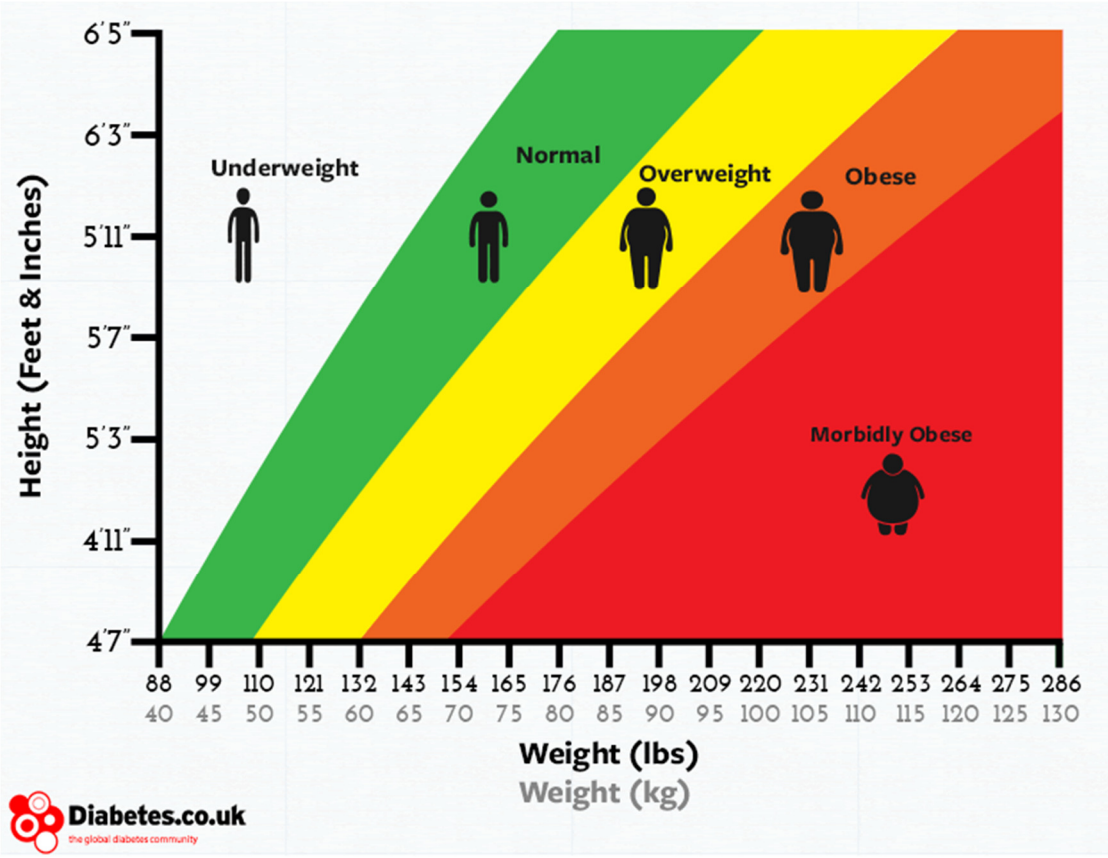

Obesity and its associated pathology was described as early as 500BC (Haslam & James, 2005; Dwivedi & Dwivedi, 2007); however historically, mankind has faced extended periods of food scarcity and obesity was rarely observed (Balke & Nocito, 1994). Changes in diet and exercise were recommended by early physicians, yet during the Middle Ages in particular, obesity was indicative of social status (Bloomgarden, 2003). The industrial revolution of the 19th century and the array of socioeconomic changes that followed, promoted increases in body weight and height in the developed world (Caballero, 2007). Increases in the Body Mass Index of the population resulted in improved survival and productivity, driving the establishment of early industrialized societies.

During the 20th century however, as the genetic height potential of populations was reached, body weight increases were maintained through the advent of technology and the adoption of a more sedentary life style. Alarming increases in cardiovascular disease were reported in the US during 1960s and 70s (US Department of Health, 1966), but it wasn't until 1995 that World Health Organization (WHO) first stated diet-induced obesity (DIO) prevalence to be of epidemic proportions (WHO, 1995). At that time, 200 million were thought to be obese. Current estimates indicate a tripling of this figure, while with the increased prevalence in the developing world, approx. 2 billion people in the world are thought to be overweight (WHO, 2014).

Excess body weight accumulation in obesity is naturally the consequence of positive energy balance. Energy intake in obese patients far exceeds energy expenditure over prolonged periods of time. The relative contribution of increased energy intake and decreased energy expenditure to the obesity epidemic is still a matter of debate. Epidemiological data with regards to the US where obesity is leading among the causes of preventable death (Danaei, et al., 2009), implicate a combination of factors. A 200kcal/day increase in daily food intake was observed during 1980-2000 (Popkin, et al., 2002), while current figures suggest consumption to exceed recommendations by approx. 50% (FAO, 2008). This can be partly attributed to increases in the consumption of sweetened beverages over fruit and vegetable, accounting to nearly 25% of daily intake (Rajeshwari, et al., 2005; Striegel-Moore, et al., 2006; US Department of Health and Human Services, 2005). The increased availability of low cost energy-dense foods and the preference to ready-meals is particularly detrimental, especially when considering low-income areas (Drewnowki & Specter, 2004). The

lack of physical activity within the US population was an issue of concern since the 1950s; however current figures suggest a mere 20% of adults currently meet the recommended physical activity guidelines (Carlson, et al., 2015).

Figure 1.2: Global Adult Obesity Prevalence 2008

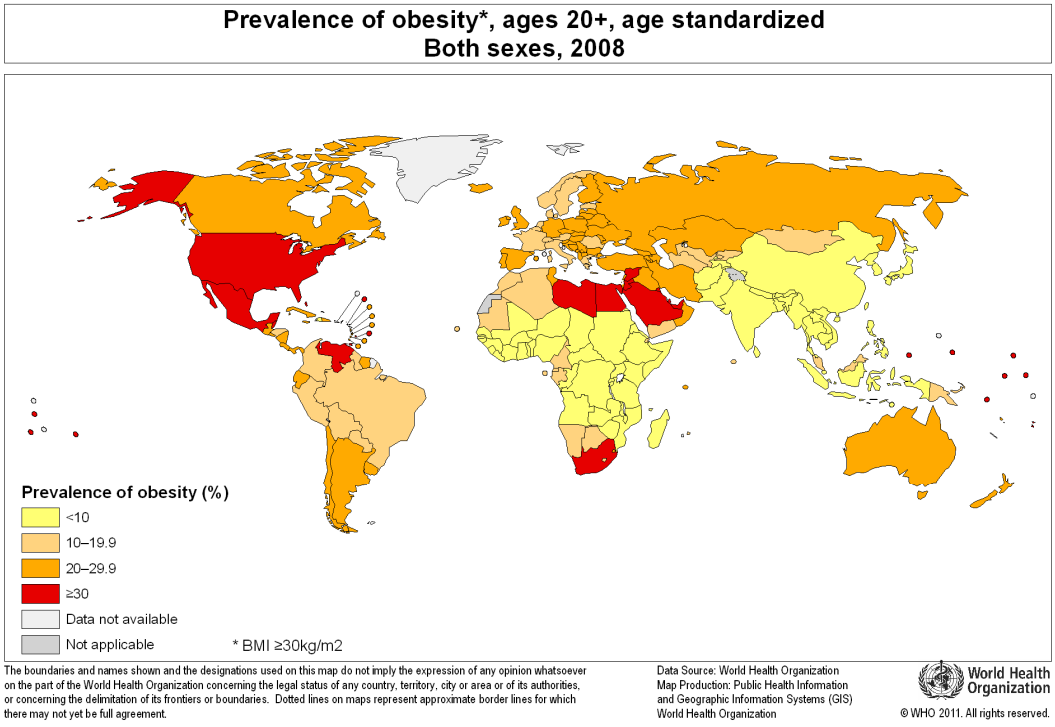

Scotland was second only to the US in terms of prevalence in a survey among the members of the Organization for Economic Co-operation and Development (Arah, et al., 2006). The total (direct and indirect) cost of obesity to Scottish society was estimated around £2 billion and thus tackling obesity is a key priority for government and public health professionals. In 2013 the Scottish Health Survey, estimated over a quarter (27.1%) of the adult population to be obese while a daunting two thirds were thought to be overweight (Bromley, et al., 2013). Prevalence was higher among women (29.3% compared to 24.9%), even though men appear more likely to be overweight (68.3% compared to 61%). Age was strongly correlated with disease prevalence (~75% of adults aged 45-74, >75% of adults aged 55-74), yet an alarming 28.8% of children aged 2-15 are also at risk of overweight or obesity. Collectively a 10% increase in obesity prevalence in people aged 16-64 since 1995 was noted, despite the efforts made such as the publication of the Revised Dietary Goals for Scotland in 1996. A recent estimation of food intake in Scotland (Barton & Wrieden, 2015), suggested that little progress was made towards those goals over 2001-2012.

On the other hand data in the years between 1998 and 2011 indicate that only a 30% of the adult population met the recommended physical activity guidelines (Bromley, et al., 2013).

Figure 1.3: Obesity Prevalence Scotland

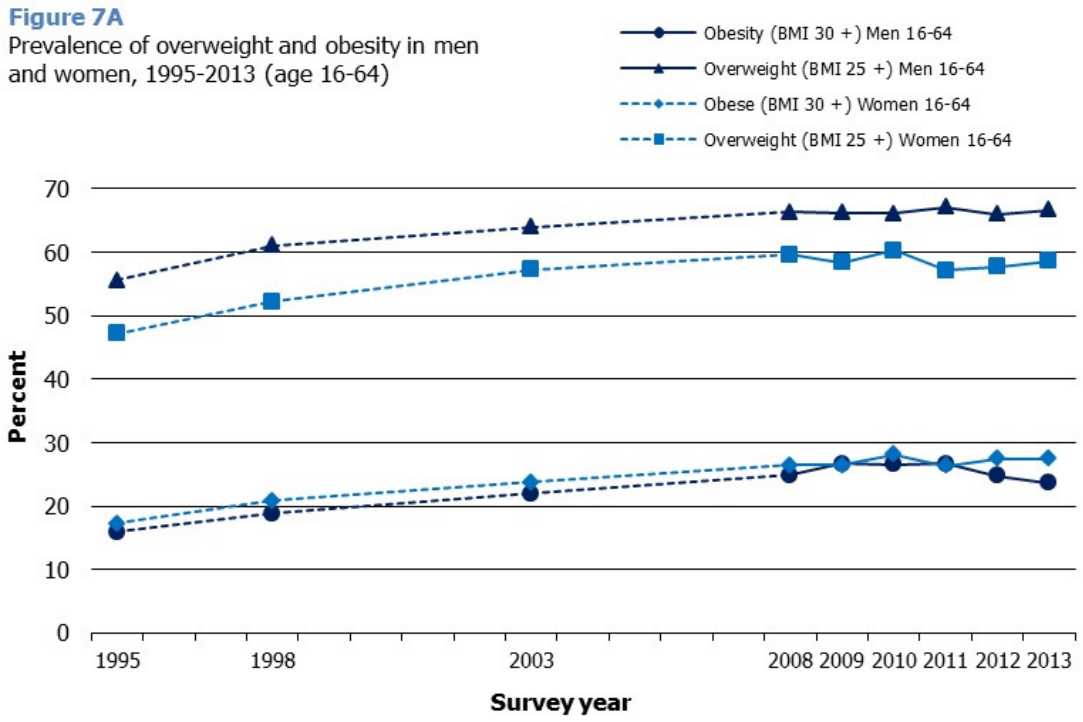

Adapted from Bromley C. et al. (2013)

Prolonged exposure to positive energy balance in obesity not only increases BMI and adiposity, but also the risk of development of the most common form of metabolic disease, Type 2 Diabetes mellitus (Lewis, et al., 2002). Earlier clinical studies indicated obesity to be strongly associated with diabetes in men (Chan, et al., 1994), while a 28-fold greater risk of developing the disease was reported in obese women (Colditz, et al., 1995). The International Diabetes Federation estimates the world diabetic population to approach 400million of whom at least 80% are overweight or obese (IDF, 2014). Type 2 diabetes (T2D) accounts for approx. 90% of the diabetic population and is characterized by hyperglycaemia and the development of insulin resistance (Kahn, 1998). Prior to the discovery of insulin in 1920 by Dr Frederick Banting and the subsequent establishment of insulin replacement therapy as treatment, diabetic disease was a synonym to death (Anon., 1966; Best, 1942). Insulin therapy is targeted towards lowering glucose levels to desired norms, as sustained

hyperglycemia is also associated with severe micro- and macro-vascular disease (Pickup, 2004; Venieratos, et al., 2010)

Despite being the subject of extensive research in the past century, diabetes remains the 4th commonest cause of death in the developed world (IDF, 2014). The current diabetic population of the UK is around 4 million, and is expected to reach 5 million by 2025. The estimated the cost of diabetes treatment in the UK in 2012 was around 14.5billion GBP, with the annual cost of treatment per patient around £1,800-2,500 GBP (Kanavos, et al., 2012). The projected annual cost of diabetes to the NHS is expected to increase to £17billion in the next 25 years. In Scotland - a nation of 5million, the diabetic population is believed to be close to 250,000 patients and is currently increasing by 13,000/year (Diabetes UK, 2015). The aforementioned high prevalence of obesity in the adult Scottish population though a combination of socioeconomic factors, is an obvious precursor to this statistic.

Figure 1.4: Type 2 Diabetes in Scotland

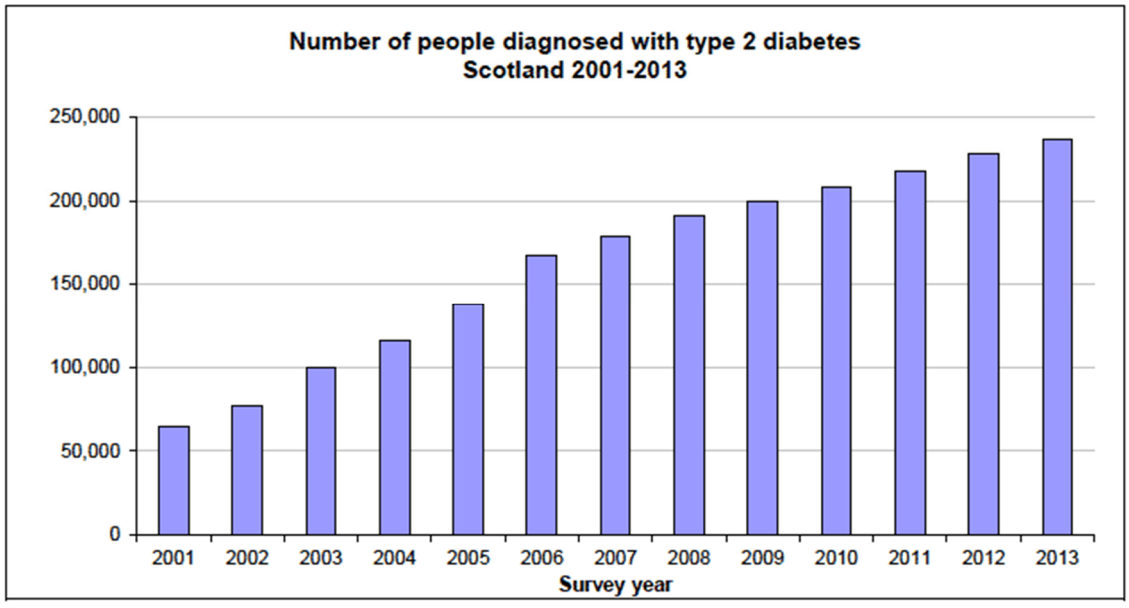

Adapted from Bromley C. et al. (2013)

Various initiatives directed towards improving public awareness have thus far been ineffective in decreasing disease prevalence and the population of obese and diabetic patients is still on the rise. The combined annual cost of diabetes to Scottish society is currently around £2 billion and the disquieting increases in obesity prevalence can only be expected to drive further increases to this figure. This figure relates to a

number of disease-associated pathologies (e.g. retinopathy, neuropathy, nephropathy, stroke and cardiovascular events) that require medical attention due to their direct impact on patient life quality and expectancy (Barness, et al., 2007). Research in the pathophysiology of disease development is still ongoing as the precise molecular mechanisms underlying this are still somewhat elusive. Diet induced obesity and diabetes comprise a serious threat to public health, and advancements in the understanding of disease development that could provide the basis for improved treatment would be of significant socioeconomic value.

Figure 1.5: Type 2 Diabetes Disease-associated Pathology

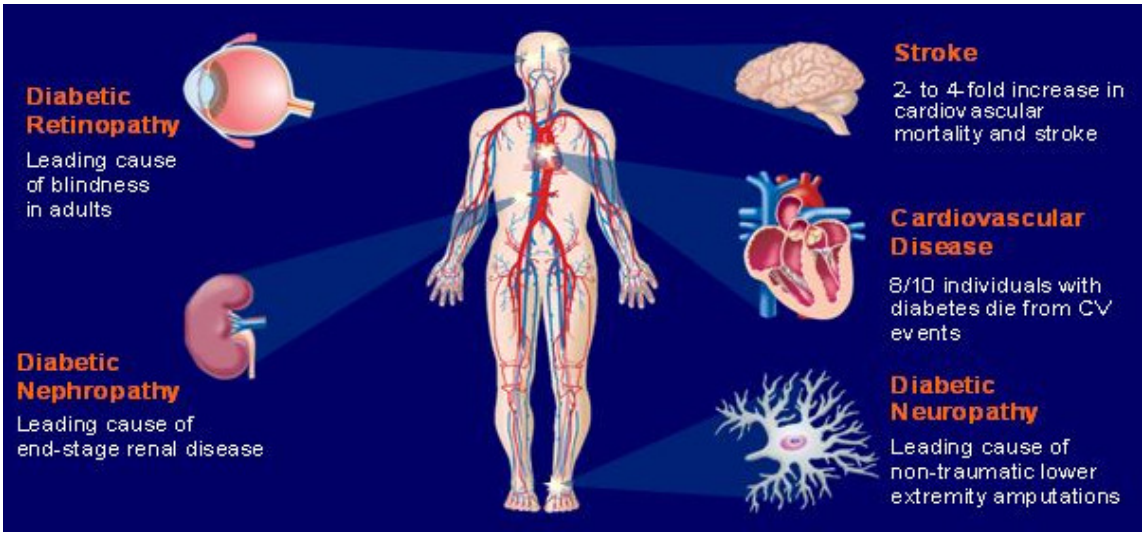

Adapted from Saltiel & Olefsky (2001)

Type 2 Diabetes Pathology

Type 2 diabetes is characterised by relative insulin deficiency and reduced insulin sensitivity in insulin target tissues (e.g. muscle, liver and adipose tissue) that promotes the dysregulation of glucose homeostasis. Patients experience impaired insulin-stimulated glucose uptake in muscle (Cusi, et al., 2000) and adipose tissue (Yki-Jarvinen, 2002), while the inhibition of glucose output from the liver is also disrupted (Nakatani, et al., 2004) as a consequence. Traditionally, chronic exposure to high fat diet alone is considered to lead to insulin resistance and the development of T2D (Reaven, et al., 1988; Walker, et al., 1966).

The secretion of insulin from pancreatic β cells is a highly regulated process targeted to account for the hyperglycaemia observed following food intake. Glucose up-take from muscle and fat is stimulated; liver gluconeogenesis is inhibited, while free fatty acid levels are decreased through the inhibition lipolysis and increases in lipogenesis (Kahn & Flier, 2000). The action of insulin and the induction of hypoglycaemia are countered by the release of glucagon from pancreatic α cells and catecholamines from the adrenals (Taborsky, et al., 1998). Glucagon release from pancreatic α cells promotes gluconeogenesis at the liver and inhibits β cell secretions. Maintenance of glucose homeostasis is physiologically achieved through the rigorous and dynamic maintenance of these relationships (Cannon, 1929; Stumvoll, 2004; Boner-Vier, 2000).

Figure 1.6: Physiological Regulation of Glucose Homeostasis in Humans

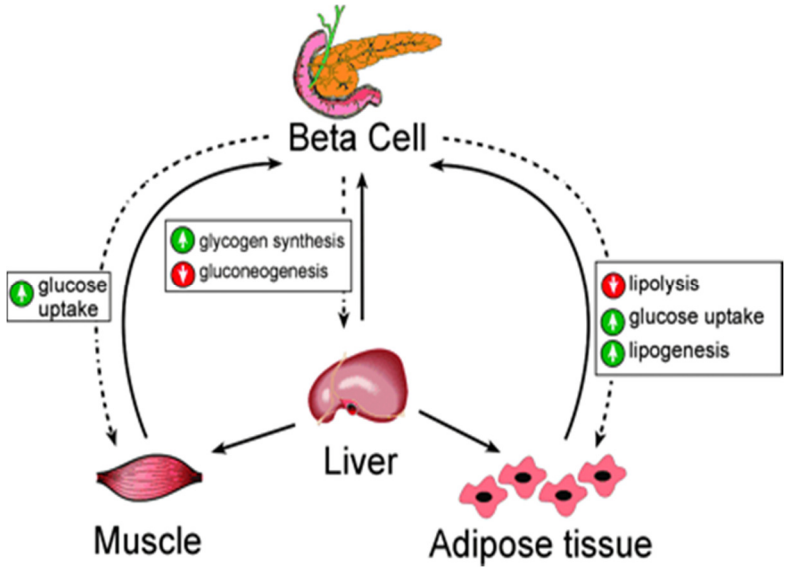

Adapted from Taborsky G.J. et al. (1998)

A reduced ability of insulin to stimulate intracellular signal transduction pathways for peripheral glucose uptake and hepatic glucose production inhibition (insulin resistance); leads to increases in circulating plasma insulin levels in most patients with Type 2 Diabetes. Glucose up-take in response to insulin is primarily driven by the hormone acting on muscle (and to a lesser extent fat) to promote glucose-transporter-4 (GLUT-4) translocation to the membrane, following recruitment of insulin receptor substrate-1 (IRS-1) and activation of tyrosine kinase activity (Klip & Paquet, 1990; Stolic, et al., 2002). Insulin resistant states are characterized by down-regulation of GLUT-4 in both muscle and adipose tissue while increases in intracellular lipid intermediates promote serine/threonine kinase activity; inhibit the action of insulin via receptor substrate-1 (IRS-1) and disrupting glucose-uptake (Yu & al., 2002; Pickersgil, et al., 2007; Lee & al., 2006).

Adipose tissue on the other hand is responsible for the uptake free fatty acids in circulation (Jensen, 2002; Shadid, et al., 2007), while the ability of fat to expand in response to metabolic challenges is instrumental to homeostasis maintenance (Gray & Vidal-Puig, 2007). Insulin regulates genes in adipocytes that promote fatty acid synthesis and lipogenesis, while the oxidation of fatty acids is inhibited (Kahn & Flier, 2000). High fat diets lead to the accumulation of free fatty acids in plasma and tissue, due to disruption of the inhibitory effects of insulin on hormone-sensitive lipase (HSL) and reduction in the activity of the lipogenic receptor PPARγ (Guilherme, et al., 2008) in adipocytes and in hepatocytes.

Figure 1.7: Insulin Resistance in Type 2 Diabetes

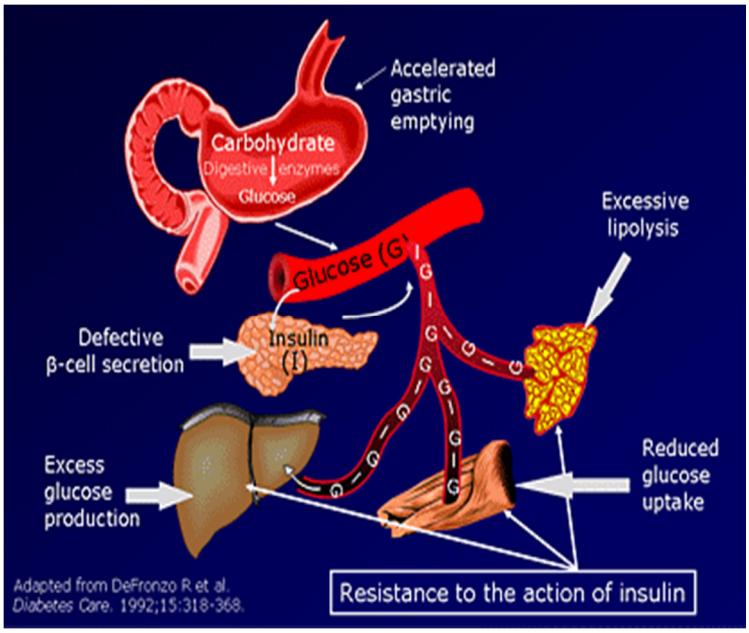

In the liver, the primary regulated step that determines glucose uptake is glucose phosphorylation by glucokinase, and not glucose transport. Approximately a third of dietary glucose is stored by the liver as glycogen and released in the post-absorptive state through the activation of glycogenolysis (Pagliassotti & Cherrington, 1992). However the chronic exposure to hyperglycaemia and dietary carbohydrates typical of DIO, results in the accumulation of metabolic intermediates that initially impair and progressively suppress the activity of glucokinase driving insulin resistance (Torres, et al., 2011; Torres, et al., 2009).

The establishment of insulin resistance in target tissues promotes sustained increases in insulin release from the β cell, to counter hyperglycaemia. However, B cells have very low anti-oxidative enzymes and are under considerable endoplasmic reticulum (ER) stress, even under physiological conditions (Donath, et al., 1999; Robertson, et al., 2004). The maintenance of hyperinsulinaemia observed in DIO and T2D, increases oxidative and endoplasmic reticulum stress in pancreatic β cells further promoting their dysfunction (Donath, et al., 2005; Robertson, 2007). The number and mass of β-cells is reduced, while the pulsatility of insulin release is disturbed (Schofield & Sutherland, 2012; Song, et al., 2000; Porksen, et al., 1996; Butler, et al., 2003); leading to a vicious cycle of disordered secretory function of the β cell that is inadequate to overcome the establishment of insulin resistance at target tissues and drive glucose uptake.

Neuroendocrine Regulation of Glucose Homeostasis and Energy Expenditure

Disruption of glucose homeostasis regulation is a fundamental aspect of DIO and the progression to T2D. The brain is a particularly energy demanding organ and accounts for approximately 25% of the total body glucose utilization in mammals (Ebert, et al., 2003), but its role in metabolic disease was overlooked for decades. Traditionally, brain glucose up-take was viewed to take place independently of insulin and the hormone itself was falsely considered to be too large to cross the blood brain barrier (Baskin, et al., 1987). During the past 20 years significant progress has been made in the role of the brain in metabolic disease. The neuronal pathways that link the central nervous system with autonomic innervation of the pancreas were delineated, while the role of the hypothalamus in controlling food intake and energy homeostasis is being increasingly acknowledged.

Figure 1.8: Neuroendocrine Regulation of Glucose Homeostasis

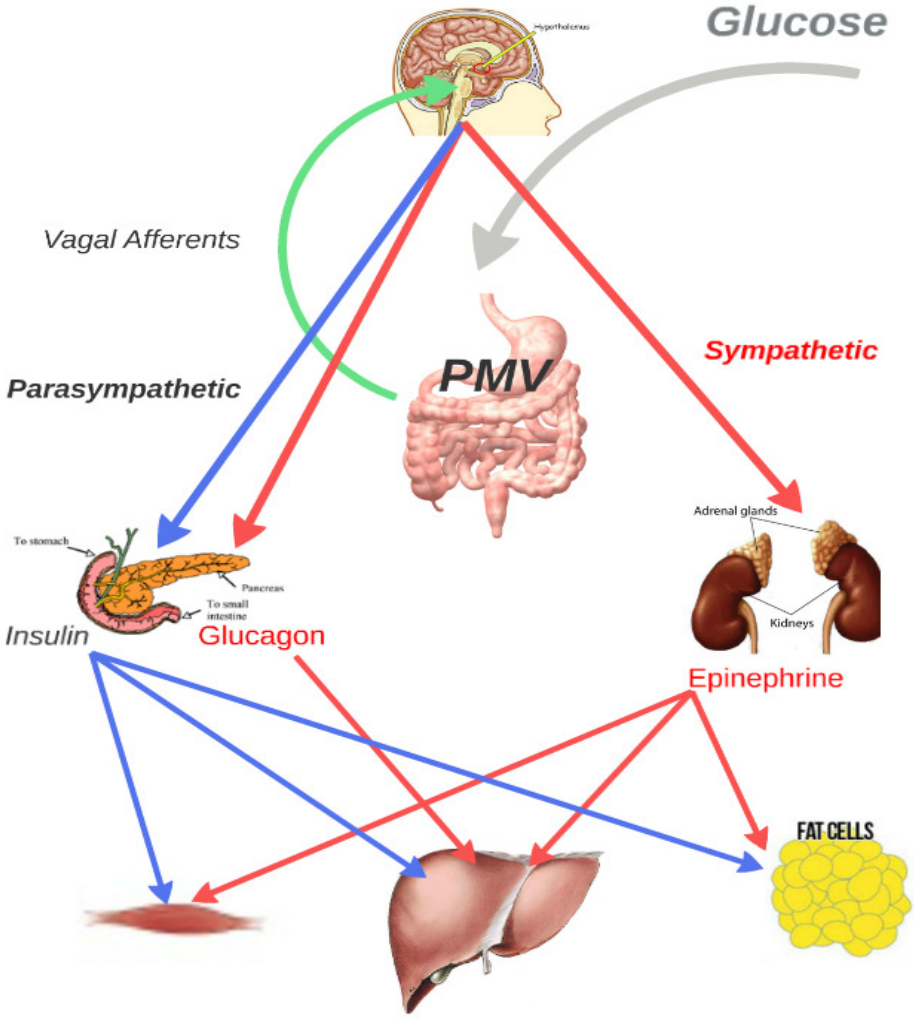

Pancreatic β cells have been demonstrated to be subject to regulation by neuronal and hormonal stimuli. This is thought to be largely a feature of the array of G-protein coupled receptors (GPCRs) expressed at these cells. Expression of GPCRs acting via the heterotrimeric G_q protein (e.g. muscarinic acetylcholine receptor - m3AChR) allows for parasympathetic stimulation of glucose-stimulated insulin secretion (GSIS) (Gilon & Henquin, 2001). Sympathetic innervation on the other hand, inhibits β cell GSIS through activation of α2 adrenoceptors coupled to G_i by agents such as noradrenaline and epinephrine from the adrenals (Ahren, 2000). Conversely, catecholamines stimulate glucagon release from α cells via β2 adrenoceptors.

The appearance of glucose in the oral cavity induces the cephalic phase of insulin secretion that is dependent on neuronal connections from taste buds project to the brainstem to activate the parasympathetic vagus nerve and stimulate GSIS from the β cell (Berthoud & Jeanrenaud, 1982; Berthoud & Powley, 1990). Parasympathetic innervation of the β cell and its stimulating effects on GSIS has been documented by a number of early studies using rodents, and researchers speculated the presence of central glucose-sensing populations (Kaneto, et al., 1975; Berthoud, et al., 1980; Lundquist, 1982; N'Guyen, et al., 1994). Studies during the late 70s first suggested the hindbrain and hypothalamus to act in concert to detect changes in nutrient availability and to calibrate autonomic tone by independently adjusting the function of the pancreas. Regulation of glucagon secretion by distinct sites within the hindbrain was initially demonstrated using administration of the glucose anti-metabolic 5-thioglucose (Ritter, et al., 1981; Ritter, et al., 2000), while lesions of the ventromedial nucleus in anesthetized rats induced hyperinsulinaemia that was suppressed by vagotomy (Berthoud & Jeanrenaud, 1979). In support of these early studies, extra-carotid injection of glucose in rats was shown to induce a transient increase in insulin secretion that was accompanied by the activation of neurons of the paraventricular and arcuate hypothalamus (Guillod-Maximin, et al., 2004; Jansen, et al., 1997).

Changes in circulating blood glucose are paralleled in the brain, inducing changes in the activity of neurons in the dorsal vagal complex at the hind brain (nucleus tractus solitarius, area postrema and dorsal motor nucleus of the vagus) as well as neurons in the ventromedial, arcuate, paraventricular and lateral hypothalamus, receiving input from vagal afferents (Mizuno & Oomura, 1984; Ritter, et al., 2000; Hudson & Ritter, 2004; Dallaporta, et al., 1999; Berthoud & Powley, 1990; Yang, et al., 2004). Glycaemic signals detected at the brainstem are directly or indirectly transmitted to

the hypothalamus via the basolateral medulla or the parabranchial nucleus (Yuan & Yang, 2002), where they are thought to be integrated to determine autonomic output (Thorens, 2011). These specialised cells resemble the function of pancreatic β cells, even though the precise molecular mechanisms of glucose-sensing are still being intensively studied (Marty, et al., 2007; Steinbusch, et al., 2015).

The ventromedial hypothalamus (VMH) is an important centre of integration of glucose-sensing signals and a regulator of sympathetic output to the pancreas (Burdakov, et al., 2005; Thorens, 2011). Direct administration of the glucoprivic agent 2-deoxy-D-Glucose (2-DG) into the VMH on the one hand induces glucagon secretion (Borg, et al., 1995), while the infusion of glucose into the nucleus suppresses glucagon secretions in response to systemic hypoglycaemia (Borg, et al., 1997). Lesions of the nucleus causes dramatic increases in insulin release, that were demonstrated to be the consequence of increases in parasympathetic output to the pancreas, increasing β cell proliferation and mass (Kiba, 2004; Kiba, et al., 1996). By integrating input from the hepatoportal vein and motivational cues from the medial amygdala (Zhou, et al., 2010); the VMH acts as the orchestrator of autonomic output from the dorsomedial, paraventricular and lateral nuclei to modulate pancreatic function (McCrimmon, et al., 2006).

In addition to regulating the release of pancreatic hormones, the hypothalamus is involved in appetite control, and mediates the action of adipostatic hormonal and neuronal mediators, such as leptin (Friedman & Halaas, 1988). A product of the *ob* gene, leptin is derived primarily from white- and to a certain extent brown adipose tissue (Moinat, et al., 1995; Tsuro, et al., 1996). Leptin acts in the brain (Satoh, et al., 1997), even though a variety of other tissues also express the hormone (Hoggard, et al., 1997; Hoggard, et al., 1997; Spicer & Francisco, 1997; Bado, et al., 1998; Wang, et al., 1998). Circulating leptin levels correlate with body weight and adiposity (Ahima, et al., 2000; Barsh, et al., 2000; Schwartz, et al., 2000; Maffei, et al., 1995), that are regulated by satiety and energy expenditure stimulating effects of the hormone (Berglund, et al., 2012; Baver S.B., et al., 2014; Williams, et al., 2001).

The arcuate nucleus (ARC), is situated at the base of the third ventricle, and the lack of tight junctions in the capillaries of the median eminence allows the ARC to be more directly exposed to circulating nutrients (e.g. glucose) and endocrine factors (e.g. insulin, leptin, ghrelin and incretins) than other brain regions (Broadwell & Brightman, 1976; Elmquist, et al., 1998). Specialized neuronal populations within the

ARC sense glucose and stimulate the release of pancreatic hormones (Claret, et al., 2007), while dense discrete populations of leptin and insulin receptor positive neuropeptide-secreting neurons allow for the regulation of energy balance in relation to body status (Plum, et al., 2006). Characteristically, direct injection of insulin (van Dijk, et al., 1997), leptin (Cowley & al., 2001) or glucose (Ahmed & Lauterio, 1993) in the ARC is sufficient to acutely reduce food intake and energy expenditure (Dunbar & Lu, 1999).

Figure 1.9: Neuroendocrine Regulation of Energy Expenditure

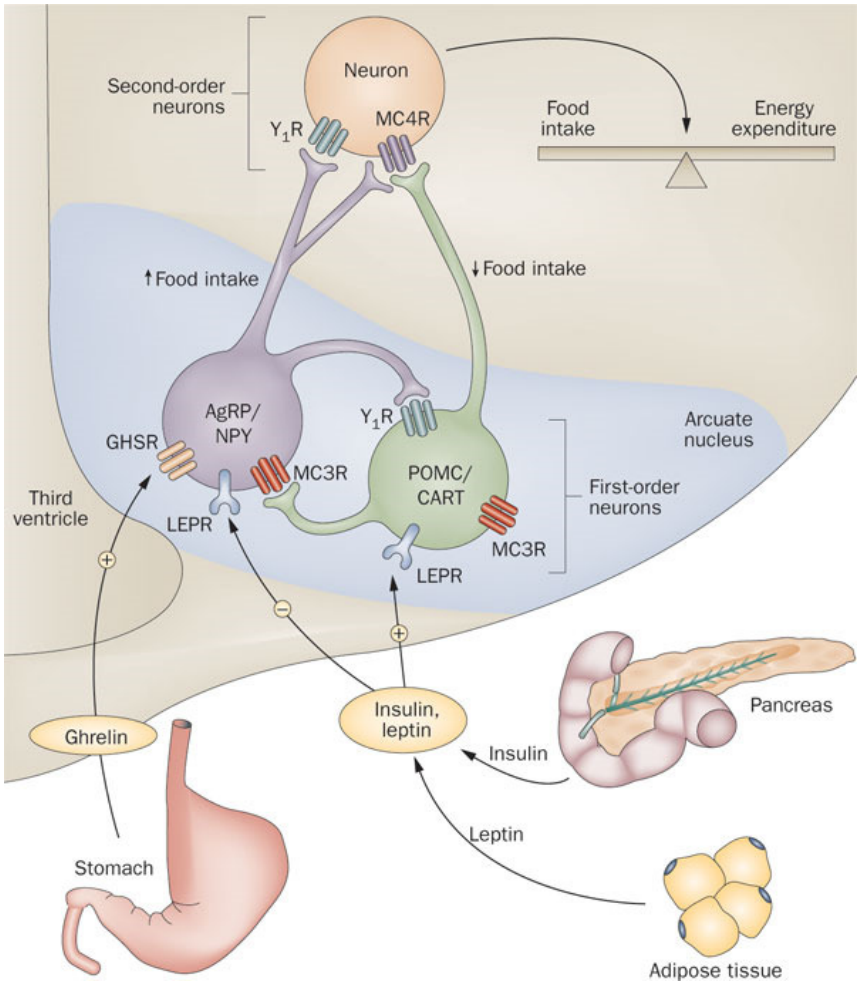

Adapted from Vetter M.L. et al. (2010)

The ARC contains orexigenic neuropeptide Y (NPY) and Agouti-related peptide (AgRP); and anorexigenic pro-opiomelanocortin (POMC) and cocaine and amphetamine-regulated transcript (CART) neurons (Broberge, et al., 1998B; Wilson, et al., 1999; Elias, et al., 1998). Neurons in the ARC (and NTS) are the primary source of anorexigenic cleavage product of POMC, α-melanocortin stimulating hormone (α-MSH), acting at the melanocortin-4 receptor in the PVN and LH, where the balance of orexigenic and anorexigenic activity is thought to be integrated and

propagated onto autonomic preganglionic neurons of the medulla and spinal cord (Swanson & Sawchenko, 1983; Elmquist, et al., 1998). Through the induction of separate yet synergistic signaling events, insulin and leptin act to promote the expression of products of POMC, inhibiting the activity NPY/AgRP expressing neurons (Plum, et al., 2006; Belgardt, et al., 2009; Ersnt, et al., 2009).

NPY/AgRP neurons of the hypothalamus are fundamental in stimulating feeding behaviour through the gut-brain axis (Luquet, et al., 2005). Stomach emptying in the context of fasting promotes increases in circulating ghrelin from the gastrointestinal tract promoting orexigenic activity in the brain (Wren, et al., 2000). This is paralleled by decreases in circulating leptin and insulin, and decreases in anorexigenic α-MSH and CART activity in the hypothalamus (Ahima, et al., 2000; Myers, et al., 2008). Other gut hormones such glucagon-like peptide-1 (GLP-1) and peptide tyrosine tyrosine (PYY) are also secreted from the gut, to limit meal size (Small & Bloom, 2004) by paracrine stimulation of pancreatic secretions (Smeets, et al., 2008; Ellingsgaard, et al., 2011), as well as directly or indirectly promoting the activity of anorexigenic neurons of the hypothalamus (De Silva & Bloom, 2012; Shirazi, et al., 2013).

Progressive increases in circulating leptin during feeding inhibit food intake and increase sympathetic outflow and energy expenditure by suppressing NPY/AgRP and increasing POMC activity in the ARC (Elias, et al., 1999). Chronic high-fat feeding, promotes down-regulation of anorexic α-MSH and CART in the ARC, while lack of POMC (Tung, et al., 2006; Diane, et al., 2014) or functional melanocortin receptors (Tarnow, et al., 2003; Butler, et al., 2000) causes hyperphagia and obesity. Mimicking the effects of DIO chronic intra-cerebroventricular administration of NPY in the ARC, promotes body weight gain, hyperphagia, hyperinsulinaemia, hyperlipidaemia and hyperleptinaemia (Sainsbury, et al., 1997; Zarjevski, et al., 1993).

Increases in sympathetic activity in response to the action of anorexigenic hormones such as leptin in the hypothalamus, enhance energy expenditure (Jequier, 2002; Konturek, et al., 2005; Valassi, et al., 2008). This involves stimulation of lipolysis, thermogenesis in muscle and fat and secondary increases in heat loss through the skin by vasoconstriction and dilation (Cannon & Nedergaard, 2004; Whittle, et al., 2011; Contreras, et al., 2014). Retrograde labelling studies have identified white adipose tissue to be innervated by neurons tracing to the brainstem (noradrenergic neurons of

the LC), the hypothalamic nuclei (ARC, DMH, LHA, and VMH) and the forebrain (Bamshad, et al., 1998; Shi & Bartness, 2001; van Baak, 2001).

Sympathetic activation of lipolysis in WAT is regulated by orexin neurons of the LH that modulate β3-adrenergic receptor output to the tissue. The activity of anorexigenic and orexigenic neuronal populations of the ARC modulates activity in the LH, and indeed a number of studies have demonstrated that stimulation of the melanocortin system promotes increased catecholamine release and lipolysis. Innervation of BAT has also been demonstrated to be synaptically connected with a number of hypothalamic neuronal populations including the VMH, PVN, ARC and suprachiasmatic nucleus (Elmquist, 2002; Bamshad, et al., 1999; Oldfield, et al., 2002). The VMH is particularly important in the thermoregulatory role of the BAT and electrical stimulation of the nucleus induces β-adrenergic-dependent increases in tissue temperature (Perkins, et al., 1981; Yoshida & Bray, 1984; Holt, et al., 1987). Steroidogenic factor 1-expressing neurons are expressed in the VMH, and project to autonomic centres and other hypothalamic regions involved in sympathetic outflow such as the ARC and PVN (Lindberg, et al., 2013). A number of studies have indicated these neurons to be particularly important in promoting thermogenesis and weight loss induced by increases in sympathetic output in response to leptin (Tanida, et al., 2013; Kim, et al., 2011).

Finally, energy expenditure and satiety are known to be influenced by mood and arousal states that commonly override homeostatic signals (Saller & Stricker, 1976; Breisch, et al., 1976). Neuronal networks stimulating arousal such as serotoninergic neurons in the dorsal & median raphe nuclei, the noradrenergic networks in the locus coeruleus and histaminergic tuberomammilary nucleus, modulate the activity of satiety-regulating neurons of the hypothalamus (Burke & Heisler, 2015). These neurons are thought to regulate motivated feeding behaviour and increase energy expenditure through positive modulation of the melanocortin system; stimulating POMC and inhibiting direct- and indirect effects of NPY/AgRP neurons. Peripheral effects of serotonin (5-HT) agonists were shown to be associated with an array of side effects during the 1990s, but in recent years the effects of activation of specific receptor subtypes within the hypothalamus were outlined (Xu, et al., 2010). This led to the development of 5-HT_{2C}R agonists that have been shown to display efficacious in promoting energy homeostasis, including glucose homeostasis and insulin sensitivity (Joo & Lee, 2014).

Hypothalamic nuclei, thus play a fundamental role in the detection of changes nutrient availability and act to modulate the balance between food intake, energy storage and energy expenditure. Specialized neuronal populations within the hypothalamus are involved in glucose-sensing, while distinct populations of orexigenic and anorexigenic neurons express leptin and insulin receptors. By integrating input from the autonomic nervous system and hindbrain, the activity of distinct neurons of the hypothalamus orchestrates short- and long-term management of changes in nutrient availability through promoting appropriate neuroendocrine and behavioural responses. Maintenance of the dynamic regulation of signaling cascades and excitability within neuronal networks of the hypothalamus, represent fundamental aspects of the ability of the body to manage perturbations of energy homeostasis. The effects of circulating factors such as pancreatic hormones and the multifunctional protein leptin in the maintenance of homeostasis, are dependent on the balance of activity within these networks. However, much is still unknown and research in the molecular mechanisms that lead to the dysfunction of these neuroendocrine networks in DIO and T2D are still being heavily investigated.

Metabolic Dysregulation in Type 2 Diabetes: The role of Inflammation

The initial step leading to the development of T2D remains somewhat elusive. More recent research efforts have discovered an important role for chronic inflammation in the impairment of insulin signaling via systemic and local effects. Metabolic inflammation in this context is unlike that of the response to infection or injury in that it lacks the classical symptomatology observed (tissue swelling, heat and pain) but is discernible at the molecular levels (Gregor & Hotamisligil, 2011; Cai, 2009). Obese patients are understood to experience chronic low-grade inflammation, as suggested by increases in plasma levels of C-reactive protein, inflammatory cytokines (Kalofoutis, et al., 2006) and the multifunctional proteins leptin (Friedman & Halaas, 1988) and osteopontin (Kiefer, et al., 2008).

Figure 1.1.1: Cytokines and Chronic Inflammation

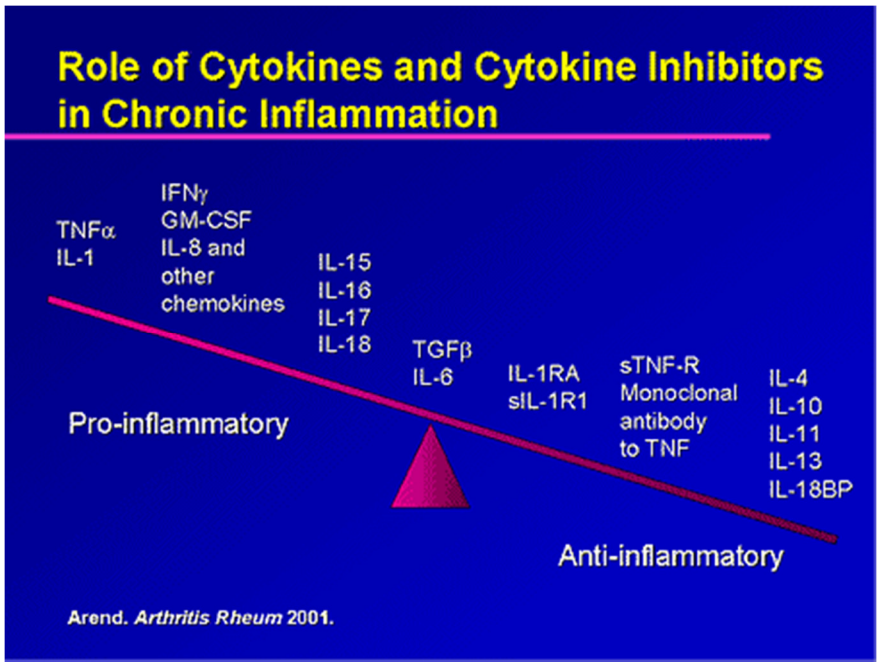

Inflammatory cytokines such as TNF-α, IL-1β and IL-6 are products of NF-κB activity (Brasier, 2006). NF-κB is a protein complex expressed in all animal cell types that acts in the regulation of DNA transcription in the response to various stress stimuli and promotes cell survival (Gilmore, 2006; Perkins, 2007). Cytokines are secreted in response to stimuli such as oxidative stress (Pereda, et al., 2006), infection (Cooper, et al., 2011; Gee, et al., 2009) and UV radiation. Cytokine signaling is often observed to act in a feed-forward manner, culminating in activation of IKKβ-NF-κB and the c-jun kinase (JNK) arm of the mitogen-activated protein kinase (MAPK).

Similarly, hyperinsulinaemia and the accumulation of free fatty acids and glucose that takes place in response to DIO and T2D induces increases in circulating cytokines via these pathways (Milanski, et al., 2009; Hirosumi, et al., 2002).

Earlier work indicated recruitment of tissue macrophages to visceral adipose tissue in obesity to induce the appearance of TNF-α and to aggravate insulin resistance (Hotamisligil, et al., 1993; Visser, et al., 1999; Kim & al., 2005). TNF-α was found to be over-expressed in muscle and adipose tissue of obese humans, while its exogenous administration led to insulin resistance (Hotamisligil, et al., 1995; Krogh-Madsen, et al., 2006). In other experiments using human *ex vivo* pancreatic β cells, exposure to high glucose increased expression of Interleukin-1β (IL-1β) via NF-κB activity which was also observed in islets from obese, but not control subjects. *Ex vivo* data indicated increased NF-κB activity to promote insulin resistance in patients by disrupting β cell secretory function and increasing vulnerability to the hyperglycaemia observed in DIO (Maedler, et al., 2002).

In the brain, increases in NF-κB activity are known to be detrimental to the survival to acute and prolonged ischemia (Stephenson, et al., 2000; Wang, et al., 2010). However, more recently it has been suggested that NF-κB activation during transient middle cerebral artery occlusion, is associated decreases in infarct size, while its suppression following hypoxia produced exacerbation of neural deficits over time (Teoh, et al., 2003; Van Den Tweel, et al., 2006; Pires, et al., 2014). Forebrain-specific neuronal inhibition of NF-κB rendered neurons more susceptible to neurotoxic insults (Fridmacher, et al., 2003), while accumulating evidence indicate NF-κB activity in hippocampal neurones to be a positive modulator learning and memory (Meffert, et al., 2003; Kaltschmidt & Kaltschmidt, 2009). In the hypothalamus, promotion of serine kinase activity via NF-κB signaling cascades has recently emerged as a harbinger of metabolic dysregulation.

The frequent and sustained increases in circulating free fatty acids observed in DIO rodents were demonstrated to directly promote hypothalamic metabolic inflammation and coincided with up-regulation of sympathetic output (Barnes, et al., 2003; Chsnokova & Mlmed, 2002) and down-regulation of the parasympathetic pathway (Mashaly & Provencio, 2008). A combination of receptor independent as well as toll-like-receptor dependent effects of cytokines and chemokines are activated in response to increases in endoplasmic reticulum (ER) and oxidative stress in response to chronic

HFD. These changes possibly take place as adaptive responses to DIO-associated insults, however their persistent engagement is suggested to contribute to dysregulation of pulsatile relationships between neuroendocrine centers associated with metabolic regulation (Zhang, et al., 2013; Chsnokova & Mlmed, 2002; Berglund, et al., 2012; Xu, et al., 2010).

Characteristically, chronic administration of low dose TNF-α in the rodent brain was shown to induce insulin insensitivity and reduced thermogenesis (Romanatto, et al., 2007; Arruda, et al., 2011). Increases in IKKβ activity in the ARC in particular were suggested to be particularly detrimental, and down-regulation of IKKβ (Zhang, et al., 2008) and JNK (Belgardt, et al., 2010) using the nervous system-specific Nes-Cre promoter were protective against obesity and glucose intolerance. Indicative of a broader role in metabolic dysregulation, accumulation of NF-κB gene products in POMC neurons in earlier studies, promoted the cachectic effects of sickness response (Jang, et al., 2010; Challis, et al., 2004). Additionally, DIO-induced activation of the IKK-β-NF-κB signaling pathway was associated with depletion of hypothalamic stem cell population, suggesting that perhaps the dysfunction observed in DIO and T2D is a form of accelerated aging (McNay, et al., 2012; Mihaylova, et al., 2014).

Inflammatory signaling cascades are driven by the tissue- and context-specific expression of cytokines involved in both the initiation and resolution of the response in relation to the insult. DIO is suggested to promote the institution of a pro-inflammatory state and down-regulation of anti-inflammatory cytokines that promote its resolution. For example, the deficiency of the main anti-inflammatory cytokine Interleukin-10 in mice, exacerbates brain inflammatory responses to ischaemia without preventing lesion resolution (Perez-de Puig, et al., 2013). Cytokines exhibit particular pleiotropy and redundancy which relates to the expression of cytokine adaptor molecules in multiple cell lineages, as well as the shared signaling pathways by virtue of similarities between cytokine receptor motifs (Ozaki & Leonard, 2002). The precise contributions of cellular and molecular factors that participate in the hypothalamic cytokine signaling networks in the metabolic response to HFD could provide novel avenues for pharmacological treatment of metabolic disorders.

IL-6; a pleiotropic JAK/STAT of all trades

Interleukin-6 (MW=21-28kDa) is a cytokine of pleiotropic character involved in the regulation a milieu of immune, hematopoietic and metabolic processes. Initially characterized as B-cell stimulatory factor-2 in the 1960s, IL-6 is a glycosylated four-helical protein that was first successfully cloned in 1986 and described by Kishimoto and others (Kishimoto, 1987; Sehgal, et al., 1987). Work at the beginning of the 1990s identified the cytokine to be central in the mounting of the acute phase response of inflammation (Heinrich, et al., 1990), while the involvement of IL-6 in the transition from innate to acquired immunity, and protection against septic shock was also confirmed (Kopf, et al., 1994; Van Snick, 1990; Vink, et al., 1990).

A number of regulatory sequences have been shown to promote IL-6 production and secretion by through the IL-6 gene. Supershift analysis indicated the functional role of NF-κB, cAMP response element-binding protein (CREB), the nuclear factor for IL-6 (NF-IL-6) and the activator protein-1 (AP-1) in regulating IL-6 expression (Castell, et al., 1988; Wang, et al., 1995; Grassl, et al., 1999), while more recently a role for circadian gene products was also demonstrated (Sato, et al., 2014). Under resting conditions, NF-κB is found in the cytosol as a dimer of the p65 and p50 transcription factors, in association with IκB (Baeuerle & Baltimore, 1988). Stress and infection induce the phosphorylation of IκBα and IκBβ by IKKinase (Huxford, et al., 1998; Verma, et al., 1995), prompting their ubiquitination and degradation by proteasome 26S (Karin, 2000). Increased phosphorylation of the p65 NF-κB subunit allows for the dimer to move into the nucleus (Phelps, et al., 2000), where interactions with the p300/CREB-binding protein (Tang, et al., 2007), allow for binding at NF-κB sites resulting in the production of IL-6.

IL-6 Binding and Signaling

IL-6 mediates its signaling via binding with nanomolar affinity to its receptor (IL-6Rα), a four-helical protein of 184 amino acids. Three distinct binding sites allow the IL-6 receptor to propagate its specific signaling pathway via recruitment of the cytokine and binding to a gp130 dimer. Site 1, formed by the C-terminal residues of helix D and the C-terminus of the AB-loop determine the receptor's IL-6 specificity. Site 2 consists of intermediate portions of helices A and C, while site 3 consists of N-terminal residues of the AB loop and C-terminal residues in the D helix. (Fiers, et al., 1987; Rose-John, et al., 1990)

Binding of IL-6 to IL-6Rα does not directly lead to signaling. It is rather the formation of an IL-6/IL-6Rα complex that allows for association with gp130 protein, which dimerizes on binding and mediates intracellular signaling via JAK/STAT. This results in recruitment of JAK (Janus-activated Kinases) at proline-rich domains. Gp130-associated JAK kinases tyrosine-phosphorylate their cytoplasmic domains to enable phosphorylation-activation of STAT3 and STAT1 (less) (Hemmann, et al., 1996; Heinrich, et al., 1998). Activation of SH2 domain-containing tyrosine phosphatase allows for the induction of Mitogen-Activated Protein Kinase (MAPKs) (Muller, et al., 2001) and Phosphatidylinositide 3-Kinase (PI3K) pathways, an event of particular importance in both cancer (Birkenkamp, et al., 2000; Hideshima, et al., 2001) and cardiac physiology (Kodama, et al., 2000).

The STAT family of transcription factors encompasses 7 mammalian members (1-4, 5a, 5b, 6), but IL-6 cytokines have been shown to induce specific activation of STAT3 and to a lesser extent STAT1 through gp130.STAT3 binds to phosphorylated YxxQ motifs, while STAT1 requires phosphorylation of YXPQ receptor motifs (Garhatz, et al., 1996). Subsequently, STATs are phosphorylated on a single tyrosine residue (Y701 for STAT1, Y705 for STAT3), leading to the formation of active STAT dimer association at SH2 domains. Interestingly, in separate studies (Kim, et al., 2004) have also indicated the existence of non-phosphorylated as well as IL-6 activated-phosphorylated STAT3 and STAT3 pools in plasma membrane rafts.

Tyrosine phosphorylation of the gp130 receptor in the context of IL-6 signaling, has been also shown to recruit the mitogen-activated protein kinase (MAPK) and phosphatidylinositol 3-kinase (PI3-K) pathways via the JAK-mediated

phosphorylation of SHP2 (SH2-domain-containing tyrosine phosphatase) site Tyr^{759} (Stahl, et al., 1995; Zhang, et al., 2002). The subsequent SHP2-dependent activation is the consequence of interactions of the SHP2 Tyr^{542} and Tyr^{580} C-terminal domains with the Grb2-SOS (growth factor-receptor-bound protein/Son of Sevenless) complex (Schaper, et al., 1998). Further complexity is provided to this mode of signaling by the tyrosine phosphorylation of Gab1, a scaffolding protein that is targeted via pleckstrin-homology (PH) to the plasma membrane (Takahashi-Tezuka, et al., 1998). Gab1 contains binding sites for Grb2, SHP2, PI-3K, Crk, phospholipase Cγ and the c-Met receptor (Schaeper, et al., 2000).

IL-6 signaling is associated with cell survival and proliferation via the combination of the mitogenic effects of the ERK/MAPK pathway and the anti-apoptotic effects of STAT3 phosphorylation (Takahashi-Tezuka, et al., 1998; Fukada, et al., 1996). Up-regulation of *Bcl-2* via *Stat3* and the inhibition of cell cycle inhibitor p27 via ERK1/MAPK signaling, are recognized as instrumental to ischaemia/reperfusion injury consolidation in cardiac myocytes (Stephanou, 2004) and more recently demonstrated neuroprotective effects of IL-6 to NDMA-induced excitotoxicity (Wang, et al., 2009). The effects of IL-6 signaling on the MAPK signaling cascade are not limited to survival, but extend to stress-activated JNK and p38 MAPK activity (Bode, et al., 2001; Zauberman, et al., 1999), promoting elements of cytokine signaling feedback inhibition.

Activation of gp130 and more specifically the recruitment of PI3-K pathway via the hydrophobic core of the SH2 domain Tyr^{657}, has been suggested to regulate cardiac myocyte survival in doxorubicin-induced apoptosis through facilitating the function of Bcl-xL (Negoro, et al., 2001). Interestingly, more recent work has suggested phosphorylation of PKB via SHP2 in the context of *classical* IL-6 signal transduction to be sufficient to induce cardioprotection in rat myocytes, in the absence of JAK/STAT activation (Fahmi, et al., 2013). Earlier work suggested *Hyper*-IL-6 signaling (described in subsequent section) to promote liver regeneration (Peters, et al., 2000), while more recently IL-6/STAT3-mediated proliferation and PI-3K-mediated cell growth, have been described as pivotal in the treatment of liver dysfunction and disease (Fujiyoshi & Ozaki, 2011; Nechemia-Arbely, et al., 2011).

Figure 1.1.2: Schematic representation of the molecular pathway involved in IL-6 signal transduction:

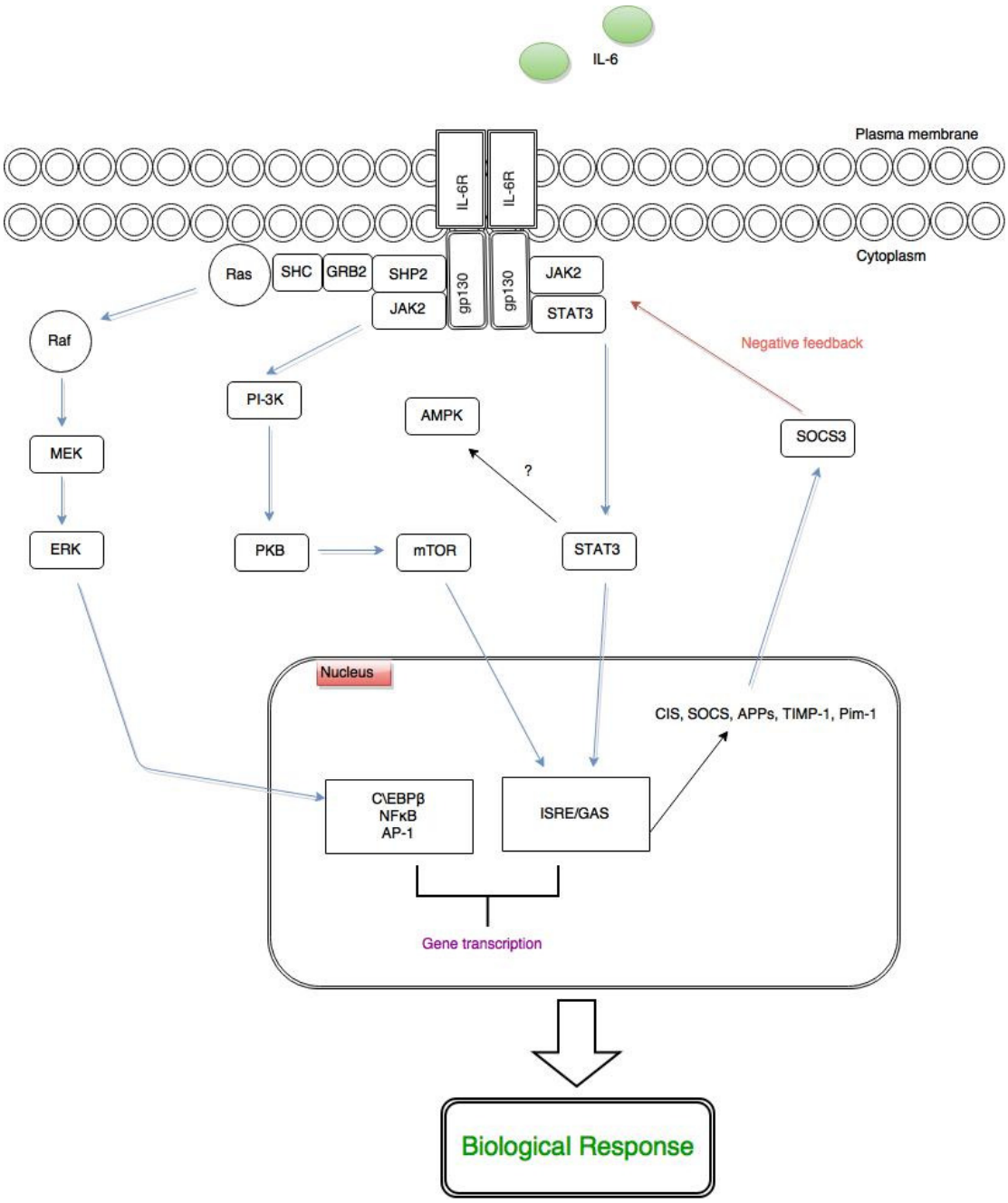

On the other hand IL-6/PI3-K signaling is particularly prominent in certain forms of cancer, and was demonstrated to be crucially involved in up-regulation of anti-apoptotic Mcl-1 in basal cell carcinoma cells (Kuo, et al., 2001). Interactions of the PI3-K arm of IL-6 signaling in particular with androgen signaling has been suggested to be detrimental to the advancement of prostate cancer (Xie, et al., 2004) and to

regulate cancer growth (Culig, et al., 2002; Culig, et al., 2005) and survival (Wegiel, et al., 2008).

IL-6 has been also observed to transiently phosphorylate AMP-activated Kinase (AMPK), a signaling event first speculated by experiments investigating the activity of AMPK in the context of exercise-induced IL-6 release (MacDonald, et al., 1987); and was later underlined by the effects of IL-6 KO on exercise in mice (Kelly, et al., 2004). A recent review of IL-6 signaling pathways, suggested AMPK phosphorylation to occur via STAT3 (Sarvas, et al., 2013), while the current dogma suggests IL-6 mediated increases in cAMP and the AMP: ATP ratio to underlie AMPK phosphorylation (Kelly, et al., 2004).

SOCS-3 is the primary direct negative feedback regulator of IL-6 signaling (Niemand, et al., 2003; Alexander & Hilton, 2004). It is a member of the *suppressor of cytokine signaling* family of 8 related proteins (CIS and SOCS-1 to 7), induced in response to activation of STAT proteins, but is known to be most potently induced by IL-10 independently of STAT (Cassatella, et al., 1999). SOCS-3 has been extensively characterized to specifically act towards termination of gp130 and Ob-Rb signaling in a variety of tissue (Croker, et al., 2003; Mori, et al., 2004; Yasukawa, et al., 2003). More recent *in vivo* mouse studies where the SOCS-3 gene was conditionally deleted (Croker, et al., 2012); confirmed the role of the protein in IL-6 response regulation as well as its requirement for survival during inflammatory responses.

Glucagon was demonstrated to act independently of de novo protein synthesis to inhibit IL-6 mediated gene expression in a pituitary adrenocorticotropic hormone (ACTH)-secreting cell line (Bousquet, et al., 2000), as well as more recently, in hepatocytes (Khouri, et al., 2011). Increases in activated adenylyl cyclase-induced calcium flux (and/or potentially PKC) (Tian & Laychock, 2001), can thus act to promote the induction of SOCS-3 as an additional means of cytokine signaling regulation.

Soluble and Membrane-bound IL-6 Signaling

As mentioned, the ubiquitously expressed gp130 protein has no measurable affinity for IL-6 or its receptor outside the spectrum of their complex (IL-6Rα/IL-6) (Taga, et al., 1989). A soluble form of the receptor exists, catalyzed by ADAM (A Desintegrin and Metalloprotease) 10 & 17-mediated proteomic cleavage in mice and by both proteomic cleave and/or alternative mRNA splicing in humans (Croucher, et al., 1999).

Figure 1.1.3: Schematic representation of Classical and Trans-signaling mechanism

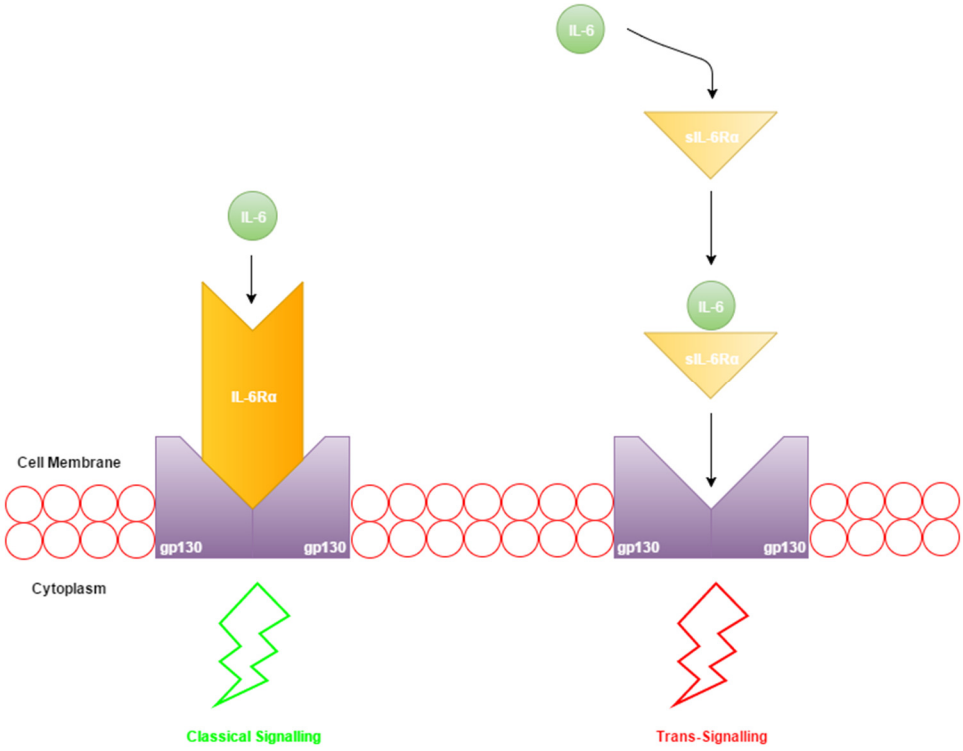

Rapid cleavage and generation of the sIL-6Rα have been associated with the activation and proteomic cleavage by ADAM17 in response to TNF-α, IL-1β and certain bacterial toxins. On the other hand ADAM10 has been found to participate in the constitutive, slow shedding of the receptor under basal or un-stimulated conditions. (Marin, et al., 2002; Matthews, et al., 2003). The soluble form of the receptor binds to gp130 with similar affinity to the membrane bound isoform. The ubiquitous expression of gp130 renders all cell moieties IL-6-responsive and allows, in part, for the endocrine, paracrine and autocrine function of the cytokine (Jones, et al., 2001).

The influence of IL-6 on major body processes and the neuroendocrine regulation of metabolism

IL-6 signaling has been recognized to modulate a vast array of events in different target tissues. The ubiquitous expression of the gp130 adaptor molecule; the release of the soluble form of the receptor from immune cells and of IL-6 from key homeostatic regulators, provide the framework through which IL-6 signaling co-ordinates activity in a spectrum of settings and cell types. Release of inflammatory mediators such as IL-6 from adipose tissue in the face of DIO contributes to the emergence of pathology however the mechanisms through which adipose inflammation contributes to disorders of glucose homeostasis remain incompletely understood (Galic, et al., 2010; Virtue & Vidal-Puig, 2010; Lontchi-Yimagou, et al., 2013; Richardson, et al., 2013). Exposure to hyperinsulinaemia in humans increases IL-6 expression (Kroqu-Madsen, et al., 2004) and release from tissue (Mohamed-Ali, et al., 1997). More recently, metabolic inflammation at level of the hypothalamus, has been suggested to be key to the development of DIO and the progression to T2D and the role of individual components of cytokine signaling is still being heavily investigated (Zhang, et al., 2008; Wang, et al., 2010).

In early studies in mice over-expressing interleukin-6 and the soluble receptor gene, a dramatic increase in hematopoietic progenitor cells at the liver and spleen was observed (Peters, et al., 1997). However, other aspects of the phenotype included visibly absent fat pads and significantly smaller stature, an effect that albeit not apparent in the single transgenic over-expressing sIL-6Rα mice spurred considerable interest on the metabolic implications of IL-6 signaling. In accord with other studies by Hotamisligil et al. who first reported a role for adipose-derived TNF-α in the development of DIO and T2D, these early studies encouraged speculation of the role of IL-6 in metabolism (Ling, et al., 2004; Bastard, et al., 2000).

In the absence of inflammation, the cytokine exhibits a prominent role in hematopoiesis (Otsuka, et al., 1994; Laharrague, et al., 2000) and is released from adipocytes (Coppak, 2001), myocytes (Loppnow & Libby, 1990; Neumann, et al., 1995; Pedersen, et al., 1998) as well as endothelia (Hedges, et al., 1992; Kishikawa, et al., 2002) in various concentrations in response to an array of stimuli. The growing interest in the role of the cytokine in metabolism resulted a number of studies that benefited from the use IL-6 deficient mice, and further supported the role of the

cytokine in promoting the action of insulin (Wunderlich, et al., 2010; Matthews, et al., 2010). More recent evidence suggests the action of IL-6 in the hypothalamus to mediate decreases in food intake and body weight as well as increases in leptin and insulin sensitivity (Flores, et al., 2006; Ropelle, et al., 2010; Shirazi, et al., 2013; Schele, et al., 2013).

The hypothalamus is a brain region that acts as the interface between the nervous and endocrine systems, orchestrating the activation of the hypothalamic-pituitary-adrenal and –thyroid axis, which act towards the maintenance of homeostasis in physiology and disease (Tsigos & Chrousos, 2002; Engelmann, et al., 2004). Distinct hypothalamic nuclei have been found to play integral role in the regulation of feeding behavior, satiety and energy expenditure (Williams, et al., 2001). The Jansson group (University of Gothenburg) recently published studies where IL-6 receptor localization in the human and mouse hypothalamus was characterized using fluorescent immunohistochemistry, indicating the medial hypothalamus to be the region exhibiting the highest expression (Schele, et al., 2012). IL-6Rα-positive neurons were identified in several areas of the mouse hypothalamus involved in the regulation of homeostasis regulation, body composition and energy expenditure. Receptor immunoreactivity was identified in the ARC, VMH, PVN, DMN and LH in close proximity to NPY positive fibres.

IL-6 is thought as an important dynamic regulator of physiology and disease, through local and systemic effects that have not been fully characterized *in vivo* (Mauer, et al., 2014; Wolf, et al., 2014). We were thus encouraged to examine role of central IL-6 signaling in the development of metabolic dysregulation in response to DIO and towards this, a tissue-specific IL-6Rα knock-down transgenic was generated. Interpretation of the phenotype observed during these studies using this transgenic could only be attempted in the context of the wide range of biological activity displayed by IL-6, which we summarize in this section.

Hematopoiesis

In mammalian systems, hematopoietic stem cells in bone marrow, give rise to all lineages of blood as well as immune cells. Bone marrow is found in the medullary cavities of skeletal bones, and is home to a dense network of medullary vascular sinuses. Hematopoietic stem cells and their progenitors are packed in the microenvironment (or niches) within bone marrow, and regulate bone formation. Early work indicated IL-6 to contribute to the proliferative capacity of bone-forming osteoblasts *in vitro* (Taichman & Emerson, 1994), as well as the formation of multi-lineage blast cell colonies and stem cells (Bernad, et al., 1994). Consistent with this, over-expression of the cytokine in rodents, augments the hematopoietic potential of animals, increasing progenitors in various tissues (Peters, et al., 1997).

The fate of stem cells of the hematopoietic system are known to be influenced by specialized inflammatory micro-environments and was initially thought to be regulated by parathyroid hormone (PTH) thought activation of Notch signaling (Calvi, et al., 2003). The critical role of IL-6 signaling in promoting PTH-mediated increases in osteoblasts were initially demonstrated in culture, while increases in hematopoietic progenitor cells observed in PTH-treated control animals were abolished in IL-6-deficient animals (Pirih, et al., 2010).

More recently, the interdependence of IL-6 and PTH mediated hematopoietic cell expansion was shown to involve the combined effects of *classical* and *trans*-signaling (Cho, et al., 2013). Absence of PTH-mediated hematopoietic cell expansion observed in IL-$6^{-/-}$ marrow cultures, was found to be restored by sIL-6Rα treatment. sIL-6Rα treatment did not induce any increases in osteoblast proliferation or differentiation *in vitro*, but was found to contribute to the anabolic actions of PTH by supporting $CD11b^{+}Gr\text{-}1^{+}$ cells and macrophages ($F4/80^{+}$) of the hematopoietic system. In other studies involving the use of IL-6 and IL-6 receptor deficient mice, the modulatory role of IL-6 signaling in wound healing, which is a measure of the ability of the hematopoietic system to generate new stem cells was demonstrated (McFarland-Mancini, et al., 2010).

Immune Regulation

Cytokines such as IL-6 are produced in response to perturbations of homeostasis, such as endotoxaemia, endotoxic lung, trauma as well as acute infections (Kishimoto, et al., 1992; Zitnik & Elias, 1993). IL-6 release from monocytes was first described to stimulate thymocytes and T lymphocytes almost 30 years ago now (Lotz, et al., 1988), an event that is dependent on monocyte depletion, indicative of the regulatory role of the cytokine in cell immunity. Up-regulation of TNF-α, IL-1β and IL-6 are required for the induction of the acute phase response, which includes fever, corticosterone release, and hepatic production of acute phase proteins (Baumann & Gauldie, 1993). Macrophages and lymphocytes, as well as endothelia activate NFκB signaling cascades culminating in the release cytokines such as IL-6 into circulation in response to exogenous stimuli and/or stress (Nguyen & Benveniste, 2002). This subsequently promotes the production of pro-inflammatory Th17 cells and eventually the mounting of the acute phase response (Castell, et al., 1988; Mackiewicz & Kushner, 1989; Wang, et al., 1995).

Lipopolysaccharide (LPS) is a vital component of bacterial cell membranes and known to induce the synthesis of pro-inflammatory cytokines IL-1, IL-6 and TNFα in both the periphery, as well as various parts of the brain in the presence of a stressor or infection (Besendovsky & Del Rey, 1996; Romero, et al., 1993). P38 MAPK was first recognized to be involved in regulation of pro-inflammatory cytokine biosynthesis in response to various stress stimuli (Lee, et al., 1994; Beyaert, et al., 1996); but is also believed to be involved in the feed-forward action of cytokines**.** In accordance with the early idea of overlapping cytokine networks (Akira, et al., 1990), Patil et al. (2004) have shown that inhibition of p38 activity by SB203580 reduces IL-1β-induced increases in IL-6 synthesis and mRNA stability. In further support, SB203580 treatment in mice and rats was found to reduce circulating IL-6 and TNFα in the context of both acute and chronic inflammation (Badger, et al., 1996; Zhou, et al., 2014).

IL-6 thus participates in the network of cytokines involved in mounting of the acute phase response, a system that exhibits particular redundancy in its relationships (Koj, 1985). However, IL-6 signaling is a requirement at the level of the liver in particular, and effective response to trauma or infection is thought to be dependent on the presence of IL-6 (Kopf, et al., 1994). This was re-emphasized in more recent work

using mouse models of bacterial infection, where IL-6$^{-/-}$ mice experienced increased neutrophilia on the one hand, but more importantly reduced bacterial clearance. Re-constitution of the sIL-6R system in IL-6$^{-/-}$ mice, improved mortality rate though ameliorating these effects (Onogawa, 2005) in agreement with the protective role of the cytokine in the development of septic shock (Diao & Kohanawa, 2005; Barton & Jackson, 1993).

Acute-phase induced apoptosis promotes IL-6Rα shedding through caspase-dependent but PKC-, MAPK- and ROS- independent mechanisms (Chalaris, et al., 2007). Rapid cleavage and generation of the sIL-6Rα are regulated by the proteomic cleavage action of ADAM10 and ADAM17. TNFα and IL-1β, as well as certain bacterial toxins, are known inducers of ADAM17 metalloproteinase activity (Marin, et al., 2002; Matthews, et al., 2003). Inhibition of ADAM17 during apoptosis by small pharmacological molecules or the expression of dominant negative ADAM17 variant resulted in inhibition of shedding from the neutrophils of mice subjected to the air pouch model of acute inflammation (Koenen, et al., 2009). sIL-6Rα/IL-6 complexes formed during apoptosis are biologically active and found to trans-signal in non-apoptotic cells examined (Rose-John, 2012; Rose-John, et al., 2007).

Shedding of the IL-6Ra during acute phase-mediated neutrophil apoptosis, directs IL-6 *trans-signaling* on endothelia. Although this event is acutely detrimental to endothelia, it primes the secretion of chemokines, it was found to be a requirement for the recruitment of monocellular phagocytic cells towards inflammation resolution (Rose-John, 2012; Rose-John, et al., 2006). Blockade of sIL-6Rα binding onto IL-6 by a soluble-gp130 analogue (sgp130Fc) resulted in normalization of the neutrophil influx observed upon stimulation, however the subsequent recruitment of monocytes was severely impaired (Rose-John, 2012; Rose-John, et al., 2007).

Monocytes are primary immune regulators of the acute phase of inflammation (Lotz, et al., 1988). They replace T cells in the 24-48hour period following initial infiltration, in order to protect tissue from local over-accumulation of neutrophils. Using IL-6 deficient mice, early studies were able to demonstrate that circulating IL-6 participates in the regulation of cytokine levels during this event *in* vivo. Transgenic mice experienced augmented pro-inflammatory responses to endotoxaemia, underlining the anti-inflammatory nature of IL-6 (Xing, et al., 1998), independently of

the main anti-inflammatory mediator IL-10 (de Vries, 1995). Monocytes are currently understood to utilize the combined action of IL-6 and TGF-β, which inhibits the conversion of nTregs to Th17 as part of negative feedback mechanisms to the initial pro-inflammatory response (Gao, et al., 2012). Their synergy along with a down-regulation of the IL-6Rα, underlie the production of not only helper cells characterized by the production of IL-17, TNF-α and IL-6 itself, but also the induction FOXP3+ and the differentiation of iTregs, responsible for the transition to inflammation resolution (Gao, et al., 2012).

In acquired immunity development, the successful transition from the acute to the resolving phase, is accompanied by leukocyte recruitment (Hoebe, et al., 1995). This involves an initial influx of neutrophils, which is followed by their replacement with more sustained mononuclear cell populations (McLoughlin, et al., 2003; Topley, et al., 1996). IL-6 cytokine governs T-cell activity and defines not only the pattern of monocyte differentiation, but also the direction of dendritic cell maturation (Jones, 2005). During the resolving phase, IL-6 suppresses CXCL1, CX3CL1 and CXCL8, while it promotes CXCL5 and CXCL6 release among other monocyte-attracting chemokines. The action of IL-6 and the expression IL-1 (Gabay, et al., 1997) and TNF-α receptor antagonists result in the induction of neutrophil apoptosis and leukocyte transmigration (Romano, et al., 1997; Hurst, et al., 2001; Kaplanski, et al., 2003). The interaction of IL-6 signaling and trans-signaling along with other cytokine cascades are central to determining aspects of both the immediate response to stress and constitutes a priming event to a similar future insult (Gao, et al., 2012; Scheller, et al., 2011). Collectively, it appears that in the experience of a non-specific stress insults; the induction of *trans-signaling* in the presence of the stimulus acts to promote the action of *classical* signaling and the expression of anti-apoptotic genes in the recovery period.

Liver Acute Phase Response and Metabolism

Acute Phase Response:

The role of IL-6 in the induction of the acute phase response at the liver have been the subject of considerable research. Serum IL-6 increases proportionately to systemic inflammation under regulation of a cytokine network involving TNF-α, IL-1 and IL-6 (Fournier, et al., 2000). For example, chronic hepatitis B virus (HBV) infection, is associated with up-regulation of IL-6 expression through NFκB by the hepatitis B virus X-protein in particular, which induces CRP and other acute-phase proteins from the liver in humans (Lee, et al., 1998; Zhu & Paddock, 1999; Schaper, et al., 1997). Chronic liver disease was demonstrated to be associated with increases in serum IL-6 and sIL-6Rα that drive increases in the major acute phase protein α1-Acid glycoprotein (AG) (Heinrich, et al., 1998; Hirano, 1998).

On the other hand, the naturally occurring negative feedback regulator of IL-6 *trans-signaling*, sgp130 was found to be significantly elevated in cirrhosis patients and exhibited correlation with various important biomarkers of the disease (Migita, et al., 2006). Serum IL-6 and soluble receptor levels are thus important regulators of both liver function and degree of impairment in chronic liver disease. In other studies where hepatectomy was used to evaluate the role of IL-6 signaling in liver function, IL-6 deficient mice showed impaired regeneration compared to controls (Blindenbacher, et al., 2003; Ling, et al., 2002). In line with the above, experiments with IL-6 transgenic and IL-6/sIL-6Rα double transgenic mice, signified the need for the combination of classical IL-6 and *trans-signaling*, for efficient hepatocellular proliferation following injury. The use of the inhibitor of *trans-signaling* sgp130Fc inhibited hepatocellular proliferation following chemically induced damage and specific blockade of *classical* signaling reduced concavalin A-induced liver damage (Scheller J. et al. 2011). The cytokine is thus central to the induction of the acute phase response at the liver and instrumental to the beneficial effects of inflammation in the recovery period.

Metabolic regulation:

High fat feeding is associated with increases in adipose-derived IL-6, and was demonstrated to promote liver insulin resistance through inhibition of the insulin receptor substrate IRS-1 (Sabio, et al., 2008), by promoting increases in pJNK and SOCS-3, as well as NF-κB-IKK-β (Cai, et al., 2005). However, hepatocyte-specific disruption of the IL-6Rα was shown to induce hepatic inflammation and glucose intolerance (Wunderlich, et al., 2010; Ouchi, et al., 2011). Thorough studies in IL-6 deficient mice indicated enhanced weight gain and the development of hepatic inflammation and steatosis upon genetic disruption of the cytokine (Matthews, et al., 2010). It is currently thought that adipose-derived IL-6 contributes to insulin resistance, whereas muscle-derived IL-6 is thought to promote it through the inhibition of gluconeogenic pathways.

Insulin resistance and dyslipidaemia observed in DIO and diabetes, induce a pathophysiological increase in glucagon release (Vons, et al., 1991; Reaven, et al., 1987; Larsson & Ahren, 2000). Elevated glucagon to insulin ratio at the liver both drives the persistence of insulin resistance and leads to hyperglycaemia (Eledrisi, et al., 2006).

Glucose-6-Phosphatase (G6Pase) is a metabolic enzyme involved in the final step of the gluconeogenic pathway, converting Fructose-6-phosphate to glucose. Liver IL-6 signaling has been suggested to inhibit gluconeogenesis through reduction of Glucose 6-Phosphatase (G6Pase) and glycogen levels (Metzger, et al., 1997), and more recently, the anti-gluconeogenic effects of IL-6 through inhibition of G6Pase was demonstrated in primary hepatocytes (Christ, et al., 2000; Inoue & al, 2004) and corroborated *in vivo.* Phosphorylation of liver STAT3 during euglycaemic-hyperinsulinaemic clamps was shown to promote insulin sensitivity by inhibiting liver Glycogen Synthase Kinase-3 (GSK-3) protein and mRNA (Inoue, et al., 2006; Moh, et al., 2008). In conjunction with previous studies using neuronal-specific insulin receptor KO mice (Bruning, et al., 2000), the role for IL-6 in the brain-liver axis being heavily investigated, however it is still not clear whether the cytokine is the primary driver of the induction of pSTAT3 *in vivo* (Mauer, et al., 2014).

Exercise and the Working Muscle

It is now widely understood that upon exercise-mediated muscle contraction, the stimulation of cytokine production is also induced, as a means of enhancing the delivery of substrate to the working tissue (Pedersen & Hojman, 2012). Northoff and Berg (1991) first reported IL-6 to be acutely up-regulated in human plasma in response to exercise, while Bruunsgaard et al. (1997) initially speculated the production of the cytokine to involve the action of leukocytes in response to exercise-induced local damage at the level of the working muscle (Northoff & Berg, 1991; Bruunsgaard, et al., 1997).

Eccentric exercise was shown to be a strong inducer of IL-6 release from muscle (Smith, 1991) and Ostrowski et al. (1998) concluded this to be dependent on duration and intensity of exercise activity. However the precise origins of IL-6 were not demonstrated and initial evidence suggested found both prolonged running and 2 hours of concentric exercise to be unable to induce IL-6 release from blood monocytes (Starkie, et al., 2000). Around the same time, (Pedersen, et al., 2001) had suggested IL-6 as a myokine whose concentrations in plasma increase dramatically in response to intense exercise (e.g. rowing), in many cases much higher than in obesity and diabetes. Increases observed, though significant compared to lean subjects (2-3fold) are nowhere near proportional to the levels previously reported in the context of exercise, where IL-6 increases up to 100-fold depending on the duration and intensity of exercise (Ostrowski, et al., 1998).

Along those lines, IL-6 infusion during exercise, was shown to increase the ability of the system to dispose glucose, while the appearance of IL-1 receptor antagonist and IL-10 in circulation prompted to anti-inflammatory signaling cascade activation; further confirming the existence of cytokine cascades (Febbraio & Pedersen, 2002). Shortly after, (Petersen & Pedersen, 2005) showed that IL-6 is the first cytokine to appear in circulation following the post-exercise period, increasing 100-fold from baseline levels, revealing that skeletal muscle harbors IL-6 gene and protein expression.

Contrasting the findings by Starkie et al. (2000) recent work by Reihmane, et al., suggests that maximal exercise induces the release of myeoloperoxidase which correlates with IL-6 increases in serum (Reihmane, et al., 2013). This was also

verified by the Starkie group, that concluded exercise-induced IL-6 release can only be partly attributed to neutrophils; (Starkie, et al., 2003; Starkie, et al., 2001) as eccentric and concentric muscle exercise normalized for individual lactate thresholds, was found to elicit similar IL-6 plasma responses. It is thus now understood that eccentric and maximal (Chaar, et al., 2011) exercise-induced plasma increases in IL-6 are not accompanied by increases in adhesion molecules that would implicate leukocytes.

The precise intracellular mechanisms underlying contraction-induced IL-6 release from myocytes was also the subject of considerable research. Individual values of activated AMPK correlated with IL-6 release after 60 minutes of cycling exercise in the glycogen-depleted state, suggestive of a link between AMPK activity, plasma IL-6 release and carbohydrate availability (MacDonald, et al., 1987). Some 20 years later, IL-6 has been suggested to activate AMPK in skeletal muscle by increasing intracellular cAMP and the AMP: ATP ratio (Kelly, et al., 2004), while AMPK-dependent pathways (Glund & Krook, 2008) have been confirmed to influence IL-6 release from isolated oxidative skeletal muscle.

Research work failed to identify an association either between carbohydrate ingestion and skeletal muscle AMPK signaling (Lee-Young & al, 2006); or glycogen levels and IL-6Rα gene expression (Keller, et al., 2005a) even though IL-6 release appeared to be affected by carbohydrate bioavailability. Despite this, IL-$6^{-/-}$ mice were indeed found to experience significantly diminished AMPK activity in both muscle (-75%) and adipose (-50%) tissue, an effect that was accompanied by dyslipidaemia, insulin & leptin resistance, glucose intolerance and mature-onset obesity (Wallenius, et al., 2002). Activation of AMPK by IL-6 signaling appears to contribute to the maintenance of the required kinase activity for effective management of metabolism over time, a notion that was further supported by Kelly M. et al. (2004) using IL-6 KO mouse, that displayed diminished AMPK activity even at rest, in both muscle and adipose tissue.

Interestingly it was recently demonstrated that exercise has ATP-sensitizing effects on muscle, that allow for Ca^{2+} dependent IL-6 release and the establishment of a cytokine autocrine loop through activation of JNK and p38 MAPK signaling (Fernandez-Verdejo, et al., 2014; Bustamante, et al., 2014; Spangenburg, et al., 2006). This would

explain the lack of direct correlation to carbohydrate bioavailability, in agreement with the regulatory role of the purinergic system on cytokine signaling (Gabel, 2007; Noma, et al., 2013). The release of IL-6 from muscle tissue, would appear to contribute the insulin-sensitizing effects of exercise at the level of the liver (Matthews, et al., 2010; Kraakman, et al., 2013), possibly through the expression of protective chemokines (Pedersen, et al., 2011).

Effects on the Pancreatic Islet Cells and Insulin Secretion

Dysregulation of the insulin signaling is one of the characteristic features of DIO and T2D. Chronic exposure to hyperglycaemia, hyperlipidaemia, ER and oxidative stress directly contribute to β cell dysfunction and promote insulin resistance (Unger, 1995; Kahn & Flier, 2000; Maedler, et al., 2002). T2D patients experience impaired insulin-stimulated glucose uptake in muscle (Cusi, et al., 2000) and adipose tissue (Yki-Jarvinen, 2002), while the inhibition of glucose output from the liver is also disrupted (Nakatani, et al., 2004). Under physiological conditions, hyperglycaemia promotes rapid release of insulin from the β cell, followed by a more moderate K_{ATP} channel-independent release that follows.

Beta cell insulin release into portal circulation in response to glucose is done under the maintenance of an intrinsic rhythm of intracellular Ca^{2+} and K^{+} oscillations (Del Prato, et al., 2002; Menge, et al., 2011). Upon successful binding to the insulin receptor and appropriate recruitment of Insulin Receptor Substrate-1 (IRS-1), rapid tyrosine phosphorylation of insulin receptor complexes as well as downstream mediators of insulin signaling, culminate in activation of Protein Kinase B (Akt), pSTAT3, Forkhead box O1 (FoXO1) protein is achieved in target tissues (Alessi, et al., 1997; Alessi, 2001; Brazil & Hemmings, 2001; Matsuzaki, et al., 2003; Campos, et al., 1996). Insulin receptor activation in muscle and fat promotes glucose up-take through the recruitment of GLUT4 transporters to the membrane via the activation of small GTP-binding protein TC10 (Saltiel & Kahn, 2001; Chiang, et al., 2001). This is thought to involve pPKB-mediate inhibition of Rab-GDP interactions, promoting GLUT4 translocation to the membrane (Miinea, et al., 2005; Elmendorf & Pessin, 1999; Zeigerer, et al., 2004).

Islets, are indeed able to release insulin in isolation, however the integration of the influence of diffusible factors and cell-to-cell interactions is required for pancreatic insulin release *in vivo* (Schofield & Sutherland, 2012; Song, et al., 2000; Porksen, et al., 1996; Butler, et al., 2003). In type 2 diabetes, the number and mass of β-cells is reduced, while and the pulsatility of insulin release in disrupted (Hellman, 2009). This results in elevated secretion of insulin at baseline, which contributes to the development of hepatic insulin resistance. Research work during the 1990s yielded conflicting results with regards to the effect of IL-6 on pancreatic β cell insulin secretion. Some studies suggested IL-6 to suppress β cell GSIS (Sandler, et al., 1990; Southern, et al., 1990) and others towards the end of the decade suggested enhanced GSIS (Shimizou, et al., 2000). In subsequent work where freshly isolated islets were pre-incubated with IL-6, significant increases in β cell viability were observed in response to pro-apoptotic insults (IL-1β, TNF-α, IFN-γ), while impairment of insulin secretion was suppressed (Choi, et al., 2004). The sensitizing effects of IL-6 on β cell insulin secretion were then corroborated in transgenic mice over-expressing IL-6 in muscle cells (Franckhauser, et al., 2008). Chronic elevations in IL-6 promoted hyperinsulinaemia and reduced body weight, even though glucose-stimulated insulin secretion was disrupted and liver inflammation was markedly increased.

More recently, evidence presented by the Donath group (University Hospital Basel) in particular ,confirmed expression of the IL-6Rα in pancreatic islets and demonstrated IL-6 to stimulate β cell insulin secretion and increase pancreatic α cell mass (Ellingsgaard, et al., 2011; Ellingsgaard, et al., 2008). The beneficial effects of exercise-induced contracting muscle-derived IL-6, were intriguingly suggested to be the consequence of increases in GLP-1 secretion from L cells in the intestine and α-cells in the pancreas.

Glucagon-like peptide 1 (GLP-1) is produced in the intestine and brain in during prandial periods as well as in response to exercise (Donath & Burcellin, 2013). It is known to stimulate exercise anorexia and insulin secretion from the pancreas (Donath & Burcellin, 2013). GLP-1 receptor agonists that have currently been proven beneficial towards food intake and body weight regulation. Central IL-6 signaling was recently demonstrated to play a role in mediating the effects of such agonists (Shirazi, et al., 2013). IL-6 was found to be massively (11x) up-regulated in the hypothalamus in response to GLP-1 receptor agonism, while inhibition of IL-6 biological activity

resulted in attenuation of the effects of the analogue on food intake. IL-6 would thus appear to promote the action of insulin via its effects involving both the brain as well as the periphery.

Effects on Adipose Tissue

The role adipose tissue as an endocrine organ (Zhang, et al., 1994) and the accumulation of inflammatory signaling at this site in the development of diabetic disease have been extensively studied in the past 20 years (Aguilar-Valles, et al., 2015; Trayhurn & Wood, 2004; Guilherme, et al., 2008; Hotamisligil, et al., 1993; Kern, et al., 2001). In the absence of an immune response, IL-6 is largely derived from white adipose tissue and circulating cytokine levels have indeed been shown to correlate with adipose tissue mass as well as long- and short-term changes to food intake (Bastard, et al., 2000; Orban, et al., 1999), and serum IL-6 is increased in obese individuals and decreases with weight loss (Kopp, et al., 2003).

Infusion of recombinant human IL-6 into healthy humans was initially shown to increase lipolysis (Van Hall, et al., 2003) through pSTAT3, but not pAMPK-mediated effects (Wolsk, et al., 2010). However its central administration in experimental mice, was demonstrated to induce acute increases in energy expenditure, suppress food intake acutely, and to reduce fat mass more effectively than peripheral administration (Rothwell, et al., 1991; Plata-Salaman, 1996; Wallenius, et al., 2002). Furthermore, IL-6 over-expression in the brain potentiated the action of leptin in promoting energy expenditure through fat oxidation (Lnczowski, et al., 1999; Spiegelman & Flier, 2001).

Up-regulation of IL-6 in adipose tissue can thus be viewed a component of the physiological response to counter exposure to HFD, acting towards increasing energy expenditure and reducing food intake (Cao, 2014). Increased macrophage infiltration into adipose tissue in the context of DIO and diabetes, was previously suggested to be concomitant with hypothalamic inflammation, preceding dramatic increases in adiposity and promoting the establishment of insulin resistance (Xu, 2003; Wellen, 2003). White adipose tissue (WAT) - infiltrating macrophages are characterized by increased expression of TNF-α, IL-6 and iNOS, glycolytic metabolism and dendritic-like morphology; effectively shifting form an anti-inflammatory towards a pro-

inflammatory phenotype (Murray & Wynn, 2011). Alternatively activated, M2 macrophages on the other hand promote tissue homeostasis through the release of IL-10 and TGF-β and their reliance on β-oxidation as opposed to glycolysis (Lang, et al., 2002; Murray & Wynn, 2011). Classification of M1 and M2 macrophages relates to their activation cascade. IFN-γ, IL-1β (Th1-cytokines) and microbial products polarize M1 macrophages, while IL-4 and IL-13 (Th2-cytokines) polarize anti-inflammatory M2 macrophages (Gordon & F.O., 2010). Given the prominent role of IL-6 *trans-signaling* in promoting M1 polarization, the effect of its specific blockade was evaluated in mice. Unfortunately, blocking *trans-signaling* does prevent macrophage infiltration in adipose tissue, but failed to inhibit the establishment of insulin resistance in HF-fed animals (Kraakman, et al., 2015).

This phenotype might again, relate to the multifaceted nature of IL-6 signaling. Besides its *de facto* pro-inflammatory role in WAT, IL-6 has been suggested to act alike IL-10 to induce IL-4 Receptor α chain (IL-4Rα) expression in macrophages, polarizing the IL-4/STAT6 anti-inflammatory axis (Herbert, et al., 2004; Vats, et al., 2006). It was recently demonstrated that in mice bearing myeloid-specific IL-6Rα inactivation, experience increased inflammation and a shift in macrophage polarization towards M1, resistance to IL-4 mediated alternative polarization and enhanced insulin resistance (Mauer, et al., 2014). The sensitizing effect of IL-6 on this axis, might be particularly important in the context of obesity where anti-inflammatory processes are disrupted (Wu, et al., 2011) and might explain the phenotype observed in studies by Kraakman et al.

Earlier work suggested IL-6 to act in the brain and to drive increases in energy expenditure and thermogenesis (Lnczowski, et al., 1999; Spiegelman & Flier, 2001). Chronic central administration of recombinant IL-6 in rats was shown to induce thermogenesis in innervated brown adipose tissue (BAT) through the induction of Uncoupling protein 1 (UCP1) (Li, et al., 2002). UCP1 expression involves the action of transcription factors (Kelly, et al., 1998; Puiserver, et al., 1998) such as peroxisome proliferator activated receptor γ (PPARγ) and the PPARγ co-activator-1α (PGC-1α) in response to sympathetic nervous system activation (Sydoux & Giradrier, 1978). More recently, the ability of exercise training, as well as cold exposure to induce UCP1 up-regulation (Ringholm, et al., 2013) and inguinal (but not epididymal) WAT browning (Bostrom, et al., 2012), have been shown to be driven by IL-6 (Knudsen, et al., 2014).

In other intricate studies, BAT transplantation in mice was found to be sufficient towards the improvement of glucose homeostasis in DIO mice, but interestingly not from IL-6 deficient mice (Stanford, et al., 2013).

IL-6 is thus an important regulator of the ability of the body to drive increases in thermogenesis and counter increases in body weight and adiposity. Interestingly, it was recently demonstrated the local presence of M2 macrophages, is instrumental to the up-regulation of energy dissipation through BAT in the context of cold or excess feeding (Nguyen, et al., 2011), which was corroborated by the deletion of the IL-4 receptor in myeloid cells disrupting the function of BAT. When considering the priming effects of IL-6 in the shift to the M2 phenotype via IL-4Rα/STAT6 in conjunction with the role in BAT-mediated thermogenesis, increases in circulating IL-6 in obesity might be more indicative of resistance to the beneficial effects of the cytokine through their prolonged engagement.

Figure 1.1.4: The Pleiotropic Role of Central and Peripheral IL-6 signaling in Physiology and Disease

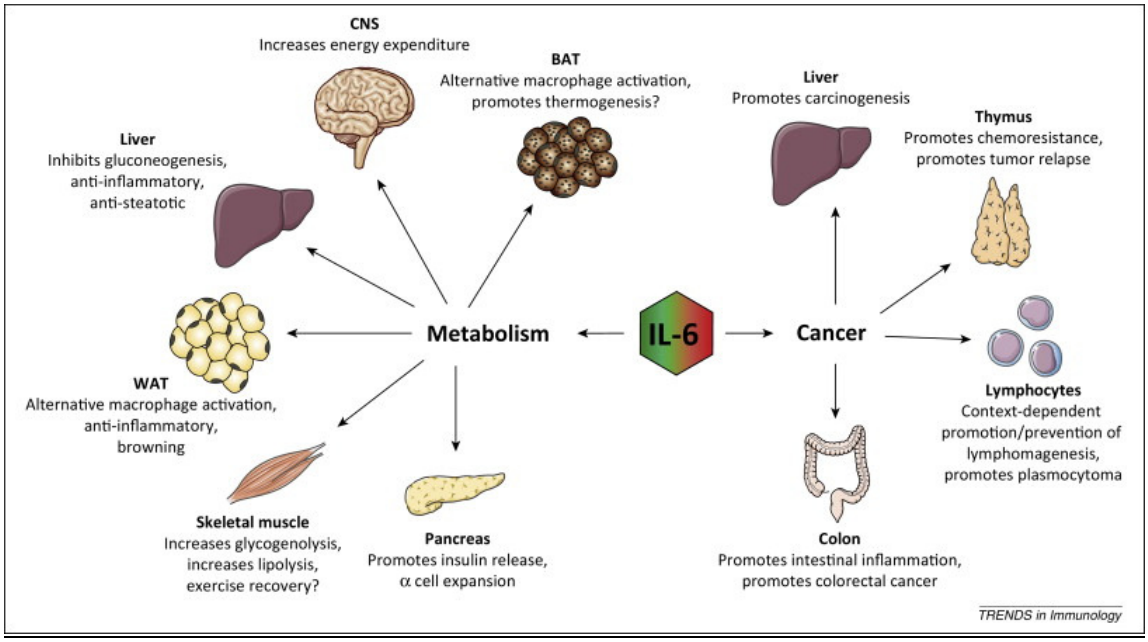

Adapted from Mauer J. et al. (2014)

Hypothesis and Experimental Approach

The initial and progressive accumulation of low-grade inflammation is increasingly understood to be of significance in the pathology of DIO and the progression to T2D. Cytokines are adipose-derived mediators involved in the acute phase as well as the resolving phase of inflammation. Increases in circulating cytokines such as IL-6 have been found to correlate with diabetic disease progression in obese patients (Kopp, et al., 2003; Ofstad, et al., 2013). The majority of published work investigating the role of IL-6 in metabolic disease, has been focused on its role in the periphery, benefiting from the use of whole body- or liver-specific knock-out or IL-6 deficient animals. A number of more recent studies have highlighted the importance of hypothalamic inflammation in metabolic disease (Fukuda, et al., 2011; Mori, et al., 2004; Yasukawa, et al., 2003; Zhang, et al., 2008).

Interleukin-6 drives metabolic inflammation in adipose tissue in response to HFD (Kraakman, et al., 2015), but has been also shown to act in the brain to promote energy expenditure through thermogenesis and fat oxidation (Wallenius, et al., 2002). Furthermore, activation of the IL-6Rα in the brain has been shown to promote the action of insulin and leptin (Shirazi, et al., 2013; Mori, et al., 2004; Ropelle, et al., 2010). In separate studies conducted at the McCrimmon lab, in a neuronal glucose-sensing hypothalamic cell line (GT1-7), repeated exposure to IL-6 was found to induce a glucose-sensing defect (G.T. Denwood data not shown).

The majority of published work investigating the role of IL-6 in metabolic disease so far, has been benefited from the use of whole body- or liver-specific knock-out or IL-6 deficient animals (Matthews, et al., 2010; Wunderlich, et al., 2010). Given the complex role exhibited by the cytokine in diabetic disease development, we were encouraged to examine the hypothesis that down-regulation of central IL-6 signaling would induce a defect in the metabolic response to HFD. To test this experimentally, we crossed NesCre1 (Dahlstrand, et al., 1995) and IL-6Rα$^{flox/flox}$ (MacFarland-Mancini, et al., 2010) mice which resulted in the nervous-system specific down-regulation of the IL-6Rα. Down-regulation of the receptor was validated in the novel transgenic, and mice on SC and HFD were studied and characterized over a period of 20 weeks using an array of metabolic phenotyping tests.

Chapter 2: Materials and Methods

List of Reagents, ELISA Kits, Antibodies and mRNA probes Used

Reagents

Acrylamide – Acrylamide/Bis-acrylamide, 30% solution A3574 Sigma-Aldrich®

Adenine – A2786 Sigma-Aldrich®

Agarose – A9539 Sigma-Aldrich®

Ammonium Persulphate – APS- A3678 Sigma-Aldrich®

Ascorbic Acid - L-Ascorbic acid A5960 Sigma-Aldrich®

Benzamidine – Benzamidine hydrochloride 99% 434760 Sigma-Aldrich®

Beta-mercaptoethanol – 2-Mercaptoethanol M6250 Sigma-Aldrich®

Blue/Orange Loading Dye, 6X – G1881 Promega®

Bradford Reagent – B6916 Sigma-Aldrich®

Bromophenol Blue – B0126 Sigma-Aldrich®

BSA - Bovine Serum Albumin A2153 Sigma-Aldrich®

$CaCl_2$ – Calcium Chloride C1016 Sigma-Aldrich®

Citric acid – 251275 Sigma-Aldrich®

Collagenase (Liberase TL – Roche 5401020001)

D-Mannitol – M4125 Sigma-Aldrich®

dNTP Mix – U1511 Promega ®

Dulbecco's Modified Eagle Medium (DMEM) – 21063-029 Life Technologies ®

EDTA – Ethylenediaminetetraacetic acid – E9884 Sigma-Aldrich®

EGTA – Ethylene glycol-bis (2-aminoethylether)–N, N, N', N'-tetracetic acid - E3889 Sigma-Aldrich®

Ethanol – 459844 Sigma-Aldrich®

Ethidium Bromide – E7637 Sigma-Aldrich®

Extraction Buffer – E7526 Sigma-Aldrich®

Foetal calf serum – 10270-106 Life Technologies ®

Glucose – D-Glucose - G8270 Sigma-Aldrich®

Glycine – G8898 Sigma-Aldrich®

GoTaq Buffer – M7911 Promega ®

GoTaq Hot Start Polymerase – M5001 Promega®

Hank's Buffered Salt Solution - HBSS 14025092 Life technologies®

HCl – 435570 Sigma-Aldrich®

Histoclear – HS200 National Diagnostics ®

Insulin - Actrapid®, Novo Nordisk

Interleukin-6 from mouse – II9646 Sigma-Aldrich®

KCl – P9541 Sigma-Aldrich®

Leptin – Recombinant Mouse Leptin CF – 498-OB-05M R&D Systems

Methanol – 320390 Sigma-Aldrich®

$MgCl_2$ – Magnesium Chloride - M8266 Sigma-Aldrich®

$MgCl_2x6H_2O$ – Magnesium Hexahydrate - M9272 Sigma-Aldrich®

Na_3VO_4 – Sodium Orthovanadate – S6508 Sigma-Aldrich®

NaCl – Sodium Chloride – S7653 Sigma-Aldrich®

NaF – Sodium Fluoride – 201154 Sigma-Aldrich®

$NaH_2PO4_X2H_2O$ – Sodium phosphate dibasic dehydrate – 71662 Sigma-Aldrich®

$NaHCO_3$ – Sodium bicarbonate – S6014 Sigma-Aldrich®

Neutralization Buffer B – N3910 Sigma-Aldrich®

Nuclease-free Water (not DEPC-treated) – Thermo Fisher Scientific® AM9932

Paraformaldehyde – 158127 - Sigma-Aldrich®

Penicillin/streptomycin – PEN/STREP - 15140-122 Life Technologies®

PMSF – 36978 – ThermoFisher Scientific®

Ponceau S Solution – P7170 Sigma-Aldrich®

Ribose – R7500 Sigma-Aldrich®

Sodium Dodecyl Sulphate – SDS- 436143 Sigma-Aldrich®

Sodium Pyruvate – P5280 Sigma-Aldrich®

Sucrose – S0389 Sigma-Aldrich®

TEMED (N, N, N', N'-Tetramethylethylenediamine) – 411019 Sigma-Aldrich®

Tissue Preparation Solution – TPS - T3073 Sigma-Aldrich®

TRITON X-100 – X100 Sigma-Aldrich®

Trizma Buffer – T4661 Sigma-Aldrich®

Trizol® Reagent – 15596-026 ThermoFisher Scientific

Tween-20 – P2287 Sigma-Aldrich®

Vectashield anti-fade mounting medium with DAPI – H-1000 Vector Laboratories®

ELISA Kits Used

- Mouse IL-6 Quantikine ELISA M6000B (R&D Systems®)
- Mouse/Rat Insulin, Glucagon Kit K15145C-1 (MSD®)
- Mouse/Rat Leptin Quantikine ELISA Kit MOB00 (R&D Systems®)
- SuperScript™ II Reverse Transcriptase – Invitrogen®
- Ultra-sensitive Rat Insulin ELISA kit 90060 (CrystalChem®)

Antibodies Used for Western Blotting

Anti-GAPDH Primary Antibody: GAPDH (D16H11) XP® Rabbit mAb #5174 – Cell Signaling Technology®

Anti-Mouse Fluorescent secondary antibody: IRDye® 680LT anti-mouse IgG – Licor®

Anti-Phospho-STAT3: Phospho-Stat3 (Tyr705) (D3A7) XP® Rabbit mAb #9145 – Cell Signaling Technology®

Anti-Rabbit Fluorescent secondary antibody: IRDye® 680LT anti-Rabbit IgG – Licor®

Antibodies Used for Immunohistochemistry

Anti-Insulin antibody produced in Guinea Pig ab7842– Abcam®

Anti-Glucagon antibody produced in Rabbit SAB451137 - Sigma Aldrich ®

Alexa Fluor® 488 AffiniPure Goat Anti-Rabbit IgG 11-545-144 - Jackson ImmunoResearch®

Alexa Fluor® 647 AffiniPure Fragment Donkey Anti-Chicken IgY 703-606-155 - Jackson ImmunoResearch®

Anti-IL-6R antibody (ALEXA Fluor 488) produced in rabbit ABIN902559 - antibodies-online®

Anti-NeuN antibody produced in Guinea Pig ABN90 - Millipore®

Anti-GFAP antibody produced in Chicken ab4674- Abcam®

Cy ™3 AffiniPure Donkey Anti-Guinea Pig IgG 706-165-148 - Jackson ImmunoResearch®

Mouse Colonies and Breeding Strategy

All mice used for the purposes of these studies were housed in the local Animal Resource Unit with water and chow pellet available ad libitum, under a 12-hour dark/light cycle. All procedures were approved under license in accordance to the Animal (Scientific Procedures) under Project License 60/4120. C57Bl/6 mice were used as a wild-type model and represent the most widely used inbred strain and the first to have its genome completely sequenced. Importantly, C57Bl/6 mice fed a high-fat diet develop mild to moderate hyperglycaemia and hyperinsulinaemia as well as obesity (Winzell & Ahren, 2004; Schreyer, et al., 1998). C57Bl/6 were used as the background strain for both the IL6Ra$^{flox/flox}$ and NesCre1 models utilized to generate NesCreIL-6R KD mice in this study.

B6 (SJL)-*Il6ra*$^{tm.1.1Drew}$*/J* animals (IL-6Rα$^{flox/flox}$) were obtained from Jackson Laboratories. The target endogenous gene (in this case *Il-6ra*), is modified by homologous targeting in embryonic stem cells. A loxP site was inserted upstream of exon 4 and an frt-flanked neomycin resistance (neo) cassette followed by a second loxP site downstream of exon 6 of the *Il6ra* gene. Flp mediated recombination removed the neo cassette leaving exons 4 through 6 floxed (Sauer, 1998). These mice were generated at the University of Cincinnati through work lead by Prof. Angela Drew, and provide the framework for tissue specific deletion of the IL-6Rα gene, by crossing with strains bearing recombinase activity (McFarland-Mancini, et al., 2010). Primers for the IL-6Rα lox-P sites were obtained from Sigma Aldrich towards identification of IL-6Rα$^{flox/flox}$ homozygote colony founders (2 male, 2 female).

NesCre1 (B6.Cg-Tg (Nes-cre) 1Kln/J) mice were obtained from Dr. Simon Arthur's group at the MRC Protein phosphorylation unit, University of Dundee (Graus-Porta, et al., 2001) and maintained in a C57Bl/6 background. These mice were first generated by work lead by Prof. Rudiger J. Klein, at the Max Planck Institute of Neurobiology. Nestin is an intermediate filament protein that was initially identified in rat neuroepithelial precursor cells (Dubois, et al., 2006; Lendahl, et al., 1990; Graus-Porta, et al., 2001). A modified Cre gene was placed in between the 5.8kb rat Nestin promoter and the rat Nestin intron 2, which contains at least 2 enhancer elements. The Nestin Cre mouse was chosen as it offers the potential to generate primarily central nervous system deletion of the floxed gene, in this case the IL-6 receptor (IL-6Rα) under the control of the promoter and enhancer (Troche, et al.,

1999). However, homozygous NesCre-positive mice are embryonically lethal. Hemizygous NesCre-positive males were identified by standard PCR and subsequently crossed with IL-6Rα$^{flox/flox}$ mice, to generate NesCre1IL-6Rα knock-down (NesCreIL-6Rα KD) and wild type littermates. Mice used exhibited no gross abnormalities, or differences in body weight, length and behavior.

Figure 2.1: Schematic Representation of Breeding Strategy

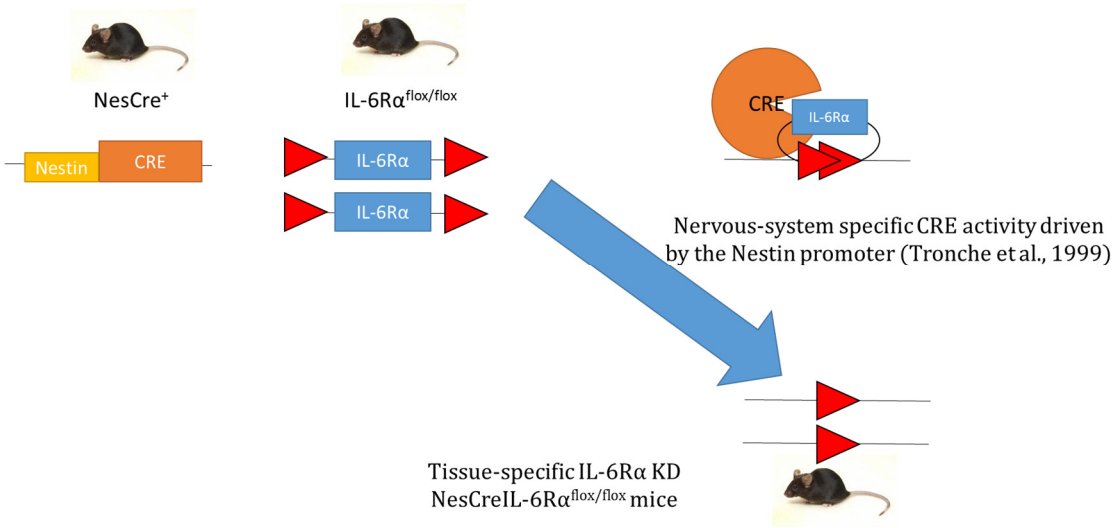

Genotyping of Nes-Cre and IL-6Raflox/flox mice by Standard PCR

Founders for the IL-6Rα$^{flox/flox}$ colony (2 female, 2 male) were ordered in directly from Jackson Laboratories®, while founders for the NesCre1 (CRE) colony obtained from Simon Arthur's lab (University of Dundee). The CRE colony was maintained by crossing founders with in-house bred C57Bl/6 wild type (WT) animals. The IL-6Rα$^{flox/flox}$ colony was maintained initially by crossing offspring of the founder mice. This was done to ensure that only homozygous IL-6Rα$^{flox/flox}$ animals were crossed with CRE. Later on in the study, new IL-6Rα$^{flox/flox}$ founders were introduced to improve breeding and avoid genetic drift (Casellas, 2011). Animals were ear-notched within the first 4 weeks of their lives and samples were stored at -20^{O}C until processing.

DNA Extraction

Ear-notch samples were suspended in suitable eppendorfs containing mixture of 100µl of *extraction buffer* (Sigma Aldrich®) and 25µl *tissue preparation solution* (TPS –

Sigma Aldrich®) at room temperature. The mixture was then briefly centrifuged to collect tissue and solution at the bottom of the tube and allowed 10 minutes at room temperature. This was followed by heating at 95^0C for 3 minutes, while the reaction was stopped by quickly removing from heat and adding 100µl of *Neutralization buffer* (Sigma Aldrich®). Samples were subsequently mixed and placed on ice. The resulting sample was deemed ready to be used to provide DNA for PCR amplification using and subsequent analysis by agarose gel electrophoresis.

Primers

Primers to confirm the presence of Cre activity were obtained from Sigma Aldrich® as advised by the Jackson® Laboratory website.

FORWARD (5') CRE PRIMER SEQUENCE:

AAATGGTTTCCCGCAGACC

REVERSE (3') CRE PRIMER SEQUENCE:

TAGCTGGCTGGTGGCAGATG

The presence of IL-6Rα loxP sites was confirmed by using primers obtained from Sigma Aldrich® in accordance to directions provided by Jackson Laboratories®:

FORWARD (5') IL-6R$\alpha^{flox/flox}$ PRIMER SEQUENCE:

GAAGGAGGAGCTTGACCTTGG

REVERSE (3') IL-6R$\alpha^{flox/flox}$ PRIMER SEQUENCE:

AACCATGCCTATCATCCTTTGG

The success of the PCR reaction was confirmed by means of a positive control primer pair obtained from Sigma Aldrich® in accordance to directions provided by Jackson Laboratories®:

FORWARD (5') oIMR 8744 PRIMER SEQUENCE:

CAA ATG TTG CTT GTC TGG TG

REVERSE (3') oIMR 8745 PRIMER SEQUENCE:

GTC AGT CGA GTG CAC AGT TT

Polymerase Chain Reaction Amplification

DNA amplification by PCR was carried out using the GoTaq® Polymerase system (Promega®). The following mixture was prepared per sample:

- 5x Go Taq Buffer – 5µl
- 2mM dNTP mix – 2.5µl
- Go Taq DNA Polymerase – 0.125µl
- Forward and reverse primers were loaded from a 10mM stock for a final concentration of 0.5µM:
  [Cre or IL-6Ra^{flox} 5' Forward Primer 10µM stock – 1.25µl]
  [Cre or IL-6Ra^{flox} 3' Reverse Primer 10µM stock – 1.25µl]
  [Positive Control Forward Primer oIMR 8744 10µM stock – 1.25µl]
  [Positive Control Reverse Primer oIMR 8745 10µM stock – 1.25µl]
- DNA – 2µl
- PCR-grade water was used to make up a final volume of 25µl/sample

Samples were then briefly centrifuged and placed in appropriate slots in the *Applied Biosystems® Veriti®* Thermal cycler. The following cycle was tailored by trial and error and was found to reproducibly allow for amplification of sample DNA. The PCR reaction was complete after 50 minutes and samples were held at 4^{O}C until recovery.

<u>Figure 2.2:</u> PCR Program used for DNA amplification

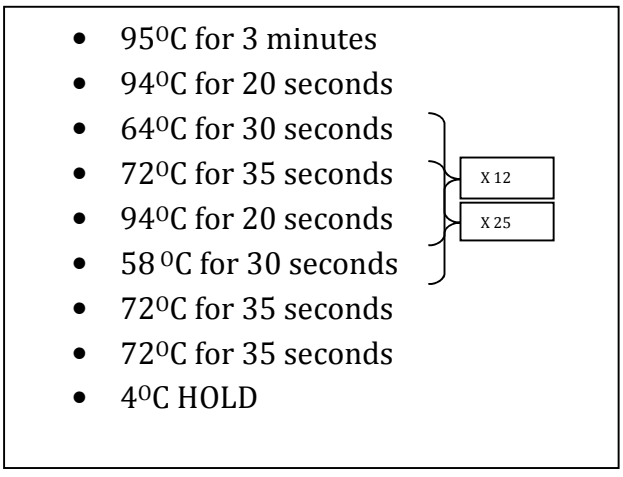

Agarose Electrophoresis

Resulting amplified samples were then mixed with 5µl of appropriate Blue/Orange 6X dye (Promega®) and briefly allowed to stand at room temperature. Products were then loaded in a 1% Agarose gel (2µl Ethidium Bromide/100ml) and ran at 120V for 40 minutes, along with an appropriate marker; 100bp DNA ladder® (Life Technologies®). Intact gels were then photographed using a UV camera and film was analyzed to identify and differentiate transgenic animals.

Where CRE Primers were used for the PCR reaction, the presence of the CRE sequence within the genome of transgenic animals was confirmed by the appearance of a 600bp. Successful identification of CRE sequences from ear notch samples was used as an indicator incorporation of the Nestin promoter. Similarly, in samples incubated with primers the IL-6Rα^{flox} sequence, the incorporation of loxP sequences flanking the IL-6Rα gene was confirmed by the appearance of a band at 671bp. Success of the PCR reaction was assessed by the appearance of the positive control band at 200bp (oIMR). NesCreIL-6Rα KD were essentially CRE-positive offspring of the NesCre^{+} x homozygote IL-6Rα$^{flox/flox}$ cross, while CRE-negative offspring were similarly identified by PCR as wild-type littermates.

mRNA quantification by Real Time PCR analysis

Wild-type (WT), NesCre+ (CRE) and NesCreIL-6Rα$^{flox/flox}$ (KD) male mice (>8 weeks old, n=7), previously confirmed by PCR were euthanized by cervical dislocation and brains were isolated and dissected. Brain tissue was divided into Frontal Cortex, Hippocampal, Hypothalamic and Cerebellar regions by anatomical identification using an appropriate mouse brain atlas (Paxinos G & Franklin KBJ 2001).

Tissue was homogenized in 1ml of Trizol® reagent (Invitrogen®) and 0.2ml of chloroform was added and vigorously mixed by shaking. Samples were then left at room temperature for 15 minutes before being centrifuged at 12,000g for 15 minutes at 4^{O}C. This allowed for phase separation, and the aqueous phase was transferred in a fresh tube where 0.5ml of isopropanol was added and mixed. The mixture was again left at room temperature for 10 minutes before being spun at 12,000g for 10minutes at 4^{O}C. The resulting supernatant was discarded and the RNA pellet was washed by the

addition of 1ml of 75% Ethanol. Washed samples were subsequently briefly mixed and centrifuged at 7,500g for 5 minutes at 4^{O}C. The ethanol supernatant was then removed and the pellet was allowed to briefly dry for 15 minutes under a fume hood. Any remaining supernatant was carefully removed using a 2µl micropipette before dissolving the pellet in 30µl of PCR grade water. To facilitate dissolution, samples were transferred for 15 minutes at 60^{O}C and mixed by pipetting.

Following successful RNA isolation the purity and concentration of samples was examined using a nano-drop spectrophotometer in combination with the ND 8000® software. First-strand cDNA synthesis was carried out using SuperScript™ II RT. 1µg of RNA from each sample was suspended in 12µl of PCR grade water along with 50-250ng random primers (Life Technologies®) and 1µl of dNTP mix (10mM each) and heated to 65^{O}C for 5 minutes. Contents were collected at the bottom of the tube using brief centrifugation and quickly placed on ice. 4µl of 5x first-strand buffer (Invitrogen®) and 2µl of 0.1M DTT was loaded and mixed with the products and left to stand at room temperature for 5minutes. 200 units of SuperScript™ II RT were then thoroughly mixed with the products before letting them to stand at room temperature for 15 minutes. Samples were then incubated at 42^{O}C for 50 minutes before inactivating the reaction by heating at 70^{O}C for 15 minutes.

Real time-PCR amplification was carried out with primers of the *Il-6ra* gene and *Cyclophillin A* as an internal control, using 6-carboxyfluorescein (FAM) as the fluorophore (Life Technologies®). Degradation of the primer probes releases the fluorophore from the quencher attached and allows for fluorescence to be detected in the quantitative PCR thermal cycler. More abundant genes produce lower values, as less thermal cycling is required for effective release of the fluorophore. Data obtained was analyzed according to the 2-ΔCT method (Schmittgen & Livak, 2008).

Brain Immunohistochemistry

Adult male mice (>8weeks, n=2) were sacrificed using an appropriate CO_2 chamber and brain was dissected and fixed in 4% paraformaldehyde in phosphate buffer solution (PBS) for 24 hours at 4°C. Tissue was embedded in paraffin and cut into 20µm sections using a microtome, to be subsequently collected in PBS. Slices collected in PBS were matched to Bregma coordinates using an appropriate mouse brain atlas (Franklin & Paxinos, 1997). Antigen retrieval was carried out by

incubating slides in 10mM citric acid pH6.0 at 100°C for 30minutes. Upon cooling to room temperature in the citric acid for 20 minutes, sections were permeabilised in PBST (PBS + 0.5% Triton X-100) for one hour.

Sections were treated for non-specific binding using 5% BSA in PBST for 1 hour at room temperature and transferred in humidified chamber. This was then used to incubate sections in 5% BSA in PBST containing primary antibody (Rabbit Anti-IL-6R 1:100 (antibodies-online®); Guinea-pig Anti-NeuN 1:100 (Millipore®) and Chicken Anti-GFAP 1:100 (Abcam®)) overnight at 4°C. On the following day, primary solution was removed and sections were washed in PBST (3x10min) at room temperature for 30 minutes. Following the final wash, sections were incubated in appropriate secondary antibodies in PBST (Anti-rabbit Alexa Fluor® 488 1:1000; Anti-guinea pig-Cy™3 1:500; Anti-chicken Alexa Fluor® 647 1:500 (Jackson ImmunoResearch®)) for 1 hour at room temperature.

Figure 2.3: Brain Slice Regions Used for Immunohistochemistry

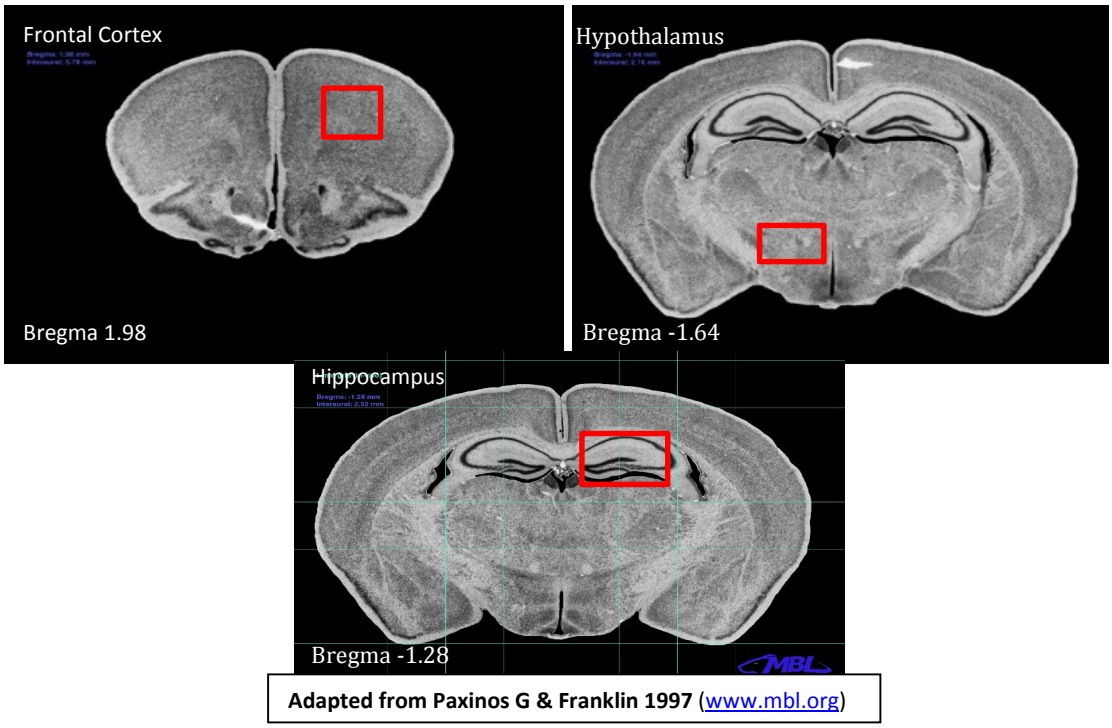

Secondary antibody was removed for a final wash in PBS (3x 10minutes) and distilled water (1x 10 minutes). Prior to mounting onto coverslips, sections were successively dehydrated in 70% ethanol for 2 minutes, 90% ethanol for 2 minutes and 100% ethanol (2x 5 minutes) and air dried for 30 minutes at room temperature. Coverslips were placed over sections along with Vectashield anti-fade mounting medium with

DAPI (Vector Laboratories®) sealed with nail varnish and stored at 4°C until imaged. Fluorescent images were acquired using a confocal laser scanning microscope (Leica® TCS SP5 II) with x100 oil-objective lens.

Cell counting was performed in region- and tissue area-matched (0.13mm^2) images from frontal cortex, hippocampal and hypothalamic brain slice tissue from each mouse to confirm IL-6Rα down-regulation, as previously described (Bologna-Molina, et al., 2011). Furthermore, images acquired were used to conduct co-localization analysis of target proteins using the Volocity ® Image Analysis Software (Barlow, et al., 2010).

Examination of peripheral and central responses to Intra-peritoneal IL-6 (50µg/kg)

To examine the ability of transgenic and control animals to respond to exogenous IL-6, adult (>8weeks old) KD, CRE and WT mice (n=2) were fasted for 4 hours and then received an IP injection of IL-6 (50mg/kg) prior to harvesting. Schedule 1 was carried out by cervical dislocation 30minutes following the injection. Central and peripheral tissue was harvested and snap-frozen using liquid nitrogen and stored in -80^{O}C.

Ex Vivo Brain Slicing Protocol for Rodent brains

To examine the ability of the mediobasal hypothalamus of KD and control animals to respond to IL-6, adult female (>8weeks old) KD, CRE and WT mice (n=7) were fasted for 4 hours prior to brain harvesting and subsequent slicing and treatment. All glassware and surgical equipment used was autoclaved daily and care was taken towards ensuring sterility of the work surfaces used.

Slicing solution: 50µM Adenine (daily), 1mM Ascorbic Acid (daily), 0.5mM $CaCl_2$, 7mM D-Glucose, 2.5mM KCl, 7mM $MgCl_2x6H_2O$, 28mM $NaHCO_3$, 1.25mM $NaH_2PO4x2H_2O$, 1mM Ribose (daily), 235mM Sucrose (daily), 3mM Sodium Pyruvate (daily).

On experimental day, 200ml aliquots of *slicing solution* per brain were prepared and frozen for 2-3 hours. Each solution was thawed on ice into an "ice slurry" constitution and oxygenated (100% O_2) for 20-30minutes before use.

Incubation Solution: 50μM Adenine (daily), 1mM Ascorbic Acid (daily), 2mM $CaCl_2$, 10mM D-Glucose, 15mM D-Mannitol, 1mM $MgCl_2x6H_2O$, 125mM NaCl, 25mM $NaHCO_3$, 1.25mM $NaH_2PO4_X2H_2O$, 1mM Ribose (daily), 110mM Sodium Pyruvate (daily).

On experimental day, 175ml aliquots of *incubation solution*/brain were prepared and oxygenated (95% O_2/5% CO_2) for 20-30minutes before and continuously during use.

4.5mM Glucose Treatment Solution: 50μM Adenine (daily), 1mM Ascorbic Acid (daily), 2mM $CaCl_2$, 4.5mM D-Glucose, 20.5mM D-Mannitol 1mM $MgCl_2x6H_2O$, 125mM NaCl, 25mM $NaHCO_3$, 1.25mM $NaH_2PO4_X2H_2O$, 1mM Ribose (daily), 110mM Sodium Pyruvate (daily)

Brain Tissue Harvest: Schedule 1 was carried out using cervical dislocation prior to decapitation. All instruments were autoclaved during the 4 hour fasting period before use. This method was used in order to minimize stress to the animal and contamination of the brain from the CO_2 gas chamber. Upon decapitation, the head was transferred into a petri dish of ice slurry of slicing solution with filter paper at the bottom. Damage to the cerebellum was to be expected. The brain was removed intact from the skull within 2 minutes. Skin and hair are removed from the scalp using a small pair of scissors. Using the same instrument a careful incision along the midline of the scalp was made, cutting from back to front, pushing upwards to avoid damage to the underlying soft tissue. While still in solution, brains were carefully removed from the skull by breaking the zygomatic and lightly pushing the brain upward from the frontal end, using the underside a small spatula.

Individual intact brains were transferred into a petri dish containing the *slicing solution* ice slurry, and rested upside down on a small piece of filter paper. Using a blade, the cerebellum and a small proportion of the frontal cortex were dissected and discarded. The remaining brain was scooped using a small spatula or appropriate instrument and excess fluid was removed using filter paper. Superglue was used to attach the brain, frontal side-up onto the stage of the vibratome. The stage was attached to Vibratome and briefly left to stand to allow the brain to dry. The slicing

stage was then filled with *slicing solution.* The surrounding exterior bathing space was filled with ice and cold water, to minimise any unwanted tissue temperature increases during slicing.

<u>Figure 2.4:</u> Ex Vivo Brain Slicing Protocol Representative photographs

Brain slicing and slice treatment:

Slices were chosen by anatomical identification of hypothalamic regions as demonstrated (Paxinos G & Franklin KBJ 2001) to contain regions of interest such as the glucosensing arcuate hypothalamic nucleus. Three 350µm slices were collected starting at approximately Bregma -1.05mm, with appearance of the arcuate hypothalamic area, up to approximately Bregma -2.05mm. Using a slice tip (cut and inverted 1ml pipette tip attached to appropriate sucker) desired slices were transferred into a petri dish. A sterile surgical blade was used to dissect out hypothalamic wedges from this region, using the third ventricle as an indicator. This would include the arcuate nucleus and aspects of the ventromedial, paraventricular and dorsomedial hypothalamus.

Using a similar tip slices were transferred into a previously oxygenated (95% O_2/5% CO_2) *incubation solution* 175ml aliquot and kept at room temperature (22°C) for 15-

20 minutes in appropriately constructed receptacles. Tissue was subsequently transferred to a 15ml flacon tube containing 5ml of *incubation solution* in a 34°C water bath. Slices were kept in the *incubation solution* with a constant supply of oxygen (95% O_2/5% CO_2), for 2 hours before being transferred into treatment solutions (4.5mM Glucose), with or without a stimulus (i.e. 20ng/ml IL-6) for 30minutes. At the end of the treatment, hypothalamic slices were transferred to an appropriate glass tube to be homogenized. Treatment solution was quickly removed and tissue was homogenized in 200µL of *lysis buffer* and stored at -80°C.

Figure 2.5: Schematic Representation of Ex vivo Slice Regions Used

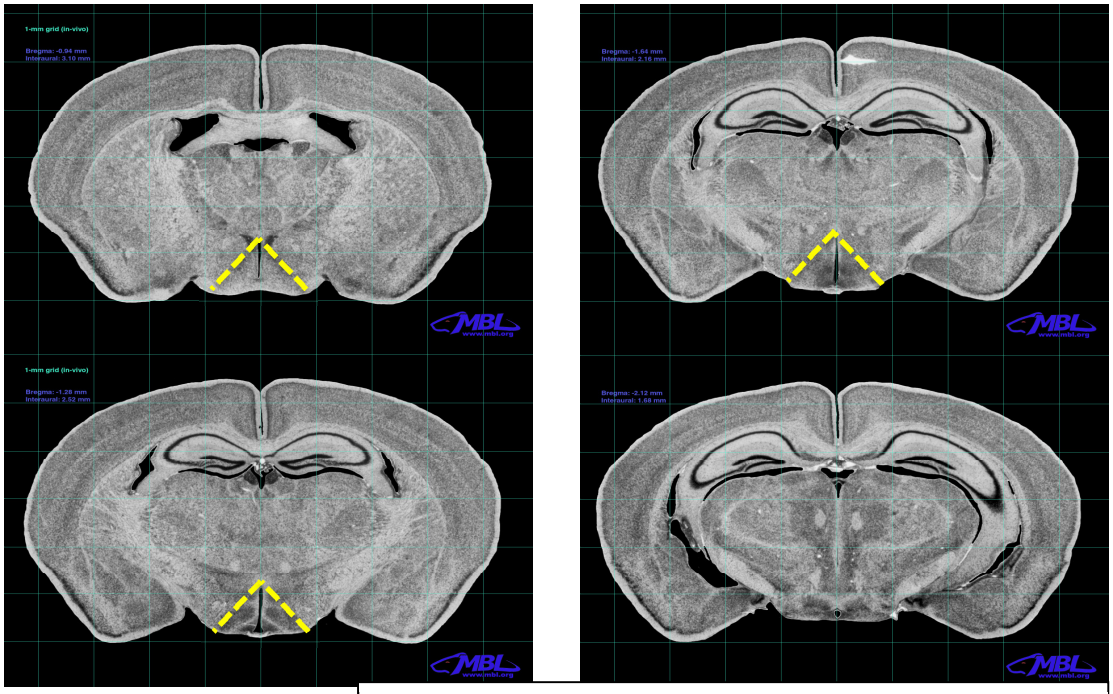

Adapted from Paxinos G & Franklin 1997 (www.mbl.org)

Western Blotting

Sample preparation

Lysis Buffer: 100mM NaCl, 10mM NaF, 25mM Tris/HCl (pH 7.4), 10mM NaPPi, 5mM EGTA, 1mM EDTA, 1mM Na_3VO_4, 1mM Benzamidine, 0.1 mM PMSF, 0.1% (v/v) β-mercaptoethanol, 1% (v/v) Triton X-100, 92mg/ml Sucrose

Sample Buffer (4x): 4ml Glycerol (99.5%), 2.5mM Tris/HCl pH 6.8, 2mM Sodium Dodecyl Sulphate (SDS), a pinch of Bromophenol blue (Sigma®) and 10% (v/v) β-mercaptoethanol added on the day of preparation.

Ex Vivo Brain Slice sample preparation: On completion of the treatment procedure, hypothalamic arcuate nuclei wedges were homogenized in 200µL of *lysis buffer* and stored at -80°C. On the following day, samples were centrifuged at 13200 rotations per minute for 30 minutes to separate the soluble and insoluble components of the lysate. The supernatant was removed, mixed and analysed for protein concentration using the Bradford Micro-Assay (0-10µg/ml protein). Appropriate lysate volumes were then suspended in (4x) sample buffer to constitute a 40µg stock.

Peripheral and Central Tissue sample preparation: Peripheral and central tissue harvested from the long-term and the short-term leptin sensitivity assessment studies was snap-frozen in liquid nitrogen and stored in -80°C. On the following day, tissue was homogenised in appropriate volumes (500µL for central and 1000µL for peripheral tissue) of lysis buffer, over dry ice to ensure no thawing of the tissue and denaturing of any resident protein. Muscle, white and brown adipose tissue was first pulverized into a thin powder by direct application of liquid nitrogen use of a mortar and a pestle over dry ice. Resulting homogenates were then briefly sonicated and centrifuged at 13200 rounds per minute (rpm) for 30minutes to separate the soluble and insoluble protein content. The supernatant was removed, mixed and analysed for protein concentration using the Bradford Micro-Assay (0-10µg/ml protein). Where lysates obtained exceeded the range of detection, diluents were prepared in distilled water. Appropriate lysate volumes were then suspended in (4x) sample buffer to constitute a 40µg stock.

Buffers

10x Tris-Glycine Running buffer: 121.1g Trizma base, 576g Glycine, 200ml of 20% SDS made up to 4L using distilled water.

20x TBS & TBST: 193.6g Trizma base and 640g NaCl were dissolved and made up to 3.2 L with ddH_2O. The pH of the solution was adjusted to 7.4 with concentrated HCl and volume made up to 4 L using ddH_2O. 2 ml of Tween-20 were added to 100ml of 20x TBS and made up to 2 L with ddH_2O, resulting in TBST (1x).

Transfer Buffer: 11.62g Trizma base, 5.86g Glycine, 1600ml dH_2O made up to 2L using 400ml Methanol (ACS grade).

Lower Gel Buffer - Tis-HCl pH 8.8: 1.5M Tris; 36.5g pH to 8.8 with concentrated HCl

Upper Gel Buffer – Tris-HCl pH 6.8: 0.5M Tris; 6.06g pH to 6.8 with concentrated HCl

SDS-PAGE

Table 1: Reagent Volumes Used for Polyacrylamide Gel Preparation

Lower Gel (10%)	**3 Gels**	**4 Gels**	**6 Gels**
dH_20	6.2ml	8.3µl	12.4ml
Tis-HCl pH 8.8	4.7ml	6.3µl	9.3ml
30% Acrylamide	5.6ml	7.5µl	11.3ml
10% SDS	165µl	220µl	330µl
TEMED	16.5µl	22µl	33µl
20% APS	83µl	110.7µl	166µl
Upper Gel (4%)	**3 Gels**	**4 Gels**	**6 Gels**
dH_20	4.2ml	5.6ml	8.4ml
Tis-HCl pH 6.8	1.9ml	2.5ml	3.8ml
30% Acrylamide	1.25ml	1.7ml	2.5ml
10% SDS	75µl	100µl	150µl
TEMED	8µl	10.7µl	16µl
20% APS	75µl	100µl	150µl

SDS-Poly-Acrylamide Gel Electrophoresis (SDS-PAGE) was utilized in order to examine the effects of experimental treatments at the protein level. Successfully casted gels were transferred to the running apparatus (Bio-Rad®) and the tank was filled with running buffer. Running buffer was prepared in a 10x stock and 2L of 1x

were prepared daily. Tris-Glycine Running buffer (1x) was used to completely fill the tanks, ensuring the space between gel plates to be completely filled. Wells were washed with running buffer using a syringe and 5µl of appropriate protein marker (Seeblue Plus2 Invitrogen ®) were loaded in the first well. 10µg of protein was loaded in each well, according to the calculations made during the Bradford assay. Upon successful loading, gels were run at 150V for approximately 1hour 45min (or until the blue dye ran out of the gels).

Proteins were separated by electrophoresis, to be transferred to a suitable membrane to be detected by using antibodies specific to target proteins of interest. Electro-blotting, uses an electric current which pulls proteins from the gel into nitrocellulose membranes used, maintaining the organization they had within the gel. A transfer cassette (BioRad®) was prepared, in which the membrane was placed on top of the gel with a stack of filter paper on either side. The entire stack was placed in appropriate transfer buffer, to allow for movement of proteins from the gel to the membrane in the presence of electric current. Transfer buffer was prepared fresh on the day of running. An ice pack was added to the tank or the whole tank was placed in an ice bucket before initiating transfer, as increases in temperature would disturb effective transfer. The tank was filled with appropriate volume of transfer buffer to fill the tank and gels transferred at 100V for 1 hour.

Protein Detection

Transfer cassettes were carefully disassembled and membranes removed from the arrangement using a forceps, to be placed in a square petri dish containing 5-10ml of Ponceau S dye (Sigma Aldrich ®) to confirm effective protein transfer. Membranes were then briefly washed in Tris-buffered saline with Tween-20 (TBST), ensuring that the membrane was free of any staining. To account for any non-specific protein binding membranes were blocked for an hour at room temperature using 10 ml of 10% non-fat milk/TBST per membrane. Membranes were then briefly (3x20minutes) washed in TBST before being treated with 10ml of primary antibody at appropriate recommended dilution overnight at 4^0C. Primary antibodies were prepared in 5% bovine serum albumin (BSA)/TBST at 1:1,000 dilution apart from GAPDH that was prepared at 1:2,000. Primary antibodies for GAPDH (GAPDH (D16H11) XP® Rabbit mAb #5174) and pSTAT3 (Phospho-Stat3 (Tyr705) (D3A7) XP® Rabbit mAb #9145) were purchased from Cell Signaling Technology ®.

On the following day, membranes were again washed (3x20minutes) in TBST at room temperature and incubated in 10ml of anti-rabbit (IRDye® 680LT anti-Rabbit IgG) or anti-mouse (IRDye® 680LT anti-mouse IgG) fluorescent secondary antibody in 5% BSA/TBST at 1:10,000. Membranes were then washed in TBST to account for any background staining (3x20minutes). This allowed protein detection and densitometry to be carried out using a Licor® chemiluminescence scanner and appropriate Licor® Odyssey software.

Study Plan for Evaluation of the role of central IL-6Rα signaling in the metabolic response to high fat diet

Male adult offspring (>8weeks) resulting from crosses of NesCre+ and IL-6Rα$^{flox/flox}$ mice genotyped and identified as NesCreIL-6Rα Knock-Down (KD) or wild-type littermate (WT) were placed on a 20-week study plan towards evaluation of the role of the receptor system in diabetic disease. Similarly, adult male NesCre+ (CRE) animals were also examined to be used as a control. For each genotype (WT, CRE and KD); 2 groups of 8-11 animals were examined for a period of 20 weeks in a 12-hour light/12-hour dark cycle. During the study groups from each genotype were assigned to be supplied either standard chow (SC; CRE n=9, KD n=9) or a 60% high-fat diet (HFD; CRE n=7, KD n=11) and water at libitum. Where a HFD was supplied, animals were allowed 3 weeks of habituating themselves to the diet, and a 50:50 mixture of HF and SC diet was provided in the first 2 weeks. In a recent report possible metabolic pitfalls of Nes-Cre mediated recombination were outlined, (Harno, et al., 2013) which arise as a consequence of differences in lean body mass and body length and absolute body weight compared to C57B/l6 mice. This was also observed in comparing CRE mice to WT mice and towards this, the CRE mice were used as a control group.

Table 2: Study Plan towards Metabolic Phenotyping of in KD and Control animals on SC and HFD

PROCEDURE	STUDY WEEK
Weighing	1-20
EchoMRI Body Composition Evaluation	3,7,12,14,20
Oral Glucose Tolerance Test	10,15,19
Intra-peritoneal Insulin Tolerance Test	6,12,14
Food Intake	9
Oral Glucose Stimulated Insulin Secretion	19

Body Composition Evaluation by echo MRI™

The echo MRI™ system was set-up and the appropriate checks were carried out using the supplier-provided software briefly before the start of the procedure. Animals were weighted briefly before entering the machine, where their body composition was recorded (fat vs. muscle mass) in triplicate. Water content was not measured. Mean body composition was calculated for each animal and means were extracted for statistical analysis.

Oral Glucose (50µg) Tolerance Test

Experimental animals were fasted 4 hours prior to the start of the procedure. At Time 0 basal blood glucose levels were measured using a Contour® Glucose meter by drawing blood from the tail vain of animals. Subsequently, mice were administered an oral dose of 50mg glucose by means of a gavage needle and allowed to move freely. Blood glucose levels were measured using tail vain sampling from freely moving animals 15, 30, 45, 60, 90 and 120 minutes following administration. On completion and upon inspection, animals were supplied with food according to their diet.

Figure 2.6: Schematic Representation of Oral Glucose Tolerance Protocol

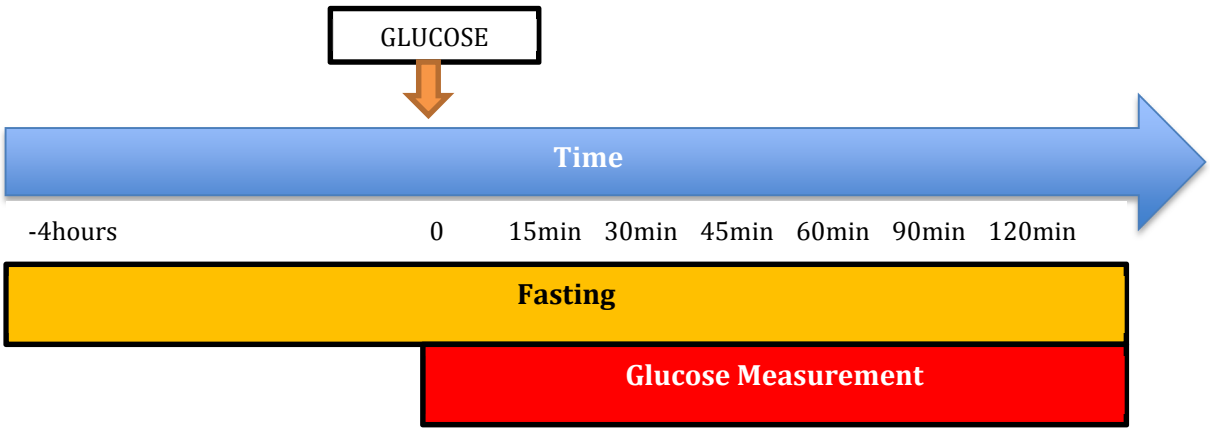

Intra-peritoneal Insulin (1U/100g) Tolerance Test

On experimental day, animals were fasted for at least 4 hours prior to the start of the procedure and baseline (Time0) glycaemia was recorded using a Contour® Glucose meter by drawing blood from the tail vain of animals. Mice were then administered an intra-peritoneal (IP) injection of 1U of insulin/kg weight and allowed to move freely. Following administration, glycaemic levels were measured using tail vain sampling from freely moving animals 15, 30, 45, 60 and 90 minutes. On completion and upon inspection, animals were supplied with food according to their diet. In cases where hypoglycaemic bouts were encountered animals were administered an intra-peritoneal dose of 50mg glucose, allowed to recover and excluded from the remainder of the experiment.

Figure 2.7: Schematic Representation of Intra-peritoneal Insulin Tolerance Protocol

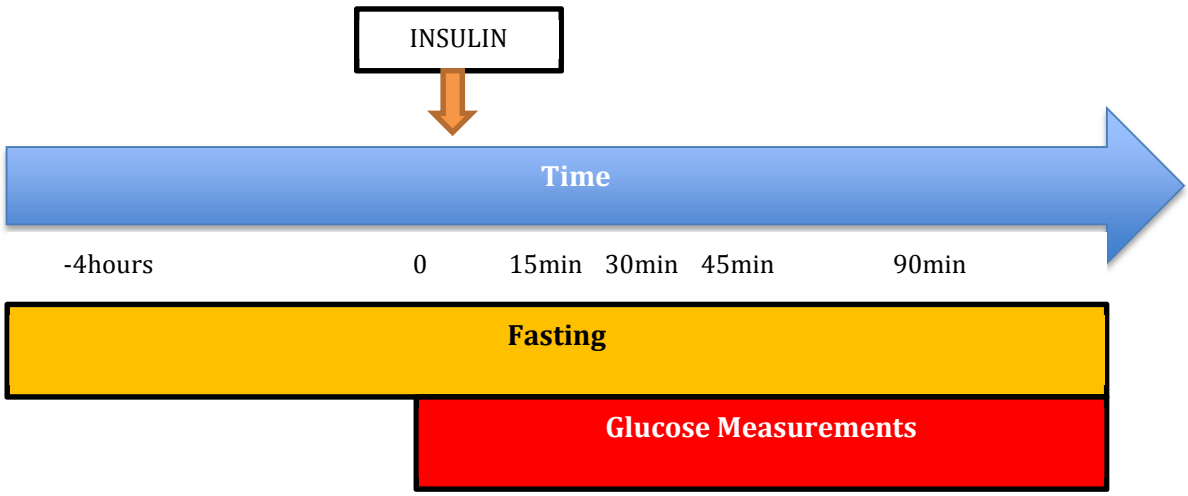

Oral Glucose Stimulated Insulin Secretion

Similarly to the oral glucose-tolerance tests, mice were fasted for 4 hours prior to measurement of baseline glycaemia (Time 0) using tail vain blood. Larger samples of blood were collected at each time point (approx. 30µl) for evaluation of the endogenous secretion of insulin by means of an ultra-sensitive enzyme-linked immunoabsorbent assay (ELISA) provided by CrystalChem ®. Similarly, mice were administered an oral dose of 50mg glucose by means of a gavage needle and allowed to move freely, but larger volume of tail vain blood were collected at 3, 15 and 30 minutes following administration. Samples from each animal at their respective time points were collected in EDTA-coated tubes and centrifuged at 1300g for 10 minutes to separate blood serum. Serum was collected and immediately stored at -80^{O}C for

processing. On completion of the experiment and upon inspection, animals were supplied with food according to their diet.

Figure 2.8: Schematic Representation of Oral Glucose Stimulated Insulin Secretion

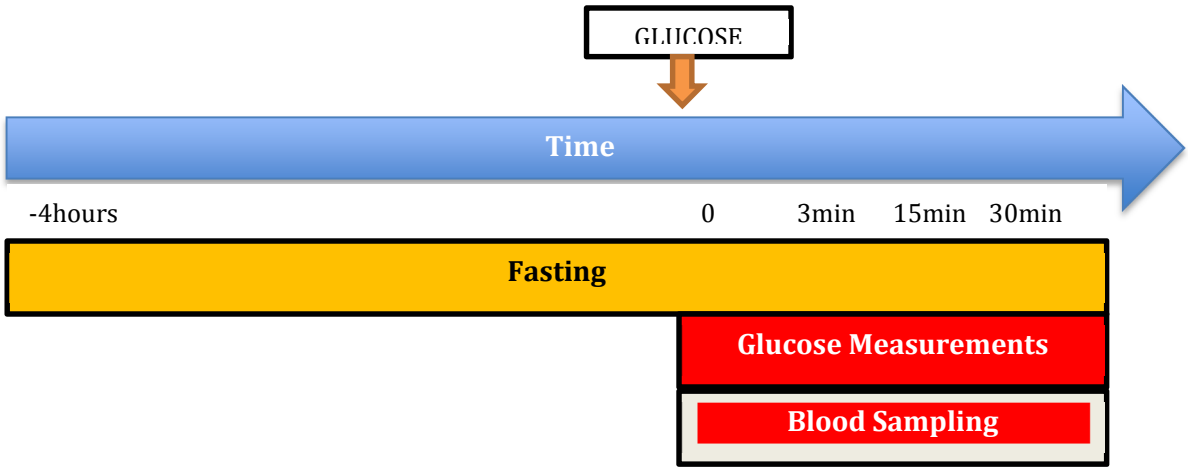

Food Intake Evaluation

Animals participating in the phenotyping study plan were separated from their normal cage-mates at the start of experimental day, and placed into individual cages for the subsequent 24hours, whereby food intake was evaluated at 4, 8 and 24hours (W9). Following completion of the protocol animals were returned to their normal cages.

Tissue Harvest

Following the end of the study plan and subsequent examination using CLAMS (described below); experimental animals (on SC or HFD) were fasted for 4 hours prior to being euthanized. Frontal Cortex, Hippocampal, Hypothalamic and Cerebellar regions were isolated by anatomical identification using an appropriate mouse brain atlas (Paxinos G & Franklin KBJ 2001). Heart, kidney, lung, liver, muscle, pancreas, spleen, white- and brown adipose tissue was isolated in accordance with the anatomy of the laboratory mouse. Harvested tissue was snap-frozen using liquid nitrogen and stored in -80^{O}C. Trunk blood (approx. 30µl) was collected in tubes containing appropriate anti-coagulant (EDTA) for isolation of plasma and examination of hormone levels by ELISA. Samples were collected and centrifuged at 1300g for 10 minutes to separate blood plasma. Plasma was collected and immediately stored at -80^{O}C for processing.

Metabolic phenotyping using the CLAMS® Activity Monitor

The activity monitoring system was started and appropriate measurements and equilibration was allowed, according to the manufacturer's specifications (Columbus Instruments®). Following the end of the 20-week study plan, experimental animals were weighted briefly before being examined using the CLAMS® Animal Monitoring System. KD and control animals were provided a 12:12 dark: light cycle, and their respective diets (SC or HFD) and water ad libitum. Measurements were taken over 48hours, following an initial 24hour acclimatization period. The well-being and the availability and accessibility to food and water of the animals was checked regularly during this period. Similarly, care was taken to ensure that software output parameters concerning the functionality of the animal monitoring system remained within suggested specifications. Output files produced allowed for monitoring and comparison of metabolic parameters (mean total food intake, mean activity and mean respiratory exchange ratio) during the 2 phases of the daily light cycle.

Figure 2.9: Representative Photograph from the CLAMS/Oxymax® System

In vivo Leptin (50µg/kg) sensitivity assessment

As examination of the effects of leptin without accounting for the stress of intra-peritoneal injections on body weight and food intake was not possible within the context of the 20-week study plan, a separate experiment was set up. A small cohort (n=6) of female adult (>8weeks) age-matched animals on SC was used. KD, CRE and WT SC animals were injected were kept on standard chow on a 12:12 night to dark cycle were used. Animals were separated from their cage mates and housed individually for a total of 3 weeks. An IP injection of saline was administered every day at dusk for the first 2 weeks of the protocol. Body weight and general health of the animals was recorded daily.

Body weight and additionally, daily food intake was recorded over a 5-day period during the 3rd week. All animals received an IP injection of saline on the first day. On the second day, an IP injection of 50µg/kg leptin was administered to half the experimental animals from each genotype and the rest received an IP injection of saline (control group). On the 3rd day, the control group received IP leptin, while the previously leptin-treated animals received IP saline. In this way, we were able to maintain an internal control for the effects of leptin on body mass and food intake. IP Saline was administered to all animals for the 4th and 5th day.

Table 3: Schematic Outline of the Leptin Sensitivity Assessment Protocol

PROCEDURE	SYMBOL
IP Saline	
IP Leptin	
IP Leptin/Saline & Tissue Harvest	
Food Intake and Body Weight Assessment	

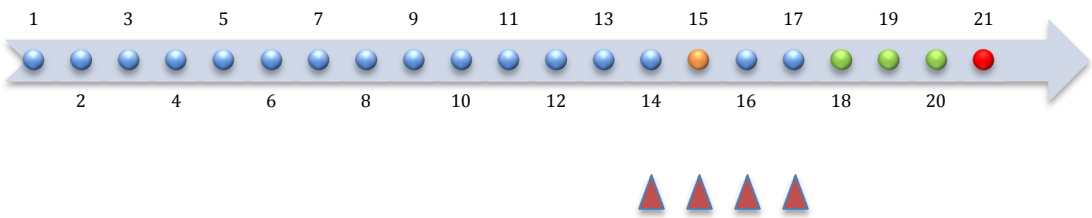

Animals were allowed to recover over the weekend. At the start of the 4th week, animals were fasted for 4 hours and schedule 1 was carried out by cervical dislocation 1 hour following a 3rd round of IP leptin injections to half the animals for each

genotype (n=3), while the rest (n=3) received saline. Central and peripheral tissue was harvested and snap-frozen using liquid nitrogen and stored at -80^{O}C. Tissue was processed for western blotting as described in previous sections.

Ex vivo pancreatic β cell Isolation and Stimulation

Collagenase Solution: A 10ml aliquot of Hank's Buffered Salt Solution (Life technologies HBSS 14025092) was supplemented with 100µl of 25mg/ml Collagenase (Liberase TL – Roche 5401020001) was prepared per animal. 0.75ml was then dispensed in a separate falcon tube to collect pancreatic tissue upon dissection.

Quenching Buffer: 500ml of HBSS was supplemented with 50 ml of 10% foetal calf serum and 5ml of penicillin/streptomycin and stored at 4^{o}C.

Overnight Solution: Dulbecco's Modified Eagle Medium (DMEM) was supplemented with 1000mg of glucose, 50 ml of 10% foetal calf serum and 5ml of penicillin/streptomycin and stored at 4^{o}C.

Tissue Isolation: KD, CRE and WT adult female mice (>8weeks, n=8) were sacrificed using an appropriate CO2 chamber. The bile duct was identified and carefully cleared of connective tissue. By following the physiological direction of the duct, ventrally from the liver, its route to the pancreas can be identified. The small intestine was clamped proximally to the point of contact of bile duct and pancreas. The bile duct was carefully incised using spring scissors and a micro-renethane cannula attached to a needle was inserted and held in place by suturing. The pancreas was subsequently inflated using approx. 5ml of collagenase solution per animal and carefully dissected out to be collected in 0.75ml of ice cold *Collagenase solution*. Pancreatic tissue was then incubated at 37^{o}C for 15 minutes. Tissue was subsequently exposed to 10ml of *Quenching buffer* and shaken vigorously for 15sec. An appropriate 500µm net was fitted over a 50ml falcon tube and pancreatic tissue in *Quenching buffer* was poured through. The tube and net were washed with an additional 10ml of *Quenching buffer* and centrifuged for 1 minute at 12,000rpm. Quenching buffer was aspirated and replaced by fresh 20ml to re-suspend the pellet formed. Following 3 washes, the pellet was suspended in 5ml of *Quenching buffer* and placed on ice.

Islet Identification: Pancreatic tissue was transferred to a 90mm Petri dish. Islets were identified under a light microscope and picked out by using head-polished glass Pasteur pipettes and a rubber tip. They were quickly transferred to Calcium and Magnesium-free HBSS and incubated in *Overnight Solution* at 37ºC (95% O2, 5%CO2). 24 hours late, islets were incubated in 20mM DMEM solution (5% FBS) at 37ºC (95% O2, 5%CO2) for one hour, before media was quickly frozen at -80ºC to subsequently examined in terms of insulin and glucagon content by ELISA.

Pancreatic Immunohistochemistry

Tissue Isolation: KD and CRE adult female (>8weeks, n=4) were sacrificed using an appropriate CO_2 chamber and pancreas was dissected and fixed in 4% paraformaldehyde in phosphate buffer solution (PBS) for 24 hours at 4°C. Tissue was embedded in paraffin and cut into 5µm sections using a microtome provided by the University of Dundee Tissue bank. Sections were collected and coated on glass microscope slides.

Pancreatic Slice Staining: Slides were incubated at 60°C for 45 minutes and then immersed in Histoclear for 30 minutes to remove wax. They were quickly immersed in an appropriate rack containing 100% ethanol for 10 minutes followed by fresh 100% ethanol for five minutes and a final wash in running water for 10 minutes.

Slides were incubated in 10mM citric acid pH6.0 at 100°C for 30minutes. Upon cooling to room temperature in the citric acid, sections were permeabilised in PBST (PBS + 0.5% Triton X-100) for one hour. Following this antigen retrieval step, wells were drawn around tissue sections on the slide, using a PAP pen.

Sections were then blocked using 5% BSA (*blocking solution*) in PBST and then incubated with primary antibody in *blocking solution* (insulin (Abcam®) 1:100 and glucagon 1:100(Sigma-Aldrich ®) in a humidified chamber overnight at 4°C. Following a 30minute wash in in PBST (3x10min) sections were incubated in appropriate secondary antibodies in PBST (Cy™3 (Jackson ImmunoResearch®) 1:250 and Alexa Fluor® 488 (Life Technologies®) 1:500) for 1 hour at room temperature. Secondary antibody was removed and sections were washed in PBS (3x 10minutes) and water (1x 10 minutes).

Sections were successively dehydrated in 70% ethanol for 2 minutes, 90% ethanol for 2 minutes and 100% ethanol (2x 5 minutes) and allowed 30 minutes to dry at room temperature. Coverslips were placed over sections along with Vectashield anti-fade mounting medium with DAPI (Vector Laboratories®) that were sealed with nail varnish and allowed to dry. Stained sections were stored at 4°C in the dark until image acquisition. Fluorescent images were acquired using a confocal laser scanning microscope (Leica® TCS SP5 II) with x40 oil-objective lens.

Chapter 3: Validation of NesCre-mediated IL-6Rα Knockdown in Mice

The main aim of my studies was to generate and validate the brain-specific down-regulation of the IL-6Rα mice as to interrogate the role of central cytokine signaling in DIO and T2D. Cre/lox technology has been widely used in science to generate tissue specific genetic mutants, aimed at the investigation of specific gene functions in everyday physiology and disease (Utomo & al., 1999). It utilized the 34kb-long P1 bacteriophage *loxP* sequence (a sequence that is normally absent in mammalian tissue) and the activity of the *cre* gene that codes for a protein that mediates DNA recombinase activity when locating *loxP sequences*. As a consequence of these properties, where *loxP* sites are successfully inserted into the genome of organisms expressing Cre, the Cre protein leaps into action, causing recombination at the locus flanked by *loxP* (Utomo & al., 1999; Pechisker, 2004).

Figure 3.1: Schematic Representation of Cre Technology -mediated Gene Disruption

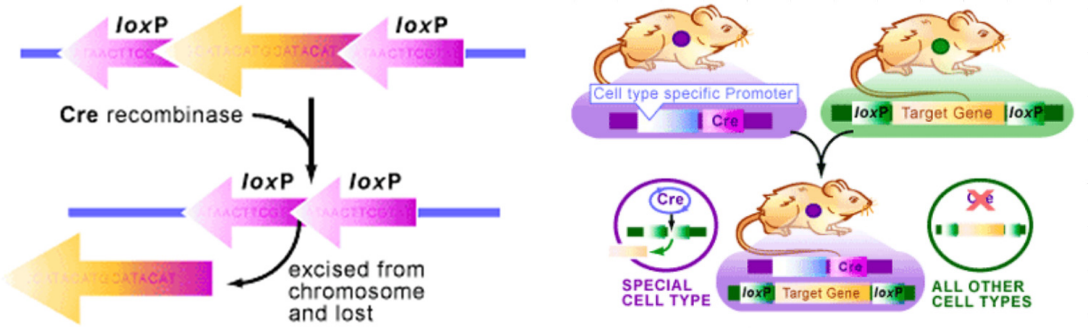

Adapted from Pechisker, 2004

A variety of Cre models are commercially available, that allow for tissue specific targeting of Cre activity. Crossing such mice with mouse strains that bear a target gene flanked by 2 *loxP* sites in direct orientation, would result in offspring that experience inactivation of the target gene in cells expressing Cre recombinase activity (Kuhn & Torres, 2002; Le & Sauer, 2000). Nestin Cre mice have been previously used in a number of studies investigating the effects of brain-specific disruption of target proteins in metabolism (Zhang, et al., 2008; Loh, et al., 2012; Pedroso, et al., 2014). Nestin Cre mice (B6Cg-Tg (Nes-cre) 1 Kln/J) were thus crossed with homozygous IL-6Rα floxed mice, towards the generation of a mice where the cytokine receptor system was disrupted in the brain, specifically.

Identification and Verification of B6.Cg-Tg (Nes-cre) 1Kln/J mice by PCR

NesCre mice (Graus-Porta, et al., 2001) were generously donated by Dr Simon Arthur's lab (MRC Protein Phosphorylation Unit, the University of Dundee) and samples were obtained for genotyping purposes. Initial verification of NesCre mice was carried out following the standard PCR (Jackson Laboratories®), using the GoTaq® Polymerase system (Promega®). DNA extracted from colony founders was used as a positive control. As shown in **Figure 3.**2, using a 1% Agarose gel, a band at 600 base pairs was evident in Nes-Cre-positive animals, as predicted by the sequence of the Cre primers used. The appearance of band at 200bp was incorporated in the protocol, by using primers for a non-coding region in mouse DNA as described in **Methods**. This acted as control for the success of PCR reactions.

Figure 3.2: Identification of animals bearing Cre activity by Standard PCR

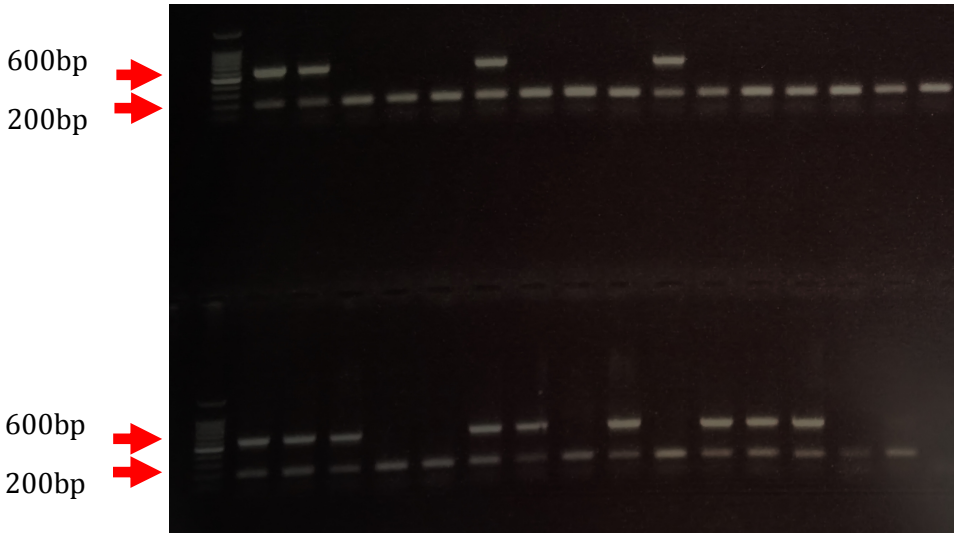

Figure 3.2: Image taken from a random set of animals from our NesCre X WT crosses. In lanes 1 & 2 DNA extracted from the colony founders examined for the presence of CRE activity. As predicted by our primer-set, CRE activity was confirmed by the appearance of a band at 600bp. The success of PCR reactions was assessed by the appearance of a band at 200bp, coded from a ubiquitously expressed DNA fragment in the mouse genome.

Identification and Verification of B6; SJL-Il6ratm1.1Drew/J mice

In a similar fashion, incorporation of the loxP sites in IL-6Rα$^{flox/flox}$ mice was confirmed by standard PCR in accordance to the Jackson Laboratories® directions, using the KOD Hot Start Polymerase ® system. As shown in **Figure 3.3**, using a 1% Agarose gel, a band at 671 base pairs was evident in transgenic animals. As mentioned above, primers for non-coding regions of the mouse genotype allowed assessing the success of PCR reactions by the appearance of band at 200bp.

Figure 3.3: Identification IL-6Rα$^{flox/flox}$ animals by PCR

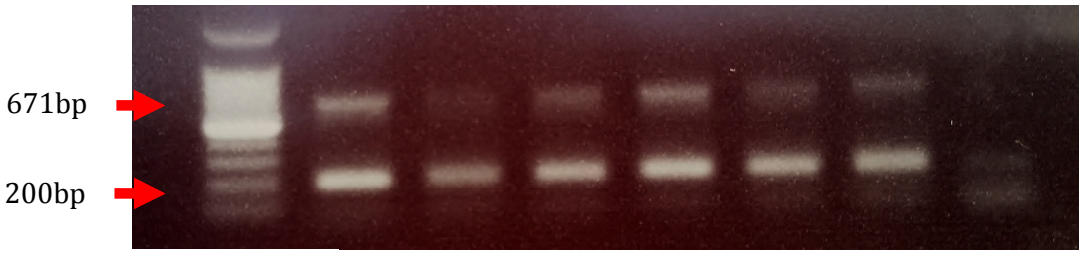

Figure 3.3: The image was taken using DNA extracted from a random set of animals from our IL-6Rα$^{flox/flox}$ colony. DNA extracted from the colony founders was used as a positive control, whereby the incorporation of the loxP sites flanking the IL-6Rα gene results in the appearance of a band at 671bp. Guidelines provided by the Jackson Laboratory®, suggested the appearance of a single band at 530bp to indicate WT animals, while a doublet at 530 and 671bp indicates that animals are heterozygotes for the loxP site. Homozygous IL-6Rα$^{flox/flox}$ mice were bread and naturally no heterozygote or WT offspring were identified. Positive control band can be observed at 200bp, confirming sample amplification.

Crossing the CRE positive heterozygote animals with homozygote IL-6Rα$^{flox/flox}$ mice was expected to yield IL-6Rα knock-down in at least 1 in 4 of their resulting offspring. The incorporation of at least one loxP site in the genome from the homozygote IL-6Rα$^{flox/flox}$ parent should result in down-regulation of the IL-6Rα system in tissue where the Nestin promoter is active. Subsequently, in tissue where the Nestin promoter is expressed, Cre activity will be promoted and disruption of the gene was expected to take place. Since the offspring of heterozygote Nes-Cre and homozygote IL-6Rα$^{flox/flox}$ mice are guaranteed to have at least one copy of the flox gene, genotyping for the presence of CRE activity, allowed us to distinguish between Nestin-Cre IL-6Rα KD and wild-type litter-mates of the cross.

Examination of Brain IL-6Rα Gene Expression by Real Time-PCR

To validate the effects of the breeding strategy, Real Time-PCR was used to assess IL-6Rα mRNA expression in the brain of animals previously classified as WT, NesCre+ and NesCreIL-6Rα KD by standard PCR. *IL-6ra* mRNA abundance in the frontal cortex, hippocampus, hypothalamus and cerebellum of adult (>8weeks) WT, CRE and KD mice (n=7-8) was calculated using the 2-ΔCT method and normalized to similarly calculated Cyclophillin A abundance. Statistical analysis of normalized data was carried out using the Mann Whitney U-test. This allowed for non-parametric examination of the null hypothesis that *Il-6ra* mRNA expression was similar in the brain of KD and control animals, against the alternative hypothesis that control animals exhibit increased receptor mRNA compared to the KDs.

Figure 3.4.1: Comparison of *IL-6ra* mRNA between NesCre IL-6Rα WT and Nes-Cre+ mice

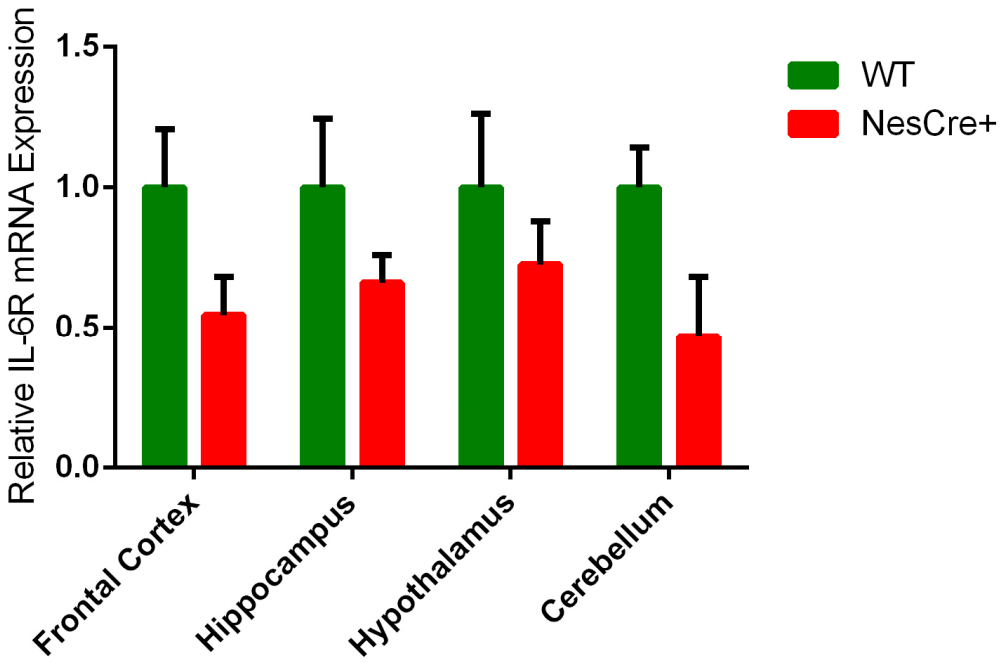

Figure 3.4.1: Adult (>8weeks old) male mice (WT n= 7; NesCre+ n=7) were used from each genotype. Error bars indicate +/-SEM. Relative IL-6ra mRNA expression was compared using the 2-ΔCT method, in cortical (p=0.06), hippocampal (p=0.14), hypothalamic (p=0.22) and cerebellar (p=0.049) brain tissue.

Cerebellar *IL-6ra* mRNA was significantly (55%) decreased in CRE compared to WT animals (p=0.049), but not in the frontal cortex (p=0.06), hippocampus (p=0.14) or

hypothalamus (p=0.22) even though an overall trend of reduced *IL-6ra* mRNA was observed **(Figure 3.4.1)**. In the frontal cortex, IL-6 receptor mRNA in NesCre+ mice was just over 50% the receptor mRNA expression of WT animals. Similarly, in the hippocampus a 40% reduction in IL-6Rα mRNA was observed, while in the hypothalamus a 35% reduction was noted. Since we have chosen to target the IL-6Rα system and evaluate its role in metabolism, the comparative between WT and NesCreIL-6Rα KD animals would not be appropriate. Since KD animals are NesCre+ themselves, the down-regulation would only be relevant in comparison to CRE animals.

Figure 3.4.2: Comparison of *IL-6ra* mRNA between NesCreIL-6Rα KD and NesCre+ mice

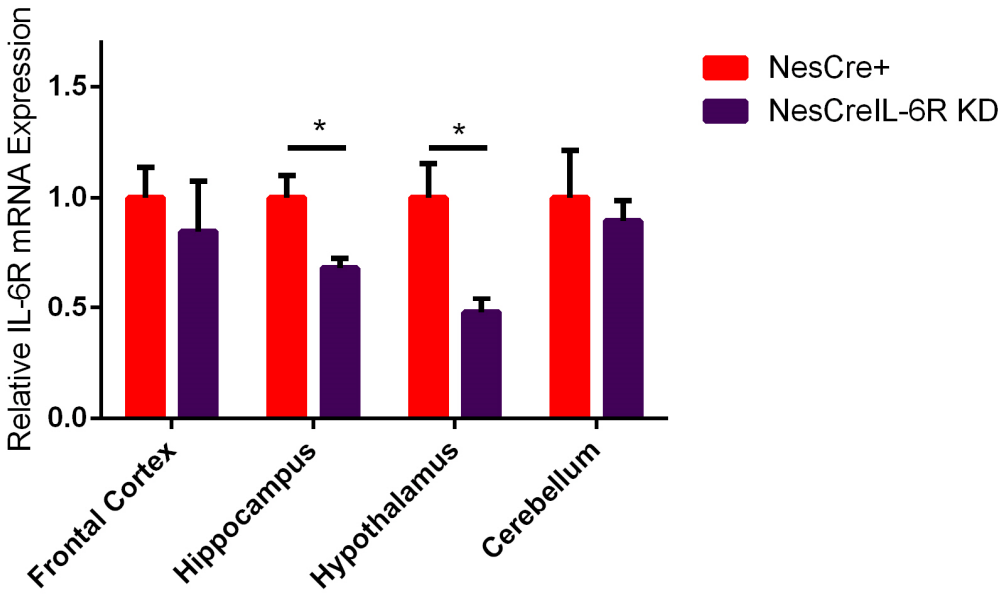

Figure 3.4.2: Comparison of Il-6ra mRNA between NesCreIL-6Rα KD and NesCre+ mice

Adult (>8weeks old) male mice (KD n= 6; NesCre+ n=7) were used from each genotype. Error bars indicate +/-SEM. Relative IL-6ra mRNA expression was compared using the 2-ΔCT method, in frontal cortex (p=0.56), hippocampus (p=0.0183), hypothalamus (p=0.128) and cerebellum (p=0.68).

Despite this, the Nes-Cre promoter system does however induce to brain-targeted disruption of *Il-6ra* mRNA when comparing in CRE and KD brains. Significant down-regulation of receptor mRNA was observed in the hippocampus (p=0.0183) and hypothalamus (p=0.0128) of KD compared to CRE controls, but not in the Frontal Cortex (p=0.56) or Cerebellum (p=0.68) **(Figure 3.4.2)**. In the hippocampus a 32% reduction in IL-6Rα mRNA was observed, while a 50% down-regulation in receptor mRNA (47.80% +/-6.4%, p=0.0128) was observed in the hypothalamus. In the frontal

cortex (84.7+/-22.8%, p=0.56) and cerebellum (89.5+/-9.3%, p=0.68), KD animals exhibited modest reductions in receptor mRNA expression compared to control animals.

Il-6ra mRNA in the 3 genotypes was fairly ubiquitous, even though the hippocampus and hypothalamus exhibited the highest expression **(Figure 3.4.3)**. Significant differences were observed in WT animals only when comparing hippocampal to cerebellar *Il-6ra* mRNA expression (p=0.005). In NesCre+ mice both hippocampal (p=0.02) and hypothalamic (p=0.05) *Il*-6ra mRNA was significantly elevated compared to the cerebellum, but not the frontal cortex (p=0.34 and p=0.54). On the other hand, differences in receptor expression among the different brain regions failed to reach significance in NesCreIL-6Rα KD mice.

Figure 3.4.3: Comparison of *Il-6ra* mRNA between Brain Regions in KD and control mice

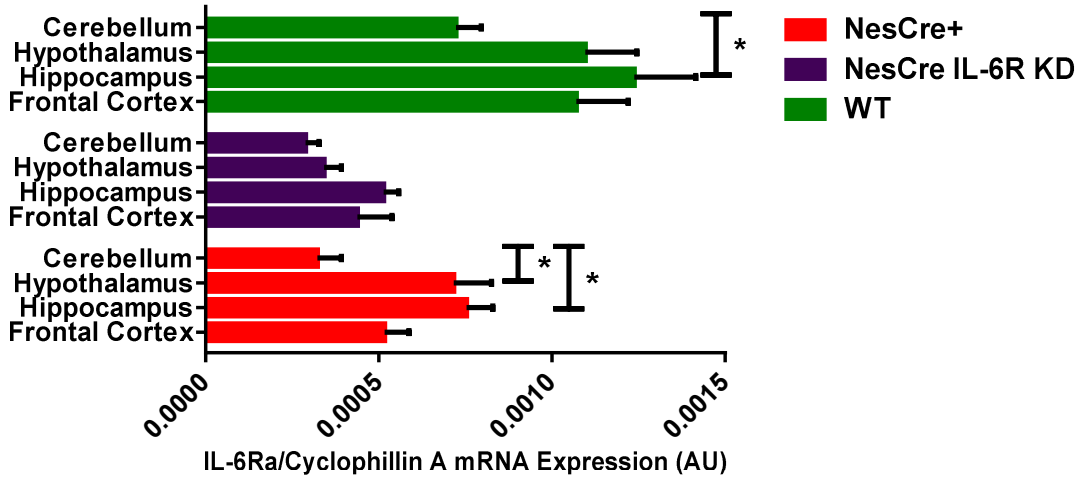

Figure 3.4.3: Comparison of Il-6ra mRNA between Brain Regions in KD and control mice

Adult (>8weeks old) male mice (**PURPLE:** KD n= 6; **RED:** NesCre+ n=7; **GREEN:** WT n=7) were used from each genotype. Error bars indicate +/-SEM. Relative IL-6ra mRNA expression was compared using the 2-ΔCT method normalized to Cyclophillin A. **WT:** Frontal Cortex vs. Hippocampus, p=0.65; Frontal Cortex vs. Hypothalamus, p>0.99; Frontal Cortex vs. Cerebellum, p=0.09; Hippocampus vs Hypothalamus, p=0.78; Hippocampus vs Cerebellum, p=0.05; Hypothalamus vs Cerebellum, p=0.07. **NesCre+:** Frontal Cortex vs. Hippocampus, p=0.39; Frontal Cortex vs. Hypothalamus, p=0.54; Frontal Cortex vs. Cerebellum, p=0.56; Hippocampus vs Hypothalamus, p=0.99; Hippocampus vs Cerebellum, p=0.02; Hypothalamus vs Cerebellum, p=0.05. **KD:** Frontal Cortex vs. Hippocampus, p=0.96; Frontal Cortex vs. Hypothalamus, p=0.93; Frontal Cortex vs. Cerebellum, p=0.79; Hippocampus vs Hypothalamus, p=0.71; Hippocampus vs Cerebellum, p=0.51; Hypothalamus vs Cerebellum, p=0.99.

Examination of the pSTAT3 Response to IL-6 in Brain Tissue

To functionally assess the effects of Nes-Cre-mediated down-regulation of the IL-6 receptor gene in transgenic and control animals, a standard dose of IP IL-6 (50µg/kg) in animals previously genotyped by standard PCR. Responses were not quantified as the cost associated with treating a number of animals from each genotype with IL-6 was a limitation (n=2).

Figure 3.5.1: Hypothalamic pSTAT3Responses to IP IL-6 (50µg/kg) injection

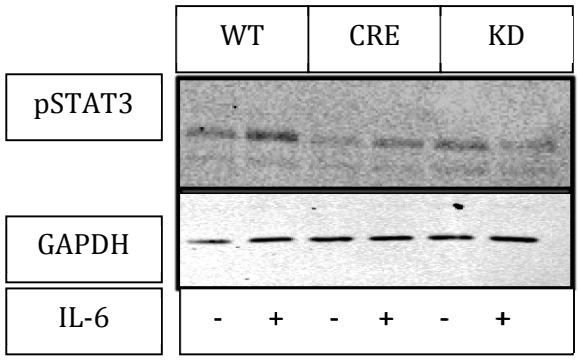

Figure 3.5.1: Adult male mice (>8weeks) from each genotype were used. Loading Order: (1) WT; (2) WT + IL-6; (3) CRE; (4) CRE + IL-6; (5) KD; (6) KD + IL-6. Representative blot, n=2 from each genotype. pSTAT3 – 79/88 kDa; Loading Control: GAPDH – 37 kDa (Cell Signaling®).

Despite our attempts to confirm our initial findings at mRNA level using an antibody against the IL-6Rα, we were unable to secure an antibody that was sensitive and specific enough for the validation of such subtle effects in such a complex organ such as the brain. Targeting of the receptor using *IL-6Rα*$^{flox/flox}$ mice leads to disruption of the cytokine-binding domain. Since most commercial antibodies available are targeted to the terminal domains of the receptor, quantification of differences at protein level was not possible. We thus examined the pSTAT3 response to a standard dose of peripheral IL-6 in KD, CRE and WT brain (hippocampus, hypothalamus and cerebellum). Despite our attempts to assay and illustrate the pSTAT3 response to IL-6 in the frontal cortex, we were unsuccessful in a number of attempts.

Figure 3.5.2: Hippocampal pSTAT3 Responses to IP IL-6 (50µg/kg) injection

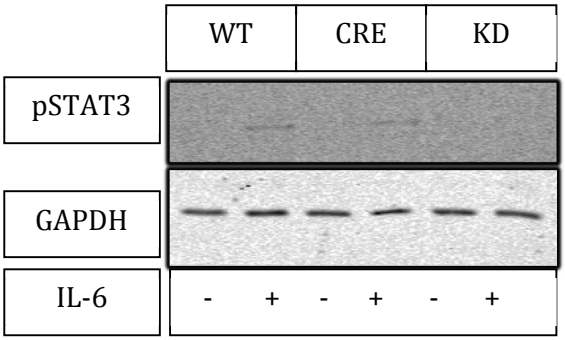

Figure 3.5.2: Adult male mice (>8weeks) from each genotype were used. Loading Order from left to right: (1) WT; (2) WT + IL-6; (3) CRE; (4) CRE + IL-6; (5) KD; (6) KD + IL-6. Representative blot, n=2 from each genotype. pSTAT3 – 79/88 kDa; Loading Control: GAPDH – 37 kDa (Cell Signaling®).

As mentioned in the introduction, circulating interleukin-6 is able to pass the blood brain barrier and mediate its associate signaling cascades in the brain. Figures in this section demonstrate IP IL-6 treatment to induce increases in phosphorylated STAT3 protein in all brain regions examined. The hypothalamus was our main region of interest and encouragingly, hypothalamic pSTAT3 response to IP IL-6 was negligible to baseline in KD animals **(Figure 3.5.1)**. This was in stark contrast to the clear up-regulation in pSTAT3 observed in WT and CRE animals (n=2), albeit differences in the magnitude of the response were apparent.

Figure 3.5.3: Cerebellar pSTAT3 Responses to IP IL-6 (50µg/kg) injection

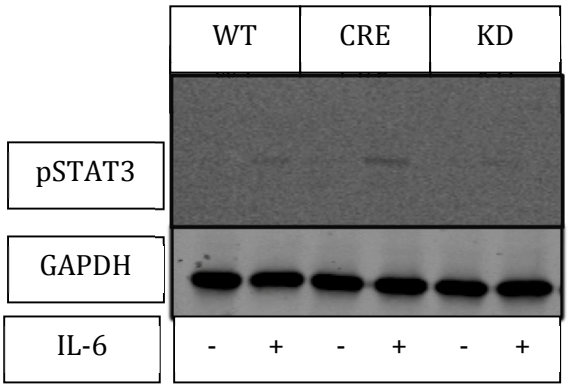

Figure 3.5.3: Adult male mice (>8weeks) from each genotype were used. Loading Order from left to right: (1) WT; (2) WT + IL-6; (3) CRE; (4) CRE + IL-6; (5) KD; (6) KD + IL-6. Representative blot, n=2 from each genotype. pSTAT3 – 79/88 kDa; Loading Control: GAPDH – 37 kDa (Cell Signaling®).

Examination of the pSTAT3 Response to IL-6 in the Peripheral Tissue

Isolation of peripheral tissue from control and KD animals that were IP IL-6-treated prior to harvesting served to confirm that the effects of the transgenic were confined to the central nervous tissue. As mentioned, quantifying and comparing differences in receptor protein expression using a cytokine-binding-site-specific IL-6R antibody was not possible. Consequently this experiment allowed us on the one hand to test the ability of KD animals to respond to the cytokine peripherally and to compare those responses to control animals.

Figure 3.6.1: Liver Tissue pSTAT3 Responses to IP IL-6 (50µg/kg)

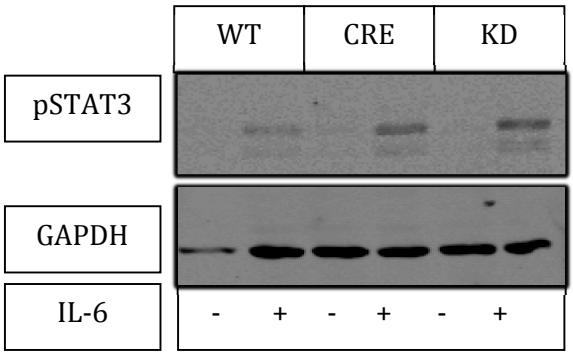

Figure 3.6.1: Adult male mice (>8weeks) from each genotype were used. Loading Order from left to right: (1) WT; (2) WT + IL-6; (3) CRE; (4) CRE + IL-6; (5) KD; (6) KD + IL-6. Representative blot, n=2 from each genotype. pSTAT3 – 79/88 kDa; Loading Control: GAPDH – 37 kDa (Cell Signaling®).

Our studies were aimed at elucidating the role of IL-6 signaling in the brain specifically in the whole body metabolic responses to chronic HFD. IL-6 has important roles in the hematopoietic system as well as in tissues involved in glucose uptake and utilization (fat, muscle, liver). The pivotal role played by the periphery in the long and short-term regulation of homeostasis and the influence of IL-6 in multi-organ cross talk involved, were highlighted in the **Introduction**. It was therefore important to confirm that any phenotype observed was not subject to non-specific recombination events in the periphery but was the consequence of disruption of central IL-6 signaling specifically.

Figure 3.6.2: Muscle pSTAT3 Responses to IP IL-6 (50µg/kg) injection

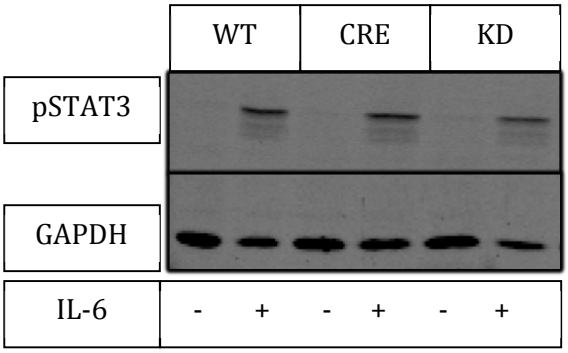

Figure 3.6.2: Adult male mice (>8weeks) from each genotype were used. Loading Order from left to right: (1) WT; (2) WT + IL-6; (3) CRE + IL-6; (4) CRE; (5) KD; (6) KD + IL-6. Representative blot, n=2 from each genotype. pSTAT3 – 79/88 kDa; Loading Control: GAPDH – 37 kDa (Cell Signaling®).

No differences were observed in the IL-6-induced induction of pSTAT3 in liver **(Figure 3.6.1),** muscle **(Figure 3.6.2)** or white adipose tissue **(Figure 3.6.3)** which is particularly important when considering the response to glucose as well as the short and long-term regulation of metabolism. KD animals examined were also found to respond similarly to control animals to IP IL-6 in the thermogenic brown adipose tissue **(Figures 3.6.4)**.

Figure 3.6.4: White Adipose Tissue pSTAT3 Responses to IP IL-6 (50µg/kg)

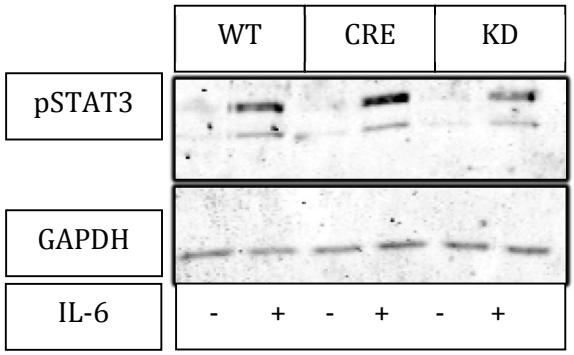

Figure 3.6.4: Adult male mice (>8weeks) from each genotype were used. Loading Order from left to right: (1) WT; (2) WT + IL-6; (3) CRE; (4) CRE + IL-6; (5) KD; (6) KD + IL-6. Representative blot, n=2 from each genotype. pSTAT3 – 79/88 kDa; Loading Control: GAPDH – 37 kDa (Cell Signaling®).

Figure 3.6.5: Brown Adipose Tissue pSTAT3 Responses to IP IL-6(50µg/kg)

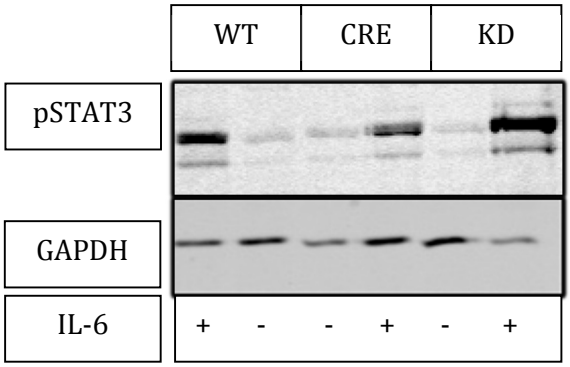

Figure 3.6.5: Adult male mice (>8weeks) from each genotype were used. Loading Order from left to right: (1) WT + IL-6; (2) WT; (3) CRE; (4) CRE + IL-6; (5) KD; (6) KD + IL-6. Representative blot, n=2 from each genotype. pSTAT3 – 79/88 kDa; Loading Control: GAPDH – 37 kDa (Cell Signaling®).

Another important aspect to be considered was the heart, as previous studies suggested scattered CRE recombination in the vasculature, ventricles and atria of the heart in some NesCre models (The Jackson Laboratory, 2014). However, as previously reported by Dubois et al. (2006) this expression is not sufficient for effective targeting of genes at cardiac tissue, which would match the minimal effects in the ability of cardiac tissue to respond to IP IL-6 in our transgenic **(Figure 3.6.6)**.

Figure 3.6.6: Cardiac Tissue pSTAT3 Responses to IP IL-6(50µg/kg)

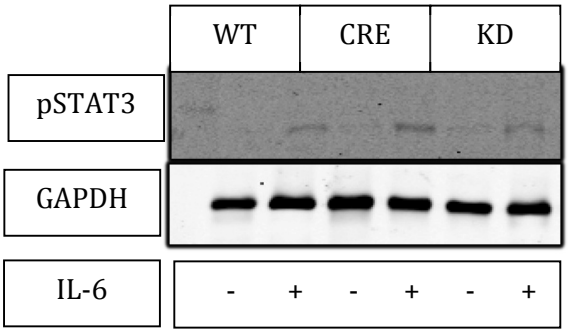

Figure 3.6.6: Adult male mice (>8weeks) from each genotype were used. Loading Order from left to right: (1) WT; (2) WT + IL-6; (3) CRE; (4) CRE + IL-6; (5) KD; (6) KD + IL-6. Representative blot, n=2 from each genotype. pSTAT3 – 79/88 kDa; Loading Control: GAPDH – 37 kDa (Cell Signaling®).

Nes-Cre mice were also previously suggested to exhibit some recombination at the level of the cytokine-producing spleen and some scattered expression in lung tissue (Dubois, et al., 2006). KD animals however can be seen to respond robustly to IP IL-6 in these tissues **(Figures 3.6.7-8)**, by comparable induction of pSTAT3 to WT and CRE controls.

Figure 3.6.7: Spleen pSTAT3 Responses to intra-peritoneal IL-6 (50µg/kg) injection

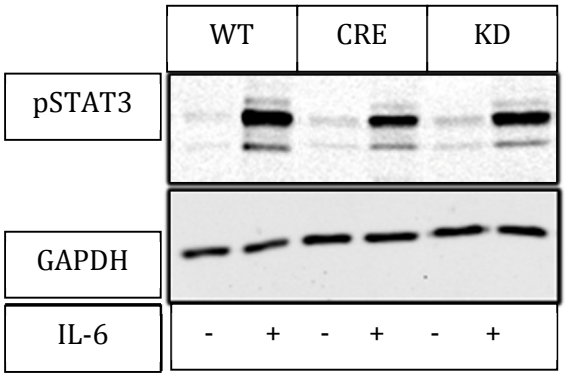

Figure 3.6.7: Adult male mice (>8weeks) from each genotype were used. Loading Order from left to right: (1) WT; (2) WT + IL-6; (3) CRE; (4) CRE + IL-6; (5) KD; (6) KD + IL-6. Representative blot, n=2 from each genotype. pSTAT3 – 79/88 kDa; Loading Control: GAPDH – 37 kDa (Cell Signaling®).

Scattered expression of CRE activity in the cortex, medulla and renal pelvis of some NesCre mice in studies carried by the Jackson laboratory (The Jackson Laboratory, 2014). Similar findings were reported by Dubois et al. (2006) using 3 different reporter genes. In our experiments we observed differences in the kidney pSTAT3 response to IP IL-6 between WT and NesCre-positive mice (CRE & KD). Despite being diminished compared to the responses observed in WT animals, CRE and KD responses appeared to be similar **(Figure 3.6.9)**. This finding further underlined the requirement for the use of CRE animals as an appropriate control for the KD.

Figure 3.6.8: Lung Tissue pSTAT3 Responses to IP IL-6 (50µg/kg)

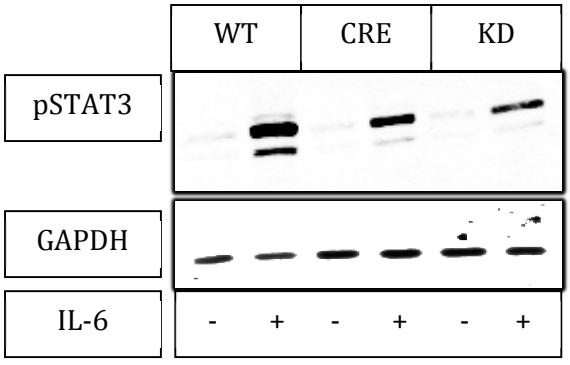

Figure 3.6.8: Adult male mice (>8weeks) from each genotype were used. Loading Order from left to right: (1) WT; (2) WT + IL-6; (3) CRE; (4) CRE + IL-6; (5) KD; (6) KD + IL-6. Representative blot, n=2 from each genotype. pSTAT3 – 79/88 kDa; Loading Control: GAPDH – 37 kDa (Cell Signaling®).

This section demonstrates that NesCreIL-6Rα KD animals respond to IP IL-6 by up-regulation of pSTAT3 in peripheral organs examined. Unlike results shown in regions of the brain, WT, CRE and KD animals examined remained sensitive to the effects of IL-6 in peripheral tissues (**Figures 3.6.1-9).** Even though this does not exclude the possibility of down-regulation of the receptor in innervated peripheral tissue, it was beyond our means to examine any such effects.

Figure 3.6.9: Kidney pSTAT3 Responses to IP IL-6 (50µg/kg) injection

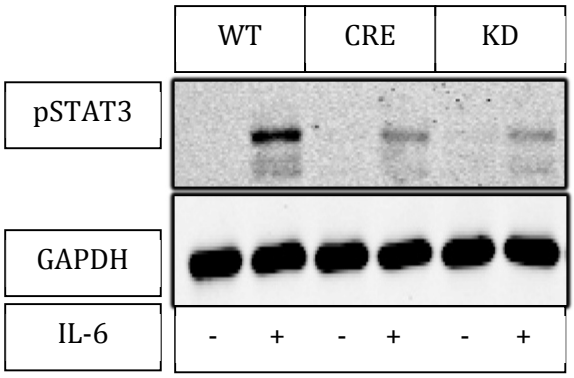

Figure 3.6.9: Adult male mice (>8weeks) from each genotype were used. Loading Order from left to right: (1) WT; (2) WT + IL-6; (3) CRE; (4) CRE + IL-6; (5) KD; (6) KD + IL-6. Representative blot, n=2 from each genotype. pSTAT3 – 79/88 kDa; Loading Control: GAPDH – 37 kDa (Cell Signaling®).

Examination of the ex vivo Hypothalamic Brain slice Response to IL-6

Examination of the effects of NesCre-mediated targeting of the IL-6Rα at mRNA level by RT-PCR and at protein level by IP IL-6 administration suggested significant effects at the level of the hypothalamus. To further assess whether the attempted transgenic approach was of functional consequence to the ability of hypothalamic tissue to respond to IL-6, an *ex vivo* approach was utilized. Ex vivo hypothalamic brain slice treatment, is a technique previously established in the Ashford laboratory to examine the acute responses of the mediobasal hypothalamus tissue to external stimuli. In preliminary studies carried out, tissue obtained and treated using this method was found to respond to an array of important stimuli such as glucose deprivation (0.1mM) in the presence of insulin (10μM). In this model glucoprivation was found to predictably induce AMPK, PKB and STAT3 phosphorylation (data not shown).

We thus proceeded to characterize the IL-6 response in the metabolically crucial mediobasal hypothalamus by examination of the change in phosphorylated STAT3 in *ex vivo* brain slices from control and KD animals. Brain slice tissue was processed and the magnitude of the IL-6 induced response was examined in terms of pSTAT3 by western blotting. Using the induction of STAT3 phosphorylation as an output measure, we were able to assess the ability of IL-6 signaling to influence metabolically active hypothalamus in control and KD animals. GAPDH protein was used as a control and statistical analysis of normalized control and IL-6 treated responses from each genotype (n=7) was carried out by using the Mann Whitney U-test. This allowed for non-parametric examination of the null hypothesis that brain slices from control and KD mice respond similarly to IL-6, against the alternative hypothesis that brain slices from control animals exhibit increased phosphorylation of STAT3 compared to KD slices.

Acute treatment (30min) of hypothalamic brain slices with 20ng/ml IL-6 in WT animals resulted in a significant up-regulation of pSTAT3 protein. By normalizing pSTAT3 to GAPDH we were able to semi-quantitatively assess this response in WT, CRE and KD IL-6 treated brain slices by comparing to suitable GAPDH-normalized genotype controls (unstimulated). IL-6 was found to induce a much more robust response in WT animals compared to both CRE and KD animals. IL-6 induced a significant ($p=0.0006$; $n=7$), induction in pSTAT3 in WT animals. Similarly, yet in

support of mRNA data suggesting diminished IL-6Rα expression in CRE animals; IL-6 treatment induced a significant (p=0.011; n=7), but more moderate induction in pSTAT3. On the other hand, in KD animals, this response failed to reach significance. In previous sections we were able to show down-regulation of hypothalamic IL-6Rα mRNA in KD animals compared to controls and similarly, decreases in the magnitude of the pSTAT3 response to IP IL-6 in a small number of animals examined. This section confirms the ability of IL-6 to influence metabolically active neurons and astrocytes in the arcuate hypothalamus of WT and CRE animals, and more importantly the disruption of this response in our NesCre-IL-6R KD.

Figure 3.7: Comparison of the effects of IL-6 (30min 20ng/ml) treatment to the induction of pSTAT3 protein in mouse hypothalamic *ex vivo* brain slices

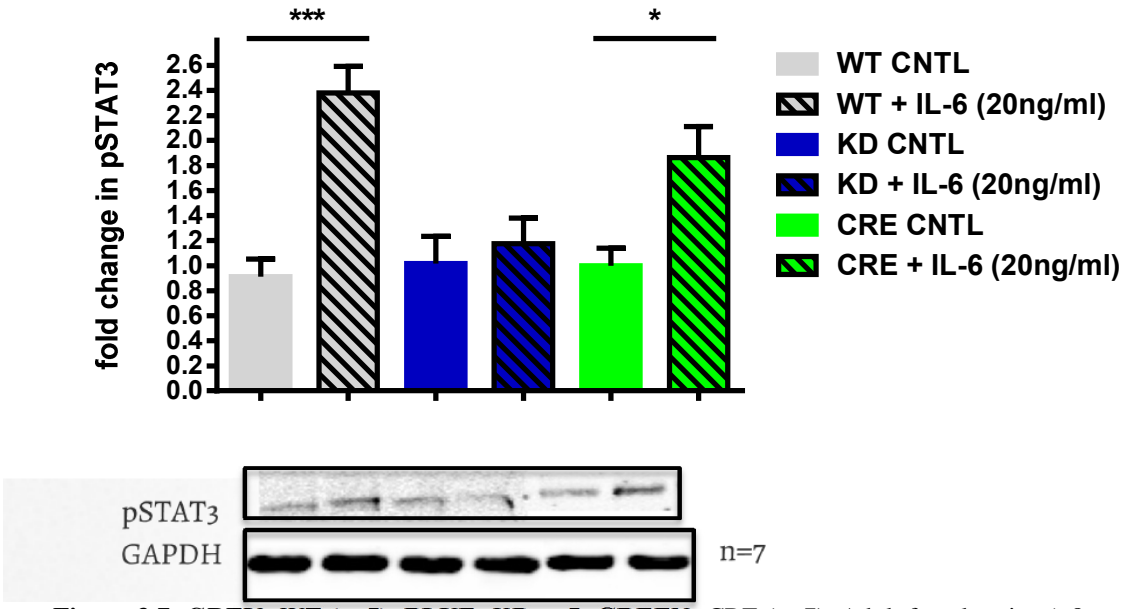

Figure 3.7: GREY: WT (n=7); **BLUE:** KD n=7; **GREEN:** CRE (n=7). Adult female mice (>8weeks) from each genotype were used. The expression of phosphorylated STAT3 protein was examined in WT, CRE and KD hypothalamic brain slices, under control conditions and following treatment with 20ng/ml IL-6. Representative western blotting bands for pSTAT3 and GAPDH under control conditions and following IL-6 treatment. Loading Order from left to right: (1) WT (2) WT +IL-6 (3) KD; (4) KD + IL-6; (5) CRE; (6) CRE + IL-6. Phospho-STAT3 expression was assayed by western blotting and quantified by densitometry with GAPDH as a loading control (Licor® Odyssey®). Statistical analysis of normalized data was carried out using the Mann Whitney U-test. IL-6 treatment promoted significant increases in pSTAT3 in relation to genotype controls in both WT (p=0.0006) and CRE (p=0.11) slices. This was not the case in KD mice, where pSTAT3 expression was largely unaffected by the treatment (p=0.6072).

Examination of Brain IL-6Rα Localization by Immunohistochemistry

IL-6Rα immunoreactivity and co-localization with neuronal and astrocytic markers was examined in frontal, hippocampal and hypothalamic brain slices from KD and control animals. Images shown in this section were captured using a Leica® TCS SP5 II microscope and subsequently analysed using the Volocity® Cellular Imaging and Analysis software (Perkin Elmer®) by Mrs. Alison Milne (Light Microscopy Facility School of Medicine, University of Dundee).

Figure 3.8.1: IL-6Rα Expression and co-localization with NeuN & GFAP in the Frontal Cortex

A - CRE **B - KD**

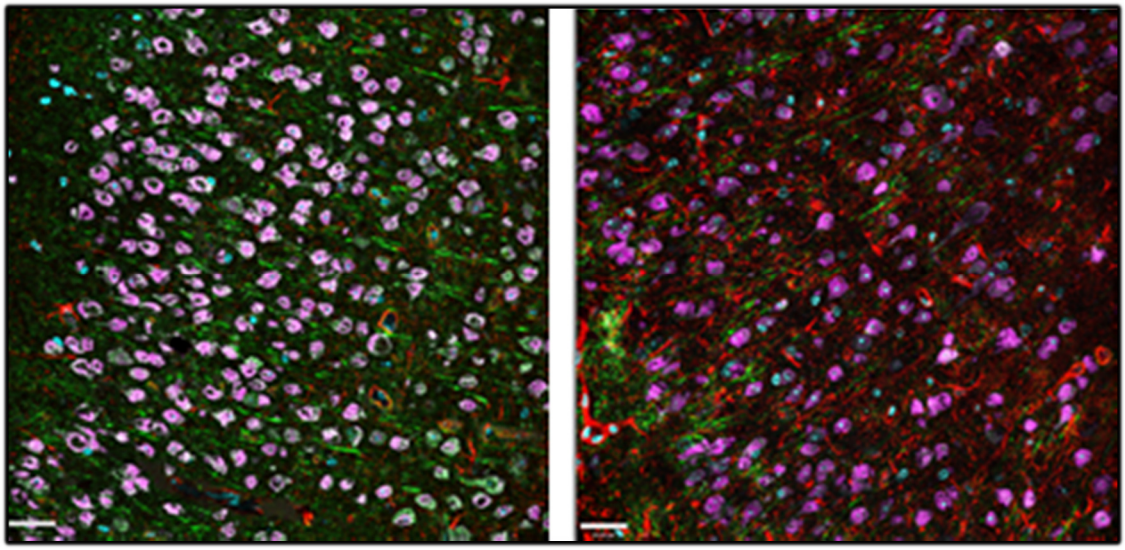

Blue: DAPI; Green: IL-6Rα; Pink: NeuN; Red: GFAP

C **D**

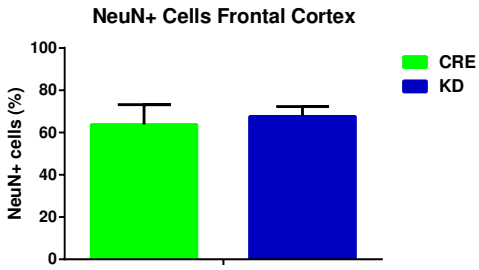

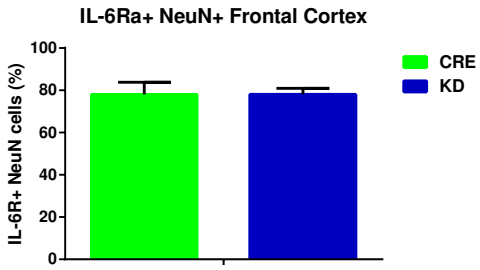

Figure 3.8.1: Adult (>8weeks) mice were used. Representative images from CRE and KD frontal cortex brain slices **(Figure 3.8.1A, B;** n=2**).** Similar numbers of NeuN+ nuclei were observed in area-matched slice from the CRE and KD frontal cortex **(Figure 3.8.1C;** CRE SC 63.7+/-9.5%, 466 cells; KD SC 67.6+/-4.7%, 383 cells). The percentage of IL-6 receptor-positive NeuN cells was not different between the 2 genotypes in examination using the Mann Whitney U-test **(Figure 3.8.1D;** CRE SC 77.9+/-5.7%; KD SC 78.0+/-2.9%; p>0.99).

Region-matched brain slices from KD and CRE mice were co-stained with antibodies for neuronal (NeuN) and astrocytic (GFAP) biomarkers, as well as IL-6Rα protein. Receptor expression was observed in both NeuN- and GFAP-positive cells in both control and KD brains **(Figure 3.8.1-3)**. However, co-localization was primarily detected in neuronal populations in both genotypes. Using manual cell counting we were able to calculate the percentage of IL-6 receptor-positive neurons in region-matched brain slices in KD and CRE mice (Bologna-Molina, et al., 2011).

Figure 3.8.2: IL-6Rα Expression and co-localization with NeuN & GFAP in the Hippocampus

A - CRE **B – KD**

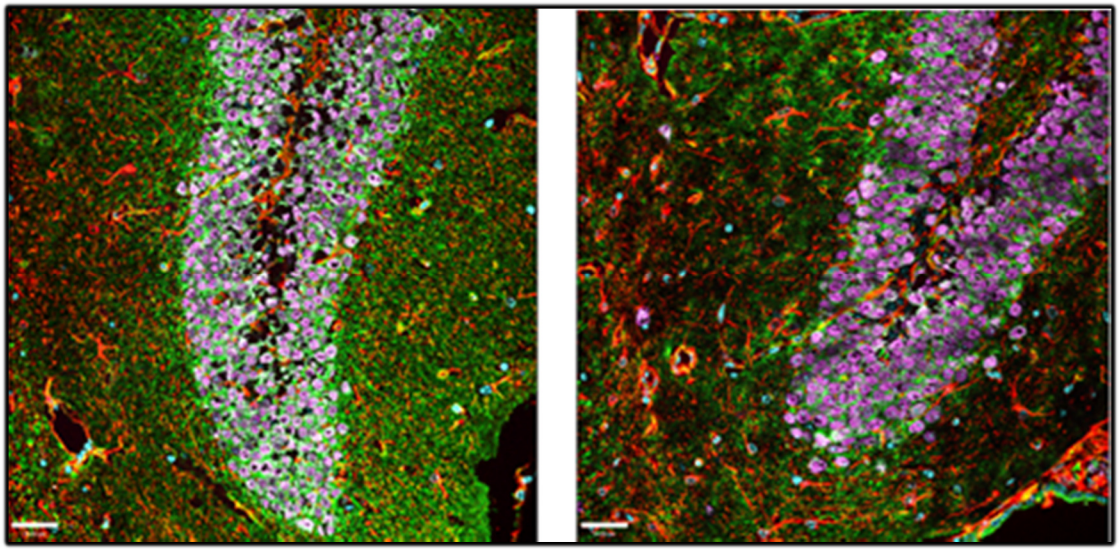

Blue: DAPI; Green: IL-6Rα; Pink: NeuN; Red: GFAP

C **D**

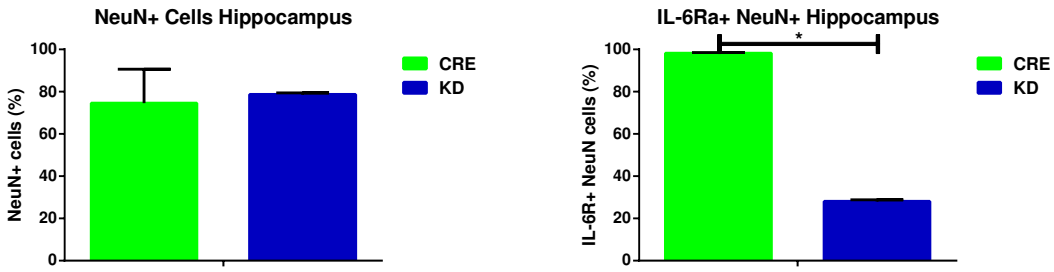

Figure 3.8.2: Adult (>8weeks) mice were used. Representative images from CRE and KD hippocampal brain slices **(Figure 3.8.2A, B;** n=2**).** The percentage of NeuN+ nuclei in area- and region-matched hippocampal slices was similar in KD and control animals **(Figure 3.8.2C;** CRE SC 74.5+/-16.2%, 616 cells; KD SC 78.6+/-0.8%%, 985 cells**)**. The percentage of IL-6 receptor-positive NeuN cells was decreased by more than 60% in the KD compared to control mice **(Figure 3.8.2D;** CRE SC 98.1+/-0.4%; KD SC 28.0+/-0.8%; p=0.0002**).**

Figure 3.8.3: IL-6Rα Expression and co-localization with NeuN & GFAP in the Hypothalamus

A - CRE **B - KD**

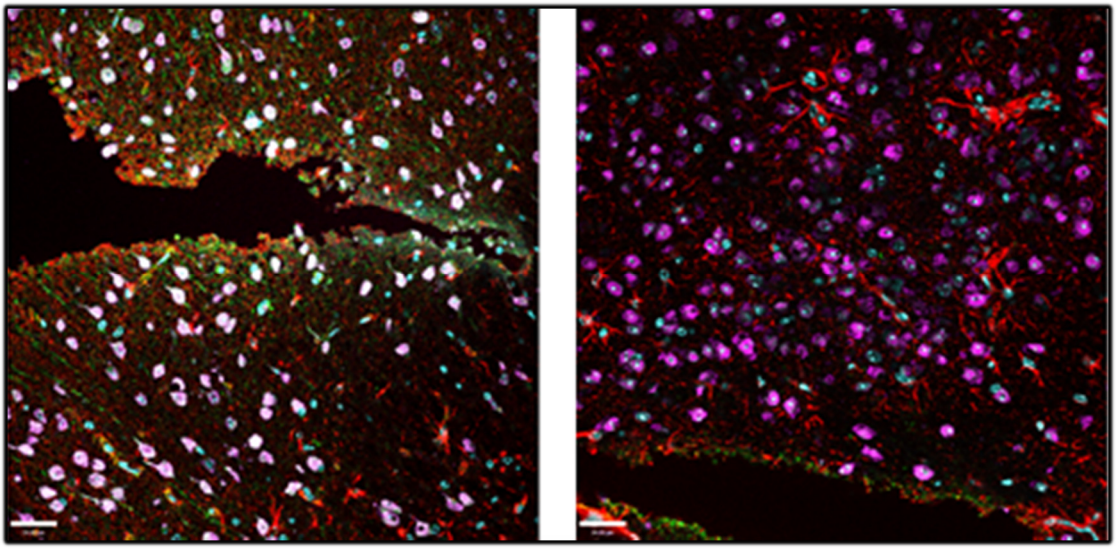

Blue: DAPI; Green: IL-6Rα; Pink: NeuN; Red: GFAP

C **D**

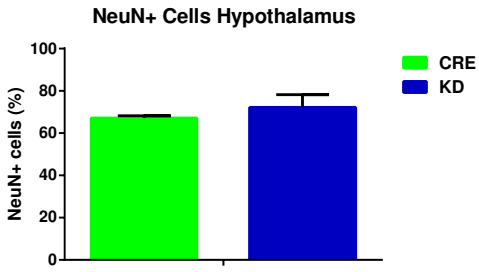

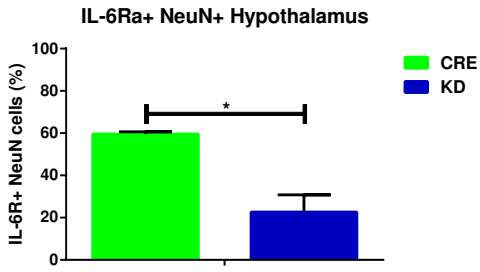

Figure 3.8.3: Adult (>8weeks) mice were used. Representative images from CRE and KD hippocampal brain slices **(Figure 3.8.3A, B;** =2**).** The percentage of NeuN+ nuclei in hypothalamic slices from KD and control animals was similar **(Figure 3.8.3C;** CRE SC 67.0+/-1.2%, 376 cells; KD SC 72.0+/-6.2%%, 386 cells**).** Approximately 60% of NeuN+ cells identified were also IL-6Rα-positive in control slices. Significant decreases were observed in KD mice, were less than 30% of NeuN cells were IL-6Rα-positive **(Figure 3.8.3D;** CRE SC 59.5+/-1.0%; KD SC 22.5+/-8.2%; p=0.0046**).**

Statistical analysis of cell counting data was carried out using the Mann Whitney U-test. This allowed for non-parametric examination of the null hypothesis that IL-6Rα protein expression in neuronal cells (stained using NeuN) was similar in the brain of KD and control animals, against the alternative hypothesis that control animals exhibit increased receptor protein in neurons compared to the KDs. The percentage of

IL-6Rα positive neurons was decreased in the KD hippocampus (p=0.0002) and hypothalamus (p=0.0046), but not the frontal cortex. This matched previous findings obtained by real-time PCR **(Figure 3.4.2).**

To further examine the effects of NesCre-mediated IL-6Rα down-regulation in neurons and astrocytes, and to resolve any possible doubt regarding the quality of staining intensity and co-localization imaging data were analysed using the Volocity® Imaging and Analysis software (Barlow, et al., 2010). This allowed for quantification of the co-localization of the receptor with neuronal (NeuN) and astrocytic (GFAP) markers **(Figure 3.8.4)**.

Figure 3.8.4: Pearson's Correlation Coefficient for Brain IL-6Rα co-localization with NeuN and GFAP

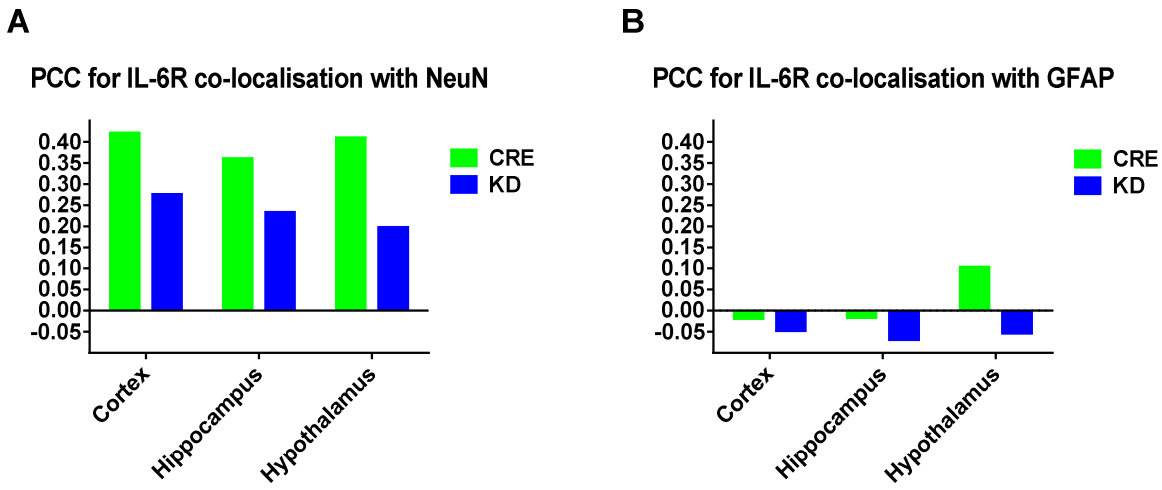

Figure 3.8.4: Adult female mice (>8weeks) from each genotype were used (n=2). Pearson's Correlation Co-efficient (PCC) was calculated for the IL-6Rα with neuronal NeuN and astrocytic GFAP from region-matched images from each genotype. **PCC IL-6Rα/NeuN:** Frontal Cortex: CRE 0.421, KD 0.275; Hippocampus: CRE 0.36, KD 0.232; Hypothalamus: CRE 0.409, KD 0.197. **PCC IL-6Rα/GFAP:** Frontal Cortex: CRE -0.018, KD -0.047; Hippocampus: CRE -0.016, KD -0.068; Hypothalamus: CRE 0.103, KD -0.053.

Recent studies suggest that calculation of a thresholded Pearson's correlation coefficient (PCC) using only intensity values over a determined threshold in relevant channels produces numerical values that more accurately describe biological protein expression relationships. PCC is a statistical analysis designed to measure the strength of a linear relationship between 2 variables, such as fluorescent intensities from images. The Volocity ® software subtracts the mean pixel intensity of an image from the intensity of each pixel within the image, generating a product of the difference from the mean that is summed for the entire dataset and divided by the maximum

possible sum of the product of the differences from the mean (Alder, et al., 2008). PCC generates a range of values, with +1 representing a perfect positive correlation, to -1, representing a perfect negative correlation, while 0 represents a random distribution. This method was used to further probe the validity of the receptor down-regulation achieved in neuronal and astrocytic cells through computerized assessment of co-localization intensities of the IL-6Rα signal in relation to NeuN and GFAP while avoiding observer bias and variability often associated with cell counting methods (Matos, et al., 2006; Barlow, et al., 2010).

A weak positive correlation was observed between NeuN and IL-6Rα in control animals, which was decreased the KD brain across all regions examined. There was no correlation between astrocytic GFAP and the IL-6Rα in Frontal Cortex and Hippocampus of control and KD animals. However in the hypothalamus, a weak positive correlation reported in CRE animals was contrasted by a weak negative correlation in the KD. The small number of animals used in these experiments was a limitation. It was however beyond our current means to further elaborate our studies. Results in this section are consistent with previous reports suggesting NesCre floxed mice to exhibit primarily neuronal but also astrocytic Cre recombinase activity. Further studies would be required to outline the precise contributions of astrocytes and metabolically active neuronal populations to the phenotype.

Summary

Chapter 3 served to confirm the brain specific down-regulation of the IL-6Rα in NesCreIL-6Rα KD compared to control animals. The expression of CRE recombinase and the incorporation of loxP sites for the receptor were initially confirmed by PCR **(Figures 3.2-3)**. Brain-specific disruption of the IL-6Rα system in the brain was demonstrated using in vivo **(Figures 3.5, 3.6)** and ex vivo **(Figures 3.7**) approaches, as well as using real-time PCR (**Figure 3.4)** and immunohistochemistry **(Figures 3.8)**. Furthermore, results in this section indicated CRE and not WT mice to be the appropriate control group for the NesCreIL-6Rα KD mouse. Importantly, down-regulation of the receptor system was confirmed in the metabolically-sensing hypothalamus, even though further studies would be required to outline the effects on individual neuronal and glial populations. Research over past years has consistently shown chronic high-fat feeding to activate pro-inflammatory pathways and related stress signaling in the rodent hypothalamus, promoting DIO and metabolic disease (Zhang, et al., 2008; Purkayastha, et al., 2011; Cai & Liu, 2011). To assess the role of central IL-6 signaling in the development of DIO and Type 2 Diabetes, KD and CRE mice were metabolically characterized over a period of 20 weeks on standard chow and high-fat-diet **(Chapter 4)**.

Table 4: NesCreIL-6Rα KD Characterization

METHOD	OUTCOME
Real Time PCR	↓*Il-6ra* mRNA compared to CRE controls • 35% in the hippocampus • 50% in the hypothalamus
In vivo IP IL-6 (50µg/kg) Administration	No effect in IL-6 induced increase in STAT3 phosphorylation in: • Heart • Kidney • Liver • Lung • Muscle • Spleen • Brown Adipose Tissue • White Adipose Tissue Disruption of IL-6 induced increase in STAT3 phosphorylation in: • Hypothalamus • Hippocampus
Ex vivo treatment of mediobasal hypothalamic slice tissue with IL-6 (20ng/ml)	Unlike hypothalamic brain slices from control animals; IL-6 failed to induce a significant increase in STAT3 phosphorylation in KD slices.
Brain Immunohistochemistry	↓IL-6Rα protein expression in NeuN+ cells compared to CRE controls in: • Hippocampus • Hypothalamus

Chapter 4: Metabolic Phenotyping of NesCre-IL-6Rα KD mice

As shown in **Chapter 3** the novel NesCreIL-6Rα$^{flox/flox}$ (KD) mouse exhibits CNS-specific disruption of the cytokine receptor in relation to control animals. In order to evaluate the role of central IL-6 signaling in the development of diet-induced obesity diabetes, a small cohort of age (8-10weeks old) - and male KD animals on SC and HFD for a total period of 20 weeks, during which they were subject to an array of metabolic phenotyping tests as outlined below. Multivariate analysis of variance was carried out to assess hypotheses regarding the effect of one or more independent variables such as diet and genotype on the parameter under examination at single time points or over time (IBM SPSS 21®). Additionally metabolic parameters governing energy expenditure were examined using the CLAMS® Animal Monitoring System prior to tissue harvest. CRE animals were used as the control group for both the SC and HFD study. Results from WT animals examined are presented in **Appendix A.**

Table 5: Schematic Outline of 20-Week Study Plan

PROCEDURE	SYMBOL
Weighting	
EchoMRI Body Composition Evaluation	
Oral Glucose Tolerance Test	
Intra-peritoneal Insulin Tolerance Test	
Food Intake	
Oral Glucose Stimulated Insulin Secretion	

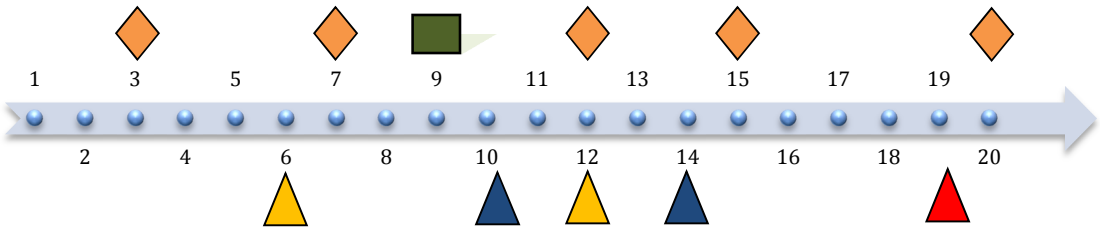

Body Weight Progression

CRE and KD on SC mice exhibited minimal weight gain over the 20-week study period (**Figure 4.1**). HF-fed animals, experienced dramatic increases in weight gain compared to SC controls ($p<0.0001$), gaining 2g of body weight/week during the first 6 weeks. Body weight gain was subsequently reduced and maintained to 1g/week until the end of the study. Brain-specific down-regulation of the IL-6 receptor failed to exert an effect on weight gain progression observed in both SC and HF-fed KDs compared to control animals ($p=0.272$).

Figure 4.1: Mean Weight Gain during the 20-week Study Plan

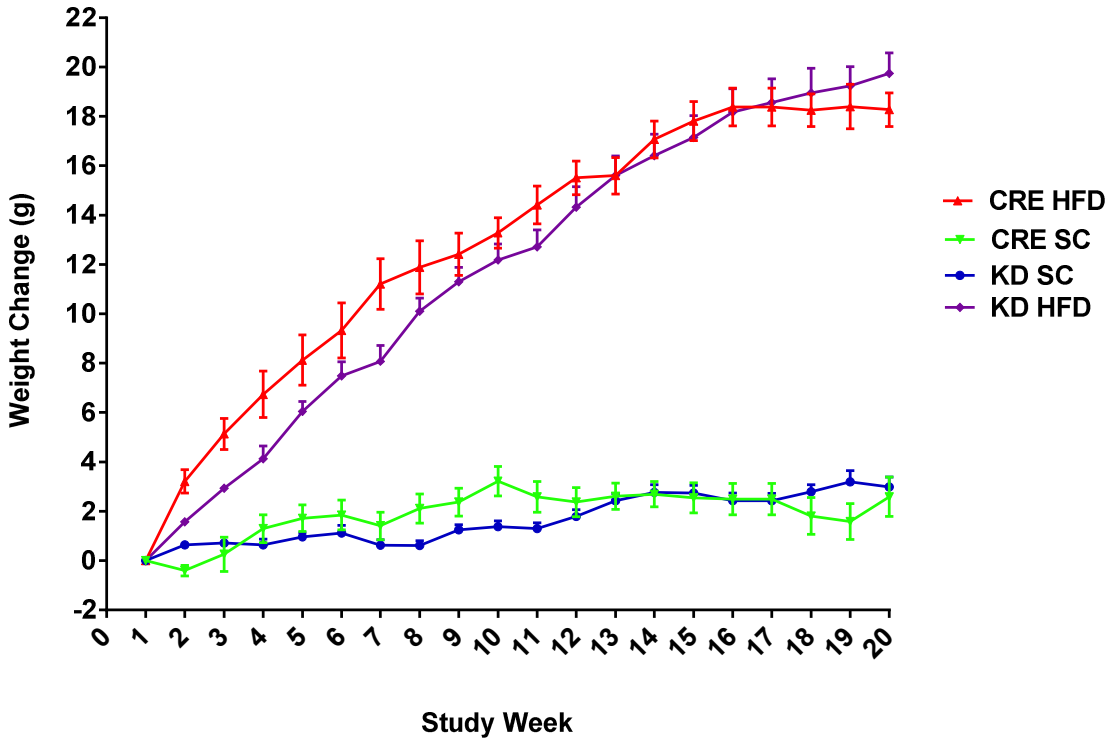

Figure 4.1: GREEN: CRE SC (n=9); **BLUE:** KD SC (n=9); **RED:** CRE HFD (n=7); **PURPLE:** KD HFD (n=11). Mean weight gain in CRE (1.9+/-0.2g; n=8) and KD SC (1.9+/-0.2g; n=9) animals was closely matched over the course of the study. Diet predictably induced significant increases in mean body weight gain in both KD (13.0+/-1.4g; n=11) and CRE (13.3+/-1.1g; n=7) HF-fed mice compared to SC controls ($p<0.0001$). No differences were apparent between the 2 genotypes in this response, and multivariate analysis (IBM SPSS 21®) indicated no significant effect of genotype ($p=0.272$) or the interaction between diet and genotype ($p=0.454$) on the body weight gain observed during the study.

Body Composition

The body composition of experimental animals was periodically examined during the course of the study by means of the Echo MRI™ system in accordance with the study plan described **(Table 4)**. This allowed for investigation of differences in percentage lean and fat body mass of CRE and KD animals on SC and HFD. Body composition data obtained through the course of the study (Study Weeks 3, 7, 15 and 20) were analysed by MANOVA (IBM SPSS® 21). Comparison of body composition at individual time points was carried out by 1-way ANOVA.

Figure 4.2.1: Body Composition at Week 3 of the Study

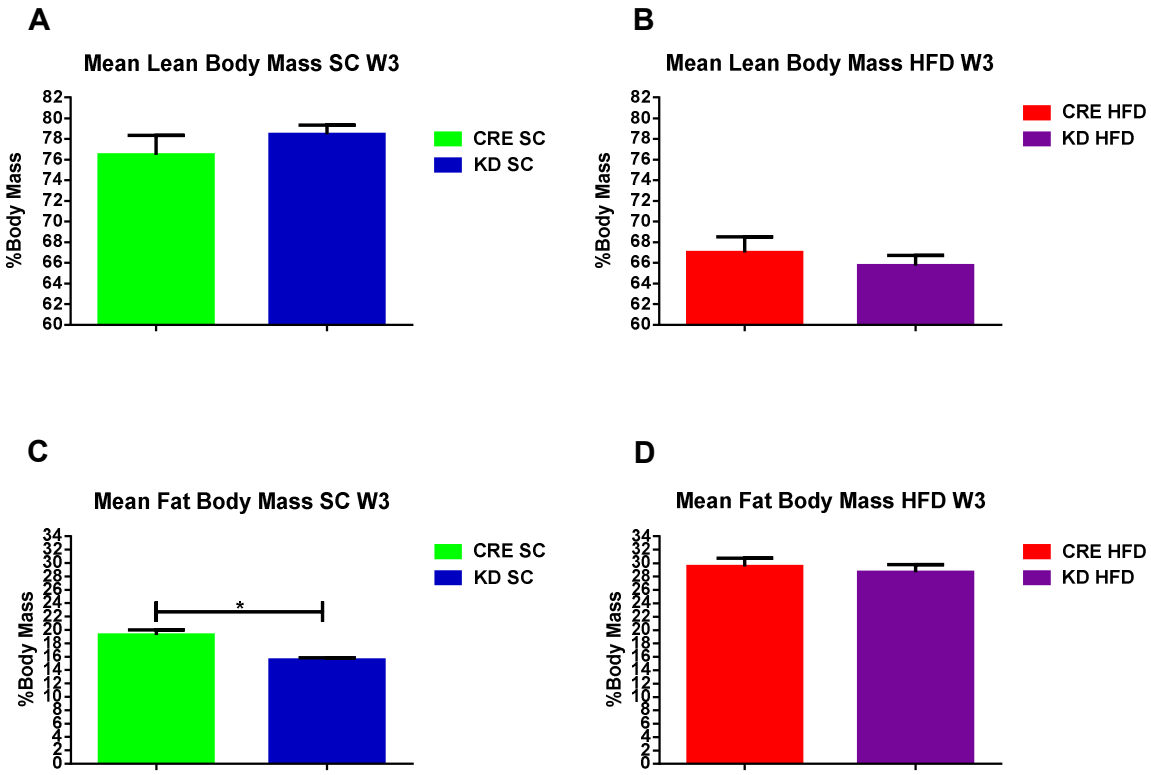

Figure 4.2.1: GREEN: CRE SC (n=9); **BLUE:** KD SC (n=9); **RED:** CRE HFD (n=7); **PURPLE:** KD HFD (n=11). KD SC mice exhibited decreased percentage body fat mass compared to CRE controls **(Figure 4.2.1C;** CRE SC 19.22+/-0.80%, n=9; KD SC 15.51+/-0.34%, n=9; p=0.001), even though no significant differences in percentage lean body were apparent between the 2 groups **(Figure 4.2.1A;** CRE 76.46+/-1.9%, n=9; KD SC 78.44+/-0.90%, n=9; p>0.99). A 10% increase in mean percentage body fat was evident across both groups following 3 weeks of HFD. No significant differences were observed between KD and control HF-fed animals in percentage lean **(Figure 4.2.1B;** CRE 65.73+/-0.99%, n=8; KD HFD 66.9922 +/-1.5214%, n=11; p=0.2052) or fat body mass at this point of the study (**Figure 4.2.1D;** CRE 29.51 +/-1.22%, n=8; KD HFD 28.62+/-1.1791%, n=11; p>0.99).

Analysis of between-subject factors indicated a significant effect of diet in the variance observed in lean ($p<0.0001$, $F=828.53$) and fat ($p<0.0001$, $F=1670.84$) composition recorded over the course of the study. Furthermore, significant differences in the percentage lean ($p<0.0001$, $F=16.32$) and fat ($p<0.0001$, $F=30.56$) body mass of the two genotypes. The interaction of genotype and diet also exerted a significant effect in the variance observed in lean ($p=0.001$, $F=15.00$) and fat ($p<0.0001$, $F=38.77$) body composition of experimental animals.

Figure 4.2.2: Body Composition at Week 7 of the Study

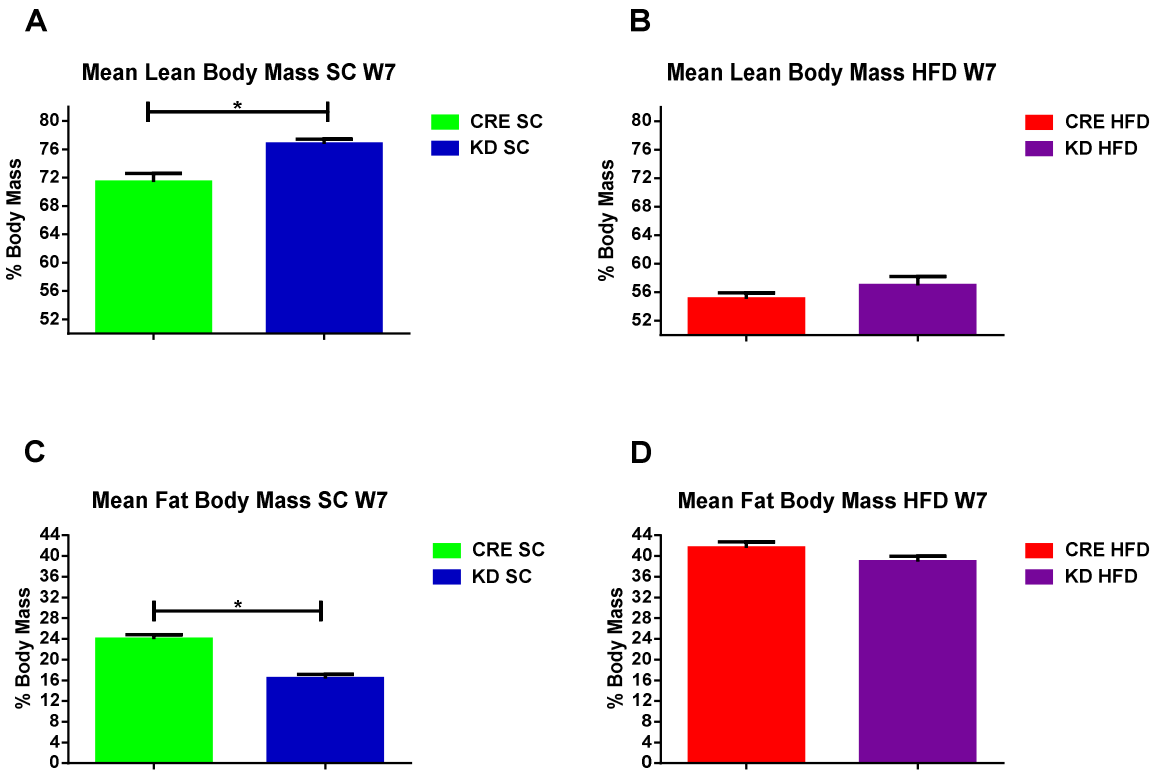

Figure 4.2.2: GREEN: CRE SC (n=9); **BLUE:** KD SC (n=9); **RED:** CRE HFD (n=7); **PURPLE:** KD HFD (n=11). KD SC mice continued to exhibit a leaner phenotype compared to control animals, and significant differences in both percentage lean (**Figure 4.2.2A;** CRE 71.41+/-1.18%; n=8; KD 76.77+/-0.65%, n=9; p=0.0293) and fat (**Figure 4.2.2C;** CRE 23.98+/-0.84%; n=8; KD 16.36+/-0.80%, n=9; p=0.007) body mass were observed at week 7 of the study. A 20% increase in body adiposity was observed in both HF-fed groups compared to SC mice at Week 7. This represented a further 10% increase since Week 3, however percentage lean (**Figure 4.2.2B;** CRE HFD 55.07% +/-0.87, n=7; KD HFD 56.98 +/-1.25 %, n=11; p=0.6572) and fat (**Figure 4.2.2D;** CRE HFD 41.56 +/-1.19%, n=7; KD HFD 38.89 +/-1.05%, n=11; p=0.31) body mass was not significantly different between the 2 groups.

KD SC mice displayed a significantly leaner phenotype compared to control animals at the beginning of the study (Week 3 - **Figure 4.2.1**). Despite the lack of differences in terms of body weight, this effect that was maintained throughout the course of the

20-week study plan (**Figure 4.1**). Percentage body fat was stable in SC animals during the study, and negligible fluctuations were observed at weeks 7, 12, 15 and 20. KD SC percentage body fat was around 18% for the remainder of the study, by contrast to a 25% observed in CRE SC mice (**Figure 4.2**).

Figure 4.2.3: Body Composition at Week 12 of the Study

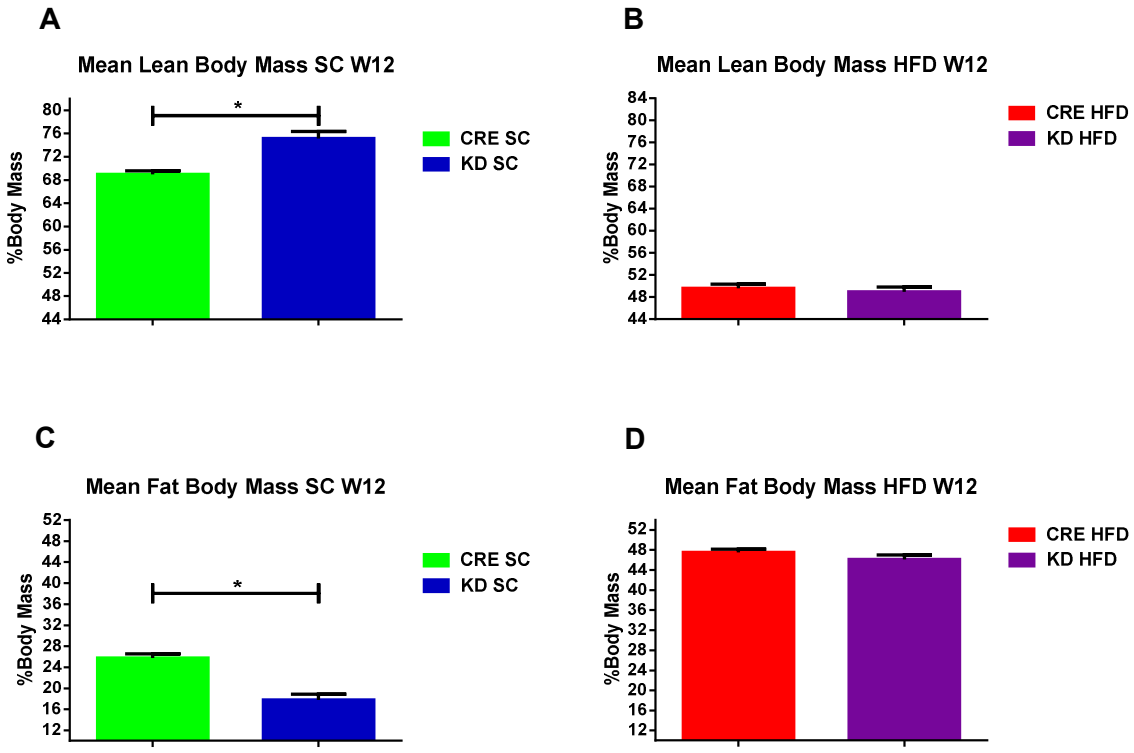

Figure 4.2.3: GREEN: CRE SC (n=9); **BLUE:** KD SC (n=9); **RED:** CRE HFD (n=7); **PURPLE:** KD HFD (n=11). The leaner phenotype observed in KD SC compared to CRE SC at Weeks 3 and 7 were preserved at Week 12 of the study. KD SC mice continued to exhibit decreased percentage body fat mass (**Figure 4.2.3C;** CRE SC 25.74+/-0.79%, n=9; KD SC 17.78 +/-1.10%, n=9; p=0.0074) and increased percentage lean body mass (**Figure 4.2.3A;** CRE SC 68.98+/-0.64%, n=9; KD SC 75.14+/-1.22%, n=9; p=0.014) compared to their controls. HF-mice mice on the other hand, exhibited a 5% increase in percentage body fat between Weeks 7 and 12, reaching 45%. CRE and KD HFD animals were nearly identical in terms of both percentage lean (**Figure 4.2.3B**; CRE HFD 49.61+/-0.75%, n=7; KD HFD 48.98+/-0.87%, n=11; p>0.99) and fat (**Figure 4.2.3D**; CRE HFD 47.48+/-0.69%, n=7; KD HFD 46.14+/-0.82%, n=7; p>0.99) body mass following 12 weeks of diet.

Three weeks of HFD induced a 10% increase in percentage body fat in both control and KD animals compared to SC animals. CRE and KD HFD percentage body fat increased to approx. 30% and significant differences in body composition observed in KD SC animals were not observed (**Figure 4.2.1B, D**). KD HFD mice closely

matched CRE HFD animals in body composition following 3 and 7 weeks of diet **(Figure 4.2.2B, D)**, where body adiposity further increased to nearly 40% of total body mass.

Figure 4.2.4: Body Composition at Week 15 of the Study

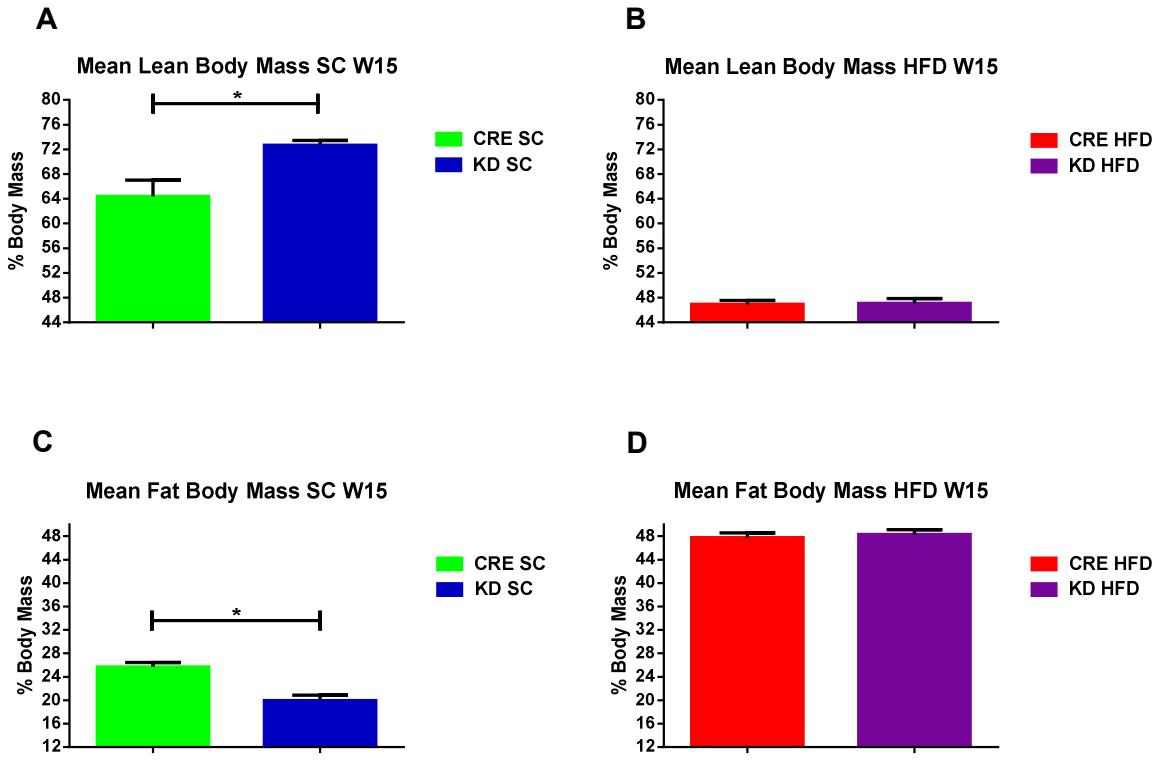

Figure 4.2.4: GREEN: CRE SC (n=9); **BLUE:** KD SC (n=9); **RED:** CRE HFD (n=7); **PURPLE:** KD HFD (n=11). Significant differences observed between KD SC and control animals in terms of percentage fat **(Figure 4.2.4C;** CRE SC 25.74+/-0.79%, n=9; KD SC 17.78+/-1.10%, n=9; p=0.002) and lean **(Figure 4.2.4A;** CRE SC 64.40+/-2.60%, n=9; KD SC 72.67+/-0.76%, n=9; p=0.001) body mass were still evident at Week 15. Similarly matching results from Week 12, KD and CRE HFD mice were identical in terms of both lean **(Figure 4.2.4B;** CRE HFD 46.93+/-0.64%, n=7; KD HFD 47.11+/-0.77%, n=11; p>0.99) and fat **(Figure 4.2.4D;** CRE HFD 47.75+/-0.81%, n=7; KD HFD 48.31+/-0.78, n=11; p>0.99) body composition. Body fat accounted for approximately 47% of total body mass in HF-fed mice following 15 weeks of diet.

Body adiposity continued to increase in HF-fed mice between Weeks 7 and 12, albeit at a slower rate. Body fat accounted for approximately 45% of total body mass in KD and CRE HFD mice, a further 5% increase from Week 7 **(Figure 4.2.2-3)**. KD HFD and control mice were nearly identical in body composition and no significant differences were observed between the 2 groups in percentage lean or fat body mass at Week 12 of the Study **(Figure 4.2.3)**.

Figure 4.2.5: Body Composition at Week 20 of the Study

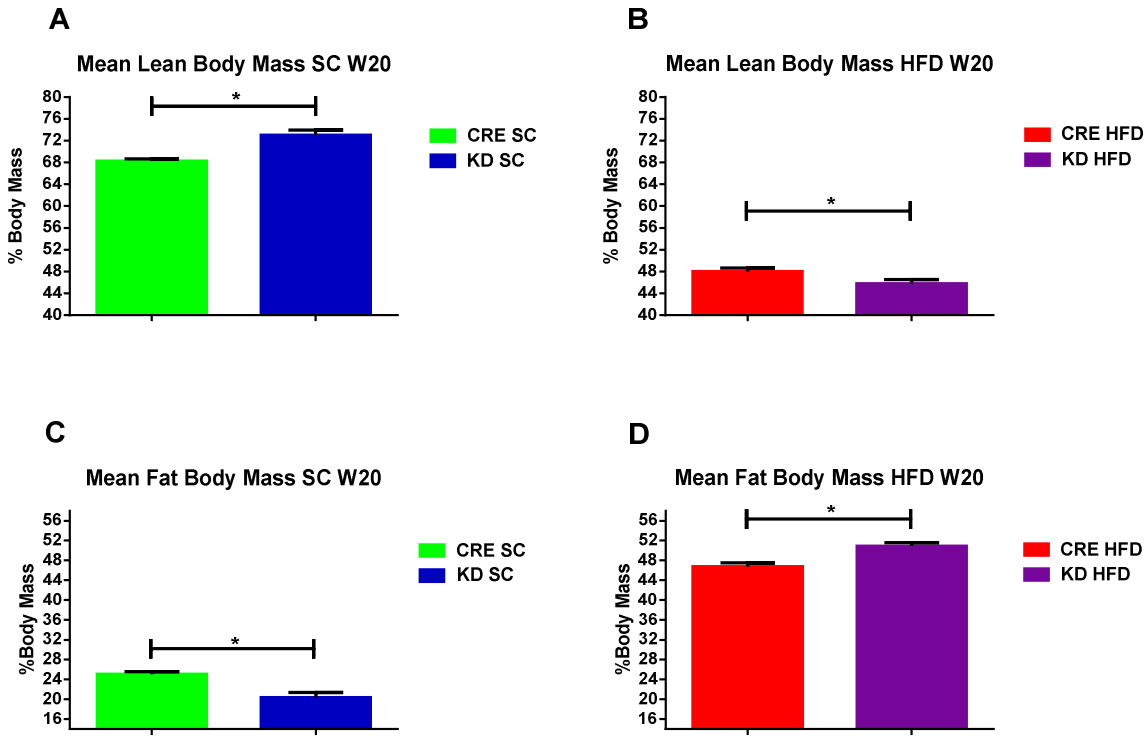

Figure 4.2.5: GREEN: CRE SC (n=9); **BLUE:** KD SC (n=9); **RED:** CRE HFD (n=7); **PURPLE:** KD HFD (n=11). Increases in mean percentage body fat mass were observed in KD SC mice at Week 20 compared to Week 15 of the Study. Despite this, percentage body fat (**Figure 4.2.5C;** CRE SC 25.03+/-0.52%, n=9; KD SC 20.35+/-1.02%, n=9; p=0.03) remained decreased and percentage lean body mass (**Figure 4.2.5A;** CRE SC 68.24+/-0.45%, n=9; KD SC 72.99+/-0.95%; p=0.002) still increased compared to CRE SC mice. By stark contrast, percentage body fat mass in CRE HFD was significantly decreased compared to KD HFD mice after 20 weeks of diet (**Figure 4.2.5D;** CRE HFD 46.78+/-0.75%, n=9; KD HFD 50.91+/-0.64%, n=11; p=0.04). Differences observed in percentage lean body mass failed to reach significance (**Figure 4.2.5B;** CRE HFD (48.00 +/-0.64%, n=7; KD HFD 45. 75 +/-0.80%, n=11; p=0.36).

Between Weeks 12 and 15 of the study, body composition in CRE and KD HFD was largely unchanged (**Figure 4.2.3-4**). CRE HFD percentage body fat was around 47% at Week 12 and marginal fluctuations were observed on examination at Weeks 15 and 20 of the study (**Figures 4.2.3-5**). KD HFD percentage body fat mass increased to approx. 51% between Weeks 15 and 20, and significant differences were observed in between the 2 groups at the end of the study (**Figure 4.2.5B, D**).

Daily Food Intake

The daily food intake of experimental animals was evaluated on Week 9 of the study plan. Mice on SC and HFD were housed individually overnight, and food intake measurements were taken on the subsequent day at 4, 8 and 24 hours. Statistical analysis was conducted using a 1-way ANOVA (SPSS®).

Figure 4.3: Examination of Daily Food Intake at Week 9 of the Study

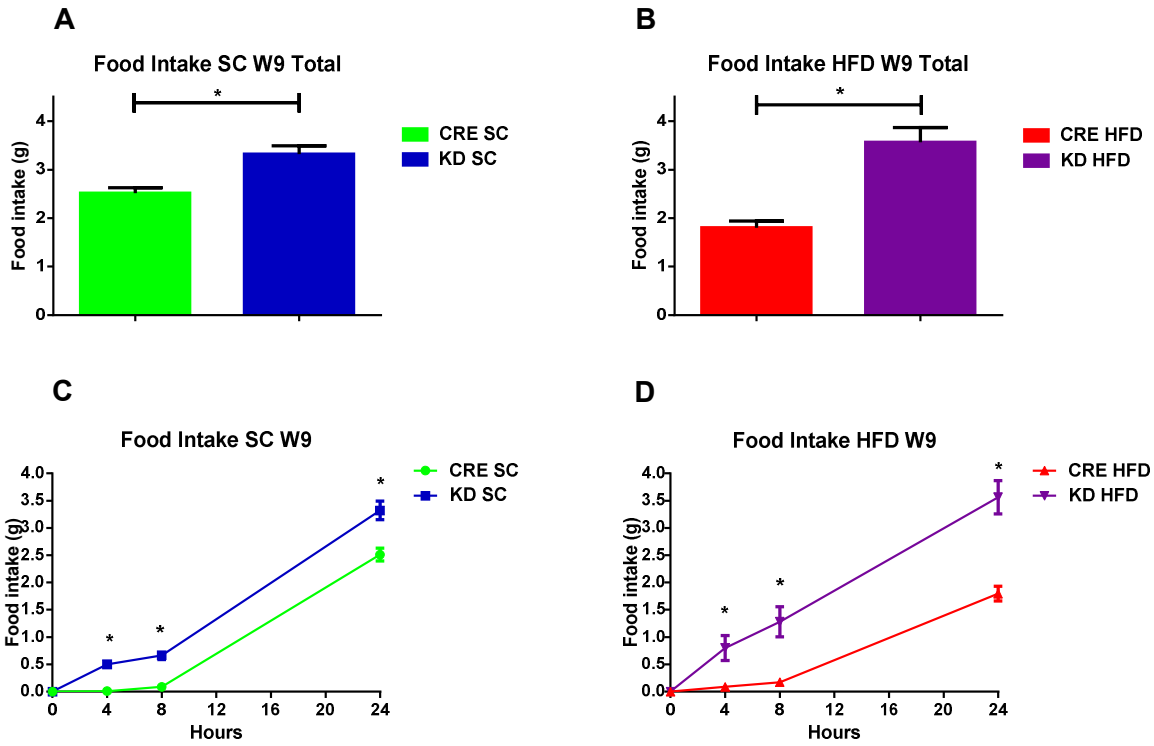

Figure 4.3: GREEN: CRE SC (n=9); **BLUE:** KD SC (n=9); **RED:** CRE HFD (n=7); **PURPLE:** KD HFD (n=11). Consistent with the anorexic effects of central IL-6 signaling, total food intake was significantly increased in KD compared to CRE SC mice (**Figure 4.3A**; CRE SC 2.5+/-0.1g, n=9; KD SC 3.3+/-0.2g, n=9; p=0.03). Increased food intake was also observed in KD mice at 4hours (**Figure 4.3C;** CRE SC 0.0g; KD SC 0.5+/-0.1g; p<0.0001) and 8hours (**Figure 4.3C;** CRE SC 0.0g; KD SC 0.7+/-0.1g; p<0.0001). Matching the trend observed in SC groups, the total food intake of KD HFD animals was nearly double compared to control animals and significant differences were observed (**Figure 4.3B**, CRE HFD 1.8+/-0.1g, n=7; KD HFD 3.6+/-0.3g, n=11; p<0.001). Correspondingly statistical analysis confirmed a significant effect of genotype on the food intake of mice on HFD at 4hours (**Figure 4.3D;** CRE HFD 0.1+/0.1g; KD HFD 0.8+/-0.2g; p=0.019) and 8hours (**Figure 4.3D;** CRE HFD 0.2+/-0.1g; KD HFD 1.3+/-0.3g; p=0.004).

Mice are nocturnal animals and thus the large majority of activity and food intake takes place at night. Indeed, more than 90% of food intake in CRE mice on SC and

HFD was recorded over the latter part of the protocol (8-24hours). This relationship was disrupted in KD mice, even though the greater part of food intake was still observed overnight. Significant increases were detected in the KD SC food intake at 4hours ($p<0.0001$) and 8hours ($p<0.0001$) of the protocol, where eating was negligible in control animals **(Figures 4.3C, D)**. This effect was accentuated in KD HFD mice (n=11) where 40% of the food intake was recorded within the first third of the protocol. Similarly significant differences were observed in the food intake of KD and CRE HFD mice at 4 ($p=0.019$) and 8 hours ($p=0.004$). Total food intake through the 24hour period was also significantly increased in both the SC ($p=0.003$) and HF-fed ($p<0.0001$) KD mice compared to their respective controls **(Figure 4.3A, B)**.

Intra-Peritoneal Insulin Tolerance Test

The responsiveness of experimental animals to the effects of intra-peritoneal injection of insulin (1U/kg body mass) was examined at 6, 9 and 15 weeks of the experimental study, following a 4 hours fast**.** Exogenous administration of insulin via this route is known to acutely reduce circulating blood glucose levels in mammals. Statistical analysis of Insulin Tolerance Tests (ITT) was carried out by MANOVA (IBM SPSS 21®). Blood glucose responses from experimental animals were tabulated as a function of time from administration of insulin, while genotype (CRE or KD) and diet (SC or HFD) were set as between-subject variables. Additionally, baseline glycaemia was assessed in experimental animals on SC and HFD, and statistical analysis was carried out using a 2-way ANOVA.

The ability of SC animals to respond to IP insulin was unaffected by the course of the study, and blood glucose in KD and control mice was indeed reduced following insulin administration at 3 different time points during the study **(Figures 4.4.1-3).** Down-regulation of the IL-6Rα in the CNS of KD animals was of little consequence to the ability of the transgenic to respond to insulin. Blood glucose responses to insulin in KD SC and HFD mice were indistinguishable compared to control animals at Week 6 of the study **(Figure 4.4.1A, B**– ITT1). Statistical analysis of the blood glucose response to ITT1 in KD and CRE mice over the course of 90minutes, revealed no significant effect of genotype ($p=0.11$). Furthermore, blood glucose during ITT1 in KD and CRE HFD mice was similar to SC controls and statistical

analysis indicated no significant effect of diet (p=0.16) or the interaction of diet and genotype (p=0.06) in the response.

Figure 4.4.1: ITT1 at Week 6 of the Study

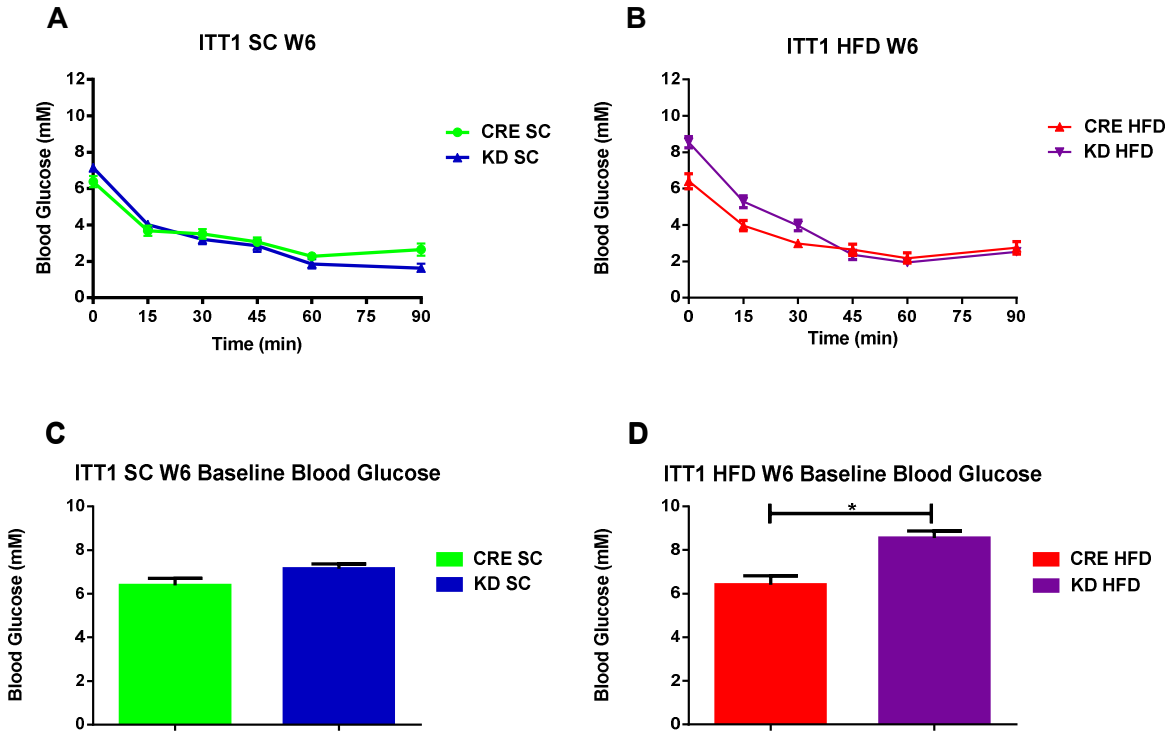

Figure 4.4.1: GREEN: CRE SC (n=9); **BLUE:** KD SC (n=9); **RED:** CRE HFD (n=7); **PURPLE:** KD HFD (n=11). Results were plotted as means +/-SEM. Statistical analysis of between-subject factors, indicated no significant effect of genotype (p=0.11, F=2.73) in the variance observed. KD and CRE SC blood glucose responses during ITT1 were nearly identical **(Figure 4.4.1A)**. Diet failed to exert a significant effect on the blood glucose response to ITT following 6 weeks of HF-feeding, despite differences between SC and HFD mice **(Figure 4.4.1B;** p=0.16, F=2.05**)**. The interaction of genotype and diet was not statistically significant (p=0.06, F=3.8), even though marginal differences were observed between the KD and CRE HFD response. On the other hand, diet (p=0.0035, F=4.84), genotype (p<0.001, F=20.28) and their interaction (p=0.04, F=4.54) exerted a significant effect on baseline glycaemia as indicated by 2-way ANOVA. Blood glucose at rest was similar in KD and CRE SC mice **(Figure 4.4.1C** CRE SC 6.4 +/-0.3 mM Glucose, n=8; KD SC 7.2 +/-0.2 mM Glucose, n=9; p=0.15). KD HFD mice exhibited significant increases compared to SC groups following 6 weeks of diet (p=0.002), but this was not the case for the CRE HFD (p>0.99) and significant differences were observed between the 2 HF-fed groups **(Figure 2.4.1D;** CRE HFD 6.4 +/-0.4 mM Glucose; n=7; KD HFD 8.5545 +/-0.3123 mM Glucose, n=11; p=0.002**)**.

Comparison of baseline glycaemia in control and KD animals at Week 6 **(Figure 4.4.1C, D)** indicated a significant effect of genotype (p<0.001, F=20.28), diet (p=0.0035, F=4.84), and their interaction in the variance observed (p=0.04, F=4.54). KD and CRE SC blood glucose levels were nearly identical and no significant

differences were identified at this point (p=0.37). Blood glucose at rest in CRE HFD mice was not statistically different to CRE SC mice (p>0.99), by contrast to KD HFD animals where significant increases were observed compared to both KD SC (p=0.02) and CRE HFD mice (p=0.002).

Figure 4.4.2: ITT2 at Week 9 of the Study

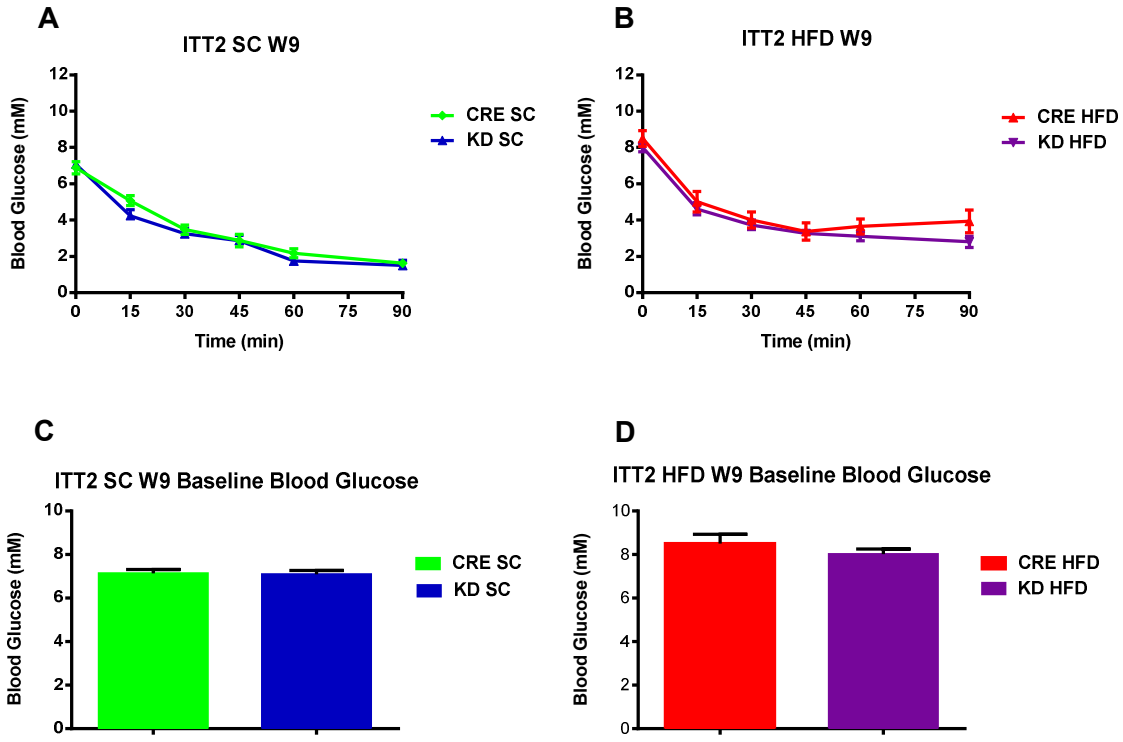

Figure 4.4.2: GREEN: CRE SC (n=9); **BLUE:** KD SC (n=9); **RED:** CRE HFD (n=7); **PURPLE:** KD HFD (n=11). Results were plotted as means +/-SEM. No significant effect of genotype (p=0.5, F=0.47) was reported in statistical analysis of variance observed in the blood glucose response of KD and CRE mice to ITT2. Blood glucose responses to ITT2 at Week 9 in KD SC mice mirrored results in control mice **(Figure 4.4.2A)**. Nine weeks of high fat feeding failed to exert a significant effect on the blood glucose response to ITT2, despite differences between SC and HFD mice **(Figure 4.4.2B;** p=0.11, F=2.76). There was no significant interaction of genotype and diet (p=0.57, F=0.33), reflected in the closely matched blood glucose profiles of KD and CRE HFD mice. Statistical examination of resting glycaemia at week 9 indicated a significant effect of diet (p<0.001, F=20.20), but not of genotype (p=0.15, F=2.22) or their interaction (p=0.75, F=0.09) in the variance observed. Blood glucose at rest was similar in SC mice **(Figure 4.4.2C** CRE SC 7.1+/-0.2 mM Glucose, n=9; KD SC 7.0+/-0.2 mM Glucose, n=9; p=0.96) and comparable increases were recorded KD (p=0.02) and CRE HFD (p0.007) mice in response to diet **(Figure 4.4.2D** CRE HFD 8.5+/-0.4 mM Glucose, n=7; KD HFD 8.0+/-0.2 mM Glucose, n=9; p=0.72).

Baseline glycaemia in KD mice at Study Week 9 paralleled levels observed in SC and HFD controls **(Figure 4.4.2C, D;** p=0.15, F=2.22). Significant increases were observed in HF-fed mice compared to SC groups (p<0.001, F=20.20), but there was

no significant interaction of genotype and diet (p=0.75, F=0.09) in the variance observed. Likewise, there was no significant differences between KD and control mice during ITT2 (p=0.5, F=0.47), while blood glucose responses were largely unaffected by diet **(Figure 4.4.2A, B;** p=0.5, F=0.47**)**.

Figure 4.4.3: ITT3 at Week 15 of the Study

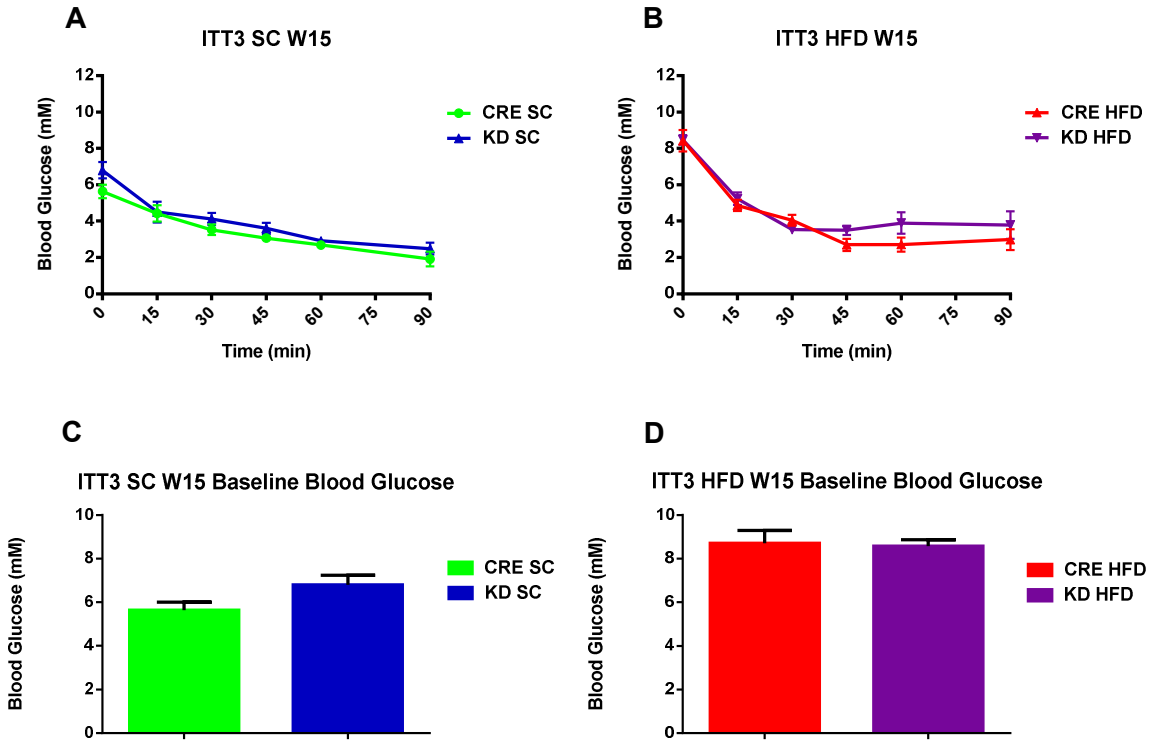

Figure 4.4.3: GREEN: CRE SC (n=9); **BLUE:** KD SC (n=9); **RED:** CRE HFD (n=7); **PURPLE:** KD HFD (n=11). Results were plotted as means +/-SEM. Significant differences were observed between SC and HF-fed mice in the blood glucose response to ITT at Study Week 15 (p=0.03, F=5.38). However, blood glucose responses to ITT3 in KD mice on SC **(Figure 4.4.3A)** and HFD **(Figure 4.4.3B)** were similar to their respective controls. Matching results in ITT1&2 statistical analysis of ITT3 indicated no significant differences between KD and CRE mice (p=0.41, F=0.72), and no significant interaction between genotype and diet (p=0.71, F=0.14). Resting blood glucose levels observed in KD mice at week 15 were not different to their CRE controls (p=0.23, F=1.151). Significant differences in resting blood glucose were maintained between SC **(Figure 4.4.3C;** CRE SC 5.6+/0.4mM Glucose; KD SC 6.8+/-0.4mM Glucose) and HF-fed **(Figure 4.4.3D;** CRE HFD 8.7+/-0.6mM Glucose; KD HFD 8.6+/-0.3mM Glucose) mice at week 15 of the study (p<0.0001, F=33.62). There was no significant interaction of diet and genotype in the variation observed (p=0.13, F=2.39).

Increases observed in the resting blood glucose of HF-fed compared to SC mice were maintained on examination at Study week 15 **(Figure 4.4.3C, D;** p<0.0001, F=33.62**)**. Furthermore, significant differences were reported in the blood glucose response of SC and HF-fed mice to ITT3 **(Figure 4.4.3A, B;** p=0.03, F=5.38). However,

differences observed at baseline and during ITT3 in KD and CRE mice failed to reach significance.

Collectively, KD blood glucose responses to ITT1-3 were not different to control mice on SC or HFD during the course of the study. Differences observed between SC and HFD groups only reached significance at Study week 15. Importantly even though CRE HFD baseline glycaemia was similar to SC groups at week 6, KD HFD exhibited hyperglycaemia compared to all 3 groups. Hyperglycaemia was observed in both CRE and KD HFD compared to SC animals on subsequent examination at weeks 9 and 15.

Oral Glucose Tolerance Test and Glucose-Stimulated Insulin Secretion

To further assess the ability of experimental animals to regulate glycaemic levels, glycaemic levels in response to oral administration of a standard dose of 100µl of a 50% glucose solution (oGTT) was examined at weeks 10 and 14. Resting and glucose-stimulated blood glucose responses were recorded over 120min. A modified protocol was used at Study week 19 to examine changes in circulating blood hormones. Results were analyzed using repeated measures MANOVA (IBM SPSS 21®). Blood glucose levels recorded during oGTT were tabulated as a function of time from administration of glucose with genotype (CRE or KD) and diet (SC or HFD) set as between-subject variables. Additionally, baseline glycaemic levels recorded prior to the challenge were analyzed separately by 2-way ANOVA.

The ability of the body to regulate glycaemic levels is an important component of current diabetic therapy, and good glycaemic management is understood to reduce associated complications and morbidity (Voiqt, et al., 2015; Healy & Dungan, 2015; Aronoff, et al., 2004). Significant differences were observed in the ability of KD and CRE mice to clear glucose on examination at Study Week 10 ($p=0.005$, $F=9.98$). Blood glucose in response to the challenge was significantly elevated in KD mice compared to controls on both SC and HFD. Additionally, analysis of the influence of between-subject factors in the variance observed, revealed a significant effect of diet ($p<0.0001$, $F=40.33$), but no significant interaction of genotype and diet ($p=0.17$, $F=1.996$). On the other hand, significant differences observed in baseline glycaemia between SC and HF-fed mice at Study Week 10, were not accompanied by differences between KD and CRE animals.

Figure 4.5.1: oGTT1 at Week 10 of the Study

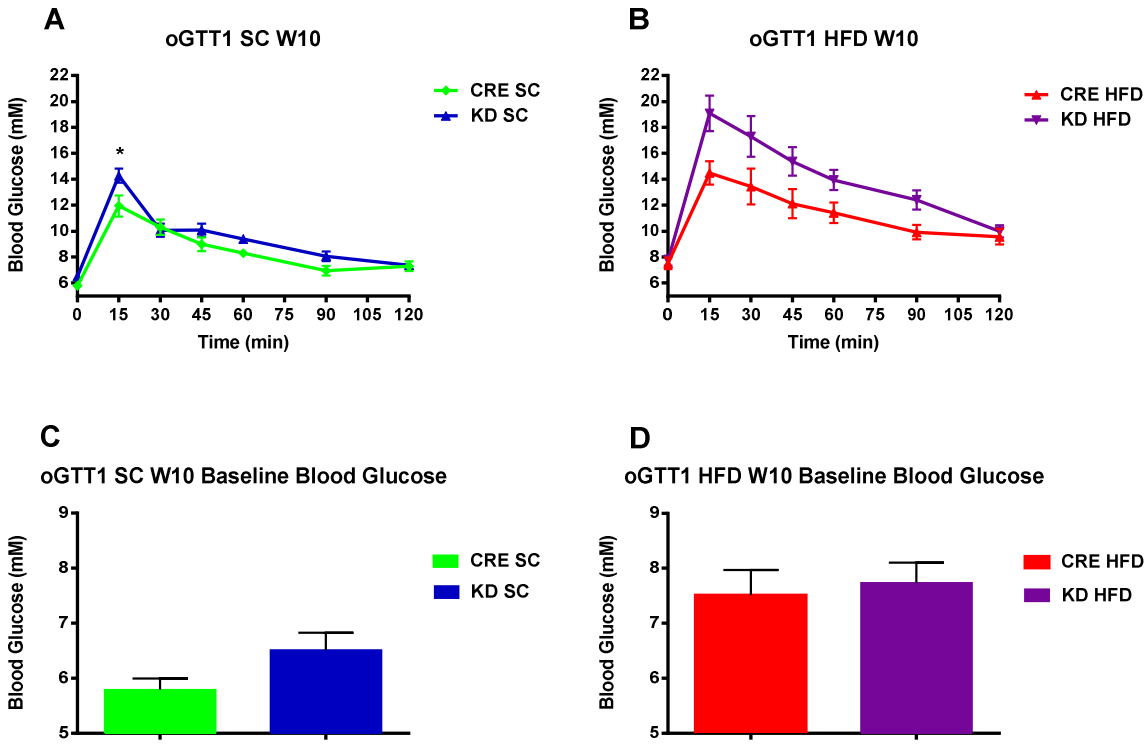

Figure 4.5.1: GREEN: CRE SC (n=9); **BLUE:** KD SC (n=9); **RED:** CRE HFD (n=7); **PURPLE:** KD HFD (n=11). Results were plotted as means +/-SEM. Statistical analysis of oGTT1 at Study Week 10 revealed significant differences between KD and CRE responses (p=0.005, F=9.98), while a significant differences were also observed between SC and HF-fed (p<0.0001, F=40.33). However, the interaction between the two did not reach significance at this point (p=0.17, F=1.996). Significant increases were observed in the baseline glycaemia of HF-fed mice compared to SC (p=0.0003, F=17.22), however there was no significant effect of genotype (p=0.2, F=1.74), or the interaction of diet and genotype (p=0.48, F=0.51) in the variance observed. Baseline glucose levels were similar in KD and CRE SC animals **(Figure 4.5.1C;** CRE SC 5.8+/-0.2mM; KD SC 6.5 +/-0.3mM; p=0.73), however the mean acute (15min) response to oGTT1, revealed a deficit in glucose clearance in the KD SC compared to CRE controls **(Figure 4.5.1A;** CRE SC 11.9+/-0.8mM; 14.3+/-0.5Mm; p=0.0003). Similarly, despite the lack of differences at baseline **(Figure 4.5.1D;** CRE HFD 7.5+/-0.5mM; KD HFD 7.7+/-0.4Mm; p>0.99), KD HFD exhibited marginal differences in glucose clearance compared to CRE HFD mice at 15minutes of oGTT1 **(Figure 4.5.1B;** CRE HFD 14.4875 +/-0.9054mM Glucose; KD HFD 19.1+/-1.4mM Glucose).

Significant differences observed in the blood glucose response to oGTT1 of KD and CRE mice were not maintained when re-examined at Study Week 15 **(Figure 4.5.2;** p=0.08, F=0.09). In contrast, significant differences observed in the glucose clearance of HF-fed and SC mice in oGTT1 were still evident at Study Week15 **(Figure 4.5.2A, B;** p>0.0001, F=30.99**)**. Mean resting blood glucose levels at Study week 14 paralleled results obtained at week 10. Baseline glycaemia prior to oGTT2 was not

different between KD and CRE mice **(Figure 4.5.2C, D;** p=0.11, F=2.68), while significant increases were observed in both HF-fed groups compared to SC animals (p<0.0001, F=31.06).

Figure 4.5.2: oGTT2 at Week 14 of the Study

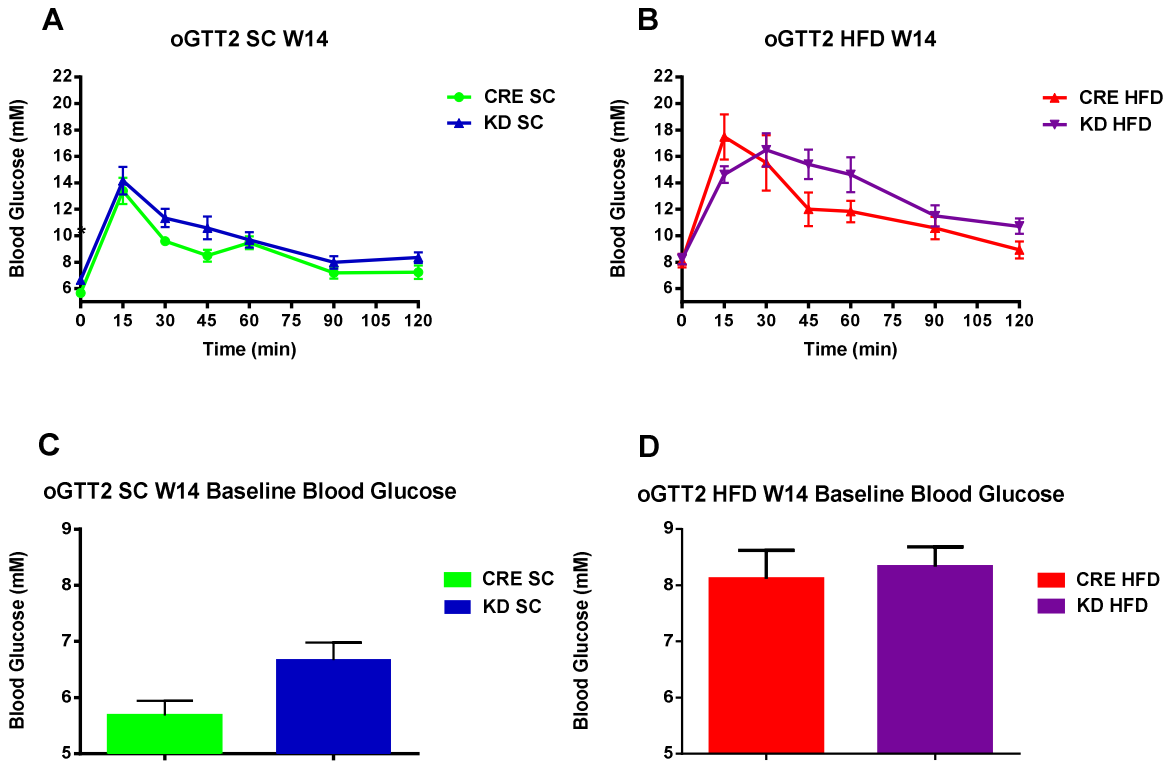

Figure 4.5.2: GREEN: CRE SC (n=9); **BLUE:** KD SC (n=9); **RED:** CRE HFD (n=7); **PURPLE:** KD HFD (n=11). Results were plotted as means +/-SEM. **Figure 4.5.2A, B**: Differences observed between KD and control animals in the failed to reach significance by MANOVA (p=0.08, F=3.23).Glucose clearance in HFD groups was disrupted compared to SC mice (p<0.0001, F=30.99). No significant effect of the interaction of genotype and diet in the variance observed (p=0.94, F=0.005). **Figure 2.5.2C, D:** Glucose levels recorded were significantly elevated (p<0.0001, F=31.06) in HFD **(Figure 4.5.2D;** CRE HFD 8.1+/-0.5mM Glucose; KD HFD 8.3+/-0.4mM Glucose) compared to SC **(Figure 4.5.2C;** CRE SC 5.7+/-0.3mM Glucose; KD SC 6.7+/-0.3mM Glucose) mice, but differences observed between the two genotypes failed to reach significance (p=0.11, F=2.68).

During the modified oGTT protocol used at week 19, larger blood volume was collected from experimental animals at smaller intervals over 30minutes**.** This allowed for examination of changes in circulating plasma insulin (GSIS) and glucagon levels in response to an oral glucose challenge in experimental animals.

Correspondingly to results from Study Weeks 10 and 14, there was no significant effect of genotype (p=0.91; F=0.01) or its interaction with diet (p=0.37, F=0.84) in the

variance observed in resting blood glucose levels at Week 19 **(Figure 4.5.3C, D)**. Baseline glycaemia was significantly increased in both groups on HFD compared to SC mice, and statistical analysis confirmed a significant effect of diet ($p<0.0001$, $F=32.97$). Conversely, glycaemia during oGTT3 was significantly increased in KD mice compared to diet-matched controls **(Figure 4.5.3A, B;** $p<0.0001$, $F=25.97$**)**, while aggravated hyperglycaemia in HF-fed mice underscored the influence of diet in the response ($p<0.0001$; $F=23.58$). Hyperglycaemia compared to diet-matched controls was maintained throughout oGTT3 in KD mice. Blood glucose responses to oGTT3 peaked at 15min in CRE mice, but this was not the case in the KD where further increases were observed at 30min.

Examination of plasma insulin levels during oGTT3 (oGSIS), revealed a substantial deficit in the ability of SC and HFD KDs to release insulin in response to glucose loading **(Figure 4.5.4)**. Analysis of the variance observed in GSIS confirmed significant differences between KD and CRE mice KD animals ($p=0.049$; $F=4.40$). Chronic HF-feeding induced increases in baseline and GSIS compared to SC mice, indicative of the significant effect of diet in the response ($p=0.009$, $F=8.44$). Increases observed in plasma insulin levels in control mice during GSIS were suppressed in KD animals. KD SC mice exhibited severe disruption of basal as well as glucose-stimulated insulin secretion throughout the protocol **(Figure 4.5.4A)**. Baseline plasma insulin levels were similar in KD and CRE HFD; however administration of glucose failed to promote increases in plasma insulin in KD mice **(Figure 4.5.4B)**.

Figure 4.5.3: Modified oGTT3 at Week 19 of the Study

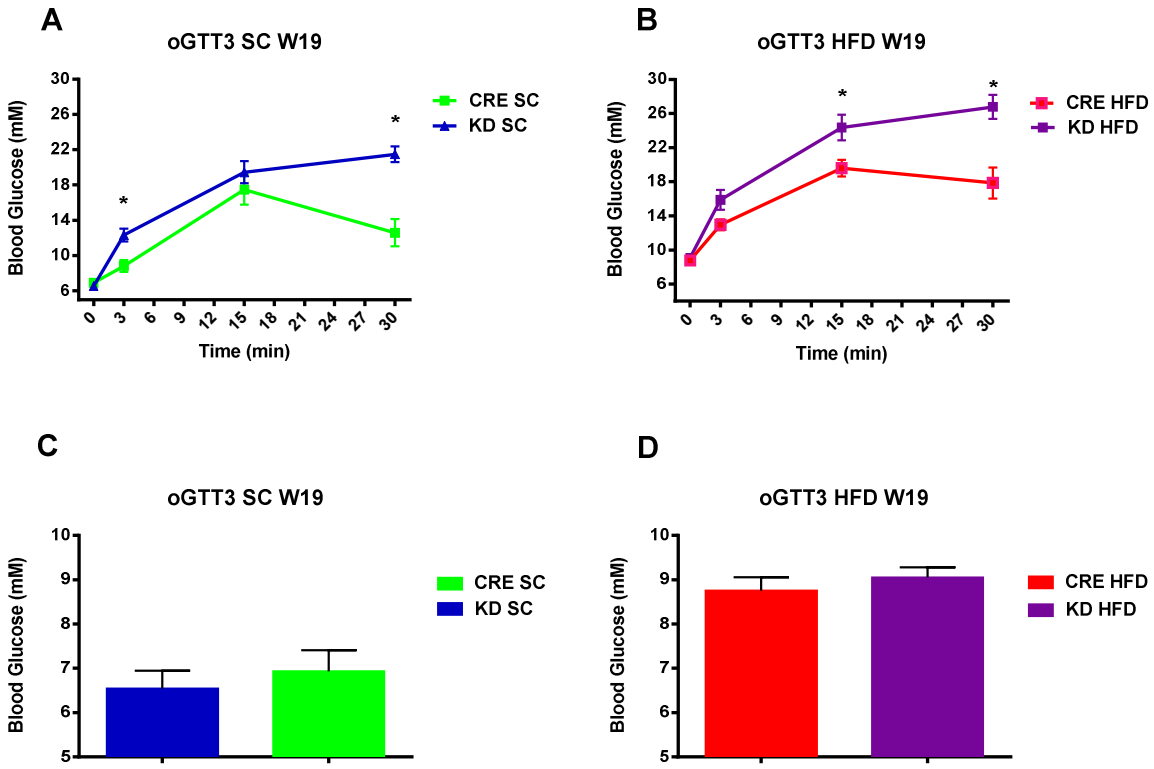

Figure 4.5.3: GREEN: CRE SC (n=9); **BLUE:** KD SC (n=9); **RED:** CRE HFD (n=7); **PURPLE:** KD HFD (n=11). Results were plotted as means +/-SEM. A significant effect of genotype ($p<0.0001$, $F=25.97$), diet ($p<0.0001$, $F=23.58$) was identified by MANOVA. Blood glucose levels rose acutely following glucose administration in both groups of animals on SC. The KD SC response was significantly elevated at 3min **(Figure 4.5.3A;** CRE SC 8.8+/-0.7mM Glucose; KD SC 12.3+/-0.7mM Glucose; $p=0.02$) and 30min **(Figure 4.53A;** CRE SC 12.6+/-1.5mM Glucose; KD SC 21.5+/-0.9mM Glucose; $p<0.0001$). Pronounced increases were observed in the acute blood glucose of CRE and KD HFD animals compared to SC mice **(Figure 4.5.3A, B;** CRE HFD 12.9+/-0.6Mm Glucose; KD HFD 15.5+/-1.0). Glycaemic levels were elevated in KD HFD compared to CRE HFD throughout oGTT3. This effect was of significance at 15min **(Figure 4.5.3B;** CRE HFD 19.6+/-1.0mM Glucose; KD HFD 24.2+/-1.1mM Glucose; p=) and 30min **(Figure 4.5.3B;** CRE HFD 17.9+/-1.8mM Glucose; KD HFD 26.5+/-1.2mM Glucose; $p<0.0001$) following the challenge. **Figure 4.5.3C, D:** Increases observed in the resting blood glucose of HF-fed (CRE HFD 8.8+/-0.3mM Glucose; KD HFD 9.1+/-0.2mM Glucose) compared to SC mice (CRE SC 6.9+/-0.5mM Glucose; KD SC 6.5+/-0.4mM Glucose) highlighted the significant effect of diet in the variance observed at Study week 19 ($p<0.0001$, $F=32.97$). There were no significant differences between the 2 groups on HFD ($p=0.37$, $F=0.84$).

The dramatic effects observed in terms of plasma insulin **(Figure 4.5.4A, B)** as well as the inhibitory role IL-6 is known to exert on gluconeogenesis (Metzger, et al., 1997; Moh, et al., 2008; Wunderlich, et al., 2010), encouraged us to examine plasma glucagon levels in experimental animals. Glucagon levels are kept low under

normoglycaemic conditions, while as mentioned, hyperglucagonaemia is observed in DIO and long-term diabetes, arising from the establishment of insulin resistance and dyslipidaemia. As plasma volume became a limiting factor, it was only possible to assess plasma glucagon levels using a small number of samples from each group at baseline and following 30min of glucose administration **(Figure 4.5.4D)**.

Figure 4.5.4: oGSIS at Week 19 of the Study

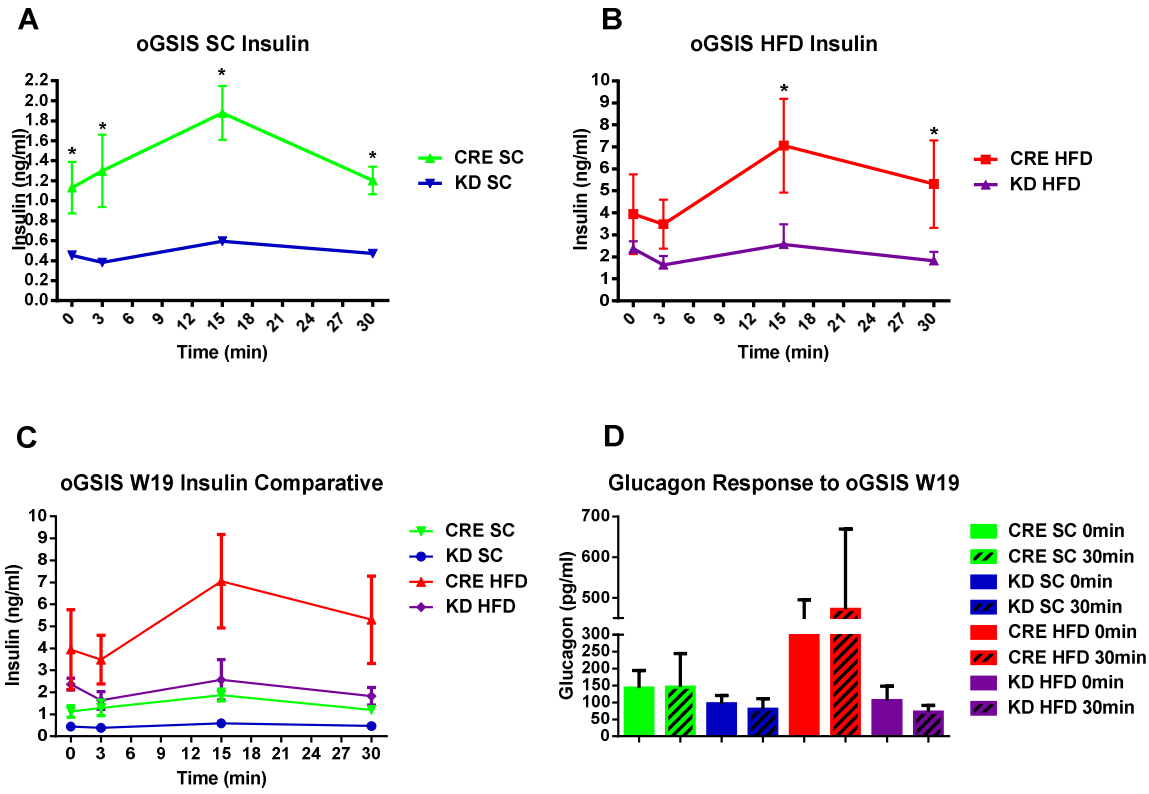

Figure 4.5.4A-C: GREEN: CRE SC (n=6); **BLUE:** KD SC (n=6); **RED:** CRE HFD (n=7); **PURPLE:** KD HFD (n=7). Results plotted as means +/-SEM. MANOVA indicated a significant effect of genotype (p=0.049, F=4.40) and diet (p=0.009), but no significant interaction between the 2 factors (p=0.33, F=1.01) in the variance observed. **Figure 4.5.4A**: Decreases in baseline insulin levels were evident in KD SC animals compared to CRE controls (CRE SC 1.13+/-0.26pg/ml; KD SC, 0.45+/-0.03pg/ml; p<0.001). This effect persisted through the 3, 15 and 30min time points (all p<0.01). **Figure 4.5.4B:** Resting plasma insulin levels were similar in CRE and KD HFD mice (CRE HFD 3.94+/-0.27pg/ml; KD HFD 2.37+/-0.27pg/ml; p=0.13). Significant increases to baseline were observed in CRE HFD at the 15min time point (7.059+/-2.128pg/ml; n=6, p=0.0062). Plasma insulin was significantly different in KD HFD compared to CRE HFD at 15 (p<0.0001) and 30 min (p<0.0004).

Figure 4.5.4D: GREEN: CRE SC (n=4); **BLUE:** KD SC (n=4); **RED:** CRE HFD (n=3); **PURPLE:** KD HFD (n=3). Results plotted as means +/-SEM. MANOVA of plasma glucagon levels at during GSIS indicated a significant effect of genotype (p=0.04, F=5.51), but not of diet (p=0.25, F=6397.78)

or their interaction (p=0.15, F=2.50) in the variation observed. **Figure 4.5.4D; 0min:** CRE SC 142.47+/-51.97pg/ml Glucagon; KD SC 95.95+/-24.63pg/ml Glucagon; p>0.9; **30min:** CRE SC 145.49+/-98.42pg/ml Glucagon; KD SC 79.81+/-31.23pg/ml Glucagon; p>0.9. Marginal differences between the HF-fed groups failed to reach significance in pair-wise comparison. **Figure 4.5.4D; 0min:** CRE HFD 311.87+/-183.67pg/ml Glucagon; KD HFD 105.67+/-42.60pg/ml Glucagon; p=0.92; **30min**: CRE HFD 471.99+/-197.35pg/ml Glucagon; KD HFD 71.32+/-19.91pg/ml Glucagon; p=0.1366.

Mean plasma glucagon in SC mice were similar, yet increases observed in CRE HFD mice were suppressed in KD HFD. A significant effect of genotype was reported in statistical analysis of variance (p=0.04, F=5.51), however differences observed in pair-wise comparison of KD and diet-matched controls were not significant **(Figure 4.5.4D)**. Data in this section clearly indicate a deficit GSIS in KD mice, and possibly a disruption in the physiological antagonistic relationship to glucagon. Significant differences were correspondingly observed in the ability of KD and CRE mice to clear glucose at 2 different points during the study (Week10 & 19, but not 14). Regardless, KD mice were still able to clear glucose during GTT, and insulin was detectable in blood plasma during GSIS. To further examine the origin of this defect in the KD, *ex vivo* GSIS and insulin glucagon staining, was examined in isolated pancreatic islet cells.

Metabolic Phenotyping using the CLAMS/Oxymax® Activity Monitor

Following the completion of the Study Plan **(Table 4)** protocol animals were examined using the CLAMS/Oxymax® Activity monitoring system. Mice were housed individually in specialized activity monitoring cages and allowed 24 hours to familiarize with the new environment. A 12:12 dark: light cycle was maintained, and their access to water and respective diet in powder were provided ad libitum. Food intake, activity, heat and respiratory exchange ratio were recorded over the subsequent 48-hour period. Comparison of metabolic parameters within each phase of the cycle as well as differences between the 2 phases, and the associated influence of genotype and diet was assessed by MANOVA (IBM SPSS®).

Figure 4.6.1: Mean Food Intake in CLAMS over 48 hours

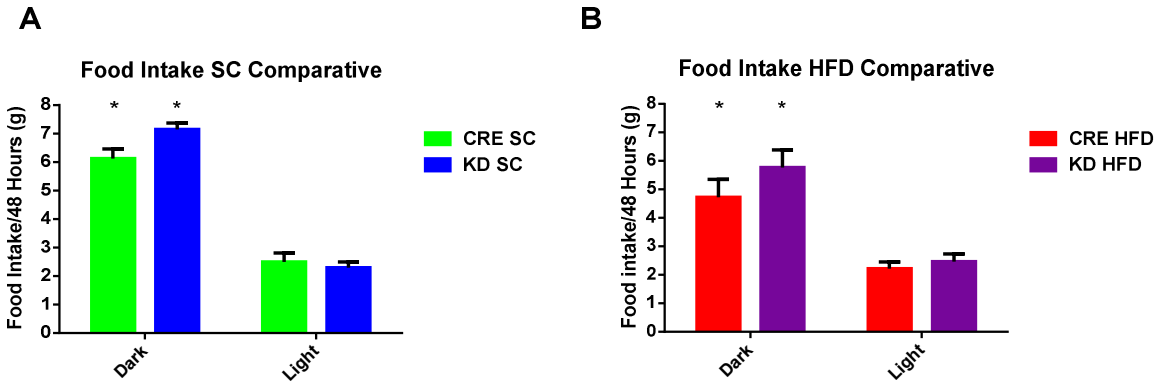

Figure 4.6.1: GREEN: CRE SC (n=9); **BLUE:** KD SC (n=9); **RED:** CRE HFD (n=7); **PURPLE:** KD HFD (n=11). Results plotted as means +/-SEM. Food intake was significantly increased during the dark compared to the light phase in both SC **(Figure 4.6.1A;** $p<0.0001$, $F=117.21$) and HFD **(Figure 4.6.1B;** $p<0.0001$, $F=33.58$). Differences observed in the total food intake of KD and control mice on SC ($p=0.18$, $F=1.91$) and HFD ($p=0.21$, $F=1.64$) were not statistically significant. **Dark Phase:** CRE SC 6.1+/-0.3g; KD SC 7.1+/-0.2g; CRE HFD 4.7+/-0.6g; KD HFD 5.8+/-0.6g. **Light Phase:** CRE SC 2.5+/-0.3g; KD SC 2.3+/-0.2; CRE HFD 2.2+/-0.2; KD HFD 2.5+/-0.2g.

Food intake in experimental animals was significantly elevated during the dark phase of the light cycle **(Figure 4.6.1)**. Approx. 75% of total food intake took place during the dark phase in both SC and HF-fed mice. However there was no significant effect of genotype, despite marginal differences observed in the food intake of KD and diet-matched controls **(Figure 4.6.1;** SC: $p=0.40$, $F=0.93$; HFD: $p=0.31$, $F=1.18$). Significant differences observed at Study week 9 were not maintained on examination using the CLAMS/Oxymax®, which could relate to differences in the environment and food access in the metabolic phenotyping cages.

Figure 4.6.2: Mean Activity during CLAMS

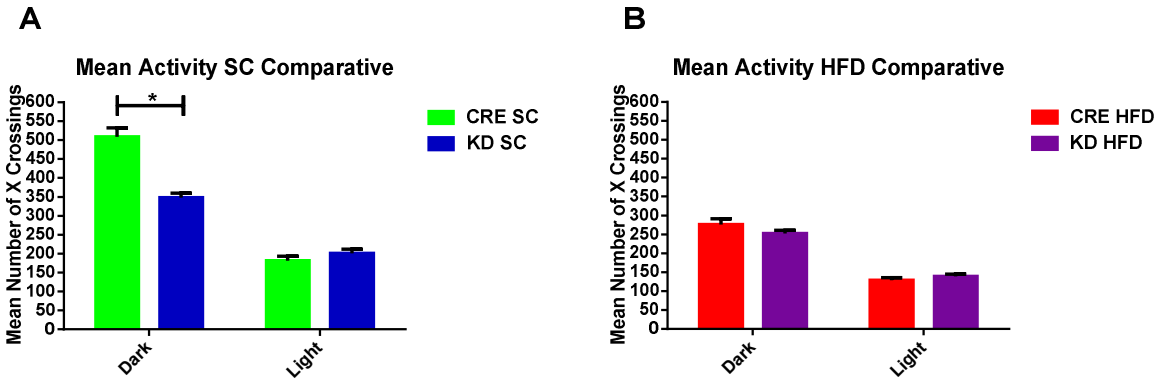

Figure 4.6.2: GREEN: CRE SC (n=9); **BLUE:** KD SC (n=9); **RED:** CRE HFD (n=7); **PURPLE:** KD HFD (n=11). Results plotted as means +/-SEM. Mean activity in SC ($p<0.0001$, $F=214.0$) and HFD ($p<0.0001$; $F=199.4$) mice was significantly influenced by the phase of the light cycle **(Figure 4.6.2A, B)**. CRE SC and KD were significantly more active during the dark phase ($p<0.0001$). **Figure 4.6.2A; Dark Phase:** CRE SC 508.5+/-23.6AU; KD SC 347.5+/-12.06AU; $p<0.001$. Activity was equally suppressed in CRE and KD SC mice during the light phase **(Figure 4.6.2A;** CRE 181.6+/-12.55AU; KD 198.5+/-12.01AU; $p=0.82$). **Figure 4.6.2B; Dark Phase:** CRE HFD 276.3+/-15.07AU; KD HFD 252.1+/-8.44AU $p=0.68$; **Light Phase:** CRE HFD 130.3+/-7.55AU; KD HFD 142.1+/-5.47AU; $p=0.85$. Activity was similarly decreased compared to SC mice in both CRE and KD HFD. Significant differences to SC mice during the dark ($p<0.0001$, $F=110.6$), but not the light phase of the cycle ($p=0.11$, $F=2.61$).

As mentioned in previous sections, activity, food intake and thermogenesis are stereotypically elevated in the dark phase of the cycle of nocturnal animals. Chronic HF-feeding has been shown to induce increases in thermogenesis through changes in adiposity and decreased activity. Mean locomotor activity of experimental animals on SC and HFD recorded by the CLAMS/Oxymax® Animal Monitoring system was consistent with this notion. Down-regulation of the IL-6Rα in SC mice was associated with significant decreases in activity **(Figure 4.6.2A;** $p<0.0001$) and thermogenesis compared to control mice **(Figure 4.6.3A;** $p<0.0001$). Activity was decreased in HF-fed mice in the dark phase, however there was no significant effect of diet on activity in the light phase **(Figure 4.6.2B;** $p=0.11$, $F=2.61$). On the other hand significant increases in thermogenesis were observed in HFD compared to SC mice during both phases of the cycle **(Figure 4.6.3B;** Dark: $p<0.0001$, $F=599.4$; Light: $p<0.0001$, $F=475.1$). KD and CRE HFD mice were identical in terms of activity **(Figure 4.6.2B;** Dark: $p=0.68$; Light: $p=0.85$). Significant differences in thermogenesis were only observed during the light phase **(Figure 4.6.3B;** Dark: $p=0.007$; Light: $p>0.0001$).

Figure 4.6.3: Mean Heat Generated during CLAMS

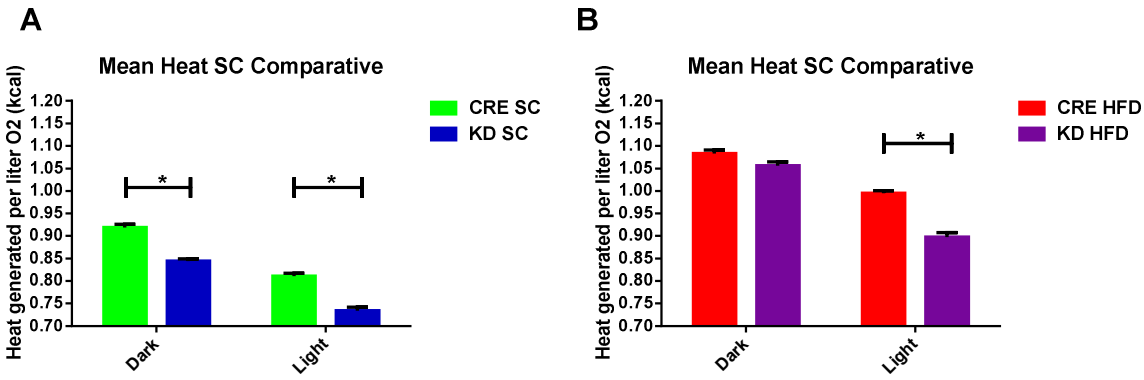

Figure 4.6.3: GREEN: CRE SC (n=9); **BLUE:** KD SC (n=9); **RED:** CRE HFD (n=7); **PURPLE:** KD HFD (n=11). Results plotted as means +/-SEM. Matching data recorded in terms of activity, heat generated was significantly influenced by the light cycle ($p<0.0001$, $F=440.7$) and thermogenesis was increased in KD ($p<0.0001$) and control SC ($p<0.0001$) mice during the dark phase. In further accord, thermogenesis was significantly influenced by genotype differences in both the dark ($p<0.0001$, $F=44.03$) and light phase ($p<0.0001$, $F=119.5$). **Figure 4.6.3A; Dark Phase**: CRE SC 0.92+/-0.007 kcal/L O_2; KD SC 0.84+/-0.005kcal/L O_2; $p<0.0001$. **Light Phase:** CRE SC 0.81+/-0.006kcal/L O_2; KD SC 0.73+/-0.008kcal/L O_2. **Figure 4.6.3B; Dark Phase:** CRE HFD 1.08+/-0.008kcal/L O_2; KD HFD 1.06+/-0.009kcal/L O_2; $p=0.007$. Thermogenesis was significantly influenced by diet during both the dark ($p<0.0001$, $F=599.4$) and light phases ($p<0.0001$, $F=199.5$). Heat generated in KD ($p<0.0001$) and CRE HFD ($p<0.0001$) mice was significantly elevated compared to SC mice. **Figure 4.6.3B; Light Phase** CRE HFD 0.99+/-0.005kcal/L O_2; KD HFD 0.90+/-0.01kcal/L O_2; $p<0.0001$. Increased thermogenesis was observed in both KD ($p<0.0001$) and CRE HFD ($p<0.0001$) mice compared to SC. KD animals exhibited significantly decreased heat generation compared to CRE HFD during the light phase.

Respiratory exchange ratio (RER) can be used to indirectly assess the metabolic substrate being consumed by the body towards energy production. RER values close to 1.0 are indicative of metabolism relying predominantly on carbohydrate as a fuel source, 0.85 suggests a mix of fat and carbohydrate, while 0.70 indicates that fat is the predominant fuel source (Christiansen & Hansen, 1939). Typically RER is close to 1.0 in SC mice during the feeding dark phase of the light cycle, and closer to 0.7 in HF-fed animals. Consequently during the light phase where food intake is naturally restricted, increased reliance on stored fat as metabolic fuel, RER is also around 0.7.

Figure 4.6.4: Mean RER during CLAMS

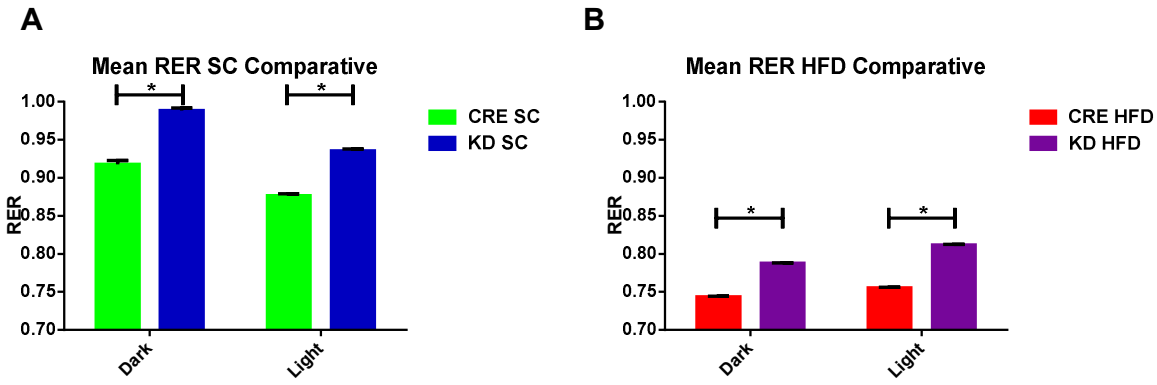

Figure 4.6.4: GREEN: CRE SC (n=9); **BLUE:** KD SC (n=9); **RED:** CRE HFD (n=7); **PURPLE:** KD HFD (n=11). The variance observed in RER was significantly influenced by the light phase as expected **(Figure 4.6.4A, B;** p<0.0001, F=73.40). Genotype differences also exerted a significant effect on the variance observed in both the SC and HF-fed groups. KD SC displayed significantly increased RER compared to CRE controls suggesting increased reliance on carbohydrate during the dark phase **(Figure 4.6.4A;** CRE SC 0.92+/-0.004; KD SC 0.99+/-0.003; p<0.0001, F=344). By contrast to the dark phase, CRE SCs were observed to rely on mixed fuel during the light phase. KD SC animals continued to rely on carbohydrate during the non-feeding light phase by stark contrast to control animals **(Figure 4.6.4A**; CRE SC 0.88+/-0.03**;** KD SC 0.94+/-0.003; p<0.0001, F=3406**)**. HFD induced significant disruption of the mean RER of animals during both phases of the light cycle in comparison to SC animals **(Figures 4.6.4A, B;** Dark: p<0.0001, F=409.1; Light: p<0.001, F=891.4). Consistent with the high fat content of the diet and their increased body fat, CRE HFD in particular exhibited increased reliance rely on fat metabolism during both phases of the light cycle **(Figure 4.6.4B;** CRE HFD Dark:0.74+/-0.001; Light: 0.76+/-0.001). This effect was disrupted in KD HFD animals that were seen to rely on a mixture of carbohydrate and fat in both the dark (0.82+/-0.0007, p<0.0001) and light (0.81+/-0.0008, p<0.0001) phases of the light cycle **(Figure 4.6.4B**).

Unsurprisingly the light cycle exerted a significant effect on the variance observed in the RER of both SC (p<0.0001, F=183.3) and HF-fed mice (p<0.0001, F=433.1). Additionally, significant differences were observed between the HFD and SC groups in both phases (Dark: p<0.0001, F=409.1; Light: p<0.0001, F=891.4), as expected. Intriguingly increased reliance on carbohydrate oxidation compared to diet-matched controls was maintained through both phases of the cycle in both SC and HF-fed KDs **(Figure 4.6.4A, B;** p<0.001, F=73.4). Results obtained using the animal monitoring system suggested the brain-specific disruption of the IL-6 receptor to induce decreased activity and thermogenesis as well as a deficit in the ability of KD mice to utilize fat as a fuel. No significant differences were observed in terms of food intake.

Plasma Leptin and IL-6 at the End of the Study

Increases in IL-6 (Kalofoutis, et al., 2006) and leptin (Friedman & Halaas, 1988) plasma levels have been associated with the development of diabetic disease. Circulating leptin levels have been known to correlate with adiposity and increase dramatically in response to DIO (Maffei, et al., 1995), while appetite and body weight are acutely suppressed in response to central leptin.

Figure 4.7.1: Plasma Leptin at the End of the Study

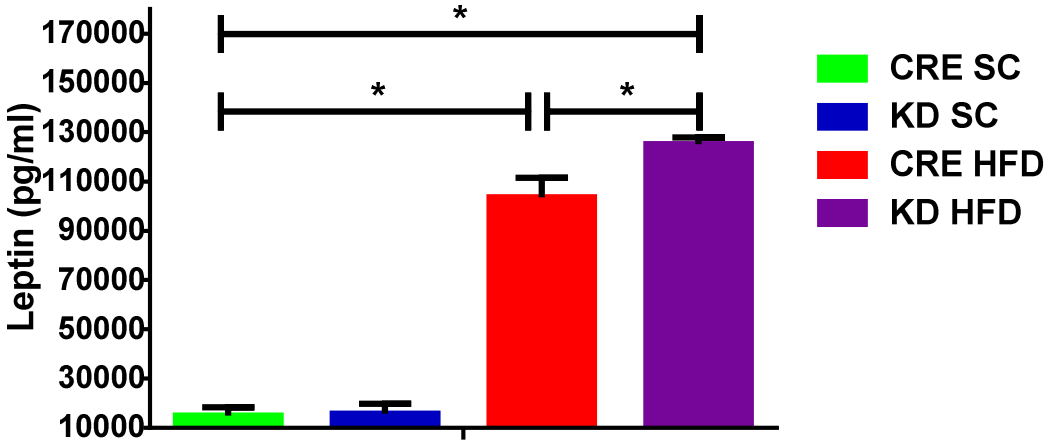

Figure 4.7.1: GREEN: CRE SC (n=5); **BLUE:** KD SC (n=5); **RED:** CRE HFD (n=5); **PURPLE:** KD HFD (n=5). Results plotted as means +/-SEM. Plasma leptin levels were significantly influenced by diet, and 10-fold increases were observed in HF-fed mice compared to age- and genotype-matched SC ($p<0.0001$, $F=395$). 2-way ANOVA also indicated a significant effect of genotype ($p=0.04$, $F=5.027$), but no effect of the interaction of genotype and diet in the variance observed ($p=0.05$, $F=4.36$). Circulating leptin levels in KD SC were analogous to levels observed in control mice (CRE SC 14919+/-34.02pg/ml; KD SC 15683+/-3006pg/ml; $p<0.99$). Increases observed in response to chronic HF-feeding were significantly augmented in KD HFD mice compared to CRE HF-fed mice (CRE HFD 103578+/-7991pg/ml; KD HFD 125164+/-2881pg/ml; $p=0.03$).

Inflammatory signaling in the central nervous system has been suggested to participate in neuroendocrine signaling networks dedicated to regulation of body weight, body composition and satiety levels (Zhang, et al., 2008). Brain-specific down-regulation of the IL-6 receptor was demonstrated in NesCreIL-6Rα KD mice in **Chapter 3**. Differences observed in the body composition **(Figures 4.2)** and food intake **(Figures 4.3)** of KD mice during the study encouraged me to examine circulating plasma leptin & IL-6 levels. The influence of genotype and diet in the differences observed in plasma IL-6 and leptin were assessed separately by 2-way ANOVA.

Figure 4.7.2: Plasma IL-6 levels at the End of the Study

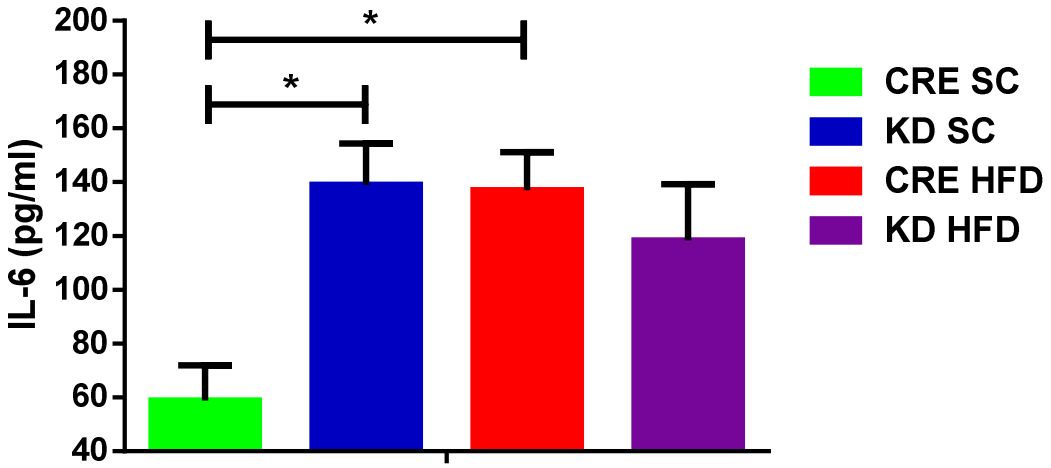

Figure 4.7.2: GREEN: CRE SC (n=5); **BLUE:** KD SC (n=5); **RED:** CRE HFD (n=5); **PURPLE:** KD HFD (n=5). Results plotted as means+/-SEM. Statistical analysis circulating IL-6 levels indicated a significant effect of the interaction of genotype and diet (p=0.008, F=9.27) in the variance observed but no significant effect of genotype (p=0.076, F=3.6), or diet alone (p=0.095, F=3.15). A two-fold increase in plasma IL-6 was observed in KD SC mice compared to age-matched control mice (CRE SC 58.82+/-13.03pg/ml; KD SC 138.9+/-15.41pg/ml; p=0.014). Chronic HF-feeding promoted significant increases in plasma IL-6 in control mice (p=0.017), but no differences were observed between SC and HF-fed KDs (p=0.81). Equivalent plasma IL-6 levels detected in KD and CRE HFD mice (CRE HFD 175.8+/-14.22; KD HFD 199.2+/-20.95pg/ml; p=0.85).

Despite differences in food intake **(Figure 4.3)** and body composition **(Figure 4.2)**, there was no significant difference between KD and CRE SC mice in terms of circulating plasma leptin **(Figure 4.7.2;** p<0.99). On the other hand, chronic HF-feeding was associated with 10-fold increases in plasma leptin levels in both KD and control mice compared to age-matched SCs **(Figure 4.7.1;** p<0.0001, F=395). The effect of genotype in the variance observed related to differences between KD and control mice on HFD **(Figure 4.7.1;** p=0.04, F=5.027). Plasma leptin was significantly elevated in KD HFD mice compared to controls, reflecting differences observed in body composition at the end of the study **(Figure 4.2.5)**. Previous studies have suggested regulate leptin sensitivity through central effects (Fukuda, et al., 2005; Ropelle, et al., 2010). To further interrogate the contribution of leptin to the phenotype, the sensitivity of KD and control mice to the anorexigenic and weight-reducing effects of leptin was assessed in separate experiments.

Consistent with previous studies (Kern, et al., 2001), a 2-fold induction of IL-6 was observed in response to HFD in CRE HFD compared to SC mice **(Figure 4.7.2**,

p=0.0007). This effect was not observed in KD mice, as plasma IL-6 was significantly increased in the KD compared to SC controls **(Figure 4.7.2,** p=0.0014), and no further increases were observed in response to chronic HF-feeding (p=0.81). Mean plasma IL-6 in KD mice was comparable to levels recorded in HF-fed controls, independently of diet (p=0.09, F=3.15).

Pancreatic Insulin and Glucagon

Examination of the effects of the insulin response to oral glucose in KD and control animals (on SC & HFD) *in vivo* revealed a significant deficit in basal and glucose-stimulated insulin release **(Figure 4.5.4)**. To interrogate the origin of this defect, pancreatic cell morphology was examined by immunohistochemistry, as well as the ability of *ex vivo* pancreatic cells to respond to glucose.

Figure 4.8.1: Pancreatic Islet Immunohistochemistry in SC mice

Index: Blue: DAPI; Red: Insulin; Green: Glucagon

A – WT SC

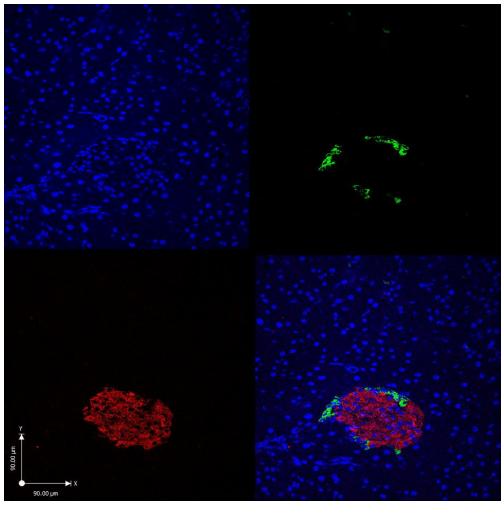

B - CRE SC

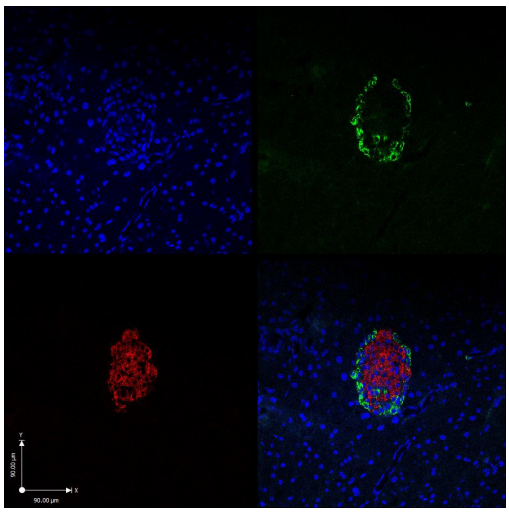

C – KD SC

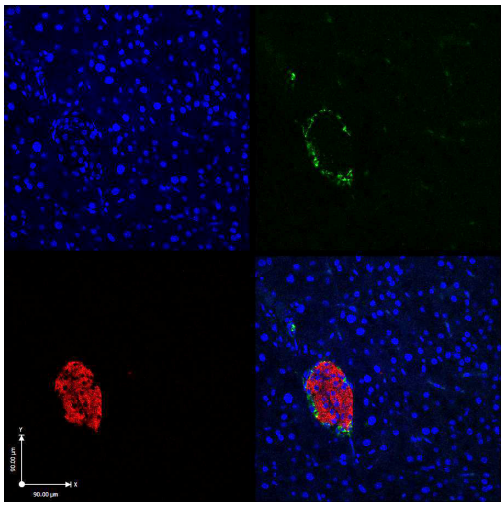

Figure 4.8.1: Adult (>8 weeks old) mice were used. A – WT SC (n=4); B – CRE SC (n=4); C- KD SC (n=4). Pancreatic Insulin and Glucagon was examined in control and NesCreIL-6Rα KD animals by immunohistochemistry. Islets identified under x40 magnification (Leica® TCS SP5 II). Images obtained from KD mice confirmed the expression of insulin and glucagon in pancreatic tissue. Similar pattern of Insulin/glucagon staining observed in KD and control islets.

Immunohistochemical examination of pancreatic tissue indicated NesCre-mediated down-regulation of the IL-6Rα to have no direct effect in the expression of insulin and glucagon protein at the pancreas. Glucagon and insulin staining are commonly used to confirm the expression of pancreatic α and β cells respectively. Our transgenic approach did not induce any effects on insulin/glucagon staining in KD SC compared to both CRE and WT animals **(Figure 4.8.1A-C).** Changes in islet morphology as a consequence of the pathophysiological effects of DIO in control animals were not different in the KD **(Figure 4.8.2A, B)**. The deficit observed in KD mice in during GSIS **(Figure 4.5.4)** was thus not associated with differences in islet morphology compared to control animals, or the ability of KD islets to express insulin and glucagon.

Figure 4.8.2: Pancreatic Islet Immunohistochemistry in HF-fed mice

Index: Blue: DAPI; Red: Insulin; Green: Glucagon

A – WT HFD **B - KD HFD**

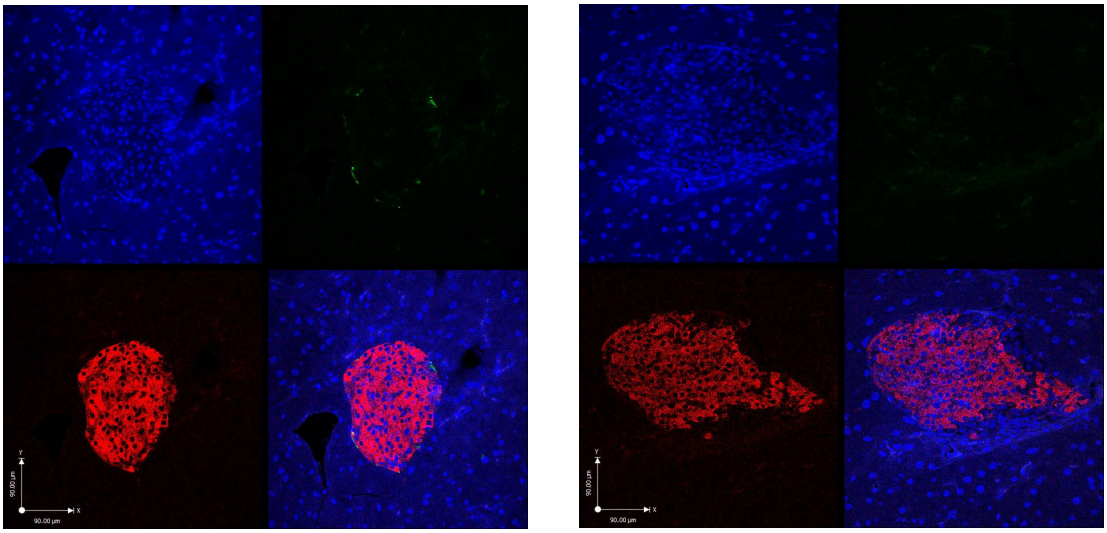

Figure 4.8.2: Adult (>8 weeks old) mice were used following chronic HF-feeding. A – WT HFD (n=2); B – KD SC (n=2). Insulin and Glucagon protein staining was examined in control and NesCreIL-6Rα KD animals by immunohistochemistry. Islets identified under x40 magnification (Leica® TCS SP5 II). Pancreatic islets identified in slides from HF-fed animals (n=2) displayed increases in size compared to SC islets. Insulin staining was pronounced, while glucagon staining was markedly decreased compared to images obtained from SC mice. This effect was observed in both KD and control islets identified.

Pancreas from age-matched WT, CRE and KD SC animals was collected with the help of Mrs Jennifer Gallagher and Dr Alison D. McNeilly. Pancreatic islet cells from

WT, CRE and KD SC animals were isolated *ex vivo* to assess the ability of endocrine tissue within islets to release insulin and glucagon. Islets were incubated in high glucose (20mM glucose) for 1 hour (Carter, et al., 2009) and Insulin and Glucagon levels secreted in media were measured by ELISA **(Figure 4.8.3)**. Results were analysed by 1-way ANOVA. No significant differences were reported between KD and CRE islets in terms of *ex vivo* glucose-stimulated insulin (p=0.110, F=2.91) or glucagon release (p=0.52, F=0.43). Even though examination of the glucose-stimulated insulin secretion of KD animals *in vivo* revealed a clear deficit in insulin release **(Figure 4.5.4)**, no significant differences were observed when islets were isolated *ex vivo*.

Figure 4.8.3: Insulin and Glucagon secretion from ex vivo Pancreatic Islets in Response to High Glucose (20mM)

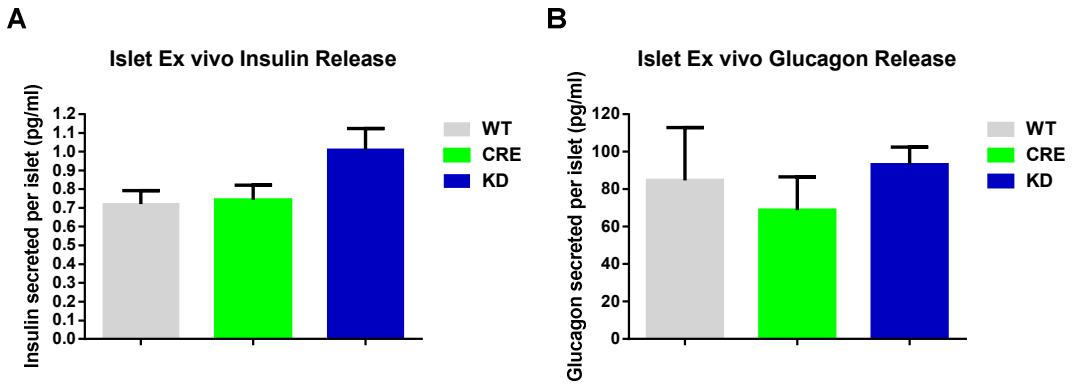

Figure 4.8.3: Pancreatic islets from adult (>8weeks) mice on standard chow were isolated *ex vivo* and stimulated with 20mM Glucose. **GREY:** WT SC (n=8); CRE SC (n=8); KD SC (n=8). Results represent mean hormone levels detected in islet media +/-SEM. Glucose-stimulated insulin release from *ex vivo* KD islets was comparable to levels observed in CRE islets (**Figure 4.8.3A;** CRE SC 0.74+/-0.08pg/ml Insulin; KD SC 1.01+/-0.11pg/ml Insulin; p=0.11; F=2.91). Similarly, glucagon secretion from *ex vivo* islets was not statistically different between CRE and KD mice (**Figure 4.8.3B;** CRE SC 68.73+/-17.87pg/ml Glucagon; KD SC 93.06+/-9.36pg/ml Glucagon; p=0.52, F=0.43)**.** WT animals were examined as an additional control group. Insulin (**Figure 4.8.3A;** WT SC 0.72+/-0.07pg/ml) and glucagon (**Figure 4.8.3B;** WT SC 84.64+/-28.21pg/ml) secretion from WT islets resembled levels detected in CRE and KD islets.

Examination of the Response to Intra-Peritoneal Leptin

Circulating leptin levels correlate with body weight and adiposity, and increases are known to promote energy expenditure and satiety through central effects (Friedman & Halaas, 1988; Cohen, et al., 2001). Hyperleptinaemia and leptin resistance have been consistently reported in obese humans and animal models of obesity (Maffei, et al., 1995; Frederich, et al., 1995). More recently, persistent increases in circulating cytokines such as IL-6 in response to chronic HF-feeding have been suggested to promote leptin resistance at the hypothalamus. The accumulation of shared negative feedback regulators (e.g. SOCS-3, EPAC-1), have been suggested to impair the ability of leptin to induce increases in STAT3 phosphorylation (Fukuda, et al., 2005; Mori, et al., 2004).

Figure 4.9.1: Examination of the effects of IP Leptin on Food Intake and Change in Body Weight in mice

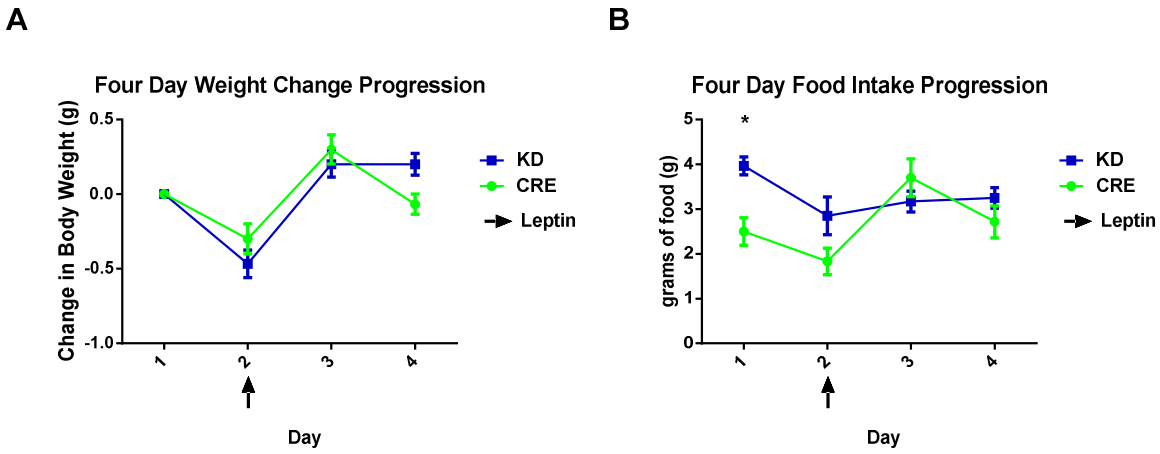

Figure 4.9.1: GREEN: CRE SC (n=6); **BLUE:** KD SC (n=6). Adult (>8weeks) female mice were used. Leptin treatment exerted a significant effect on body weight in both genotypes **(Figure 4.9.1A;** CRE SC -0.3+/-0.1g; KD SC -0.5+/-0.1g; p<0.0001, F=48.18**).** Body weight responses to leptin treatment and control conditions were nearly identical in KD and CRE SC mice **(Figure 4.9.1A;** p=0.43, F=0.62). Similarly the interaction between genotype and treatment was not statistically significant **(Figure 4.9.1A;** p=0.12, F=2.49). Food intake decreased in response to leptin treatment in both CRE and KD mice **(Figure 4.9.1B;** p=0.03, F=9.58). Statistical analysis indicated a significant effect of genotype on the variance observed in food intake **(Figure 4.9.1B;** p=0.01; F=7.09). This related to differences observed under control conditions prior (CRE SC 2.5+/-0.3g; KD 4.0+/-0.2g; p=0.03), but not in response to leptin treatment (CRE SC 1.8g+/-0.3g; KD SC 2.9+/-0.4g; p=0.19). Compensatory increases were observed in both genotypes during the 2 days following leptin treatment. CRE and KD food intake was not statistically different on Day 3 (CRE SC 3.7+/-0.4g; KD SC 3.2+/-0.3g; p= 0.74) or Day 4 (CRE SC 2.7+/-0.4g; KD SC 3.3+/-0.3g; p=0.74).

Statistical analysis of the response to the leptin sensitivity assessment protocol was carried out with regards to changes food intake and body weight over 4 days. Results were analyzed using 2-way ANOVA (IBM SPSS 21®). Leptin treatment was associated with decreases in body weight and food intake in both CRE and KD SC mice **(Figure 4.9.1).** Changes observed in body weight were independent of genotype (p=0.43, F=0.62). The effect of genotype on food intake (p=0.01, F=2.09), related to increased food intake in the KD prior to leptin treatment (p=0.03) corroborating previous findings **(Figure 4.3)**. Food intake following IP leptin was not significantly different between KD and control mice (p=0.19). Furthermore, the induction of STAT3 phosphorylation in response to IP leptin was intact in NesCreIL-6Rα KD mice **(Figure 4.9.2)**.

Figure 4.9.2: Examination of the effects of IP Leptin (50µg/kg) on STAT3 phosphorylation in hypothalamic tissue

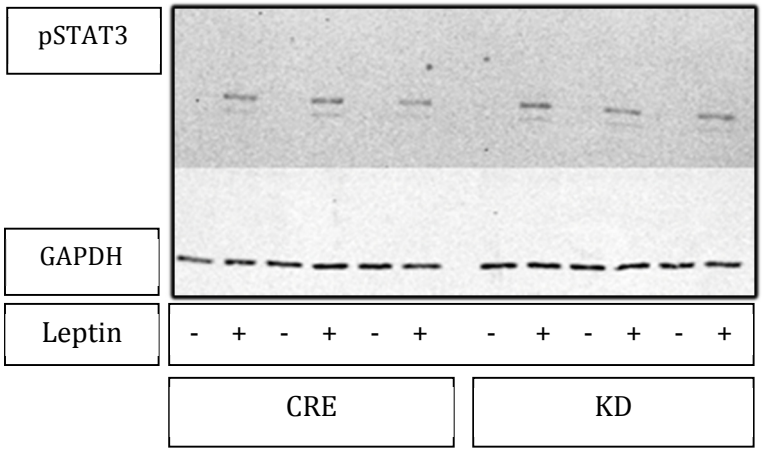

Figure 4.9.2: Adult (>8 weeks) mice were used. Half of the KD and CRE SC animals (n=6) participating in this experiment received an IP injection of Leptin (50µg/kg) (+) and the rest Saline (-), as indicated. Hypothalamic tissue was collected 1hour following leptin or saline injection. Leptin administration consistently induced up-regulation of phosphorylated STAT3 protein in the hypothalamus. pSTAT3 – 79/88 kDa; Loading Control: GAPDH – 37 kDa (Cell Signaling®)

Summary

The metabolic phenotype of the novel NesCreIL-6Rα KD on SC and HFD was examined over a period of 20 weeks, and compared to control animals **(Diagram 3)**. Body weight gain through the course of the study was closely matched between the two genotypes, both on SC and HFD **(Figure 4.1)**. Paradoxically, KD SC mice exhibited hyperphagia **(Figure 4.3)**, while body adiposity was significantly decreased compared to age-matched controls throughout the course of the study **(Figures 4.2.1-5)**. KD HFD mice were also hyperphagic compared to diet-matched controls; however following 20 weeks of HF-feeding, increased adiposity was recorded. The phenotype was not the consequence of differences in leptin sensitivity, as indicated by additional studies using a separate group of KD and CRE SC mice. The hyperphagic phenotype of the KD was not associated with differences in baseline glycaemia or insulin sensitivity during the study. Sensitivity to the hypoglycaemic effects of exogenous insulin was similar in KD and control mice on SC at Study weeks 6, 9 and 15 **(Figures 4.4.1-3)**. Evidence of insulin resistance was only apparent in KD and control HF-fed mice after 15 weeks of diet, and no differences were observed between the 2 genotypes in this response. However, glucose clearance was significantly suppressed in KD mice at Study Weeks 10 and 19 (but not 14), while basal and glucose-stimulated insulin secretion was dramatically disrupted **(Figures 4.5.1-4)**. Additional studies conducted using *ex vivo* islets from KD SC and control mice, indicated that the disruption of GSIS in KD mice *in vivo* was not due to differences in the ability of islets to produce and secrete insulin and glucagon **(Figures 4.8.1-3)**. Collectively our studies suggest central IL-6 signaling to participate in the integration of satiety signals, at least in part through the regulation of insulin release in response to changes in glucose loading.

Finally, at the end of the study, KD and control mice were examined using the CLAMS/Oxymax® system. Consistent with central IL-6 signaling promoting pyrogenesis (Rothwell, et al., 1991) and fat oxidation (Wallenius, et al., 2002); KD mice exhibited decreased activity and thermogenesis at different stages of the light cycle **(Figures 4.6.2-3)**. Furthermore, differences in RER between KD and diet-matched control mice indicated increased reliance on carbohydrate fuel in the KD even in response to HFD **(Figure 4.6.4)**.

Table 6: Summary of the NesCreIL-6Rα KD Metabolic Phenotype

Metabolic Phenotype Parameter Examined	Differences Compared to Control Mice	
	SC	**HFD**
Body Weight	**-**	**-**
Body Fat Composition	**↓**	**↑After 20 weeks**
24-Hour Food Intake	**↑**	**↑**
Plasma Leptin	**-**	**↑**
IP Leptin Sensitivity	**-**	**N/A**
Baseline Glycaemia	**-**	**-**
IP Insulin Tolerance Test	**-**	**-**
Oral Glucose Tolerance Test	**↓Glucose Clearance**	**↓Glucose Clearance**
In vivo GSIS	**↓**	**↓**
Ex vivo GSIS	**-**	**N/A**
Pancreatic Islet Insulin/Glucagon Immunohistochemistry	**-**	**-**
Food Intake in CLAMS	**↑ (ns)**	**↑ (ns)**
Activity in CLAMS	**↓ Dark Phase**	**-**
RER in CLAMS	**↑Both Phases**	**↑Both Phases**
Thermogenesis in CLAMS	**↓ Both Phases**	**↓ Light Phase**

Chapter 5: Discussion

Generation and Characterization NesCreIL-6Rα KD mice

By crossing NesCre and IL-6Rα$^{flox/flox}$ mice, we were able to generate and validate a novel transgenic where the IL-6Rα gene was disrupted in the brain specifically (NesCre-IL-6Rα KD). Wild-type (WT), NesCre+ (CRE) and KD mice were identified by standard PCR **(Figures 3.2, 3.3)**. Receptor mRNA expression in KD and control brains was initially assayed using real-time PCR and significant differences were observed between age- and sex-matched CRE and WT IL-6ra mRNA expression **(Figure 3.4.1)**. This finding as well as other recent published work suggesting differences in the metabolic phenotype of CRE and WT/C57Bl6 mice, indicated CRE mice to be the appropriate control group for the KD (Harno, et al., 2013). IL-6ra mRNA was significantly decreased in the hippocampus and the hypothalamus, but not the frontal cortex or the cerebellum of KD mice compared to CRE controls **(Figure 3.4.2)**. Brain IL-6Rα protein expression was also examined using immunohistochemistry. In region-matched slices from the hippocampus and hypothalamus of CRE and KD mice, the percentage of IL-6 receptor-positive NeuN cells was decreased in the KD group **(Figure 3.8.2-3)**. Matching mRNA expression data, IL-6Rα immunoreactivity was similar in the KD and CRE frontal cortex **(Figure 3.8.1)**. Analysis of imaging data using Volocity® (PerkinElmer®) indicated the NesCre-mediated disruption of the IL-6Ra to be primarily affect receptor co-localization with neurons, even though decreases in receptor co-localization with astrocytic biomarkers were also observed **(Figure 3.8.4).**

To functionally assess the effects of the KD, the ability of IL-6 to activate STAT3 in *ex vivo* brain slices from the mediobasal hypothalamus was examined by western blotting. IL-6 treatment in control slices promoted significant increases in pSTAT3 in this metabolically active brain region, contrasting KD responses that failed to reach significance **(Figure 3.7)**. Furthermore, KD and control mice were administered a weight-adjusted dose of intra-peritoneal (IP) IL-6 *in vivo*. IP IL-6 treatment in CRE mice induced STAT3 phosphorylation in peripheral (heart, kidney, liver, lung, muscle, spleen, brown- & white-adipose tissue) and central tissue examined (hippocampus, hypothalamus and cerebellum). Peripheral tissue from KD mice responded to IL-6 treatment in a similar fashion to control animals, confirming that peripheral receptor

expression was not disturbed **(Figures 3.6.1-9)**. However, phosphorylation/activation of STAT3 in response to IL-6 was disrupted in the KD brain across all regions examined, in further support of the brain-specific disruption of the IL-6 receptor system **(Figures 3.5.1-3)**. Consistent with previous studies using NesCre mice, results shown in **Chapter 3** confirmed brain-specific disruption of the IL-6Rα system in NesCreIL-6Rα KD mice. To examine the role of central IL-6 signaling in the development of DIO and diabetes, KD and control mice on SC and HFD were examined over a 20-week period.

Metabolic Phenotype of the NesCreIL-6Rα KD

Brain-specific IL-6Rα down-regulation in NesCreIL-6Rα KDs was associated with a dramatic suppression of *in vivo* GSIS **(Figure 4.5.4)**, but was of little consequence to the blood glucose response to insulin **(Figures 4.4.1-3)** and the body weight and food intake response to leptin **(Figure 4.9.1-2).** Body weight was closely matched between KD and control animals on SC diet, while dramatic increases observed in control animals on HFD were mirrored in HF-fed KDs **(Figure 4.1)**. Paradoxically, KD SC mice were significantly leaner than control mice, despite being hyperphagic **(Figures 4.2.1-5, 4.3, 4.9.1)**, hypoactive and less thermogenic **(Figure 4.6.2-4)**. Hyperphagia and suppression of energy expenditure was also observed in the HF-fed KDs, and the leaner phenotype was progressively reversed through the course of 20weeks of diet **(Figures 4.2.1-5, 4.6.2-4)**. The complex phenotype observed in the KD can be explained by the combined disruption of (a) the anorexigenic effects of central insulin and IL-6 signaling (Woods, et al., 1979; Wallenius, et al., 2002); (b) the lipogenic effects of GSIS in the periphery (Kahn & Flier, 2000); and (c) the thermogenic and lipolytic effects of central IL-6 signaling (Rothwell, et al., 1991; Van Hall, et al., 2003; Carey, et al., 2006)**.** Consistent with previous findings, studies using the NesCreIL-6Rα KD additionally implicate central IL-6 signaling in the coordination of insulin secretion in response to changes in nutrient availability; and to be consequently required for the induction of the anabolic and anorexic effects of the hormone.

Figure 5.1: Schematic representation of the NesCreIL-6Rα KD metabolic phenotype

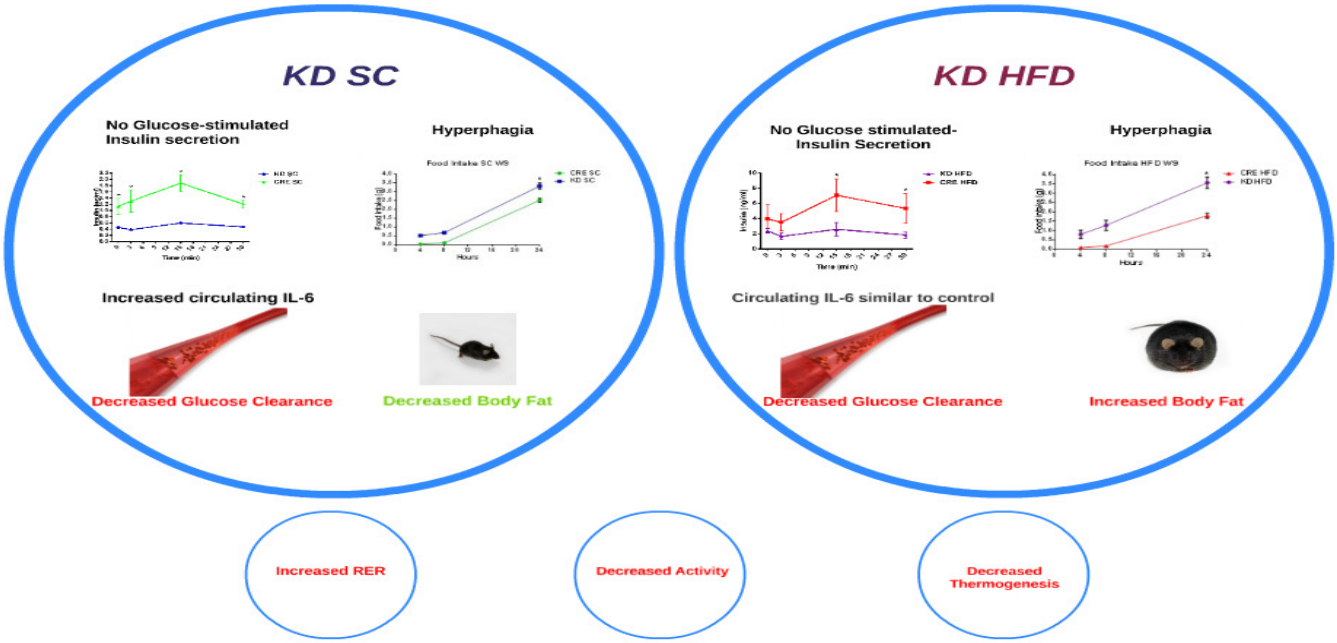

In response to glucose loading, insulin acts to inhibit liver gluconeogenesis and activates glucose up-take (Hardwick, et al., 1959; Caygill & Stein, 1972; Mohan & Bessman, 1985) lipogenesis (Kim, et al., 1998; Griffin & Sul, 2004; Seo, et al., 2004), while by passing the blood-brain barrier insulin acts in the mediobasal hypothalamus to inhibit food intake (Woods & Seeley, 2000; Schwartz, et al., 2000). The brain modulates autonomic output to the periphery, driving changes in energy expenditure in muscle and fat, as well as regulating endocrine secretions from the pancreas. The suppression of GSIS observed the KD *in vivo* was not maintained in isolated *ex vivo* islets, implicating central effects to underlie the defect **(Figures 4.8.1-3)**. Insulin secretion from the pancreatic β cell is stimulated by parasympathetic inputs (Kaneto, et al., 1975; Berthoud, et al., 1980; Lundquist, 1982; N'Guyen, et al., 1994) and inhibited by sympathetic innervation that promotes the expression of counter-regulatory hormones (Ahren, 2000; Gilon & Henquin, 2001). This is coordinated by specialised neuronal populations of the hypothalamus (Guillod-Maximin, et al., 2004; Jansen, et al., 1997) and the brainstem (Ionescu, et al., 1983; Jansen, et al., 1995; Dallaporta, et al., 1999). Glucose-dependent changes in the activity of POMC and NPY/AgRP neurons in the hypothalamus in particular, are likely implicated in the GSIS phenotype observed in the NesCreIL-6Rα KD (Claret, et al., 2007; Ersnt, et al.,

2009; Belgardt, et al., 2009). Given the GSIS defect observed in the KD, in conjunction with hyperphagia, it is possible that brain-specific disruption of the IL-6 receptor induced increases in orexigenic NPY and decreased anorexigenic POMC activity in the hypothalamus (Senaris, et al., 2011; Schele, et al., 2013); that would suppress pancreatic β cell secretions, inhibiting both the anorexic and anabolic effects of the insulin (Woods, et al., 2006; Palou, et al., 2009).

Pharmacological or diet-induced increases in circulating IL-6 have been suggested to promote enhanced GSIS in mice (Carey, et al., 2006; Franckhauser, et al., 2008). This was not the case in the NesCreIL-6Rα KD, suggesting central IL-6 to be involved in the physiological enhancement of GSIS in response to insulin resistance **(Figures 4.5.4, 4.7.2)**. Furthermore, recent studies have suggested central IL-6 signaling to be required for the induction of the anorexic effects of exendin-4, a drug that decreases NPY expression in the brain and increases sympathetic output (Perez-Tilve, et al., 2010; Dalvi, et al., 2012; Shirazi, et al., 2013; Yang, et al., 2014). The increased reliance on carbohydrate fuel, decreased thermogenesis and increased lipogenic capacity observed in HF-fed NesCreIL-6R KD mice would be consistent with this **(Figure 4.2.1-5, 4.6.2-4)**. Further studies would be required to determine the effect of the KD on the balance of anorexigenic/orexigenic neuropeptides at the brain and the expression of thermogenic and lipolytic enzymes in the periphery.

Despite suppression of GSIS, KD animals avoided overt hyperglycaemia in response to oral glucose, suggesting that compensatory events might have accounted for the defect **(Figures 4.5.1-3)**. The first phase of insulin secretion ensues within the first 2 minutes of a glucose challenge and peaks by approx. 10 min, followed by longer more prolonged phase that plateaus at 2-3hours (Gerich, 2002; Del Prato, et al., 2002). Hyperinsulinaemia is commonly observed in chronically HF-fed mice (Winzell & Ahren, 2004), and disruption of the pulsatility of insulin secretion into the portal vein has been suggested to directly contribute to the development of insulin resistance at the level of the liver (Schofield & Sutherland, 2012; Song, et al., 2000; Porksen, et al., 1996; Butler, et al., 2003). Indeed, chronic high fat feeding was associated with the disruption of the 1st and the enhancement of the 2nd phase of GSIS control animals **(Figure 4.5.4)**, indicative of the establishment of insulin resistance (Del Prato & Tiengo, 2001; Cheng, et al., 2013). This was contrasted by marginal increases in plasma insulin in the KD HFD mice that were sufficient to maintain comparable glycaemia to controls. It is thus likely that the chronic suppression of insulin secretion

observed in KD animals, promoted increased insulin sensitivity at the liver. Further studies would be required to confirm whether KD mice experienced differences in the expression of factors regulating insulin sensitivity at the liver during GSIS, such as G6Pase (Franckhauser, et al., 2008; Mauer, et al., 2014).

Conclusions

The expression of adipostatic (e.g. insulin and leptin) and inflammatory mediators (e.g. IL-6) is increased during the development of DIO (Bastard, et al., 2006), and circulating levels have been shown to correlate with diabetic disease severity (Mohamed-Ali, et al., 1997; Kroqu-Madsen, et al., 2004; Daniele, et al., 2014). Cytokine release from adipose tissue increases in response to stimuli such as oxidative stress (Pereda, et al., 2006) and hyperglycaemia (Kroqu-Madsen, et al., 2004), commonly observed in obesity and type 2 diabetes (Wellen & Hotamisligil, 2005; Tsiotra & Tsigos, 2006; Boden, 2009). More recently, sustained activation of inflammatory cascades at level of the hypothalamus has been suggested to be central to the development of DIO and the establishment of metabolic dysfunction leading to diabetic pathology (Zhang, et al., 2008; Wang, et al., 2010).

The role of IL-6 in metabolic regulation was previously highlighted in studies involving IL-6 null mice that exhibited glucose intolerance, insulin insensitivity and developed mature onset obesity (Wallenius, et al., 2002; Matthews, et al., 2010). Since then, IL-6 has been demonstrated to drive glucose uptake from muscle (Petersen & Pedersen, 2006) as well as pancreatic β cell glucose-stimulated insulin secretion (GSIS) *in vivo* and *ex vivo* (Choi, et al., 2004; Ellingsgaard, et al., 2011)*;* and to promote liver insulin sensitivity during GSIS (Wunderlich, et al., 2010). Infusion of peripheral or central IL-6 itself, inhibits food intake through the induction of anorexigenic POMC in the hypothalamus (Rummel, et al., 2006; Senaris, et al., 2011), but is also associated with increases in white adipose tissue (WAT) lipolysis and sympathetic stimulation of brown adipose tissue (BAT) thermogenesis (Rothwell, et al., 1991; Plata-Salaman, 1996; Wallenius, et al., 2002). More recently, IL-6 has been suggested to promote the action of insulin through central effects (Flores, et al., 2006; Shirazi, et al., 2013; Mauer, et al., 2014), however prolonged engagement of the cytokine signaling cascade is associated with pathology (Campbell, et al., 2014)

The suppression of baseline and glucose-stimulated insulin and glucagon levels observed in NesCreIL-6Rα KD animals indicate the cytokine to be prominently involved in the regulation of the brain-pancreas axis. Furthermore, persistent hyperphagia and inhibition of fat oxidation in the novel transgenic, implicate the cytokine in the integration of meal-related factors (e.g. glucose) at the brain and the modulation of acute- and long-term autonomic output that drive changes in metabolism in the periphery (Mauer, et al., 2014). IL-6 would appear to act centrally to regulate pancreatic insulin secretion, and perhaps increases observed in response to HF-feeding in both mice and humans represent a protective response to augment insulin secretion in the face of persistent increases in circulating nutrients.

In addition to the pyrogenic and anorexigenic effects of cytokines in the context of infection, our data suggest increases in circulating IL-6 to act at the brain to intercept prolonged exposure to hyperphagia, at least in part through enhancing insulin secretion. SC KDs exhibited hyperphagia that was accompanied by significant increases plasma IL-6, that unlike control animals were not further increased in response to HFD. Given the leaner phenotype observed in KD SC mice, it is possible that increases in circulating IL-6 act in the brain to indirectly promote increases in adipose tissue expansion through insulin. On the other hand, IL-6 acts centrally to promote thermogenesis through fat oxidation, an effect that was disrupted in KD mice, but was of no consequence on SC. However, in HF-fed KDs, the combined suppression of GSIS and reduced glucose clearance, as well as hyperphagia and inhibition of fat oxidation resulted in increased adiposity. Collectively, this composite phenotype observed in our mouse model would suggest IL-6 to be a component of the acute protective response to nutrient excess in mammals, whose prolonged engagement in DIO and type 2 diabetic humans experiences resistance, further promoting metabolic dysfunction. KD mice exhibited a form of metabolic inflexibility in terms of fuel utilization and decreased thermogenesis that likely contributed to the increased body fat observed in response to HFD. This scenario would match the phenotype observed in a number of chronic DIO and T2D patients, where the ability of the body to regulate food intake and utilize fuel is compromised (Larson, et al., 1995; Labayen, et al., 2004). Despite the dramatic inhibition of GSIS, KD mice were still able to clear glucose, through marginal fluctuations in plasma insulin levels. This might suggest central IL-6 signaling to be indirectly involved in the regulation of

insulin sensitivity at liver (Inoue, et al., 2006) or muscle tissue (Pedersen, et al., 2001).

In summary, the NesCreIL-6Rα KD exhibited brain-specific down-regulation of the IL-6Rα system with prominent effects in metabolically active mediobasal hypothalamus, which was associated with a significant effect on insulin secretion and energy expenditure. However, further studies would be required to outline the precise contribution of individual neuronal populations and compensatory changes in the expression of circulating and tissue-specific biological markers to the phenotype.

Diabetic Treatment and Interleukin-targeted therapies

Glycated haemoglobin (HbA1c) is the current recommended method of assessment of long term glycaemia in diabetic patients (Nielsen, et al., 2014). Glycated haemoglobin is formed by reversible glycation at the N-terminus and is known to increase proportionally to glucose intolerance. The practice is followed as HbA1c levels reflect the fluctuation in glucose levels over a period of 2-3 months, the typical lifespan of erythrocytes (Jeffcoate, 2004; Tahara & Shima, 1993). This provides an obvious advantage to assessment of fasted blood glucose alone, even though diet or treatment can alter HbA1c values within 6 weeks. HbA1c in health is below 42mmol/mol (<6%), ranges between 42 and 47mmol/mol (6.0-6.4%) in pre-diabetic patients and exceeds 48mmol/mol (>6.5%) in diabetes (International Expert Committee, 2009). Current regiments suffer from an array of side-effects such as weight gain, hypoglycaemia, gastrointestinal infections and bone fragility (Barnett, 2013). An over-reliance on insulin therapy should also be noted; that albeit effective in the management of hyperglycaemia and dyslipidaemia, is not subject to physiological regulation and is accompanied with other long term complications (Lavernia, 2008; Shogbon & Levy, 2000; Moghissi, 2010; Reider, et al., 2009).

Metformin is currently the first line of pharmacological treatment, although the precise mechanisms by which the biguanide is able to induce its potent anti-hyperglycaemic effects are not clear (Rena, et al., 2013). Activation of AMPK via metformin has been suggested to involve biguanide metal-binding properties (Logie, et al., 2012), which would be consistent with the metallic taste reported by patients. Metformin + insulin dual therapy is most effective at regulating glycaemia and body

weight, even compared to insulin monotherapy (Strowig, et al., 2002). Despite being particularly effective at HbA1c regulation, this choice of dual therapy increases both the incidence of hypoglycaemia while still posing the thread of cardiovascular complications associated with increased body weight (Anon., 2015; Anon., 2014).

Sulfonylureas have now been used for a number of decades (Mirsky, et al., 1956) in diabetic care and are known to lower HbA1c in monotherapy (Anon., 1985). Their action involves glucose independent inhibition of potassium flux through K_{ATP} channels at the β cell (Ashcroft & Rorsman, 1989; Smith, et al., 1990). This allows for depolarization and opening of voltage-gated Ca^{2+} channels, stimulating insulin secretion (Panten, et al., 1996). The use of sulfonylureas (Wheeler, et al., 2013) and their combination with metformin in particular, is of questionable long-term efficacy, as it has been associated with dose-related hypoglycaemia, cardiovascular complications and morbidity (Roumie, et al., 2014; Li, et al., 2014; Mogensen, et al., 2015).

Thiazolidinediones, on the other hand, target the PPARγ signaling cascade (de Douza, et al., 2001; Spiegelman, 1998), inducing an expansion of adipose tissue, which ameliorates inflammation and insulin resistance (Saraf, et al., 2011; Ikeda & Sugiyama, 2011). Unfortunately, data suggest that unwanted side effects include increases in body weight (Boden & Zhang, 2006; Hermansen & Mortensen, 2007), increased incidence of bone fractures (Riche & King, 2010; Zhu, et al., 2014), and alarmingly increased incidence of bladder cancer (Turner, et al., 2014; Tseng, 2014) and cardiovascular events (Della-Morte, et al., 2014).

When considering the aging population of the world today as well as the increasing incidence of DIO and T2D, it would appear that new pharmacotherapies are required that are associated with fewer side effects and the risk of further cardiovascular events through their use over extended periods of time. In line with other recent work (Maeder, et al., 2011; Kraakman, et al., 2013; Emamaullee, et al., 2009), studies using the NesCreIL-6Rα KD provide evidence that cytokine signaling could provide a means of manipulation of insulin secretions that would not rely on previously established pharmacotherapies or insulin replacement therapy in itself. Central and peripheral cytokine signaling are increasingly understood to participate in the beneficial effects of exercise, that is still the most common means of management of long term metabolic stress (Pi-Sunyer, 2012; Danesh, et al., 2008; Petersen & Pedersen, 2006). Possible pitfalls of interleukin-signaling based therapies were

previously exposed, in phase I studies using recombinant human CNTF in ALS patients, as some subjects developed auto-antibodies for the drug (Anon., 1995). However, advancements since then, have allowed for drugs like the highly efficacious Tocilizumab to be approved by the FDA towards the treatment for rheumatoid arthritis and Castleman Disease patients (Nishimoto, 2005; Nishimoto, et al., 2004; Maini, et al., 2006). The drug acts by blocking both modes of IL-6 signaling, but was interestingly found to been associated with hyperlipidaemia and weight gain. Similarly, recent translational has indicated the treatment of hypercholesterolaemic mice with the natural blocker of IL-6 *trans-signaling*, sgp130Fc fusion protein, ameliorated atherosclerosis, but had no effect on weight gain and serum lipid levels in response to HF-feeding in mice (Rabe, et al., 2008; Schuett, et al., 2012).

The selective pharmacological blockade of IL-6 *trans-signaling* would appear to be good strategy for targeting the accumulation of aberrant inflammatory signaling and atherosclerosis observed in DIO, however as indicated by our studies, the inhibition of the insulin-sensitizing effects of *classical signaling*, is highly unwelcome in the context of diabetic disease. Similarly studies selectively targeting activation this aspect of IL-6 cytokine family signaling in muscle and brain have been particularly promising in terms of insulin and leptin resistance (Watt, et al., 2006; Steinberg, et al., 2006). Administration of IL-6 in healthy humans was previously shown to have no direct effects on glucose utilization (Steenber, et al., 2003), despite promoting increased fat oxidation (Van Hall, et al., 2003). Perhaps in conjunction with necessary lifestyle changes and other compatible therapies, a pharmacological agent that would block *trans-signaling* and yet drive the selective activation of cytokine signaling through the membrane-bound receptor would be of therapeutic benefit.

GLP-1 is an incretin secreted by the small intestine to stimulate glucose-dependent insulin secretion, inhibits glucagon secretion, delays gastric emptying and promote satiety (Nauck, et al., 1993; Enc, et al., 2001; Lee, et al., 2002). GLP-1 analogues have shown tremendous potential, with a reported single dose glucose-lowering potency similar to one or two daily insulin injections (Drucker & Nauck, 2006). Synthetic inhibitors of DPP-4, the enzyme responsible for degradation of GLP-1 are currently used in T2D therapy (DeFronzo, et al., 2012; Vilsboll, et al., 2010). These drugs display high potency in HbA1c regulation and confer the advantage of inducing weight loss, which is not accompanied by the risk of hypoglycaemia (White, 2009; Neumiller, 2009). Common side effects in combination drug therapy include nausea

and gastrointestinal effects (Anon., 2011; Liu, et al., 2014), however most alarmingly and despite their recent introduction a link to the development of pancreatitis and pancreatic cancer has been reported in patients (Tella & Rendell, 2015; Gokhale, et al., 2014; Monami, et al., 2014; Filippatos, et al., 2014; Raz, et al., 2014). Results using the NesCreIL-6Rα, in agreement with studies published by the Donath group (Ellingsgaard, et al., 2008; Shirazi, et al., 2013), indicate central IL-6 signaling as a potential enhancer of the ability of GLP-1 agonists to promote the action of insulin. GLP-1 agonists and IL-6 action itself unlike metformin, SURs and glitazones, are not associated with increases in body weight and are of no direct consequence to blood glucose levels or the incidence of cardiovascular events. Perhaps a pharmacological agent targeting specific enhancement of the IL-6 *classical signaling* over *trans-signaling* in the hypothalamus could provide a means to limit some of the unwanted risks associated with GLP-1 agonists through decreasing the required dose. Further studies in the safety, effectiveness and compatibility of such drug combinations would be required.

Future Work

Changes in energy expenditure and the anabolic utilization of fat have been previously shown to involve interaction of hindbrain catecholamine neurons regulating corticotropin-releasing hormone neurons of the paraventricular hypothalamic nucleus that promote changes in the autonomic output of the brain (Ritter, et al., 2006; Hudson & Ritter, 2004; Li, et al., 2013). The phenotype observed in the NesCreIL-6Rα KD would be consistent with disruption of this axis, in agreement with recent studies implicating IL-6 signaling in the response to GLP-1 analogues. Towards the specific targeting of neuronal populations, a particularly good option would be the use of *Sf1 CRE* (Jackson Laboratories®) mice; that induces recombination in GABAergic and Glutamatergic neurons of the glucose-sensing ventromedial hypothalamus involved in the regulation of autonomic responses to changes in energy homeostasis. This model was successfully used for mapping of the ventromedial hypothalamus in the developing mouse brain (Cheung, et al., 2013), while previous studies indicated the action of leptin at this site to be required for regulation of body weight homeostasis (Dhillon, et al., 2006). Another particularly

good candidate when considering the food intake phenotype observed would be the *Pomc Cre* (Jackson Laboratories®) mouse that was previously used to study the action of leptin in the brain (Balthasar, et al., 2004).

Importantly, the use of CRE mice is known to be accompanied with an array of off-target effects; and the *Sf1 CRE* mouse itself is known to also induce recombination in the cerebral cortex and caudal brainstem, while scattered recombination in the adrenal, gonads and pituitary that might interfere with the phenotype (Pihlajoki, et al., 2013; The Jackson Laboratory, 2011; Harris, et al., 2014). Intracerebroventricular administration of adenoviral vectors (Xue, et al., 2008; Xue, et al., 2012) that mediate the disruption of the IL-6 receptor would confine disruption of the receptor under the regulation of region-specific promoters (e.g. AAV2/8-Cre in the VMH) would minimize non-specific effects (Unger, et al., 2007). Designer receptors exclusively activated by designer drugs (DREADD) have been shown to be of particular efficacy and specificity, and recent studies have demonstrated the specific contribution of neuronal populations of the hypothalamus and not the hindbrain to modulate satiety and energy expenditure (Zhan, et al., 2014). Additional selectivity, specificity in gene targeting has been reported for the novel CRISPR-Cas system (Sander & Joung, 2014; Ma, et al., 2014) that could also be utilized in this fashion.

Limitations

My studies began with a particular focus on the role of hypothalamic inflammation in diabetic disease. It was not however possible to acquire a transgenic model that would limit the recombination events to the hypothalamus specifically using our current means. Nes-Cre mediated down-regulation of the IL-6 receptor, albeit successful at inducing recombination centrally as well as indicating the importance of IL-6 signaling in diabetic disease development, lacked specificity.

Verification of the transgenic was attempted by several different techniques, however since our Nes-Cre mediated approach did not ablate but down-regulated the receptor system; this proved particularly challenging. In addition, the IL-6Rα$^{flox/flox}$ mouse mediates its effects by disrupting the binding site of the receptor, which made verification at the protein level impossible. This prompted us to pursue functional approaches, such as the IP administration of IL-6 to transgenic animals. Having also demonstrated down-regulation of the receptor at mRNA by real time PCR **(Figures 3.4.2)** and protein level by immunohistochemistry **(Figures 3.8.1-3)**, as well disruption of the *in vivo* pSTAT3 response to IL-6 in the brain **(Figures 3.5.1-3)** as well as the *ex vivo* mediobasal hypothalamus **(Figure 3.7)**, the phenotype observed in our *in vivo* studies is at large the consequence of central effects. In attempts to verify the down-regulation of the receptor by immunohistochemistry, we found the effects induced in NesCre-KDs to be variable, and even though primarily confined to neuronal populations some effects in astrocytic populations were observed **(Figure 3.8.4)**. However, due to the small number of animals we were able to use at this point (n=2), it was not possible to provide any meaningful quantification of the effects observed by immunohistochemistry.

Finally, it would be important to address that differences observed in 2 separate occasions in KD animals **(Figures 4.3, 4.9.1)** were not observed in examination using the CLAMS/Oxymax® animal monitoring system **(Figure 4.7.1)**. From closer examination of the feeding pattern of experimental animals during the procedure; we conclude the differences relate to the length of the study and the stress of the procedure, as a number of animals appeared to be having issues with food accessibility due to the novel environment. Shorter studies or intermittent exposure to the experimental set-up would account for these differences.

Bibliography

Adachi, A., Shimizu, N., Oomura, Y. & Kobashi, M., 1984. Convergence of hepatoportal glucose-sensitive afferent signals to glucose-sensitive units within the nucleus of the solitary tract. *Neurosci Lett,* 46(2), pp. 215-218.

Ahima, R., Saper, C., Flier, J. & Elmquist, J., 2000. Leptin regulation of neuroendocrine systems. *Front Neuroendocrinol,* 21(3), pp. 263-307.

Akira, S., 2003. Toll-like receptor signaling. *Journal of Biological Chemistry,* 278(40), pp. 38105-38108.

Akira, S., Hirano, T., Taga, T. & Kishimoto, T., 1990. Biology of multifunctional cytoines: IL 6 and related molecules (IL 1 and TNF). *FASEB,* Volume 4, pp. 2860-2867.

Alessi, D. R., 2001. Discovery of PDK1, one of the missing links in insulin signal transduction. *Biochem Society Trans,* Volume 29, pp. 1-14.

Alessi, D. R. et al., 1997. Characterization of a 3-phosphoinositide-dependent protein kinase which phosphorylates and activates protein kinase B alpha. *Curr Biol,* Volume 7, pp. 261-269.

Alexander, W. & Hilton, D., 2004. The role of suppressors of cytokine signaling proteins in regulation of the immune response. *Annu. Rev. Immunol.,* Volume 22, pp. 503-529.

Alivisatos, J. G. & McCullagh, E., 1955. Studies with glucagon in patients with insulin sensitivity. *J Am Med Assoc,* 11(159), pp. 1089-1105.

Amiel, S. A., 2009. Hypoglycemia from the laboratory to the clinic. *Diab.Care,* 32(8), pp. 1364-1371.

Anon., 2003. Atlizumab: anti-IL-6 receptor antibody-Chugai, anti-interleukin-6 receptor antibody-Chugai, MRA-Chugai. *BioDrugs,* 17(5), pp. 369-372.

Ashcroft, F., 2005. ATP-sensitive potassium chanellopathies: Focus on Insulin Secretion. *J Clin Invest,* Volume 115, pp. 2047-2058.

Azar, S. T. et al., 2002. Leptin levels in patients with Type 1 diabetes receiving intensive insulin therapy compared with those in patients receiving conventional insulin therapy. *J Endocrinol Invest,* 25(8), pp. 724-6.

Badger, A. M. et al., 1996. Pharmacological profile of SB 203580, a selective inhibitor of cytokine suppressive binding protein/p38 kinase, in animal models of arthritis, bone

resorption, endotoxin shock and immune function. *J Pharmacol Exp Ther,* 279(3), pp. 1453-1461.

Bado, A. et al., 1998. The stomach is a source of leptin. *Nature,* Volume 394, pp. 790-793.

Baeuerle, P. A. & Baltimore, D., 1988. I kappa B: a specific inhibitor of the NF-kappa B transcription factor. *Science,* 242(4878), pp. 540-546.

Bailey, S. M., Udoh, U. S. & Young, M. E., 2014. Circadian regulation of metabolism. *J Endocrinol,* Volume 222, pp. 75-96.

Banks, W. A., J., K. A. & Gutierez, E. G., 1994. Penetration of interleukin-6 across the murine blood-brain barrier. *Neurosci Lett,* Volume 179, pp. 53-56.

Bantubungi, K., Prawitt, J. & Staels, B., 2012. Control of metabolism in nutrient regulated nuclear receptors acting in the brain. *J Steroid Biochem & Mol Biol ,* Volume 130, pp. 126-137.

Barsh, G., Farooqi, I. & Rahily, S., 2000. Genetics of body weight regulation. *Nature,* Volume 404, pp. 644-651.

Bastard, J. P. et al., 2000. Elevated levels of IL-6 are reduced in serum and subcutneous adipose tissue of obese women after weight loss. *J Clin Endocrinol Metab,* 85(9), pp. 3338-3342.

Baver S.B., H. K. et al., 2014. Leptin modulates the intrinsic excitability of AgRP/NPY neurons in the arcuate nucleus of the hypothalamus. *J Neurosci,* 34(16), pp. 5486-5496.

Beall, C., Ashford, M. L. & McCrimmon, R. J., 2012. The physiology and pathophysiology of the neural control of the counterregulatory response. *Am J Physiol Regul Integr Comp Physiol,* Volume 302, pp. 215-225.

Beall, C. et al., 2012. Mouse hypothalamic GT1-7 cells demonstrate AMPK-dependent intrinsic glucose-sensing behaviour. *Diabetolo,* Volume 55, pp. 2432-2444.

Beall, C. et al., 2010. Loss of AMP-activated protein kinase alpha2 subunit mouse beta cells impairs glucose-stimulated insulin secretion and inhibits their sensitivity to hypoglycaemia. *Biochem J,* Volume 429, pp. 323-333.

Berglund, E. et al., 2012. Direct leptin action on POMC neurons regulates glucose homeostasis and hepatic insulin sensitivity in mice. *J Clin Invest,* 122(3), pp. 1000-1009.

Bernad, A. et al., 1994. Interleukin-6 is required in vivo for the regulation of stem cells and committed progenitors of the hematopoietic system. *Immun,* Volume 1, pp. 725-731.

Besedovsky, H. O. & Del Rey, A., 2011. Central and peripheral cytokines mediate immune-brain connectivity. *Neurochem Res,* Volume 36, pp. 1-6.

Besendovsky, H. O. & Del Rey, A., 1996. Immune-neuro-endocrine interactions: facts and hypotheses. *Endocr Rev,* 17(1), pp. 64-102.

Beurel, E. & Jope, R., 2009. Lipopolysaccharide-induced interleukin-6 production is controlled by glycogen synthase kinase-3 and STAT3 in the brain. *J Neuroinflammation,* 6(9).

Beverly, J. L., De Vris, M. G., Bouman, S. D. & Arseneau, L. M., 2001. Noradrenergic and GABAergic systems in the medial hypothalamus are activated during hypoglycemia. *Am J Physiol Regul Integr Comp Physiol,* 280(2), pp. R563-569.

Beyaert, R. M. et al., 1996. The p38/RK mitogen-activated protein kinase pathway regulates interleukin-6 synthesis response to tumor necrosis factor. *embo j,* 15(8), pp. 1914-1923.

Birkenkamp, K. U., Eseelink, M. T., Kruijer, W. & Vellenga, E., 2000. An inhibitor of PI3-K differentially affects proliferation and IL-6 protein secretion in normal and leukemic myeloid cells depending on the stage of differentiation. *Exp Hematol,* 28(11), pp. 1239-1249.

Bjorbaek, C. et al., 1998. Expression of leptin recepto isoforms in rat brain microvessels. *Endocrinology,* 139(8), pp. 3485-3491.

Bjorbaek, C. & Kahn, B., 2004. Leptin singaling in the central nervous system and the periphery. *Recent Prog Horm Res,* Volume 59, pp. 305-331.

Blindenbacher, A. et al., 2003. Interleukin 6 is important for survival after partial hepactomy in mice. *Hepatology,* 38(3), pp. 674-682.

Blouet, C. & Schwartz, G. J., 2009. Hypothalamic nutrient sensing in the control of energy homeostasis. *Behaviour Brain Res,* Volume 209, pp. 1-12.

Bode, J. et al., 2001. The MKK6/p38 mitogen-activated protein kinase pathway is capable of inducing SOCS3 gene expression and inhibits IL-6 induced transcription. *Biol Chem,* Volume 382, pp. 1447-1453.

Borges, M. C. et al., 2012. High-fat diet blunts activation of the nuclear factor-kappaB signaling pathway in lipopolysaccharide-stimulated peritoneal macrophages of Wistar rats. *Nutrition xxx,* pp. 1-7.

Borg, M. A. et al., 1999. Chronic hypoglycemia and diabetes impair counterregulation induced by localized 2-deoxy-glucose perfusion of the ventromedial hypothalamus in rats. *Diab,* Volume 48, pp. 584-587.

Bortolon, J. R. et al., 2012. Persistence of inflammatory response in intense exercise in diabetic rats. *Exp Diab Res.*.

Bousquet, C., Zatelli, M. C. & Melmed, S., 2000. Direct regulation of pituitary proopiomelanocortin by STAT3 provides a novel mechanism of imunno-neuroendocrine interfacing. *J Clin Invest,* 106(11), pp. 1417-1425.

Brandt, C. et al., 2012. IL-6 regulates exercise and training-induced adaptations in subcutaneous adipose tissue in mice. *Acta Physiol ,* Volume 205, pp. 224-235.

Brazil, D. P. & Hemmings, B. A., 2001. Ten years of PKB signaling: A hard Akt to follow. *Trends Biochem Sci,* Volume 26, pp. 657-664.

Briesemeister, D. et al., 2012. Differences in serum cytokine levels between wild type mice and mice with a targeted mutation suggests necessity of using control littermates. *Cytokine,* 60(3), pp. 626-633.

Bruunsgaard, H. et al., 1997. Exercise-induced increase in serum interleukin-6 in humans is related to muscle damage. *J of Physiology,* 499(3), p. 833841.

Burdakov, D., Luckman, S. M. & Verkhratsky, A., 2005. Glucose-sensing neurons of the hypothalamus. *Phil. Trans. R. Soc. B,* Volume 360, pp. 2227-2235.

Busbridge, N. J. D. M. J. et al., 1989. Central activation of thermogenesis and fever by IL-1beta and IL-1alpha involves different mechanisms. *Biochem Biophys Res Commun,* 162(2), pp. 591-596.

Campbell, I. L. et al., 2014. Trans-signaling is a dominant mechanism for the pathogenic actions of interleukin-6 in the brain. *J Neurosci,* 34(7), pp. 2503-2513.

Candilio, L., Malik, A. & Hausenloy, D., 2013. Protection of organs other than the heart by remote ischemic conditioning. *J Cardiovasc Med (Hagerstown),* 14(3), pp. 193-205.

Capoccia, S. et al., 2013. Quality and timing of stressors differentially impact on brain plasticity and neuroendocrine-immune function in mice. *Neural Plast,* Volume 2013.

Cardoso, S. et al., 2011. Impact of STZ-induced hyperglycemia and insulin-induced hypoglycemia in plasma amino acids and cortical synpatosomal neurotansmitters. *Synapse,* 65(6), pp. 457-466.

Castell, J. V. et al., 1988. Recombinant human interleukin-6 (IL-6/BSF-2/HSF) regulates the synthesis of acute phase proteins in human hepatocytes. *FEBS,* 232(2), pp. 347-350.

Chaar, V. et al., 2011. Effect of strenuous physical exercise on circulating cell-derived microparticles. *Clin Hemorheol Microcirc,* 47(1), pp. 15-25.

Chalaris, A. et al., 2007. Apoptosis is a natural stimulus of IL6R shedding and contributes to the proinflammatory trans-signaling function of neutrophils. *Blood,* 110(6), pp. 1748-1755.

Chen, W. et al., 2013. Changes of systemic and local myeloperoxidase and tumor necrosis factor-α in rats with myocardial injury induced by hind-limb ischemia-reperfusion. *Nan Fang Yi Ke Da Xue Xue Bao,* 33(5), pp. 761-764.

Chun-Xia, Y. & Tschop, M. H., 2012. Brain-gut-adipose-tissue communication pathways at a glance. *Dis Model Mech,* 5(5), pp. 583-587.

Claret, M. et al., 2007. AMPK is essential for energy homeostasis regulation and glucose sensing by POMC and AgRP neurons. *J Clin Invest,* 117(8), pp. 2325-2336.

Codeluppi, S. et al., 2014. Interleukin-6 secretion by astrocytes is dynamically regulated by PI3K-mTOR-Caclium signaling. *PLoS One,* 9(3), p. e92649.

Cohen, P. & Frame, S., 2001. The renaissance of GSK3. *Nat Rev Mol Cell Biol,* Volume 2, pp. 769-776.

Cone, R. D., 2006. Studies on the physiological functions of the melanocortin system. *Endocr Rev,* 24(5), pp. 63-67.

Cone, R. D. et al., 2001. The arcuate nucleus as a condit for diverse signals relevant to energy homeostasis. *Int J Ob and Rel Met Dis,* 24(5), pp. 63-67.

Cooperbeg, B. A. & Cryer, P. E., 2009. Beta-cell-mediated signaling predominates over direct alpha-cell signaing in the regulation of glucagon secretion in humans. *Diab Care,* 32(12), pp. 2275-2280.

Cortright, R. & Dohm, G., 1997. Mechanisms by which insulin and muscle contraction stimulate glucose transport. *Can J Appl Physiol,* 22(6), pp. 519-530.

Cotrozzi, G., Casini Raggi, V., Relli, P. & Buzzelli, G., 1997. Role of the liver in the regulation of glucose metabolism in diabetes and chronic liver disease. *Ann Ital Med,* 12(2), pp. 87-91.

Croker, B. A. et al., 2012. IL-6 promotes acute and chronic inflammatory disease in the absence of SOCS3. *Immunol Cell Biol,* 90(1), pp. 124-129.

Croker, B. et al., 2003. SOCS3 negatively regulates IL-6 signaling in vivo. *Nat Immunol,* Volume 4, pp. 540-545.

Croucher, P. I., Wang, F. & Hargreaves, P. G., 1999. Interleukin-6 receptor shedding: a possible role for members of the ADAM family. *Biochem Soc Trans,* 27(2), pp. 224-228.

Cryer, P., 2004. Glucose counterregulatory hormones: Physiology, Pathophysiology, and Relevance to Clinical hypoglycemia. *Diabetes Mellitus: A Fundamental and Clinical Text*.

Cryer, P. E., 1982. Adrenergic mechanisms in glucose counterregulation in normal and diabetic man. *Cardiovasc Res,* 16(7), pp. 370-376.

Cryer, P. E., 2008. The barrier of hypoglycemia in diabetes. *Diabetes ,* 57(12), pp. 3169-3176.

Cryer, P. E. & Gerich, J. E., 1985. Glucose counterregulation, hypoglycemia and intensive insulin therapy in diabetes mellitus. *N Engl J Med,* 313(4), pp. 232-241.

Cusin, I. et al., 1998. Chronic central leptin infusion enhances insulin-stimulated glucose metabolism and favors the epxression of uncoupling proteins. *Diabetes,* Volume 47, pp. 1014-1019.

Dahlstrand, J., Lardelli, M. & Lendahl, U., 1995. Nestin mRNA expression correlates with the central nervous system progenitor cell state in many, but not all, regions of developing central nervous system. *Brain Res Dev Brain Res,* Volume 84, pp. 109-129.

Das, S. K. & Balakrishnan, V., 2011. Role of cytokines in the pathogenesis of Non-alcoholic fatty liver disease. *Ind J Clin Biochem,* 26(2), pp. 202-209.

Das, U. N., 2001. Is obesity an inflammatory condition?. *Nutrition,* Volume 17, pp. 953-966.

Dawn, B., Xuan, Y. T., Guo, Y. & al, e., 2004. IL-6 plays an obligatory role in late preconditioning via JAK-STAT signaling and upregulation of iNOS and COX-2. *Cardiovasc Res.,* Volume 64, pp. 61-71.

De Feo, P. et al., 1986. Comparison of glucose counterregulation during short-term and prolonged hypoglycemia in normal humans. *Diabetes,* 35(5), pp. 563-569.

de Rooij, J. et al., 1998. Epac is a Rap1 guanine-nucleotide-exchange factor directly activated by cyclic AMP. *Nature,* 396(6710), pp. 474-477.

de Vris, M., Lawson, M. & Beverly, J., 2005. Hypoglycemia-induced noradrenergic activation in the VMH is a result of decreasd ambient glucose. *Am J Physiol Regul Integr Comp Physiol,* 289(4), pp. R977-981.

Dhillon, H. et al., 2006. Leptin directly activates SF1 neurons in the VMH, and its action by leptin is required for normal body-weight homeostasis. *Neuron,* Volume 49, pp. 191-203.

Dietrich, M., Liu, Z.-W. & Horvath, T., 2013. Mitochondrial dynamics controlled by mitofusins regulate Agrp neuronal activity and diet-induced obesity. *Cell,* 155(1), pp. 188-199.

Dietrich, M., Tamas, L. & Horvath, L., 2013. Hypothalamic control of energy balance: Insights into the role of synaptic plasticity. *Trend in Neuroscience,* 36(2), pp. 65-73.

Donath, M. Y. & Burcellin, R., 2013. GLP-1 effects on islets: Hormonal, Neuronal, or Paracrine?. *Diab Care,* 36(2), pp. 145-148.

Donsheng, C. & Liu, T., 2012. Inflammatory cause of metabolic syndrome via brain stress and NF-kappaB. .*AGING,* 4(2), pp. 98-115.

Dotson, S., Failing, H. J., Freeman, R. & Adler, G. K., 2008. Hypoglycemia increases serum interleukin-6 levels in healthy men and women. *Diab Care,* Volume 23, pp. 1222-1223.

Dubois, N. C., H., D. & al., e., 2006. Nestin-Cre transgenic mouse line Nes-Cre1 mediates highly efficient Cre/loxP mediated recombination in the nervous system, kidney, and somite-derived tissues. *Genesis,* 44(8), pp. 355-360.

Dunn, A. J., 2000. Cytokine activation of the HPA axis. *Ann N Y Acad Sci,* Volume 917, pp. 608-617.

Elias, C. et al., 1999. Leptin differentially regulates NPY and POMC neurons projecting to the lateral hypothalamic area. *Neuron,* 23(4), pp. 775-786.

Ellingsgaard, H. et al., 2011. Interleukin-6 enhances insulin secretion by increasing glucagon-like peptide-1 secretion from L cells and alpha cells. *Nat Med,* 17(11), pp. 1481-1490.

Elmendorf, J. & Pessin, J., 1999. Insulin signaling regulating the trafficking and plasma membrane fusion of GLUT-4 containing intracellular vesicles. *Exp Cell Res,* 253(1), pp. 55-62.

Elrick, H., 1956. Glucagon and the regulation of carbohydrate metabolism. *Nature,* 177(4515), pp. 892-893.

Erickson, M. & Banks, W. A., 2011. Cytokine and chemokine responses in serum and brain after signle and repeated injection of LPS: multiplex quantification with path analysis. *Brain Behav Immun,* 25(8), pp. 1637-1648.

Erta, M., Quintana, A. & Hidalgo, J., 2012. Interleukin-6, a major Cytokine in the Central Nervous system. *Int J Biol Sci,* 8(9), pp. 1254-1266.

Fahmi, A. et al., 2013. P42/P44-MAPK and PI3K are sufficient for IL-6 family cytokines/gp130 to signal to hypertrophy and survival in cardiomyocytes in the absence of JAK/STAT activation. *Cellular Signaling,* Volume 25, pp. 893-909.

Febbraio, M. A. & Pedersen, B., 2002. Muscle-derived interleukin-6: mechanisms for activation and possible biological roles. *FASEB,* 16(11), pp. 1335-1347.

Fei, H. et al., 1997. Anatomic localization of alternatively spliced leptin receptors (Ob-R) in mouse brain and other tissues. *Pro Natl Acad Sci,* Volume 94, pp. 7001-7005.

Feng, M., Wang, Q., Wang, H. & Guan, W., 2013. Tumor necrosis factor-alpha preconditioning attentuates liver ischemia/reperfusion injury through preserving sarco/endoplasmis reticulum calcium-ATPase function. *J Surg Res,* 184(2), pp. 1109-1113.

Fernandez-Real, J. M. & Pickup, J. C., 2012. Innate immunity, insulin resistance and type 2 diabetes. *Diabetolog.,* Volume 55, pp. 273-278.

Ferreira, R. C. F. D. F. et al., 2013. Functional IL6R358Ala Allele impairs classical IL-6 receptor signaling and influences risk of diverse inflammatory diseases. *PLoS Gen,* 9(4).

Fiers, W. et al., 1987. Gene cloning and structure-function relationship of cytokines such as TNF and interleukins. *Immunol Lett,* 16(3-4), pp. 219-226.

Fioramonti, X. et al., 2010. Ventromedial hypothalamic nitrix oxide production is necessary for hypoglycemia detection and counterregulation. *Diabetes,* 59(2), pp. 519-528.

Friedman, J., 2000. Obesity in the new millenium. *Nature,* Volume 404, pp. 632-634.

Fukuda, M., Williams, K. W., Gautron, L. & Elmquist, J. K., 2011. Induction of Leptin Resistance by Activation of cAMP-Epac Signaling. *Cell Metab.,* 13(3), pp. 331-339.

Fullerton, M. D. et al., 2013. Single phosphorylation sites in ACC1 and ACC2 regulate lipid homeostasis and the insulin-sensitizing effects of metforming. *Nature Med,* Volume 19, pp. 1649-1654.

Gabellec, M. M., Griffais, R., Fillion, G. & Haour, F., 1996. Interleukin-1 receptors type I and type II in the mouse brain: kinetics of mRNA expression after peripheral administration of bacterial LPS. *J Neuroimmunol,* Volume 66, pp. 65-70.

Gadek-Michalska, A., Tadeusz, J., Rachwalska, P. & Bugajski, J., 2013. Cytokine, prostaglandins and nitric oxide in the regulation of stress-response systems. *Pharmacol Rep,* 65(6), pp. 1655-1662.

Gao, Z. et al., 2012. Synergy between IL-6 and TGF-beta signaling promotes FOXP3 degradation. *Int J Clin Exp Pathol,* 5(7), pp. 626-633.

Garhatz, C. et al., 1996. Differential activation of acute phase response factor/STAT3 and STAT1 via the cytoplasmic domain of the interleukin 6 signal transducer gp130. I. Definition of a novel phosphotyrosine motif mediating STAT1 activation. *J Biol Chem,* 271(22), pp. 12991-12998.

Gidday, J. M., 2006. Cerebral preconditioning and ischaemic tolerance. *Nature Rev Neuro,* 7(6), pp. 437-448.

Glund, S. & Krook, A., 2008. Role of interleukin-6 signaling in glucose and lipid metabolism. *Acta Physiol. ,* Volume 192, pp. 37-48.

Gray, S. & Vidal-Puig, A., 2007. Adipose tissue expandability in the maintenance of metabolic homeostasis. *Nutr Rev,* 65(6 Pt 2), pp. S7-S12.

Green, C. J. et al., 2011. Counter-modulation of fatty acid-induced pro-inflammatory nuclear factor kappaB signaling in rat skeletal muscle cells by AMPK-activated protein kinase. *Biochem J,* Volume 435, pp. 463-474.

Greenhill, C. J. et al., 2011. IL-6 trans-signaling modulates TLR4-dependent inflammatory responses via STAT3. *J Immunol,* Volume 186, pp. 1199-1208.

Hardwood, A. J., 2001. Regulation of GSK-3: a cellular multiprocessor. *Cell,* Volume 105, pp. 821-824.

Harno, E., Cottrell, E. & White, A., 2013. Metabolic Pitfalls of CNS Cre-based technology. *Cell Metab,* Volume 18, pp. 21-28.

Hattori, R. et al., 2001. Role of STAT3 in ischemic preconditioning. *J Mol Cell Cardiol,* 33(11), pp. 1929-1936.

Heinrich, P. et al., 1998. Interleukin-6-type cytokine signaling through gp/130/Jak/STAT pathway. *Biochem J,* 334(2), pp. 297-314.

Heller, S. R. & Cryer, P. E., 1991. Reduced neuroendocrine of symptomatic responses to subsequent hypoglycemia after 1 episode of hypoglycemia in nondiabetic humans. *Diabetes,* 40(2), pp. 223-226.

Hemmann, U. et al., 1996. Differential activation of acute phase response factor/Stat3 and Stat1 via the cytoplasmic domain of the interleukin 6 signal transducer gp130. II.Src homology SH2 domains define the specificity of stat factor activation. *J Biol Chem,* 271(22), pp. 12999-13007.

Herman, A. P., Miszal, T., Romanowicz, K. & Tomaszewska-Zaremba, D., 2012. Central injection of exogenous IL-1beta in the control activities of hypothalamic pituitary-gonadal axis in anestrous ewes. *Reprod Domest Anim,* 47(1), pp. 44-52.

Herman, J., Flak, J. & Jankord, R., 2008. Chronic stress plasticity in the hypothalamic paraventricular nucleus. *Prog Brain Res,* Volume 170, pp. 353-364.

Herrmann, O. et al., 2003. Regulation of body temperature and neuroprotection by endogenous interleukin-6 in cerebral ischemia. *J Cereb Blood Flow Metab,* 23(4), pp. 406-415.

Hideshima, T., Nakamura, N., Chauhan, D. & Anderson, K. C., 2001. Bilogic sequelae interleukin-6 induced PI3-K/Akt signaling in multiple myeloma. *Oncogene,* 20(42), pp. 5991-6000.

Hoggard, N. et al., 1997. Leptin and leptin receptor mRNA and protein expression in the murine fetus and placenta. *Proc Natl Acad Sci,* pp. 11073-11078.

Hoggard, N. et al., 1997. Localization of leptin receptor mRNA splice variants in murine peripheral tissue by RT-PCR and in situ hybridisation. *Biochem Biophys Res Commun,* Volume 232, pp. 383-387.

Hotamisligil, G., 2006. Inflammation and metabolic disorders. *Nature,* Volume 444, pp. 860-867.

Hotamisligil, G., 2010. Endoplasmic reticulum stress and the inflammatory basis of metabolic disease. *Cel,* Volume 140, pp. 900-917.

Hotamisligil, G. S., Shargill, S. N. & Spiegelman, B. M., 1993. Adipose expression of tumor necrosis factor-alpha: direct role in obesity-linked insulin resistance. *Science,* 259(5091), pp. 87-91.

Hurst, J. & West, R., 2010. Taming anxiety in laboratory mice. *Nature Methods,* Volume 7, pp. 825-826.

Hurst, S. M. et al., 2001. IL-6 and its soluble receptor orchestrate a temporal switch in the pattern of leukocyte recruitment. *Immunity,* 14(6), pp. 705-714.

Huxford, T., Huang, D. B., Malek, S. & Ghosh, G., 1998. The crystal structure of the IkappaBalpha/NF-kappaB complex reveals mechanisms of NF-kappaB inactivation. *Cell,* 95(6), pp. 759-770.

IDF, 2014. *IDF Diabetes Atlas update poster 6th edition.* [Online] Available at: http://www.idf.org/sites/default/files/EN_6E_Atlas_Full_0.pdf [Accessed 2015].

Ikeda, Y. et al., 1993. Characterization of the mouse FTZ-F1 gene, which encodes a key regulator of steroid hydroxylase gene expression. *Mol Endocrin Baltimore,* Volume 7, pp. 852-860.

Imai, S., Armstrong, C. M., Kaeberlein, M. & Guarente, L., 2000. Transcriptional silencing and longevity protein Sir2 is an NAD-dependent histone deacetylase. *Nature,* Volume 403, pp. 795-800.

Inoue, H. & al, e., 2004. Role of STAT-3 in regulation of hepatic gluconeogenesis genes and carbohydrate metabolism in vivo. *Nat Med,* 10(2), pp. 168-174.

Inoue, H. et al., 2006. Role of hepatic STAT3 in brain-insulin action on hepatic glucose production. *Cell Metab,* 3(4), pp. 267-275.

Irvin, B. J., Hanson, C. L., Smith, L. H. & Daniels, C. K., 2001. Cyclic AMP- and IL6-signaling cross talk: comodulation of proliferation and apoptosis in the 7TD1 B cell hybridoma. *Exp Cell Res,* 265(1), pp. 73-79.

Jacobsen, L., Ansari, T. & McGuiness, O. P., 2006. Counterregulatory deficits occur within 24h of a single hypoglycemic episode in conscious, unrestrained, chonically cannulated mice. *Am J Physiol Endocrin & Metab,* 290(4), pp. E678-684.

Jacobs, M. D. & Harrison, S. C., 1998. Structure of an IkappaBalpha/NF-kappaB complex. *Cell ,* 95(6), pp. 749-758.

Jacoby, J. J., Kalinowski, A., Liu, M. G. & al, e., 2003. Cardiomyocyte-restricted knockout of STAT3 results in higher sensitivity to inflammation, cardiac fibrosis, and heart failure with advanced age. *Proc Natl Acad Sci U S A,* Volume 100, pp. 12929-12934.

Janicki, P. et al., 1994. Diminished brain synaptic plasma membrane Ca(2+)-ATPase activity in rats with streptozocin-induced diabetes: association with reduced anesthetic requirements. *Life Sci,* 55(18), pp. 359-364.

Jara, L. J. et al., 2006. Immune-neuroendocrine interactions and autoimmune diseases. *Clin & Devel Immun,* 13(2-4), pp. 109-123.

Jones, S. A., 2005. Directing transition from innate to acquired immunity: defining a role for IL-6. *J Immunol,* 175(6), pp. 3463-3468.

Jones, S. A. et al., 2001. The soluble IL-6 receptor: mechanisms of production and implications in disease. *FASEB,* 15(1), pp. 43-58.

Kai, A. et al., 2013. Exchange protein activated by cAMP 1 (Epac1) deficient mice develop β-cell dysfunction and metabolic syndrome. *FASEB,* Volume 27, pp. 4122-4135.

Kamimura, D., Ishihara, K. & Hirano, T., 2003. IL-6 signal transduction and its physiological roles: the signal orchestration model. *Rev Physiol Biochem Pharmacol,* Volume 149, pp. 1-38.

Kanavos, P., van den Aarweg, S. & Schurer, W., 2012. *Diabetes expenditure, burden of disease and management in 5 EU countries,* London: LSE.

Kaplanski, G. et al., 2003. IL-6: a regulator of the transition from neutrophil to monocyte recruitment during inflammation. *Trends Immunol,* 24(1), pp. 25-29.

Karin, M. B.-N. Y., 2000. Phosphorylation meets ubiquitination: the control of NF-kappaB activity. *Annu Rev Immunol,* Volume 18, pp. 621-663.

Karnani, M. & Burdakov, D., 2011. Multiple hypothalamic circuits sense and regulate glucose levels. *Am J Phys,* Volume 300, pp. R47-55.

Keller, C. et al., 2005a. Effect of exercise training, and glycogen availability on IL-6 receptor expression in human skeletal muscle. *J of App Physiol,* 99(6), p. 2075079.

Kelly, M. et al., 2004. AMPK activity is diminished in tissues of IL-6 knockout mice: the effect of exercise. *Biochem Biophys Res Commun,* Volume 320, pp. 449-454.

Khouri, C. et al., 2011. Glucagon counteracts interleukin-6-dependent gene expression by redundant action of Epac and PKA. *Biol Chem,* 392(12), pp. 1123-1134.

Kim, H. J., Higashimori, T., Park, S. Y. & al, e., 2004. Differential effects of interleukin-6 and -10 on skeletal muscle and liver insulin action in vivo. *Diabetes,* Volume 53, pp. 1060-1067.

Kim, J., Adam, R. J., Solomon, K. R. & Freeman, M. R., 2004. Involvement of cholesterol-rich rafts in IL-6 induced neuroendocrine differentiation of LNCaP prostate cancer cells. *Endocrin,* Volume 320, pp. 449-454.

Kishimoto, T., 1987. B-cell stimulatory factors (BSF's): molecular structure, biological functions, and regulation of expression. *J Clin Immunol,* 7(5), pp. 343-355.

Kishimoto, T., 2005. Interleukin-6: from basic science to medicine - 40 years in immunology. *Annu Rev Immunol,* Volume 23, p. 1.

Kishimoto, T., 2010. IL-6: from its discovery to clinical application. *Int Immunol ,* 22(5), pp. 347-352.

Klip, A. & Hawkins, M., 2005. Desperately seeking sugar; glial cells as hypoglycemia sensors. *JCI,* 115(12), pp. 3403-3405.

Knudsen, P. J., Dinarello, C. A. & Strom, T. B., 1987. Glucocorticoids inhibit transcriptional and post-transcriptional expression of interleukin 1 in U937 cells. *J immunol,* 139(12), pp. 4129-4134.

Kodama, H. et al., 2000. Significance of ERK cascade compared with JAK.STAT and PI3-K pathway in gp130-mediated cardiac hypertrophy. *Am J Physiol Heart Circ Physiol,* 279(4), pp. H1635-1644.

Koenen, R. R. et al., 2009. Regulated release and functional modulation of juncitonal adhesion molecule A by disintegrin metalloproteinases. *Blood,* 113(19), pp. 4799-4809.

Kojima, H. et al., 2005. STAT3 regulates Nemo-like kinase by mediating its interaction with IL-6 stimulated TGFbeta-activated kinase 1 for STAT3 Ser-727 phosphorylation. *Pro Natl Acad Sci,* 102(12), pp. 4524-4529.

Konner, C. A. & Bruning, J. C., 2011. Toll-like receptors: linking inflammation to metabolism. *Trends Endocrin & Metab,* 22(1), pp. 16-23.

Kontras, S. & Bodenbender, J., 1968. Studies in the inflammatory cycle in juvenile diabetes. *Am J Dis Child,* 116(2), pp. 130-134.

Kopf, M. et al., 1994. Impaired immune and acute-phase responses in interleukin-6-deficient mice. *Nature,* Volume 368, pp. 339-342.

Kristiansen, O. & Mandrup-Poulsen, T., 2005. Interleukin-6 and diabetes; the good, the bad, or the indifferent?. *Diabetes,* Volume 54, pp. 114-124.

Kuhn, R. & Torres, R., 2002. Cre/loxP Recombination system and gene targeting. *Methods Mol Biol,* 28(3), pp. 175-204.

Kurdi, M. & Booz, G. W., 2007. Can the protective actions of JAK-STAT in the heart be exploited therapeutically? Parsing the regulation of IL-6-type cytokine signaling. *J Cardiovasc Pharmacol,* 50(2), pp. 126-141.

Lant, B. & Storey, K., 2010. An Overview of stress response and hypometabolic strategies in Caenorhabditis elegans: conserved and contrasting singals with the mammalian system. *International Journal of Biological Sciences,* 6(1), pp. 9-50.

Laye, S. et al., 2000. Endogenous brain IL-1 mediates LPS-induced anorexia and hypothalamic cytokine expression. *Am J Physiol Regul Integr Comp Physiol,* 279(1), pp. R93-98.

Lee, J. C. et al., 1994. A protein kinase involved in the regulation of inflammatory cytokine biosynthesis. *Nature,* 372(6508), pp. 739-746.

Lee, S. et al., 2004. CpG oligodexynucleotides induce expression of proinflammatory cytokines and chemokines in astrocytes: the role of c-Jun N-terminal kinase in CpG ODN-mediated NF-kappaB activation. *J Neuroimmunol,* 153(1-2), pp. 50-63.

Lee-Young, R. S. & al, e., 2006. Carbohydrate ingestion does not alter skeletal muscle AMPK signaling during exercise in humans. *Am J Physiol Endocrinol and Met,* Volume 291, pp. E566-573.

Lee-Young, R. S. et al., 2011. Obesity impairs skeletal muscle AMPK signaling during exercise: role of APMKalpha2 in the regulation of exercise capacity in vivo. *Int J Obes,* 35(7), pp. 982-989.

Lendahl, U., Zimmerman, L. B. & al., e., 1990. CNS stem cells express a new class of intermediate filament protein. *Cell,* 60(4), pp. 585-595.

Levin, B., Dunn-Meynell, A. & Routh, V., 1999. Brain glucose sensing and body energy homeostasis: role in obesity and diabetes. *Am J Physiol,* 276(5 Pt 2), pp. R1223-1231.

Le, Y. & Sauer, B., 2000. Conditional Gene Knockout using cre Recombinase. *Methods Mol Biol,* Volume 136, pp. 477-485.

Liu, M. Y. et al., 2005. Multiplexed analysis of biomarkers related to obesity and the metabolic syndrome in human plasma, using Luminex 100 system. *Clin Chem,* 51(7), pp. 1102-1109.

Livak, K. & Schmittgen, T., 2001. Analysis of relative gene expression data using real-time quantitative PCR and the 2-ΔΔCT Method. *Methods,* Volume 25, pp. 402-408.

Lopez, M. et al., 2010. Hypothalamic AMPK and fatty acid metabolism mediate thyroid regulation of energy balance. *Nature Med,* 16(9), pp. 1001-1008.

Lotz, M. et al., 1988. B cell stimulating factor 2/interleukin 6 is a costimulant for human thymocytes and T lymphocytes. *J Exp Med,* 167(3), pp. 1253-1258.

Lowe, G. et al., 2013. Circulating inflammatory markers and the risk of vascular complication and mortality in people with type 2 diabetes and cardiovascular disease or risk factors: The ADVANCE study. *Diabetes,* 63(3), pp. 1115-1123.

Lumeng, C. N. & Saltiel, A. R., 2011. Inflammatory links between obesity and metabolic disease. *J Clin Invest,* 121(6), pp. 2111-2117.

Lu, M. et al., 2010. Protective effects of grape seed proanthocyanidin extracts on cerebral cortex of streptozotocin-induced diabetic rats through modulating AGEs/RAGE/NF-kB pathway. *J Nut Sci Vitam,* 56(2), pp. 87-97.

Luo, Y. et al., 2004. The levels of plasma IL-1β, IL-6 of C57BL/6J mice treated with MPTP and brain lateralization. *Cellular and Molecular Immunology,* 1(3), pp. 219-223.

MacDonald, C. et al., 1987. Interleukin-6 release from human skeletal muscle during exercise: relation to AMPK activity. *J Appl Physiol,* 95(6), pp. 2273-2277.

Mackiewicz, A. & Kushner, I., 1989. Interferon beta 3/B-cell stimulating factor 2/interleukin 6 affects glycosylation of acute phase protein in human hepatoma cell lines. *Scand J Immunol,* 29(3), pp. 265-271.

Maggio, M., Guralnik, J., Longo, D. & Ferrucci, L., 2006. Interleukin-6 in aging and chronic disease: A magnificent pathway. *J Gerontol A Biol Scie Med Sci,* 61(6), pp. 575-584.

Magistretti, P. & Pellerin, L., 1999. Astrocytes couple synaptic activity to glucose utilization in the brain. *News Physiol Sci,* Volume 14, pp. 177-182.

Mainardi, M., Pizzorusso, T. & Margherita, M., 2013. Environment, leptin sensitivity and hypothalamic plasticity. *Neur Plast,* Volume 2013, pp. 1-8.

Malaviya, A. P. et al., 2014. The 2013 BSR and BHPR guideline for the use of intravenous tocilizumab in the treatment of adult patients with rheumatoid arthritis. *Rehmatology,* 53(10), p. 1914.

Marin, V. et al., 2002. Chemotactic agents induce IL-6Ralpha shedding from polymorphonuclear cells: involvement of a metalloproteinase of the TNF-alpha-converting enzyme (TACE) type. *Eur J Immunol,* 32(10), pp. 2965-2970.

Martin-Cordero, L., Garcia, J. L., Hinchado, M. D. & Ortega, E., 2011. The IL-6 and Noradrenaline-mediated inflammation stress feedback mechanism is dysregulated in metabilic syndrome: Effect of exercise. *Cardio Vasc Diabet ,* Volume 10, p. 42.

Matsuzaki, H. et al., 2003. Insulin-induced phosphorylation of FKHR (Foxo1) targets to proteasomal degradation. *PNAS,* 100(2), pp. 11285-11290.

Matthews, V. B. et al., 2010. Interleukin-6 deficient mice develop hepatic inflammation and systemic insulin resistance. *Diabetologia,* Volume 53, pp. 2431-2441.

Matthews, V. et al., 2003. Cellular cholesterol depletion triggers shedding of the human interleukin-6 receptor by ADAM10 and ADAM17 (TACE). *J Biol Chem,* 278(40), pp. 38829-38839.

Matveyenko, A. V., Bohland, M., Saberi, M. & Donovan, C. M., 2007. Portal vein hypoglycemia is essential for full induction of hypoglycemia-associated autonomic failure with slow-onset hypoglycemia. *Am J Physiol Endocrinol Metab,* 293(3), pp. E857-864.

McCrimmon, R. J., 2007. The mechanisms that underlie glucose sensing during hypoglycaemia in diabetes. *Diab Med,* Volume 25, pp. 513-522.

McCrimmon, R. J. & Sherwin, R. S., 2010. Hypoglycemia in type 1 diabetes. *Diabetes,* 59(10), pp. 2333-2339.

McCrimmon, R. J. et al., 2006. Corticotrophin-releasing factor receptors within the ventromedial hypothalamus regulate hypoglycemia-induced hormonal counterregulation. *JCI,* 116(6), pp. 1723-1730.

McCrimmon, R. et al., 2008. Key role for AMP-activated protein kinase in the ventromedial hypothalamus in regulating counterregulatory hormone response to acute hypoglycemia. *Diabetes,* 57(2), pp. 444-450.

McFarland-Mancini, M. et al., 2010. Differences in wound healing in mice with deficiency of IL-6 versus IL-6 receptor. *J Immunol,* 184(12), pp. 7219-7228.

McGillicuddy, F. C. et al., 2011. Lack of interleukin-1 receptor I (IL-1RI) protects mice from high-fat diet-induced adipose tissue inflammation coincident with improved glucose homeostasis. *Diabetes,* 60(6), pp. 1688-1698.

McNay, D. et al., 2012. Remodelling of the arcuate nucleus energy-balance circuit is inhibited in obese mice. *J Clin Invest,* 122(1), pp. 142-152.

Meier, C. A., 1995. Advances in the understanding of the molecular basis of obesity. *Eur J Endocrinol,* 133(6), pp. 761-763.

Mihaylova, M., Sabatini, D. & Yilmaz, O., 2014. Dietary and metabolic control of stem cell function in physiology and cancer. *Cell Stem Cell,* 14(3), pp. 292-305.

Miinea, C., Sano, H., Kane, S. & al., e., 2005. AS160, the Akt substrate regulating GLUT4 translocation, has a functional Rab GTPase-activating protein domain. *Biochem J,* Volume 391 (Pt 1), pp. 87-93.

Milanski, M. et al., 2009. Saturated fatty acids produce an inflammatory response predominantly through the activation of TRL4 signaling in hypothalamus: Implications for the pathogenesis of obesity. *J Neuro,* 29(2), pp. 359-370.

Mirshamsi, S. et al., 2004. Leptin and insulin stimulation of signaling pathways in arcuate nucleus neurones: PI3K dependent actin reorganization and KATP channel activation. *BMC Neurosci,* Volume 6, pp. 5-54.

Miyahara, S., Komori, T., Fujiwara, R. & Shizuya, K., 2000. Effects of repeated stress on expression of IL-6 and IL-6 receptor mRNAs in rat hypothalamus and midbrain. *Life Sciences Pharm Lett,* 66(6), pp. 93-98.

Moh, A. et al., 2008. STAT3 sensitizes insulin signaling by negatively regulating glycogen synthase kinase-3 beta. *Diabetes,* 57(5), pp. 1227-1235.

Moinat, M. et al., 1995. Modulation of obese gene expression in rat brown and white adipose tissues. *FEBS Lett,* Volume 373, pp. 131-134.

Moore, M. et al., 2012. Regulation of hepatic glucose uptake and storage in vivo. *Adv Nutr,* 3(3), pp. 286-294.

Mori, H. et al., 2004. SOCS3 deficiency in the brain elevates leptin sensitivity and confers resistance to diet-induced obesity. *Nat Med,* Volume 10, pp. 739-743.

Moulle, V. S. et al., 2014. Lipid sensing in the brain and regulation of energy balance. *Diab & Met,* Volume 44, pp. 29-33.

Muller, M. R. et al., 2001. Immunostimulation by the synthetic lipopeptide P3CSK4: TLR4-independent activation of the ERK1/2 signal transduction pathway in macrophages. *Immunology,* 103(1), pp. 49-60.

Murry, C. E., Jennings, R. B. & al, e., 1986. Preconditioning with ischemia: a delay of lethal cell injury in ischemic myocardium. *Circulation,* 74(5), pp. 1124-1136.

Nagler, W. & Taylor, H., 1963. Diabetic come with acute inflammation of Islet of Langerhans. *JAMA,* Volume 184, pp. 723-725.

Navvaro, S. et al., 1991. Expression of interleukin and its specific receptor by untreated and PMA-stimulated human erythroid and megakaryotic cell lines. *Exp Hematol,* 19(1), pp. 11-17.

Niemand, C. et al., 2003. Activation of STAT3 by IL-6 and IL-10 in primary human macrophages is differentially modulated by SOCS3. *J of Immunol,* Volume 170, pp. 3263-3272.

Nishimoto, N., 2005. Clinical studies in patients with Castleman's disease, Crohn's disease, and rheumatoid arthritis in Japan. *Clin Rev Allergy Immunol,* 28(3), pp. 221-230.

Northoff, H. & Berg, A., 1991. Immunologic mediators as parameters of the reaction to strenuous exercise. *Int J of Sports Med,* 12(1), pp. S9-15.

O' Connor, T. M., O' Halloran, D. J. & Shanahan, F., 2000. The stress response and the hypothalamic-pituitary-adrenal axis: from molecule to melancholia. *QJM,* 96(6), pp. 323-333.

O'Donovan, A. et al., 2010. Clinical anxiety, corticol and interleukin-6: Evidence for specificity in emotion-biology relationships. *Brain, Behaviour, and Immunity,* 24(7), pp. 1074-1077.

Oshima, Y., Fujio, Y., Nakanishi, T. & al, e., 2005. STAT3 mediates cardioprotection against ischemia/reperfusion injury through metallothionein induction in the heart. *Cardiovasc Res,* Volume 65, pp. 428-435.

Ospelt, C. & Gay, S., 2010. TLRs and chronic inflammation. *Intern J Biochem & Cell Biol,* Volume 42, pp. 495-505.

Ostrowski, K. et al., 1998. Evidence that IL-6 is produced in human skeletal muscle during prolonged running. *J Physiol,* 508(3), pp. 949-953.

Papanicolaou, D. A., Wilder, R. L., Manolagas, S. C. & Chrousos, G. P., 1998. The pathophysiologic role of interleukin-6 in human disease. *Intern Med,* Volume 128, pp. 127-137.

Park, S., Kim, D. S., Kang, S. & Shin, B. K., 2014. Chronic activation of central AMPK attenuates GSIS and exacerbates hepatic insulin resistance in diabetic rats. *Brain Research Bull,* Volume 108, pp. 18-6.

Patil, C. et al., 2004. p38 MPAK regulates IL-1beta induced IL-6 expression through mRNA stability in osteoblasts. *Immunol Invest,* 33(2), pp. 213-233.

Patsouris, D., Li, P. P., Thapar, D. C. J. O. J. M. & Neels, J. G., 2008. Ablation of CD11c-positive cells normalizes insulin sensitivity in obese insulin resistant animals. *Cell Metab,* 8(4), pp. 301-309.

Peake, J. M. S. K. et al., 2005. Plasma cytokine changes in relation to exercise intensity and muscle. *Eur J Appl Physiol,* 95(5-6), pp. 514-521.

Pechisker, A., 2004. Targeting your DNA with the Cre/Lox system. *The Science Creative Quarterly,* Volume 4.

Pedersen, B. K. & Febbraio, M. A., 2008. Muscle as an endocrine organ: focus on muscle-derived interleukin-6. *Physiol Rev,* 88(4), pp. 1379-1406.

Pedersen, B. K., Steensberg, A. & Schjerling, P., 2001. Muscle-derived interleukin-6: possible biological effects. *J Physiol,* 536(2), pp. 329-337.

Petersen, A. M. & Pedersen, B. K., 2005. The anti-inflammatory effect of exercise. *J Appl Physiol,* 98(4), pp. 1154-1162.

Petersen, A. M. & Pedersen, B. K., 2006. The role IL-6 in mediating and the anti-inflammatory effects of exercise. *J Physiol Pharmacol,* Volume 10, pp. 43-51.

Petersen, F. K. & Shulman, G. I., 2006. Etiology of Insulin Resistance. *Am J Med,* 1195(5), pp. S10-16.

Peters, M. et al., 1997. Extramedullary expansion of hematopoietic progenitor cells in IL-6/sIL-6R double transgenic mice. *J Exp Med,* 185(4), pp. 755-766.

Phelps, C. B., Sengchanthalangsy, L. L., Huxford, T. & Ghosh, G., 2000. Mechanisms of I kappa B alpha binding to NF-kappa B dimers. *J Biol Chem,* 275(38), pp. 29840-29846.

Pickup, J. C., Mattock, M. B., Chusney, G. F. & Burt, D., 1997. NIDDM as a disease of the innate immune system: association of acute-phase reactants and IL-6 with metabolic syndrome X. *Diabetolog,* 40(11), pp. 1286-1292.

Pires, P. et al., 2014. Tumor necrosis factor-α inhibition attentuates middle cerebral artery remodeling but increases cerebral ischemic damage in hypertensive rats. *Am J Physiol Heart Circ Physiol,* 307(5), pp. H658-H669.

Plum, L., Belgardt, B. F. & Bruning, J. C., 2006. Central insulin action in energy and glucose homeostasis. *J Clin Invest,* 116(7), pp. 1761-1766.

Plum, L. et al., 2006. Enhanced PIP3 signaling in POMC neurons causes KATP channel activation and leads to diet-sensitive obesity. *J Clin Invest,* Volume 116, pp. 1886-1901.

Pocai, A. et al., 2005. Central leptin acutely reverses diet-induced hepatic insulin resistance. *Diabetes,* Volume 54, pp. 3182-3189.

Powell, A. M., Sherwin, R. S. & Shulman, G. I., 1993. Impaired hormonal responses to hypoglycemia in spontaneously diabetic and recurrently hypoglycemic rats. Reversibility and stimulus specificity of the deficits. *J of Clin Invest,* 92(6), pp. 2667-2674.

Pradhan, A. D. et al., 2001. C-reactive protein, interleukin 6 and risk of developing type 2 diabetes mellitus. *JAMA,* 286(3), pp. 327-334.

Purkayastha, S., Zhang, G. & Cai, D., 2011. Uncoupling the mechanisms of obesity and hypertension by targeting hypothalamic IKK-β and NF-κB. *Nat Med,* 17(7), pp. 883-887.

Qui, Z., Parsons, K. L. & Gruol, D. L., 1995. Interleukin-6 selectively enhances the intracellular calcium response to NMDA in developing CNS neurons. *J of Neuro,* 15(10), pp. 6688-6699.

Ramadori, G. et al., 2011. SIRT deacetylase in SF1 neurons protects against metabolic imbalance. *Cell Metab,* 14(3), pp. 301-312.

Reihmane, D., Jurka, A., Tretjakovs, P. & Dela, F., 2013. Increase in IL-6, TNF-alpha and mmp-9, but not sICAM-1, concentrations depends on exercise duration. *Eur J Appl Physiol,* 113(4), pp. 851-858.

Romano, M. et al., 1997. Role of IL-6 and its soluble receptor in induction of chemokines and leukocyte recruitment. *Immunity,* 6(3), pp. 315-325.

Romero, R. et al., 1993. A comparative study of the diagnostic performance of amniotic fluid glucose, white blood cell count, interleukin-6, and gram stain in the detection of microbial invasion in patients with preterm premature rupture of membranes. *Am J Obstet Gynecol,* 169(4), pp. 839-851.

Ropelle, E. R. et al., 2010. *IL-6 and IL-10 Anti-Inflammatory activity links exercise to hypothalamic Insulin and Leptin sensitivity through IKKbeta and ER stress Inhibition,* s.l.: PLoS Biol.

Rose-John, S., 2012. IL-6 trans-signaling via the soluble IL-6 receptor: importance for the pro-inflammatory activities of IL-6. *Int J Biol Sci,* 8(9), pp. 1237-1247.

Rose-John, S., Scheller, J., Elson, G. E. & Jones, S. A., 2006. IL-6 biology is coordinated by membrane-bound and soluble receptors: role in inflammation and cancer. *J Leuk Biol,* Volume 80, pp. 227-236.

Rose-John, S. et al., 1990. Studies on the structure and regulation of the human hepatic interleukin-6 receptor. *Eur J Biochem ,* 190(1), pp. 79-83.

Rose-John, S. et al., 2007. The IL-6/sIL-6R complex as a novel target for therapeutic approaches. *Expert Opin Ther Targets,* 11(5), pp. 613-624.

Rubio-Perez, J. M. & Morillas-Ruiz, J. M., 2012. *A Review: Inflammatory process in Alzheimer's disease, role of cytokines,* s.l.: ScientificWorldJournal.

Ruderman, N. B. et al., 2006. Interleukin-6 regulation of AMP-Activated protein kinase. *Diabetes,* 55(2), pp. 48-54.

Sahu, A., 2003. Leptin signaling in the hypothalamus: emphasis on energy homeostasis and leptin resistance. *Front Neuroendocrinol,* 24(4), pp. 225-253.

Sakurai, T. Y. B., Takata, T. & Yokono, K., 2002. Synaptic adaptation to repeated hypoglycemia depends on the utilization of monocarboxylates in guinea pig hippocampal slices. *Diabetes,* 51(2), pp. 430-438.

Saltiel, A. & Kahn, C., 2001. Insulin signaling and the regulation of glucose and lipid metabolism. *Nature,* 414(6865), pp. 799-806.

Sands, W. et al., 2006. Exchange protein activated by cyclic AMP (Epac)-mediated induction of suppressor of cytokine signaling 3 (SOCS-3) in vascular endothelial cells. *Mol Cell Biol,* 26(17), pp. 6333-6346.

Saraf, N. et al., 2011. Role of PPARg2 transcription factor in thiazolidinedione-induced insulin sensitization. *J Pharmacy and Pharmacology,* Volume 64, pp. 161-172.

Sarvas, J. L., Khaper, N. & Lees, S., 2013. The IL-6 Paradox: Content Dependent Interplay of SOCS3 and AMPK. *J Diabetes Metab,* 24(13), pp. S13-003.

Satoh, N. et al., 1997. The arcuate nucleus as a primary site of satiety effect of leptin in rats. *Neurosci Lett,* Volume 224, pp. 149-152.

Sauer, B., 1998. Inducible gene targeting in mice using the Cre/lox system. *Methods: A companion to methods in enzymology,* Volume 14, pp. 381-392.

Schele, E. et al., 2013. Inter-relation between IL-1, IL-6 and body fat regulating circuits in the hypothalamic arcuate nucleus. *J of Neuroendocrin,* Volume 25, pp. 580-589.

Schele, E. et al., 2012. IL-6Ralpha is co-localised with MCH in human and mouse hypothalamus. *J of Neuroendocrin,* Volume 24, pp. 930-943.

Scheller, J., Chalaris, A., Schmidt-Arras, D. & Rose-John, S., 2011. The pro- and anti-inflammatory properties of the cytokine IL-6. *Biochem Biophy Acta - Mol Cell Res,* 1813(5), pp. 878-888.

Schneeberger, M. et al., 2013. Mitofusin 2 in POMC neurons connects ER stress with leptin resistance and energy imbalance. *Cell,* Volume 155, pp. 172-187.

Schofield, C. J. & Sutherland, C., 2012. Disordered insulin secretion in the development of insulin resistance and type 2 diabetes. *Diab Med,* Volume 29, pp. 972-979.

Schuit, F., Huypens, P., Heimberg, H. & Pipeleers, D., 2001. Glucose sensing in pancreatic beta-cells: a model for the study of other glucose-regulated cells in gut, pancreas, and hypothalamus. *Diabetes,* 50(1), pp. 1-11.

Schultz, O. et al., 2010. Effects of inhibition of interleukin-6 signaling on insulin sensitivity and lipoprotein (A) levels in human subjects with rheumatoid diseases. *PLoS One,* 5(12), p. E14328.

Schwantner, A. et al., 2004. Direct determination of the interleukin-6 binding epitope of the interleukin-6 receptor by NMR spectroscopy. *J Biol Chem,* 279(1), pp. 571-576.

Schwartz, M. et al., 2000. Central nervous system control of food intake. *Nature,* Volume 404, pp. 661-671.

Scott, M. et al., 2009. Leptin targets in the mosue brain. *J Comp Neurol,* Volume 514, pp. 518-532.

Sebastian, D. et al., 2011. Mitofusin 2 links mitochondrial and endoplamic reticulum function with insulin signaling and is essential for normal glucose homeostasis. *PNAS,* 109(14), pp. 5523-5528.

Segal, K. R., Landt, M. & Klein, S., 1996. Relationship between insulin sensitivity and plasma leptin concentration in lean and obese men. *Diab,* 45(7), pp. 988-991.

Sehgal, P. B., May, L. T., Tamm, I. & Vilcek, J., 1987. Human beta-2 interferon and B-cell differentiation factor BSF-2 are identical. *Science (Wash. DC),* Volume 235, pp. 731-732.

Selam, J. L., Woertz, L., Eichner, H. & Charles, M. A., 1990. Blood glucose levels stimulating hypoglycemic counterregulation are related to chronic diabetes control. *Diabetes Res,* 13(3), pp. 117-120.

Semmler, A. et al., 2005. Systemic inflammation induces apoptosis with variable vulnerability of different brain regions. *J Chem Neuroanatomy,* 30(2-3), pp. 144-157.

Senaris, R. M. et al., 2011. Interleukin-6 regulates the expression of hypothalamic neuropeptides involved in body weight in a gender-dependent way. *J Neuroendocrinol,* 23(8), pp. 675-686.

Serrano-Marco, L. et al., 2012. TNF-alpha inhibits PPARbeta/delta activity and SIRT1 expression through NF-Kbeta in human adipocytes. *Bioch et Biophys,* Volume 1821, pp. 1177-1185.

Sharma, A. M. & Staels, B., 2007. REVIEW: Peroxisome Proliferator-activated Receptor gamma and Adipose tissue - Understanding obesity-related changes in regulation of lipid and glucose metabolism. *J Clin Endo Metab,* 92(2), pp. 386-395.

Shirazi, R. et al., 2013. Glucagon-like peptide 1 receptor induced suppression of food intake, and body weight is mediated by central IL-1 and IL-6. *Proc Natl Acad Sci USA,* 110(40), pp. 16199-16204.

Shiuchi, T. et al., 2009. Hypothalamic orexin stimulates feeding-associated glucose utilization in skeletal muscle via sympathetic nervous system. *Cell Metab,* 10(6), pp. 466-480.

Simi, A. et al., 2002. The neuroprotective agents clomethiazole and SB203580 inhibit IL-1beta signaling but not its biosynthesis in rat cortical glial cells. *J Neurochem,* 83(3), pp. 727-737.

Smith, L., 1991. Acute inflammation: the undelying mechanism in delayed onset muscle soreness. *Medicine and Science in Sports and Exercise,* Volume 23, pp. 542-551.

Smith, R. M., Suleman, N., Lacerda, L. & al, e., 2004. Genetic depletion of cardiac myocyte STAT-3 abolishes classical preconditioning. *Cardiovasc Res,* Volume 63, pp. 611-616.

Smythe, G. A. & Edwards, S. R., 1992. Suppression of central noradrenergic neuronal activity inhibits hyperglycemia. *Am J Physiol,* 263(5 Pt 1), pp. E823-827.

Sodhi, H. S., 1957. Diabetes mellitus, insulin and glucagon. *Med Times,* 85(9), pp. 1013-1019.

Song, Z. et al., 2001. Convergence of pre- and postsynaptic influences on glucosensing neurons in the ventromedial hypothalamic nucleus. *Diabetes,* 50(12), pp. 2673-2681.

Spicer, L. & Francisco, C., 1997. The adipose obese gene product, leptin: evidence of direct inhibitory role in ovarian function. *Endocrinology,* Volume 138, pp. 3374-3379.

Starkie, R. L. et al., 2000. Effect of prolonged, submaximal exercise and carbohydrate ingestion on monocyte intracellular cytokine production in humans. *J Physiol,* 528(Pt3), pp. 647-655.

Starkie, R. L. et al., 2001. Circulating monocytes are not the source of elevations in plasma IL-6 and TNF-α levels after prolonged running. *Am J Physiol,* Volume 280, pp. C769-774.

Starkie, R. et al., 2003. Exercise and IL-6 infusion inhibit edotoxin-induced TNF-alpha production in humans. *FASEB,* Volume 60, pp. 3154-3158.

Steffens, A. B., Scheurink, A. J., Luiten, P. G. & Bohus, B., 1988. Hypothalamic food intake regulating areas are involved in the homeostasis of blood glucose and plasma FFA levels. *Physiol Behav,* 44(4-5), pp. 581-589.

Steinberg, G. R. & Kemp, B. E., 2009. AMPK in health and disease. *Physiol Rev,* 89(3), pp. 1025-1078.

Steiner, D. & Oyer, P., 1967. The biosynthesis of insulin and a probable precursor of insulin by a human islet cell adenoma. *Proc Natl Acad Sci,* 57(2), pp. 473-480.

Steinman, L., 2013. Inflammatory cytokines at the summits of pathological signal cascades in brain diseases. *Sci Signal ,* 6(258), p. pe3.

Stephanou, A., 2004. Role of STAT-1 and STAT-3 in ischaemia/reperfusion injury. *J Cell Mol Med,* 8(4), pp. 519-525.

Svensson, C., 2010. IL-6: A local pain trigger?. 12(5).

Szepietowska, B. Z. W. et al., 2011. Modulation of beta-adrenergic receptors in the ventromedial hypothalamus influences counterregulatory responses to hypoglycemia. *Diabetes,* 60(12), pp. 3154-3158.

Taga, T. et al., 1989. Interleukin-6 triggers the association of its receptor with a possible signal transducer, gp130. *Cell,* 58(3), pp. 573-581.

Takahashi-Tezuka, M. et al., 1998. Gab1 acts as an adapter molecule linking the cytokine receptor gp130 to ERK mitogen-activated protein kinase. *Mol Cell Biol,* Volume 18, pp. 4109-4117.

Takao, T., Hashimoto, K. & De Souza, E. B., 1995. Modulation of interleukin-1 receptors in the neuro-endocrine-immune axis. *Int J Dev Neurosci,* 13(3-4), pp. 167-178.

Takeda, K. & Akira, S., 2004. TLR signaling pathways. *Seminars in Immunology ,* Volume 16, pp. 3-9.

Tanaka, T., Nrazaki, M. & Kishimoto, T., 2011. Anti-IL-6 receptor antibody, tocilizumab, for the treatment of autoimmune diseases. *FEBS,* 585(23), pp. 3699-3709.

Tang, C.-H.et al., 2007. Leptin-induced IL-6 production is mediated by leptin receptor, insulin receptor substrate-1, phosphatydylinositol 3-Kinase, Akt, Nf-κB, and p300 pathway in microglia. *J Immunol ,* 179(2), pp. 1292-1302.

Taniguchi, C. M. et al., 2006. Divergent regulation of gepatic glucose and lipid metabolism by PI3-K via AKT and PKClamda/zeta. *Cell Met,* Volume 3, pp. 343-353.

Teoh, N., Leclercg, I., Pena, A. & Farrell, G., 2003. Low-dose TNF-alpha protects against hepatic ishemia-reperfusion injury in mice: implications for preconditioning. *Hepatology,* 37(1), pp. 118-128.

Thorens, B., 2003. A gene knockout approach in mice to identify glucose sensors controlling glucose homeostasis. *Pflugers Arch,* 445(4), pp. 482-490.

Thorens, B., 2011. Brain glucose sensing and neural regulation of insulin and glucagon secretion. *Diabetes Obes Metab 13 Suppl,* Volume 1, pp. 82-88.

Tian, Y. & Laychock, S. G., 2001. Protein kinase C and calcium regulation of adenylyl cyclase in isolated rat pancreatic islets. *Diabetes,* 50(11), pp. 2505-2513.

Tokunaga, K., Fukushima, M., Kemnitz, J. W. & Bray, G. A., 1986. Comparison of ventromedial and paraventricular lesions in rats that become obese. *Am J Physiol,* 25(6 Pt 2), pp. R1221-1227.

Tokunaga, K. et al., 1989. Effects of food restriction and adrenalectomy in rats with VMH or PVH lesions. *Physiol Behav,* 45(6), pp. 1131-1137.

Tosello-Trampont, A. C. et al., 2012. Kuppfer cells trigger nonalcoholic steatohepatitis development in diet-induced mouse model through TNFalpha production. *JBC,* 287(48), pp. 40161-40172.

Troche, F. et al., 1999. Disruption of the glucocorticoid receptor gene in the nervous system results in reduced anxiety. *Nat Genet,* 23(1), pp. 99-103.

Tsuro, Y. et al., 1996. Immunohistochemical detection of the ob gene product (leptin) in rat white and brown adipocytes. *Horm Metab Res,* Volume 28, pp. 753-755.

Tu, H., Pan, W., Feucht, L. & Kastin, A., 2007. Convergent trafficking pattern of leptin after endocytosis mediabeted by ObRa-ObRd. *J Cell Physiol,* 212(1), pp. 215-222.

Utomo, A. & al., e., 1999. Temporal, spatial, and cell type-specific control of Cre-mediated DNA recombination in transgenic mice. *Nature Biotechnology,* 17(11), pp. 1091-1096.

Utsuyama, M. & Hirokawa, K., 2002. Differential expression of various cytokine receptors in the brain after stimulation with LPS in young and old mice. *Exp Gerontol,* 37(2-3), pp. 411-420.

Vahdat, A. et al., 2010. TNF-alpha-converting enzyme (TACE/ADAM17)-dependent loss of CD30 induced by proteasome inhibition through reactive oxygen species. *Leukemia,* 24(1), pp. 51-57.

van der Heide, L. P., Ramakers, G. M. J. & Smidt, M. P., 2006. Insulin signaling in the central nervous system: Learning to survive. *Prog in Neurobio,* 79(4), pp. 205-221.

Van Hall, G. et al., 2003. Interleukin-6 stimulates lipolysis and fat oxidation in humans. *J Clin Endocrinol Metab,* Volume 88, pp. 3005-3010.

Van Snick, J., 1990. Interleukin-6: an overview. *Annu Rev Immunol,* Volume 8, pp. 253-278.

Verma, I. M. et al., 1995. Rel/NF-kappa B/I kappa B family: intimate tales of association and dissociation. *Genes Dev,* 9(22), pp. 2723-2735.

Vink, A., Uyttenhove, C., Wauters, P. & Van Snick, J., 1990. Accessory factors involved in murine T cell activation. Distinct role of interleukin 6, interleukin 1 and tumor necrosis factor. *Eur J Immunol,* 20(1), pp. 1-6.

Virtanen, K. et al., 2002. Glucose uptake and perfusion in subcutaneous and visceral adipose tissue during insulin stimulation in nonobese and obese humans. *J Clin Endocrinol Metab,* 87(8), pp. 3902-3910.

Virtue, S. et al., 2012. Lipocalin Prostaglandin D synthase and PPARgamma2 coordinate to regulate carbohydrate and lipid metabolism in vivo. *PLOS,* 7(7), p. e39512.

Vozarova, B. et al., 2001. Circulating IL-6 in relation to adiposity, insulin action, and insulin secretion. *Obes Res,* 9(7), pp. 414-417.

Vranic, M., Ross, G., Doi, K. & Lickey, L., 1976. The role of glucagon-insulin interactions in control of glucose turnover and its significance in diabetes. *Metabolism,* 25(11), pp. 1375-1380.

Wallenius, V. et al., 2002. Interleukin-6-deficient mice develop mature onset obesity. *Nature Med,* Volume 8, pp. 75-79.

Wang, J. et al., 1998. A nutrient sensing pathway regulates leptin gene expression in muscle and fat. *Nature,* Volume 393, pp. 684-688.

Wang, P. et al., 1995. Interleukin (IL)-10 inhibits nuclear factor kappa B (NF kappa B) activation in human monocytes. IL-10 and IL-4 suppress cytokine synthesis by different mechanisms. *J Biol Chem,* 270(16), pp. 3558-3563.

Wang, P. et al., 1996. IL-10 inhibits NFkappaB activation in human monocytes. *J Biol Chem,* 270(16), pp. 9558-9563.

Wang, X.-Q.et al., 2009. Neuroprotection of interleukin-6 against NMDA attach and its signal transudction by JAK and MAPK. *Neuroscience Letters,* Volume 450, pp. 122-126.

Wang, Y.-C., Lin, S. & Yan, Q.-W., 2011. Toll-like receptors in cerebral injury inflammatory injury. *J of Neuroinflam,* Volume 8, p. 134.

Watts, A. G. & Donovan, C. M., 2010. Sweet talk in the brain: glucosensing, neural networks, and hypoglycemic counterregulation. *Front Neuroendocrinol,* 31(1), pp. 32-43.

Weigert, C. et al., 2005. Direct cross-talk of interleukin-6 and insulin signal transduction via insulin receptor substrate-1 in skeletal muscle cells. *J Biol Chem,* Volume 11, pp. 7060-7067.

Williams, G. et al., 2001. The hypothalamus and the control of energy homeostasis: different circuits, differet purposes. *Physiol Behav,* 74(4-5), pp. 683-701.

Woolson, H. D., Thomson, V. S. & al, e., 2009. Selective inhibition of cytokine-activated extracellular signal regulated kinase by cyclic-AMP via Epac-dependent induction of suppressor of cytokine signaling-3. *Cell Signal ,* 21(11), pp. 1706-1715.

Wunderlich, F. T. et al., 2010. Interleukin-6 signaling in liver-parenchymal cells suppresses hepatic inflammation and improves system insulin action. *Cell Metab,* 12(3), pp. 237-249.

Xuan, Y. T. et al., 2001. An essential role of the JAK-STAT pathway in ishemic preconditioning. *Proc Natl Acad Scie USA,* 98(16), pp. 9050-9055.

Xu, Y. et al., 2010. PI3K signaling in the ventromedial hypothalamic nucleus is required for normal energy homeostasis. *Cell Metab,* Volume 12, pp. 88-95.

Yasukawa, H. et al., 2003. IL-6 induces an anti-inflammatory response in the absence of SOCS3 in macrophages. *Nat Immunol,* Volume 4, pp. 551-556.

Zauberman, A., Zipori, D., Krupsky, M. & Ben-Levy, R., 1999. Stress activated protein kinase p38 is involved in IL-6 induced transcriptional activation of STAT3. *Oncogene,* Volume 18, pp. 3886-3839.

Zeigerer, A., BcBrayer, M. K. & McGraw, T., 2004. Insulin stimulation of GLUT4 exocytosis, but not its inhibition of endocytosis, is dependent on RabGAP AS160. *Mol Biol Cell,* 15(10), pp. 4406-4415.

Zeyda, M. & Stulnig, T. M., 2009. Obesity, inflammation, and insulin resistance - A Mini-Review. *Gerontology,* Volume 55, pp. 379-386.

Zhang, G. et al., 2013. Hypothalamic programming of systemic ageing involving IKK-β, NF-κB and GnRH. *Nature,* 497(7448), pp. 211-216.

Zhang, R. et al., 2008. Selective inactivation of Socs3 in SF1 neurons improves glucose homeostasis without affecting body weight. *Endocrinology,* Volume 149, pp. 5654-5661.

Zhang, Y. et al., 1994. Positional cloning of the mouse obese gene and its human homologue. *Nature,* Volume 372, pp. 425-432.

Zhao, H., Ren, C., Chen, X. & Shen, J., 2012. From rapid to delayed and remote postconditioning: the evolving concept of ischemic postconditioning in brain ischemia. *Curr Drug Targets,* 13(2), pp. 37-87.

Zhou, W. D. et al., 2014. SB203580,a p38 mitogen-activated protein kinase inhibitor, suppresses the development of endometriosis by down-regulating proinflammatory cytokines and proteolytic factors in a mouse model. *Hum Reprod,* 25(12), pp. 3110-3116.

Zwartkruis, F. J. & Bos, J. L., 1999. Ras and Rap1: two highly related small GTPases with distinct function. *Exp Cell Res,* 253(1), pp. 157-165.

Appendix

Metabolic Characterization of NesCre+ and NesCreIL-6Rα WT mice

Figure 3.1:

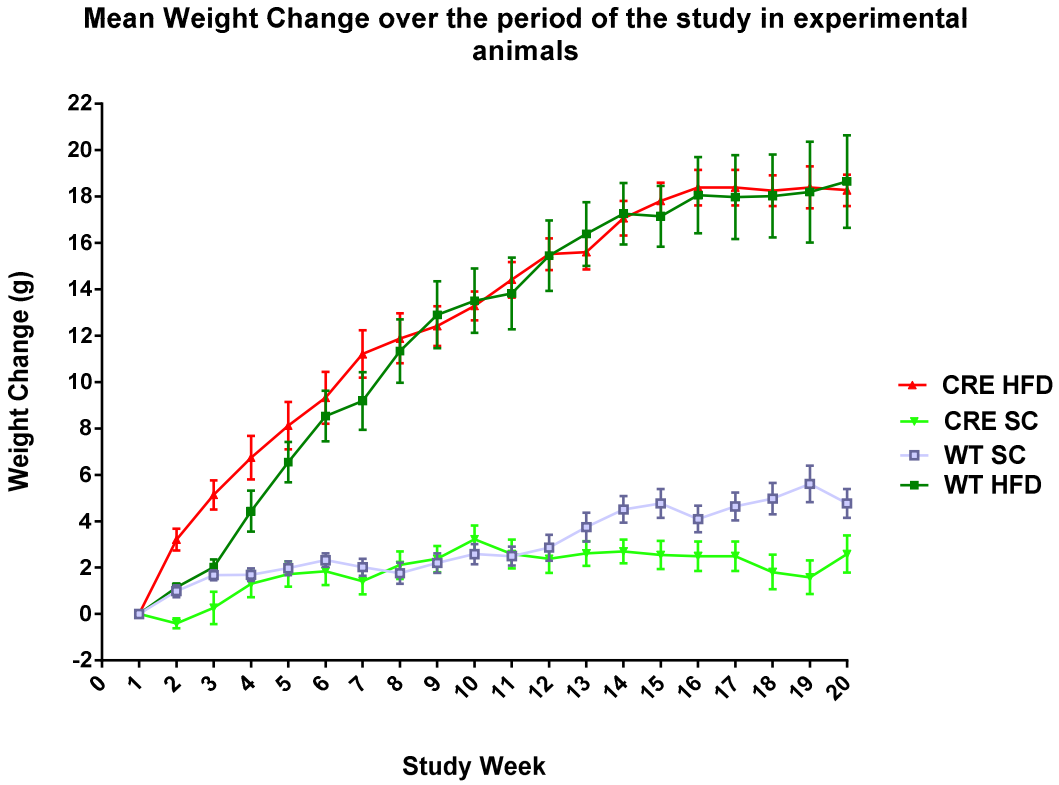

Figure 3.2:

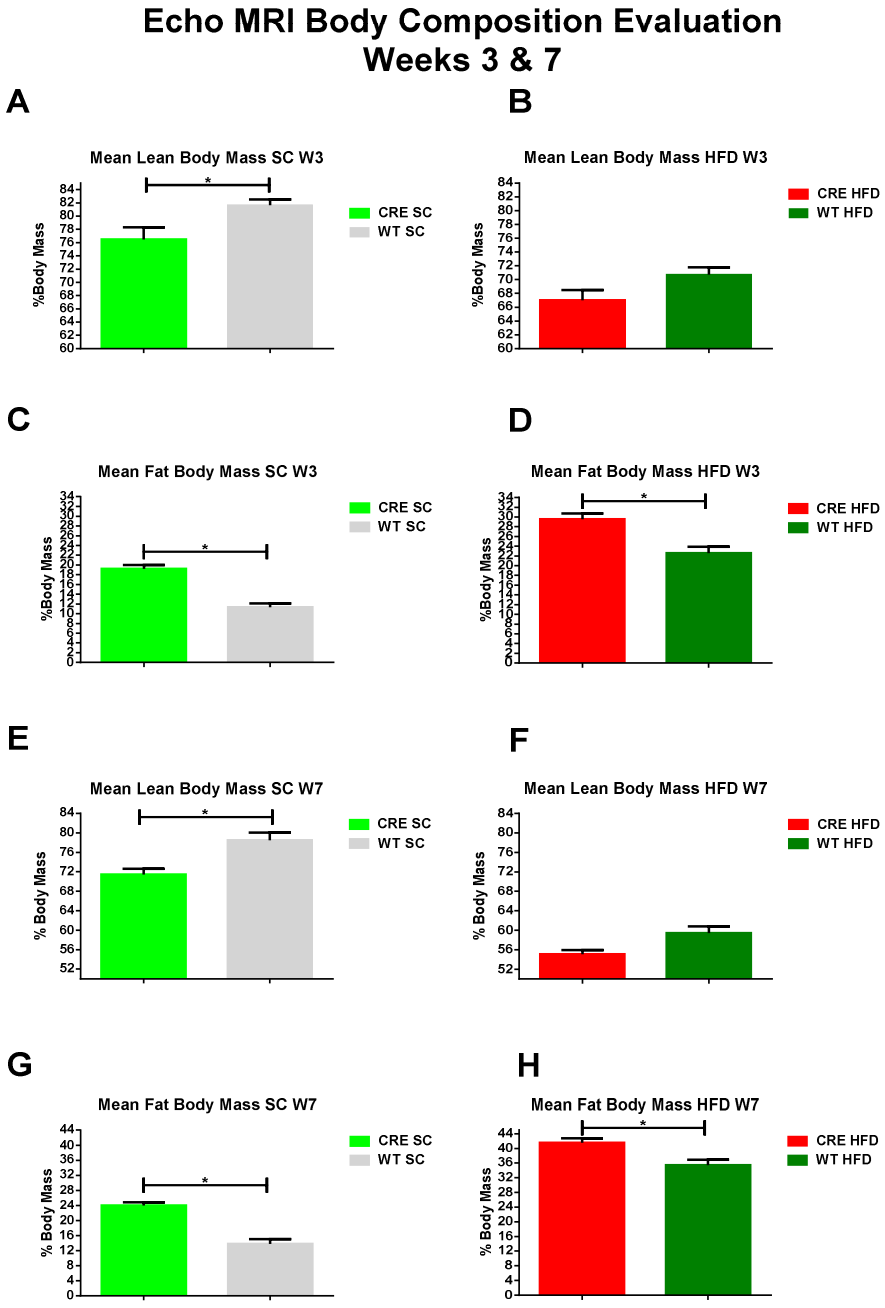

Figure 3.2:

Week3 – Mean Lean SC: CRE 76.462+/-1.8790%, n=8; WT 81.6713+/-0.9156%, n=8; p=0.0195. **Mean Fat SC:** CRE 19.22+/-0.8047%, n=8; WT 11.28+/-0.8662%, n=8; p<0.0001. **Mean Lean HFD:** CRE 65.7332+/-0.9901%, n=8; WT 70.7318+/-1.151%, n=8; p=0.2052. **Mean Fat HFD:** CRE 29.5113+/-1.2201%, n=8; WT 22.5927+/-1.2731%, n=8; p=0.0168.

Week7 – Mean Lean SC: CRE 71.4125+/-1.1801%, n=8; WT 78.4838+/-1.5456%, n=8; p=0.0032. **Mean Fat SC:** WT 13.7138+/-1.8790%, n=8; CRE 23.975+/-0.8448%, n=8; p=0.0003. **Mean Lean**

HFD: CRE 55.0714+/-0.8668%, n=7; WT 59.419+/-1.3802%; n=7**;** p=0.1033**. Mean Fat HFD:** CRE 41.5571 +/-1.1912%, n=7; WT 35.4736+/-1.4073%, n=7; p=0.0124.

Figure 3.3:

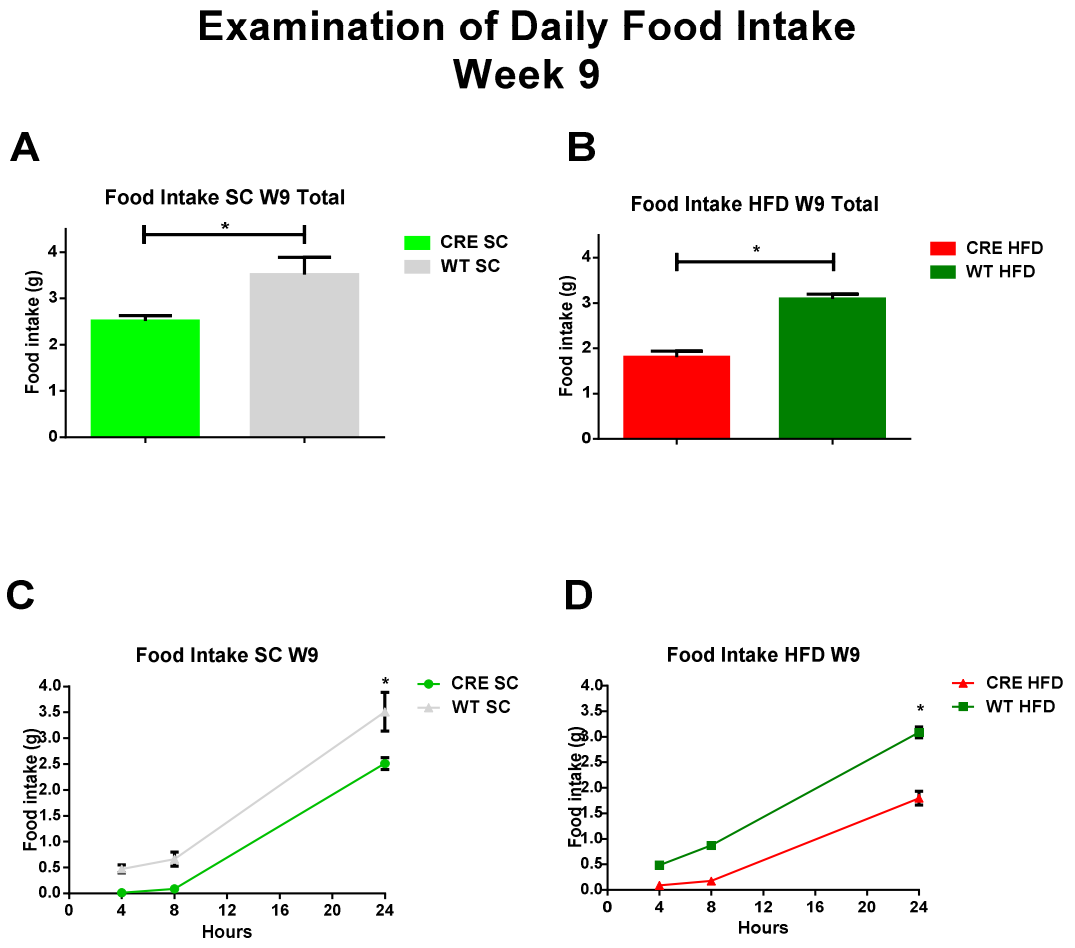

Figure 3.3:

Total food intake SC: WT=3.5125+/-0.3744g, n=8; CRE = 2.5111+/-0.1172g, n=9; p=0.012.

Total food intake HFD: WT=3.0857+/-0.1056g, n=7; CRE=1.8+/-0.1363g, n=8; p=0.0003.

Figure 3.4:

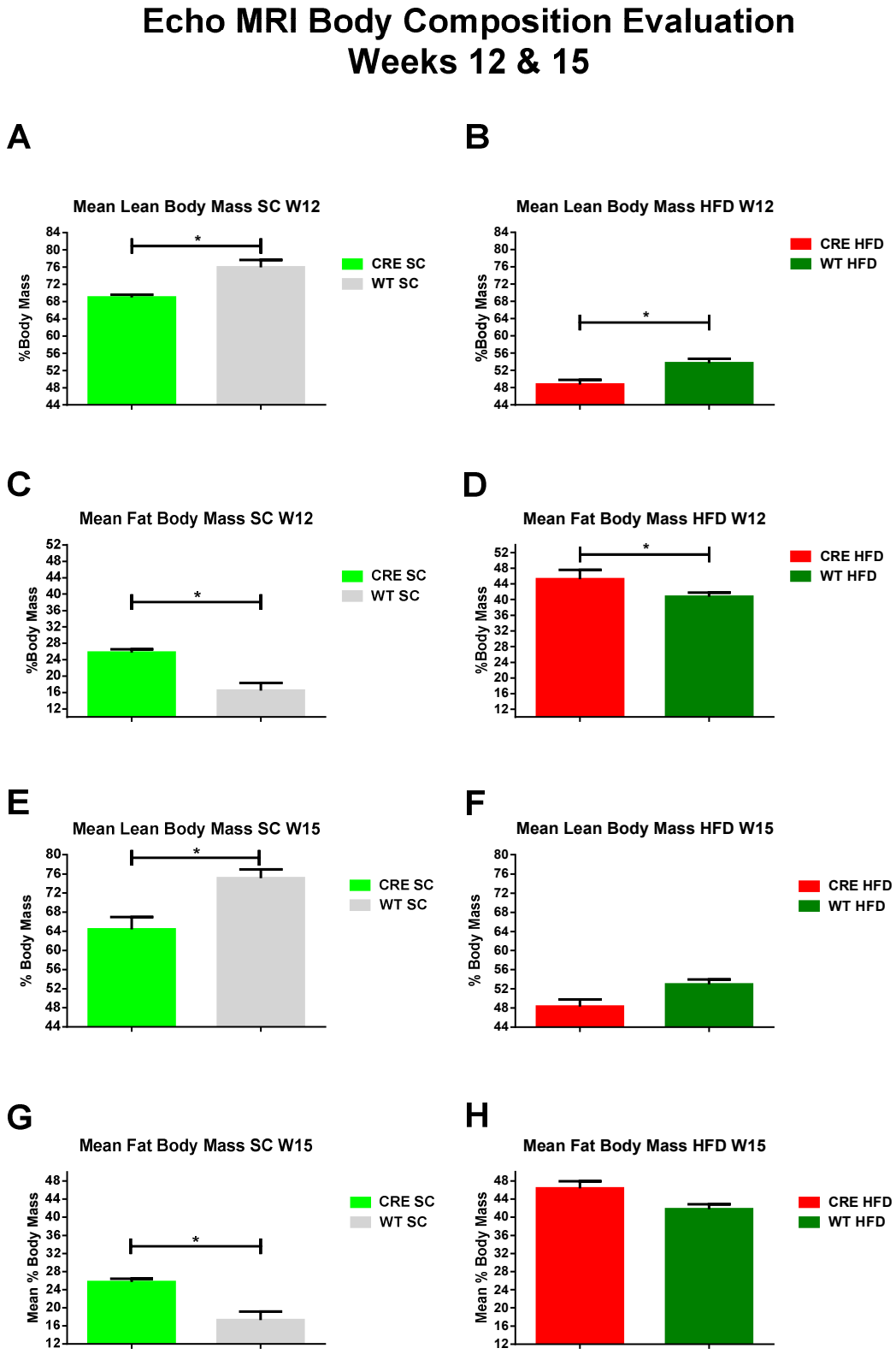
Echo MRI Body Composition Evaluation
Weeks 12 & 15
A
Mean Lean Body Mass SC W12
%Body Mass
CRE SC
WT SC
B
Mean Lean Body Mass HFD W12
%Body Mass
CRE HFD
WT HFD
C
Mean Fat Body Mass SC W12
%Body Mass
CRE SC
WT SC
D
Mean Fat Body Mass HFD W12
%Body Mass
CRE HFD
WT HFD
E
Mean Lean Body Mass SC W15
% Body Mass
CRE SC
WT SC
F
Mean Lean Body Mass HFD W15
% Body Mass
CRE HFD
WT HFD
G
Mean Fat Body Mass SC W15
Mean % Body Mass
CRE SC
WT SC
H
Mean Fat Body Mass HFD W15
Mean % Body Mass
CRE HFD
WT HFD

Figure 3.4:

Week12 – Mean Lean SC: CRE 68.9788+/-0.6403%, n=8; WT 75.9386+/-1.7187%, n=7; p=0.0048. **Mean Fat SC:** CRE 25.7389+/-0.7927%, n=8; WT 16.5014+/-1.8050%, n=8; p=0.0009. **Mean Lean HFD:** CRE 48.7588+/-1.1444%, n=8; WT 53.6969+/-0.9837%, n=8; p=0.0269. **Mean Fat HFD:** CRE 45.2050+/-2.3498%, n=8; WT 40.6984+/-1.0848%, n=8; p=0.00185.

Week15 – Mean Lean SC: CRE 65.0467+/2.3804%, n=8; WT 75.085+/-1.8322%, n=8; p=0.0011. **Mean Fat SC:** CRE 25.6788 +/-0.7322%, n=8; WT 17.3063 +/-1.8549%, n=8; p=0.0013. **Mean Lean HFD:** CRE 48.3038+/-1.4830%, n=8; WT 52.9253+/-1.0368%, n=8; p=0.00501. **Mean Fat HFD:** CRE 46.35 +/-1.5674%, n=8; WT 41.7397 +/-1.1024%, n=8; p=0.1316.

Figure 3.5:

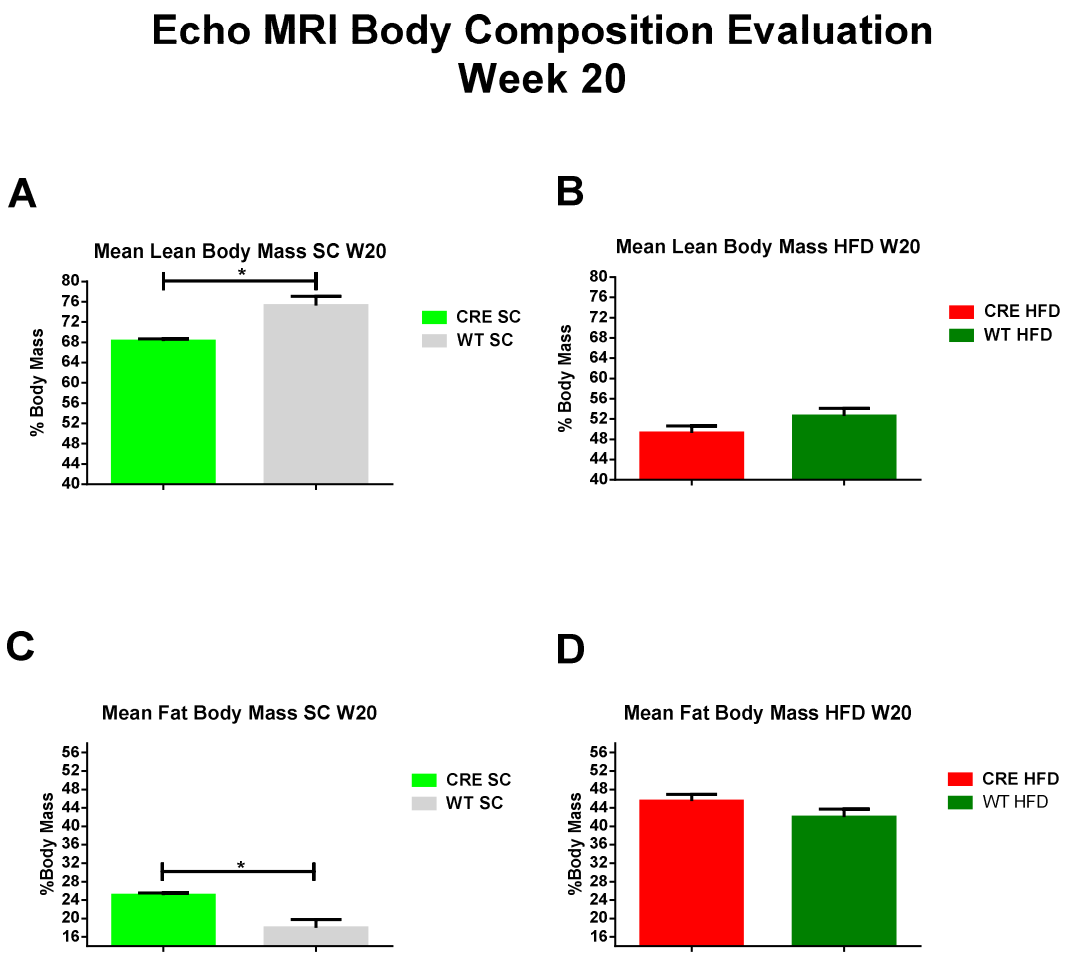

Figure 3.5:

Week20 – Mean Lean SC: CRE 68.2363+/-0.4456%, n=8; WT 75.2485+/-1.8228%, n=8; p=0.0020. **Mean Fat SC:** CRE 25.03+/-0.5203%, n=8; WT 16.5014+/-1.8050%, n=8; p=0.0057. **Mean Lean**

HFD: CRE 49.2463 +/-1.3617%, n=8; WT 53.6969+/-0.9837%, n=8; p=0.5270. **Mean Fat HFD:** CRE 45.4963 +/-1.4328%, n=8; WT (42.0338 +/-1.7235%, n=8; p=0.6940.

Figure 3.6:

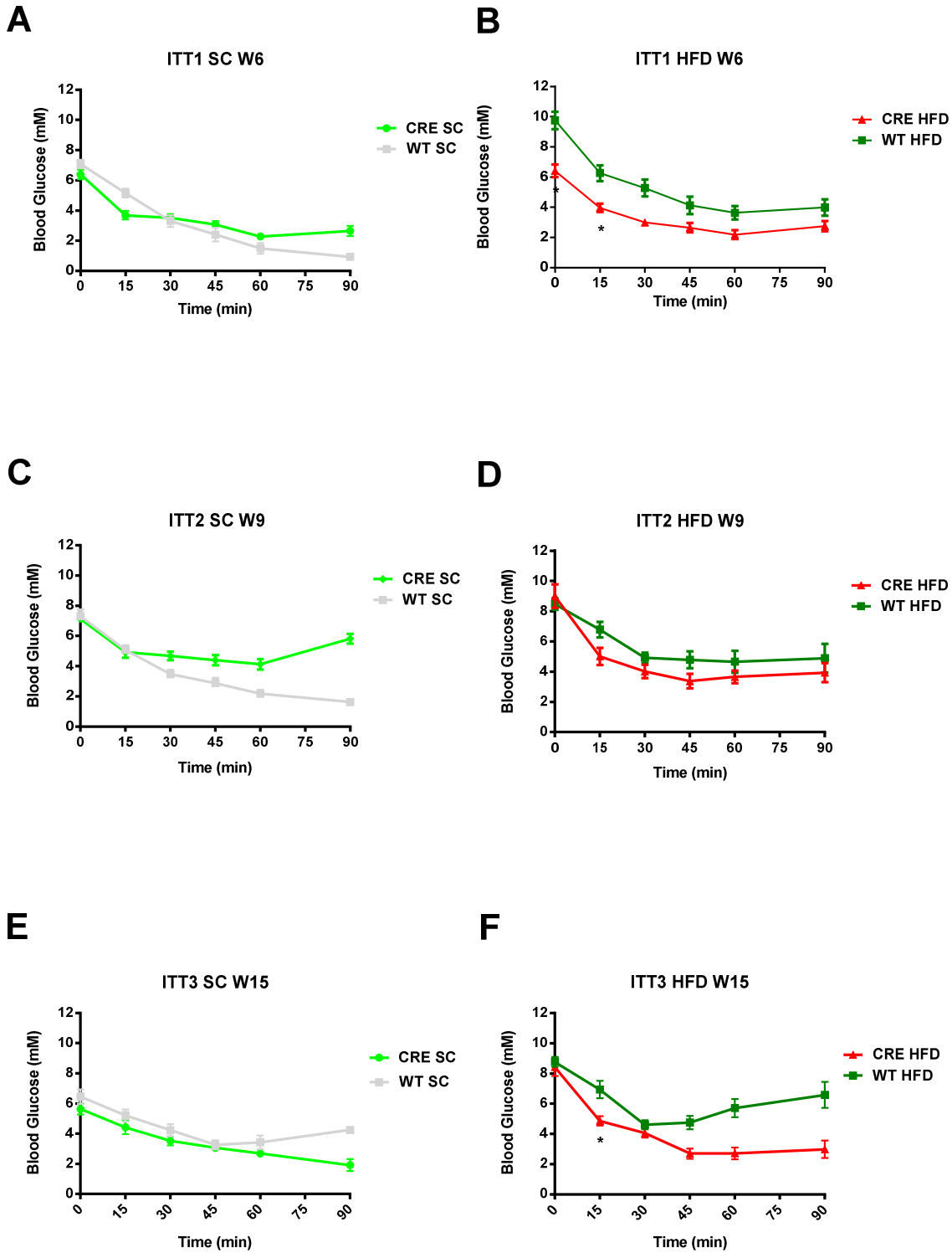

Figure 3.6:

ITT Week 6: SC Baseline: CRE 6.3889+/-0.3182mM Glucose, n=8; WT 7.0857+/-0.2890mM Glucose, n=8; p=0.5117. **SC T15:** CRE 3.6889+/-0.287926mM Glucose, n=8; WT 5.1571+/-0.2935mM Glucose, n=8; p= 0.0071. **HFD Baseline:** CRE 6.411+/-0.415mM Glucose, n=9; WT 9.75+/-0.571mM Glucose; p<0.0001. **HFD T15:** CRE 3.967+/-0.274mM, n=9; WT 6.262+/-0.526mM, n=8; p=0.0015.

ITT Week 9: SC Baseline: CRE 7.133+/-0.176mM Glucose, n=9; WT 7.3+/-0.411mM Glucose, n=8; p=0.9989. **SC T15:** CRE 4.922+/-0.355mM Glucose, n=9; WT 5.075+/-0.276mM Glucose, n=8; p=0.9996. **HFD Baseline:** CRE 9.0+/-0.774mM Glucose, n-8; WT 8.475mM Glucose, n=8; p=0.9894. **HFD T15:** CRE 5.012+/-0.571mM Glucose, n=8; WT 6.787+/-0.514mM Glucose, n=8, p=0.2.

ITT Week 15: SC Baseline: CRE 5.637+/-0.372mM, n=8; WT 6.463+/-0.477mM Glucose; p=0.4699. **SC T15:** CRE 4.425+/-0.446mM Glucose, n=8; WT 5.213+/-0.394mM Glucose, n=8; p=0.5245. **HFD Baseline:** CRE 8.425+/-0.588mM, n=8; WT 8.762+/-0.331, n=8; p=0.9973. **HFD T15:** CRE 4.863+/0.31mM, n=8; WT 6.938+/-0.574mM, n=8; p=0.0213.

Figure 3.7:

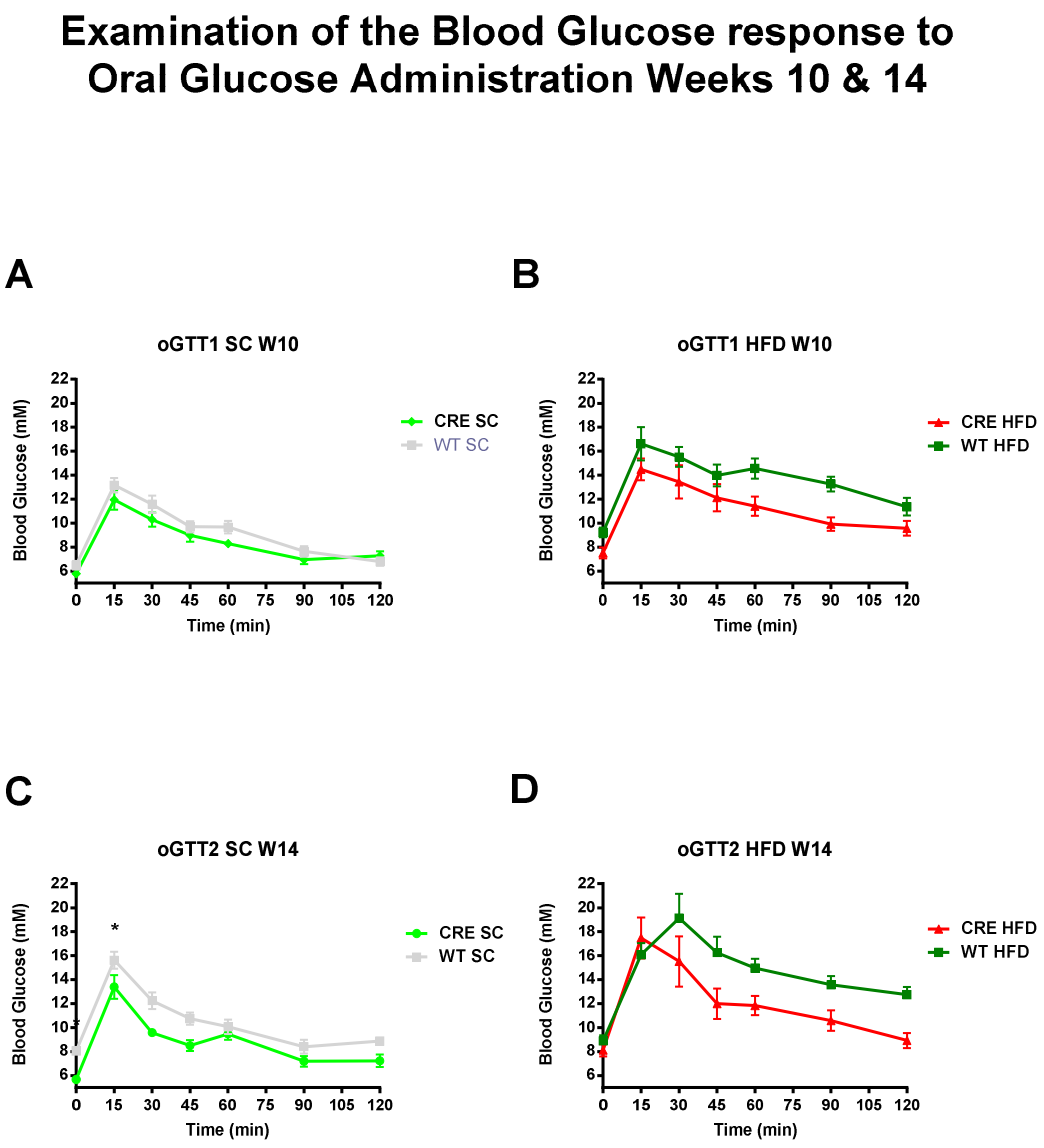

Figure 3.7:

Week 10 oGTT: SC Baseline: CRE 5.789+/-0.206mM Glucose, n=8; WT 6.488+/-0.355, n=8; p=0.9317. **SC T15:** CRE 11.944+/-0.814mM Glucose, n=8; WT 13.163+/-0.611, n=8; p=0.4773. **HFD Baseline:** CRE 7.512+/-0.456mM Glucose, n=8; WT 9.225+/-0.41mM Glucose, n=8; p=0.7291. **HFD T15:** CRE 14.488+/-0.905mM Glucose, n=8; WT 16.625+/1.383mM Glucose, n=8; p=0.4742.

Week 14 oGTT: SC Baseline: CRE 5.678+/-0.268mM Glucose, n=9; WT 8.050+/-0.270, n=8; p=0.0188. **SC T15:** CRE 13.389+/-1.002mM Glucose, n=9; WT 15.613+/-0.708, n=8; p=0.0334. **HFD Baseline:** CRE 8.113+/-0.509mM Glucose, n=8; WT 8.887+/-0.476mM Glucose, n=8; p=0.9993. **HFD T15:** CRE 17.475+/-1.71mM Glucose, n=8; WT 16.087+/0.960mM Glucose, n=8; p=0.9751.

Figure 3.8:

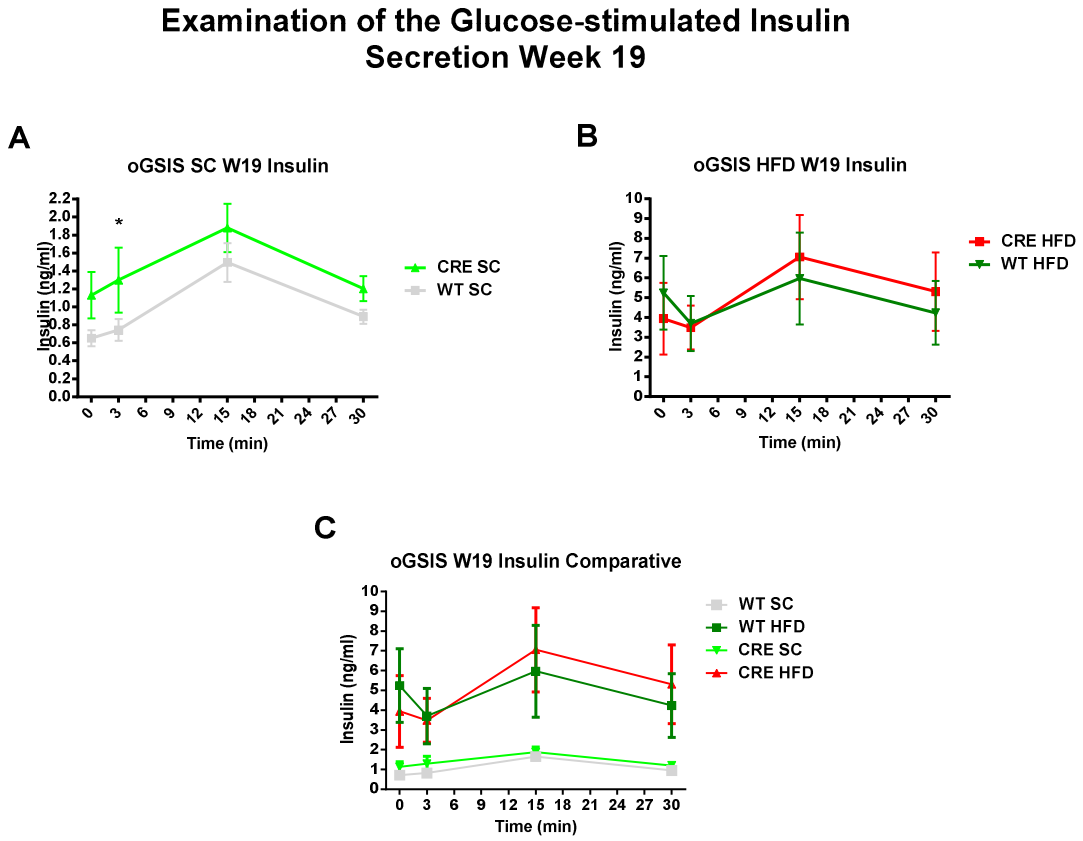

Figure 3.8:

Week 19 oGSIS: SC Baseline: CRE 1.13+/-0.257pg/ml Insulin, n=6; WT 0.711+/-0.078pg/ml Insulin, n=6; p=0.0855. **SC T3:** CRE 1.299+/-0.361pg/ml Insulin, n=6; WT 0.819+/-0.112pg/ml Insulin, n=6; p=0.0431. **SC T15:** CRE 1.878+/-0.268pg/ml Insulin, n=6; WT 1.654+/-0.17pg/ml Insulin, n=6; p=0.4745. **SC T30:** CRE 1.202+/-0.138pg/ml Insulin, n=6; WT 0.951+/-0.057pg/ml Insulin, n=6; p=0.3951.

Week 19 oGSIS: HFD Baseline: CRE 3.943+/-1.814pg/ml Insulin, n=6, WT 5.244+/-1.86pg/ml Insulin, n=6; p=0.2454. **HFD T3:** CRE 3.49+/-1.109pg/ml Insulin, n=6; WT 3.701+/-1.394pg/ml Insulin, n=6; p=0.9619. **HFD T15:** CRE 7.059+/-2.128pg/ml Insulin, n=6; WT 5.974+/-2.325pg/ml, n=6; p=0.3702. **HFD T30:** CRE 5.31+/-1.986pg/ml Insulin, n=6; WT 4.239+/-1.607pg/ml Insulin, n=6; p=0.3798.